

Thesis submitted for the degree of
Doctor of Philosophy

Palaeoceanography and
Sedimentology of a
Mid-Cretaceous
Greensand

Volume 2 - Figures and Tables

by

Stephen Francis Hart

Department of Earth Sciences
& Wolfson College
University of Oxford

Trinity, 1991



TABLE OF CONTENTS

CHAPTER 1 - INTRODUCTION AND HISTORY OF PREVIOUS RESEARCH

Fig.1: Simplified stratigraphic position of the Upper Greensand of southern England.

Fig.2: Map of the outcrop of Albian sediments in the Anglo-Paris Basin, showing the locations of areas discussed further in the text.

CHAPTER 2 - SEDIMENTARY CONDENSATION PHENOMENA AND FACIES CONTROLS IN THE UPPER ALBIAN (CRETACEOUS) OF THE ANGLO-PARIS BASIN

Fig.3: Simplified stratigraphic scheme for the Upper Albian of the Anglo-Paris Basin, based on Jukes-Browne & Hill (1900); Smith (1961); Drummond (1970); Hamblin & Wood (1976); Juignet (1980); Garrison *et al.* (1987) and the author's own work and interpretation. Ammonite zonation scheme after Owen (1976). Hatched areas indicate biostratigraphic gaps.

Fig.4: Detailed graphic log of the Upper Greensand succession between the Hooken Cliffs and Beer Head, Beer (SY 220 879 to SY 227 879).

Fig.5: Detailed graphic log of the high *auritus* subzone interval of sedimentary condensation: amalgamated glauconitic storm laminites at the Foxmould-Chert Beds contact, Dunscombe Cliff (SY 153 877), south Devon.

Fig.6: Outcrop of the interval of condensed glauconitic pebble-shell beds in the uppermost Foxmould, Whitecliff, Beer (SY 234 894). Shown graphically in Figure 7.

Fig.7: Detailed graphic log of the high *auritus* subzone interval of sedimentary condensation: glauconitic intraformational pebble-shell beds at the Foxmould Chert Beds contact, south-east Devon.

Fig.8: Basal burrowing with glauconitic sediment infill, developed in the glauconitic pebble-shell beds in the uppermost Foxmould, Whitecliff, Beer, south-east Devon (SY 234 894). Middle bed in Fig.7.

Fig.9: Basal burrowing with glauconitic sediment infill, developed in the glauconitic pebble-shell beds in the uppermost Foxmould, Whitecliff, Beer, south-east Devon (SY 234 894). Middle bed in Fig.7.

Fig.10: Basal burrowing with glauconitic sediment infill, developed in the glauconitic pebble-shell beds in the uppermost Foxmould, Whitecliff, Beer, south-east Devon (SY 234 894). Upper bed in Fig.7.

Fig.11: Basal burrowing with glauconitic sediment infill, developed in the glauconitic pebble-shell beds in the uppermost Foxmould, Whitecliff, Beer, south-east Devon (SY 234 894). Upper bed in Fig.7.

Fig.12: Two successive nodular horizons developed in the uppermost Foxmould, around Culverhole Point, between Axemouth and Lyme Regis (SY 278 893).

Fig.13: Thick interval of nodular sandstones - pebble beds, section 0.5km east of Corbin Rocks, between Axemouth and Lyme Regis (SY 293 896).

Fig.14: Field outcrop of the lower Chert Beds hardground, Little Beach - Beer Head, south-east Devon (SY 226 879).

Fig.15: Field outcrop of the lower Chert Beds hardground, Little Beach - Beer Head, south-east Devon (SY 226 879).

Fig.16: Thin development of the lower Chert Beds hardground, Whitecliff, Beer (SY 234 894). Note the chert nodules (black) replacing *Thalassinoides* burrows.

Fig.17: Burrowing developed at the base of the lower Chert Beds hardground, Whitecliff, Beer (SY 234 894).

Fig.18: Vertical profile through the uppermost Foxmould, Chert Beds and Top Sandstones, Little Beach - Beer Head (SY 226 879). Shows the reduction in quartz concentration passing into the Chert Beds; the high quartz content of the Coarse Band; the increase in quartz grain size in the upper Chert Beds pebble beds and Coarse Band; high glauconite concentrations in the uppermost Foxmould and upper Chert Beds pebble beds.

Fig.19: Detailed correlation of the uppermost Foxmould, Chert Beds and Top Sandstones across south-east Devon, indicating the lateral extent and proposed correlation of individual hardgrounds and pebble-shell beds. A = uppermost Foxmould interval of glauconite-rich sands and intraformational pebble-shell beds; B = lower Chert Beds hardground; C = Brecciated Limestone hardground; D = the Coarse Band; E = the top Upper Greensand hardground.

Fig.20: The thick nodular Brecciated Limestone hardground, slipped block, Weston Ebb, west of Branscombe (SY 175 878).

Fig.21: Outcrop of the Brecciated Limestone hardground (lower arrow) and Top Sandstones, Kempstone Rocks, south Devon (SY 161 881). The Coarse Band is developed (upper arrow), weathering back as a notch in the cliffs.

Fig.22: Well-developed rather compacted *Thalassinoides* burrow system, infilled with glauconitic carbonate sand; developed in the lower Top Sandstones, Beer Head (SY 226 879).

Fig.23: Sediment fabric of the Coarse Band, Kempstone Rocks (SY 161 881). Quartz-carbonate sand, rich in coarse rounded quartz grains.

Fig.24: The top Upper Greensand hardground at Whitecliff, Beer (SY 234 894). A well-defined planar surface marks the top of the bed, and a variably-nodular fabric is developed below.

Fig.25: Relict trough cross-bedding preserved in the top Upper Greensand hardground, Beer Head, Beer (SY 226 879).

Fig.26: Small pocket with infill of Beer Head Limestone developed between the uppermost nodules of the top Upper Greensand hardground, Beer Roads, Beer (SY 229 890).

Fig.27: Well-developed rhythmic bedding in the Foxmould, Worbarrow Bay, below Flower's Barrow, south Dorset (SY 866 804).

Fig.28: Close-up view of the rhythmic bedding shown in Fig.27, defined by an increase in the black clay content.

Fig.29: Close-up view of the muddy bed shown in Fig.28; the black mud is redistributed by burrowing activity, often as burrow linings.

Fig.30: Field outcrop of rhythmically-bedded Passage Beds succession at Compton Bay, Isle of Wight (SZ 367 853). Rhythmicity is defined by varying amounts of black mud within pale brown fine-grained siltstones.

Fig.31: Diagram illustrating the cyclicity developed within the Passage Beds of the Isle of Wight. Bed measurement is accompanied by a visual estimate of the mud concentration (1 = very weak; 7 = very strong); the data are plotted as a simple histogram. The 40 first order cycles group into 4 second order cycles.

Fig.32: Glauconite- and serpulid-rich bed developed in the upper Foxmould, below Flower's Barrow, Worbarrow Bay (SY 866 804).

Fig.33: Close-up view of the concretionary horizon shown in Fig.32, indicating the high serpulid concentrations in the sediment.

Fig.34: The Dispar Zone Ammonite Bed, a phosphatic greensand, slipped blocks west of White Nothe, south Dorset (SY 769 809).

Fig.35: Detailed correlation of the uppermost Foxmould, Exogyra Rock, Dispar Zone Ammonite Beds, Chert Beds and Eggardon Grit across south Dorset. Lower Cenomanian faulting at Mupe Bay results in the Chalk Basement Bed resting directly on the Gault. A = uppermost Foxmould glauconitic marly silts; B = Exogyra Rock; C = glauconitic marls; D = Dispar Zone Ammonite Bed; E = thin glauconite-rich bed above the DZAB; F = Chert Beds; G = Eggardon Grit.

Fig.36: Thin development of the Chert Beds at White Nothe, south Dorset (SY 772 806), lying stratigraphically between the Dispar Zone Ammonite Bed and the Eggardon Grit.

Fig.37: The Eggardon Grit, a thick nodular bed of sandy limestone at the top of the Upper Greensand, Durdle Cove, south Dorset (SY 805 806). Top of the bed is just above the hammer head.

Fig.38: A detailed correlation of selected Middle-Upper Albian sections in Normandy, France. A = Poudingue Ferrugineux; B = Gaize Inférieure; C = high *auritus* subzone greensands, basal contact the surface perforée "Cauville"; D = Gaize Supérieure; E = Craie Glauconieuse, basal contact the surface de ravinement "Octeville".

Fig.39: Glauconitic bed developed in sediments of the high *auritus* subzone, Compton Bay, Isle of Wight (SZ 367 853). Pale brown silts pass up into a bed of green, glauconitic marly silt, with a basal contact marked by a zone of sediment-mixing due to bioturbation.

Fig.40: Close-up of the burrowed basal contact shown in Fig.39.

Fig.41: Field outcrop showing the Upper Greensand succession at Gore Cliff, Isle of Wight (SZ 492 763). The Passage Beds (dark grey) in the lower part of the section pass up into pale brown silts of the Upper Greensand; the top part of the cliff is marked by the development of glauconitic marly silts with prominent chert horizons, the Chert Beds.

Fig.42: Detailed graphic log of the high *auritus* subzone interval of sedimentary condensation: thin glauconitic cycles at the top of the Gaize Inférieure, St. Jouin-Bruneval, Normandy coast.

Fig.43: Field outcrop showing the high *auritus* subzone sediments, near St. Jouin-Bruneval, Normandy coast; four greensand beds are developed in this interval (the bases of these are arrowed). Field log of the section given in Fig.42.

Fig.44: Field outcrop of three greensand beds developed in a thin Albian sequence on the eastern side of the Armorican Massif, Carrière le Livet, near Cordebugle, Normandy.

Fig.45: The lower greensand bed shown in Fig.44. Facies change is from muddy fine sands to glauconite-rich, muddy fine sands, which become marly immediately above. The base of the greensand bed is marked by an erosion surface with a coarse quartzose lag, and remanié phosphate nodules.

Fig.46: Field outcrop of the lower greensand bed shown in Fig.44. Outcrop is 5m along the section from that shown in Fig.45. The base of the greensand bed is marked by well-developed burrowing.

Fig.47: Field outcrop of erosion surface in the lower Chert Beds, interpreted as the result of Upper Albian synsedimentary faulting, Culverhole Point area (SY 278 893). The erosion surface is marked by a glauconitic, clayey pebble bed.

Fig.48: Close-up of the bed shown in Fig.47. Note the burrowed basal contact to the glauconitic pebble bed.

Fig.49: Top of the Eggardon Grit, slipped block below Flower's Barrow, Worbarrow Bay (SY 866 804). Note the erosive nature of the contact, with truncation of the nodules highlighted by the nodule-margin (burrow-wall) glauconitization.

Fig.50: Top of the Eggardon Grit, slipped block below Flower's Barrow, Worbarrow Bay (SY 866 804). Erosion of the bed has proceeded to a lower level than in Figure 49, with only traces of burrow-wall glauconitization preserved.

Fig.51: Sipped block of the Upper Greensand below Flower's Barrow, Worbarrow Bay (SY 866 804). Shows a mixed eroded-nodule assemblage, with pale nodules of the Eggardon Grit and smaller glauconitic sandstone nodules of Exogyra Rock lithology.

Fig.52: Field outcrop of the Chalk Basement Bed at Cow Corner, resting on the Exogyra Rock, as a result of Lower Cenomanian synsedimentary faulting.

Fig.53: Complex condensation horizon at the top of the Upper Greensand, Swanage Bay, south Dorset (SY 044 811). 1.2 metres of sediment contain four concretion generations, and represent the equivalent of the Chert Beds and Top Sandstones of south-east Devon (around 23 metres in thickness).

Fig.54: Generation 2 nodules in the complex condensation horizon shown in Figure 53. Pale brown concretions represent the Chert Beds lithology, and preserve burrows filled with glauconitic sediment.

Fig.55: Generation 3 nodules in the complex condensation horizon shown in Figure 53. The phosphatic concretions correlate with the Dispar Zone Ammonite Bed.

Fig.56: Thin Chert Beds Member, at Compton Bay, Isle of Wight (SZ 367 853). Well-developed concretionary horizons are present, but chert is not developed. The top of the Upper Greensand occurs at a level marked by the top of the scale rule; the beds are overlain by the Glauconitic Marl. The Chert Beds expand and become more siliceous towards the south of the island (Fig.41).

Fig.57: Cartoon illustrating the genetic relationship between nodular hardgrounds and phosphoritic greensands.

A: Halt in sedimentation above cross-stratified bioclastic grainstones, and deeper-water marly silts.

B: Development of nodularity within carbonates; glauconite concentration in deeper settings.

C: Nodules are exposed due to winnowing of the overlying sediment; an often long and complex cycle, which includes nodule boring, encrustation, glauconitization and phosphatisation occurs; increased concentrations of glauconite-rich sediment accumulate in deeper settings, a basal zone of strong burrowing and sediment mixing develops, and phosphate nodules develop.

D: Under relative transgression, sedimentation recommences, preserving the hardground and phosphoritic greensand below bioclastic packstones and silty marls.

Fig.58: Summary of stratigraphy, cyclicity and sedimentary environments of the Chert Beds and Top Sandstones Members of the Upper Greensand Formation, Beer Head, south-east Devon.

Fig.59: Glauconite-rich greensand bed marking the base of the Upper Greensand south of Eastbourne (TV 610 977). This bed is equivalent to the Coarse Band of south Devon.

Fig.60: Sequence stratigraphic subdivision of the Upper Albian sediments of the Anglo-Paris Basin, with reference to fourteen designated regional type areas. Ammonite subzonal stratigraphy is plotted as a vertical scale, with proven subzones indicated to the left of each column by a * symbol. Within each column is shown a summary of the sediment composition at a given time interval. Note that no indication of the relative thicknesses is given with this representation. Dotted lines indicate correlative conformities to candidate type II sequence boundaries. Candidate sequential interpretation is given: S.B. = sequence boundary; T.S. = transgressive surface; C.S. = condensed section; TST = transgressive systems tract; HST = highstand systems tract; SMST = shelf margin systems tract.

Table 1: Upper Albian candidate sequence stratigraphy of the Anglo-Paris Basin.

Fig.61: Comparison between the sequence stratigraphy proposed for the Anglo-Paris Basin as a result of this study, and the global cycle chart of Haq *et al.* (1988). Shows candidate sequence boundaries (filled arrows), condensed sections (open arrows), and additional minor flooding surfaces (dotted arrows).

CHAPTER 3 - STORM SEDIMENTATION IN THE UPPER GREENSAND FORMATION (CRETACEOUS) OF SOUTH-WEST ENGLAND

Fig.62: Location map showing the outcrop of the Upper Greensand and Gault across south-west England, and the localities mentioned in the text.

Fig.63: Distal storm laminites, interbedded with fully-bioturbated sediment. Two laminite beds visible, with associated calcareous concretions. Hooken Cliffs, near Beer.

Fig.64: Summary of the typical sedimentological features of a Foxmould member storm laminite bed.

Fig.65: Bioturbated top of a storm laminite bed. Hooken Cliffs, Beer.

Fig.66: Graphic logs of a selected part of the Foxmould member, demonstrating the west-east trend of thinning, fining and disappearance of storm laminite beds. Peak Hill: muddy fine sands with interbedded laminites ; Hooken Cliffs: muddy fine sands with fewer and thinner laminites ; Seaton Hole: muddy fine sands with traces of lamination ; Golden Cap: homogeneous and fully bioturbated muddy silts ; Lulworth Cove: rhythmically-bedded muddy silts (variations in silt : clay).

Fig.67: Thick, proximal storm laminite bed, with a sharp base and bioturbated top. Peak Hill, near Sidmouth.

Fig.68: Large scour at the base of a proximal storm bed, cutting down through thin, amalgamated laminite beds to the top of an underlying thick bed. Peak Hill, near Sidmouth.

Fig.69: Horizontal and low-angle cross-lamination, developed within a thick proximal laminite bed. Peak Hill, near Sidmouth.

Fig.70: Bioturbated top of the bed seen in Fig.67, showing the progression from horizontally-laminated to structureless bioturbated silt.

Fig.71: Amalgamated thin storm laminite beds, preserved within a late diagenetic calcareous concretion, Hooken Cliffs, Beer. Each bed has a concentration of serpulid-rich sediment at the base. Note the burrows in the upper part of the top laminite bed.

Fig.72: Graphic log of amalgamated thin storm laminites and storm-reworked phosphate horizon, from the Foxmould member, Hooken Cliffs, Beer.

Fig.73: Field outcrop of a lens of tabular cross-lamination preserved in the Foxmould Member, Whitecliff, Beer (SY 234 893).

Fig.74: Graphic log of variably-amalgamated, glauconite-rich, thin storm laminites at the Foxmould-Chert Beds contact, Dunscombe Cliff. Correlates with interval shown in Fig.77 and Fig.78.

Fig.75: Fully-bioturbated lithofacies, with very abundant black mud-lined *Palaeophycus* burrows. Little Beach, near Beer.

Fig.76: Fully-bioturbated lithofacies showing the *Thalassinoides-Palaeophycus* trace fossil association, preserved within a concretion. Foreshore east of Axemouth.

Fig.77: Pebble-shell beds and coquina lenses in the uppermost Foxmould, with the Chert Beds Member carbonates above. Whitecliff, Beer.

Fig.78: Graphic log and fabric data from the uppermost Foxmould pebble/shell beds seen in Figure 77, Whitecliff, Beer. Fabric data taken on pebble long axes (pebbles with >2:1 length:width ratio). Correlates with interval shown in Figure 73.

Fig.79: Detailed view of the coquina shell lens seen in Figure 77.

Fig.80: Detailed view of the upper two pebble-shell beds shown in Figure 77, showing the sediment fabric, which has a tendency towards bedding-parallel orientations of the pebble long axes.

Fig.81: Graphic log and fabric data from the upper Chert Beds pebble-shell beds at Beer Head. Fabric data taken on shell and pebble long axes (pebbles with >2:1 length:width ratio) and on shell convexity orientations.

Fig.82: Interbedded carbonate packstones/grainstones and coarse pebble-shell beds, upper Chert Beds, Beer Head (shown graphically in Figure 81).

Fig.83: Pebble-shell bed fabric. Shows a patch of pebble-rich sediment in the upper part, probably infilling a small scour. Shell material is predominantly horizontally-oriented, with a patch of imbricated shells on the left of the picture. Lower pebble-shell bed in upper Chert Beds, Beer Head.

Fig.84: Pebble-shell bed fabric. Shows the predominantly horizontal alignment of the pebble and shell material. An internal sandy lens suggests amalgamation of two beds. A shallow scour at the base of the bed, infilled with pebbles and shells, is present on the left of the picture. Lower pebble-shell bed in upper Chert Beds, Beer Head.

Fig.85: Coquina shell bed in the lower Chert Beds, showing sharp base, lower shelly layer, internal sandy lens, and overlying shelly layer with mounded top. Implies amalgamation of at least two discrete events. Little Beach, Beer.

Fig.86: Graphic log and fabric data from complex proximal shell-pebble beds, Weston Ebb. Fabric data taken on shell long axes and convexity orientations.

Fig.87: Complex proximal shell-pebble beds, upper Chert Beds, just below the Brecciated Limestone hardground, Weston Ebb (shown graphically in Figure 86). Note the internal calcarenite lenses within the uppermost coquina, and thin shell stringers in the sediment immediately below.

Fig.88: Coarse-grained coquina lens and thin shell stringers, upper Chert Beds, Weston Ebb. Note the predominantly convex-down shell stacking in the main part of the coquina lens, and the predominantly convex-up alignments at the top of the lens, and in the shell stringer below.

Fig.89: Fabric of thin pebble layer, finer-grained shell-pebble bed, and coarse shell stringer, upper Chert Beds, Weston Ebb.

Fig.90: Bedding plane view of shell bed from the Beer Head Limestone (Cenomanian), Weston Ebb. Shows the different shell assemblage to the Upper Greensand shell beds, with variably-fragmented *Merklinia* and *Amphidonte* bivalves.

Fig.91: Fabric of coarse-grained complex, proximal coquina bed, upper Chert Beds, Weston Ebb. Note the close shell stacking in predominantly convex-down orientations. Scattered patches of sediment show imbrication, and orientations up to vertical to bedding. Small intraformational pebbles are present at low concentrations throughout.

Fig.92: Gutter infilled with shell-rich sediment, developed at the base of a coarse-grained, complex, proximal coquina bed, Weston Ebb.

Fig.93: Complex pebble-shell bed, showing evidence for amalgamation of three separate pebble and shell concentrations, upper Chert Beds, Beer Head.

Fig.94: Cartoon showing the different types of basal contact to the pebble/shell beds in the Chert Beds calcarenites. (A) basal firmground burrowing and *in situ* nodules ; (B) basal firmground burrowing, all nodules reworked ; (C) no firmground burrowing, all nodules reworked ; (D) sharp base, overlain by a shell-rich bed, sometimes cross-stratified.

Fig.95: Horizontal and undulose to low-angle cross-lamination, the Chert Beds. Wave-polished block, Culverhole Point.

Fig.96: Polished slab from coquina bed, lower Chert Beds, showing the shell fabric. Predominantly horizontal shell orientations, with occasional larger shells up to vertical to the bedding. Note the stratification present within the sample; at least four thin beds are developed, differing in grain size and shell orientation. Little Beach, Beer.

CHAPTER 4 - STABLE-ISOTOPE STRATIGRAPHY OF THE UPPER ALBIAN *DISPAR* ZONE (MID-CRETACEOUS) OF SOUTHERN ENGLAND

Fig.97: Subdivision of the Upper Greensand Formation of south-east Devon, with corresponding ammonite biostratigraphy. Ammonite zonation scheme based on Owen (1976).

Fig.98: Map showing the Upper Greensand and Gault outcrop across south-west England, and the location of the section sampled, at Little Beach - Beer Head.

Table 2: Carbon- and oxygen-isotopic data from Little Beach - Beer Head, south-east Devon. Data are from whole rock samples, generated by crushing, except for the two samples marked *, which were generated by drilling a small amount of powder from fresh specimen surfaces. Normalised data reflect modification to remove postulated silica diagenesis; data normalised to the lowest $\delta^{18}\text{O}$ value.

Table 3: Detailed sample set extracted from Table 2, with corresponding normalised values.

Table 4: Isotopic data from repeated drillings of a single hand specimen showing patchy silicification, collected from the top glauconitic pebble-shell bed in the uppermost Foxmould at Whitecliff, Beer (SY 234 893).

Table 5: Carbon- and oxygen-isotopic data from oysters collected throughout the Little Beach - Beer Head section. Normalised data reflects modification to remove postulated silica diagenesis.

Fig.99: Carbon- and oxygen-stable isotope stratigraphy of the Upper Greensand (Chert Beds and Top Sandstones Members), Little Beach - Beer Head, south-east Devon. The $\delta^{13}\text{C}$ and $\delta^{18}\text{O}$ values are measured from whole-rock carbonate samples. The accompanying lithostratigraphy shows the subdivision of the Upper Greensand in south-east Devon.

Fig.100: Investigation of the isotopic modification resulting from silica diagenesis.

Fig.100A: the isotopic changes across 1.63m of the lower Chert Beds, showing the positions of prominent chert nodules and nodules of siliceous limestone.

Fig.100B: plot of $\delta^{13}\text{C}$ vs $\delta^{18}\text{O}$, showing the good positive correlation, and the best fit line, the gradient of which represents the isotopic changes caused by silicification.

Fig.100C: original carbon-isotope plot and normalised plot (dotted), removing the effects of silicification.

Fig.101: Plot of $\delta^{13}\text{C}$ vs $\delta^{18}\text{O}$ values recorded from repeated drillings of a single hand specimen showing patchy silicification, collected from the top glauconitic pebble-shell bed of the uppermost Foxmould at Whitecliff, Beer (SY 234 893).

Fig.102: Carbon-isotope stratigraphy of the Upper Greensand (Chert Beds and Top Sandstones), Beer Head - Little Beach. The three plots show measured $\delta^{13}\text{C}$ values, three point moving average of measured $\delta^{13}\text{C}$ values, and $\delta^{13}\text{C}$ values normalised to remove the variations assumed to represent changes due to silicification.

Fig.103: Plot of $\delta^{13}\text{C}$ vs $\delta^{18}\text{O}$ values for the whole rock data set (Little Beach - Beer Head section). Data from the lower Chert Beds, upper Chert Beds and the Top Sandstones plot as three distinct groups, with little or no overlap. The silicification trend established in Figure 5B is shown for the lower Chert Beds. Data from the upper Chert Beds, and possibly the Top Sandstones, also show a scatter of values inferring that a major control on recorded $\delta^{13}\text{C}$ values (low variability within each group) was silica diagenesis. The plot clearly displays the abrupt positive shift between the lower and upper Chert Beds, and shows that it is not caused by silicification.

Fig.104: Carbon- and oxygen-isotope stratigraphy of the Upper Greensand (Little Beach - Beer Head). The isotopic values are from oysters collected throughout the succession.

Fig.105: Plot of $\delta^{13}\text{C}$ vs $\delta^{18}\text{O}$ values for the oyster data set (Little Beach - Beer Head section). Data from the lower Chert Beds, upper Chert Beds and Top Sandstones plotted separately. A high degree of scatter is shown, with little indication of any secular changes. Some degree of correlation establishes a tentative silicification modification trend.

Fig.106: Carbon-isotope stratigraphy from oyster samples (Little Beach - Beer Head section). The two plots show measured $\delta^{13}\text{C}$ values, and $\delta^{13}\text{C}$ values normalised to remove the variations interpreted as due to silicification.

Fig.107: Global distribution of Upper Albian black shales (discussed in the text), plotted on an Albian (105Ma) palaeogeographic reconstruction of Funnel (1990).

CHAPTER 5 - GEOCHEMICAL ANALYSIS OF GLAUCONITIZATION PROCESSES IN THE UPPER GREENSAND FORMATION

Table 6: Microprobe chemical analyses of glauconitic grains from the Foxmould Member, Upper Greensand Formation, Beer, south-east Devon.

Table 7: Microprobe chemical analyses of glauconitic grains from the uppermost Foxmould Member, Upper Greensand Formation, Beer, south-east Devon.

Table 8: Microprobe chemical analyses of glauconitic grains from the Chert Beds, Upper Greensand Formation, Beer, south-east Devon.

Table 9: Microprobe chemical analyses of glauconitic grains from the Chert Beds, Upper Greensand Formation, Beer, south-east Devon.

Table 10: Microprobe chemical analyses of glauconitic grains from the top Upper Greensand hardground, Beer, south-east Devon.

Table 11: Microprobe chemical analyses of glauconitic grains from the Dispar Zone Ammonite Bed, Durdle Cove, south Dorset.

Table 12: Microprobe chemical analyses of glauconitic grains from the Upper Greensand at Gore Cliff, Isle of Wight.

Table 13: Microprobe chemical analyses of glauconitic grains from the basal Upper Greensand at Eastbourne.

Fig.108: Photomicrograph of glauconite filling the porosity within a bryozoan bioclast: coquina bed in lower Chert Beds Member, Upper Greensand Formation, Little Beach, Beer, south-east Devon.

Fig.109: Photomicrograph of glauconite filling the chambers of a foraminifera, and rimmed grains with two accretion phases: middle pebble-shell bed in uppermost Foxmould interval of glauconitic pebble-shell beds, Upper Greensand Formation, Whitecliff, Beer, south-east Devon.

Fig.110: Photomicrograph of glauconite filling the axial canal of a sponge spicule (transverse section): Blue Rag, Upper Greensand, Hollows Lane, Selbourne, western Weald.

Fig.111: Photomicrograph of glauconite filling the axial canal of a sponge spicule (longitudinal section): Blue Rag, Upper Greensand, Hollows Lane, Selbourne, western Weald.

Fig.112: Photomicrograph of glauconite rimming a quartz grain, and a vermicular glauconitic grain: upper thick storm laminite bed, Foxmould Member, Upper Greensand Formation, Hooken Cliffs, Beer, south-east Devon.

Fig.113: Photomicrograph of glauconite forming along cracks in a quartz grain: coquina bed in lower Chert Beds Member, Upper Greensand Formation, Little Beach, Beer, south-east Devon.

Fig.114: Photomicrograph of glauconite growing within the flakes of a muscovite grain: Foxmould Member (loose sample), Upper Greensand Formation, Hooken Cliffs, south-east Devon.

Fig.115: Photomicrograph of glauconite growing within the flakes of a muscovite grain: upper thick storm laminite bed, Foxmould Member, Upper Greensand Formation, Hooken Cliffs, Beer, south-east Devon.

Fig.116: Photomicrograph of glauconitized echinoid bioclast: coquina bed in lower Chert Beds Member, Upper Greensand Formation, Little Beach, Beer, south-east Devon.

Fig.117: Photomicrograph of glauconite replacing an aggregate of silt-sized quartz grains and mud, interpreted as a faecal pellet: coquina bed in lower Chert Beds Member, Upper Greensand Formation, Little Beach, Beer, south-east Devon.

Fig.118: Photomicrograph of glauconite replacing the muddy matrix sediment of fine-grained muddy sand: Foxmould Member (loose sample), Upper Greensand Formation, Hooken Cliffs, Beer, south-east Devon.

Fig.119: Morphologies of glauconitic grains measured by electron microprobe analysis. 119.1: Foxmould glauconites; 119.2: uppermost Foxmould glauconites; 119.3: upper Chert Beds (lower part) glauconites; 119.4: upper Chert Beds (upper part) glauconites; 119.5: top Upper Greensand glauconites; 119.6: Dispar Zone Ammonite Beds glauconites; 119.7: Upper Greensand, Gore Cliff glauconites; 119.8 Upper Greensand, Eastbourne glauconites.

Table 14: Sulphur-carbon analyses.

Fig.120: Sulphur/carbon data - the Foxmould Member, Upper Greensand, south-east Devon.

Fig.121: Sulphur/carbon data - the Upper Greensand and Gault of south Dorset.

Fig.122: Sulphur/carbon data - Passage Beds and Upper Greensand, Compton Bay, Isle of Wight.

Fig.123: Sulphur/carbon data - Gault clay, Folkstone.

CHAPTER 6 - CONTROLS ON THE WORLD-WIDE DEVELOPMENT OF THE CRETACEOUS GLAUCONITIC FACIES

Fig.124: World-wide distribution of glauconitic facies during the Ryazanian, plotted on a palaeogeographic reconstruction of Funnel (1990).

Fig.125: World-wide distribution of glauconitic facies during the Valanginian, plotted on a palaeogeographic reconstruction of Funnel (1990).

Fig.126: World-wide distribution of glauconitic facies during the Hauterivian, plotted on a palaeogeographic reconstruction of Funnel (1990).

Fig.127: World-wide distribution of glauconitic facies during the Barremian, plotted on a palaeogeographic reconstruction of Funnel (1990).

Fig.128: World-wide distribution of glauconitic facies during the Aptian, plotted on a palaeogeographic reconstruction of Funnel (1990).

Fig.129: World-wide distribution of glauconitic facies during the Albian, plotted on a palaeogeographic reconstruction of Funnel (1990).

Fig.130: World-wide distribution of glauconitic facies during the Cenomanian, plotted on a palaeogeographic reconstruction of Funnel (1990).

Fig.131: World-wide distribution of glauconitic facies during the Turonian, plotted on a palaeogeographic reconstruction of Funnel (1990).

Fig.132: World-wide distribution of glauconitic facies during the Coniacian, plotted on a palaeogeographic reconstruction of Funnel (1990).

Fig.133: World-wide distribution of glauconitic facies during the Santonian, plotted on a palaeogeographic reconstruction of Funnel (1990).

Fig.134: World-wide distribution of glauconitic facies during the Campanian, plotted on a palaeogeographic reconstruction of Funnel (1990).

Fig.135: World-wide distribution of glauconitic facies during the Maastrichtian, plotted on a palaeogeographic reconstruction of Funnel (1990).

Fig.136: Diagram showing glauconite production rates (measured in km³ per Ma) for each substage of the Cretaceous, derived from volumetric calculations for a large data set of Cretaceous glauconitic facies.

Fig.137: Diagram showing the correlation between the Cretaceous sea-level of Haq *et al.* (1990), peak glauconite production rates (GPR), and the oceanic anoxic events/subevents of Jenkyns (1980), Schlanger *et al.* (1987) and Arthur *et al.* (1990). Stippled area indicates a middle-Upper Cretaceous interval of high GPR; heavy stipple indicates the three main peaks in GPR during the interval.

GRAPHIC LOGS

KEY TO GRAPHIC LOGS

CRETACEOUS	UPPER	CENOMANIAN	CHALK
	LOWER	ALBIAN	UPPER GREENSAND GAULT LOWER GREENSAND

Fig.1: Simplified stratigraphic position of the Upper Greensand of southern England

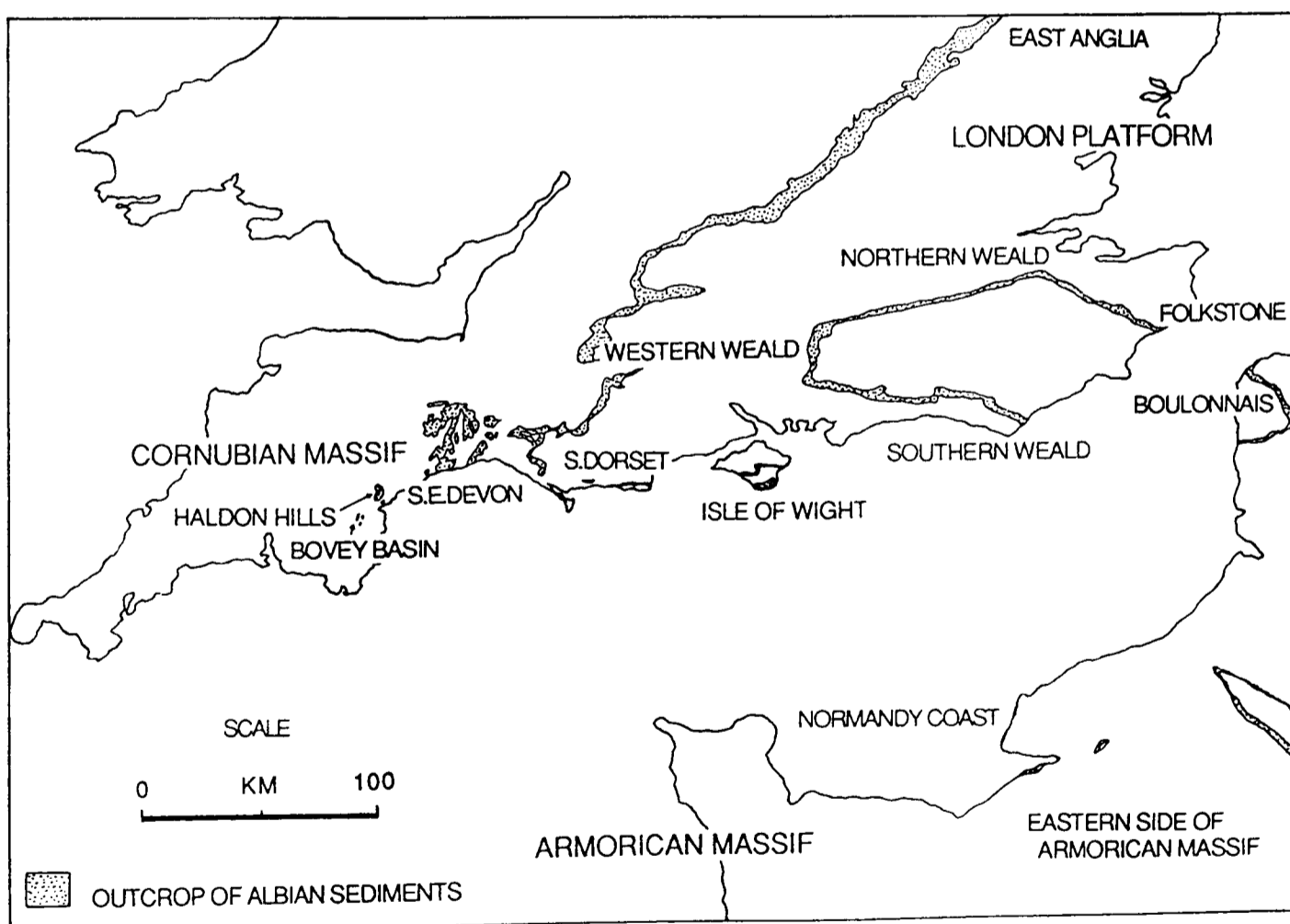


Fig.2: Map of the outcrop of Albian sediments in the Anglo-Paris Basin, showing the locations of areas discussed further in the text.

UPPER ALBIAN		AMMONITE ZONE	AMMONITE SUBZONE	HALDON HILLS	SOUTH-EAST DEVON	SOUTH DORSET	ISLE OF WIGHT	EASTBOURNE	FOLKSTONE	NORMANDY COAST
<i>dispar</i>	<i>perinflatum</i>	Ashcombe Gravels	Top Sandstones	Eggardon Grit	Chert Beds	Upper Greensand	Chert Beds	Upper Greensand	Upper Gault	Gaize supérieure
	<i>rostratum</i>	Woodlands Sands	DZAB & Chert Beds	Passage Beds				Gaize inférieure		
<i>inflatum</i>	<i>auritus</i>	Haldon Sands	Foxmould	Foxmould	Gault	Gault	Gault	Upper Gault	Upper Gault	Gault
	<i>varicosum</i>	Telegraph Hill Sands								
	<i>orbigny</i>	Hatched area	?	?						
	<i>cristatum</i>	Hatched area	?	?						

Fig.3. Simplified stratigraphic scheme for the Upper Albian of the Anglo-Paris Basin, based on Jukes-Browne & Hill (1900); Smith (1961); Drummond (1970); Hamblin & Wood (1976); Juignet (1980); Garrison et al. (1987) and the author's own work and interpretation. Ammonite zonation scheme after Owen (1976). Hatched areas indicate biostratigraphic gaps.

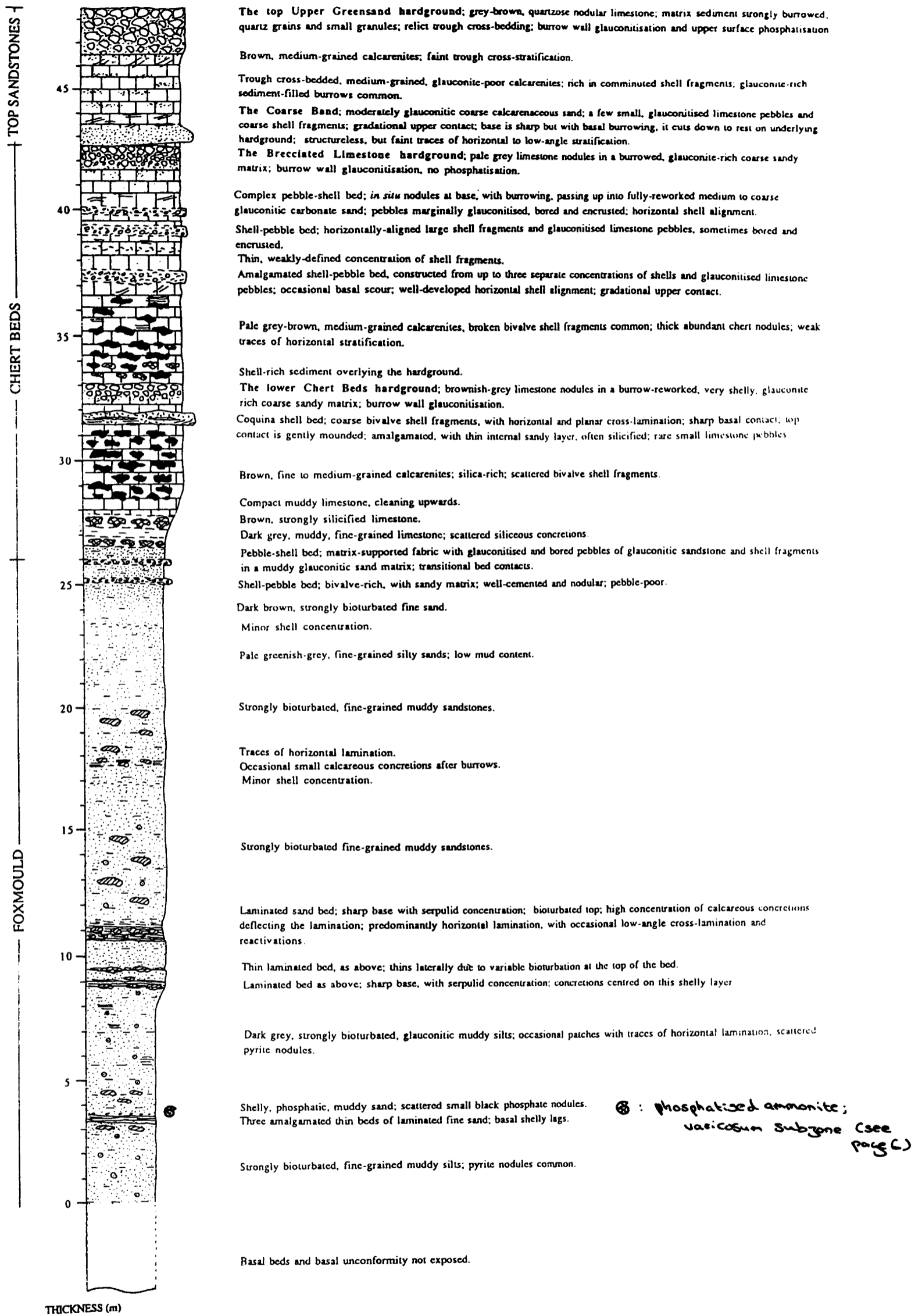


Fig.4: Detailed graphic log of the Upper Greensand succession between the Hooken Cliffs and Beer Head, Beer (SY 220 879 to SY 227 879).

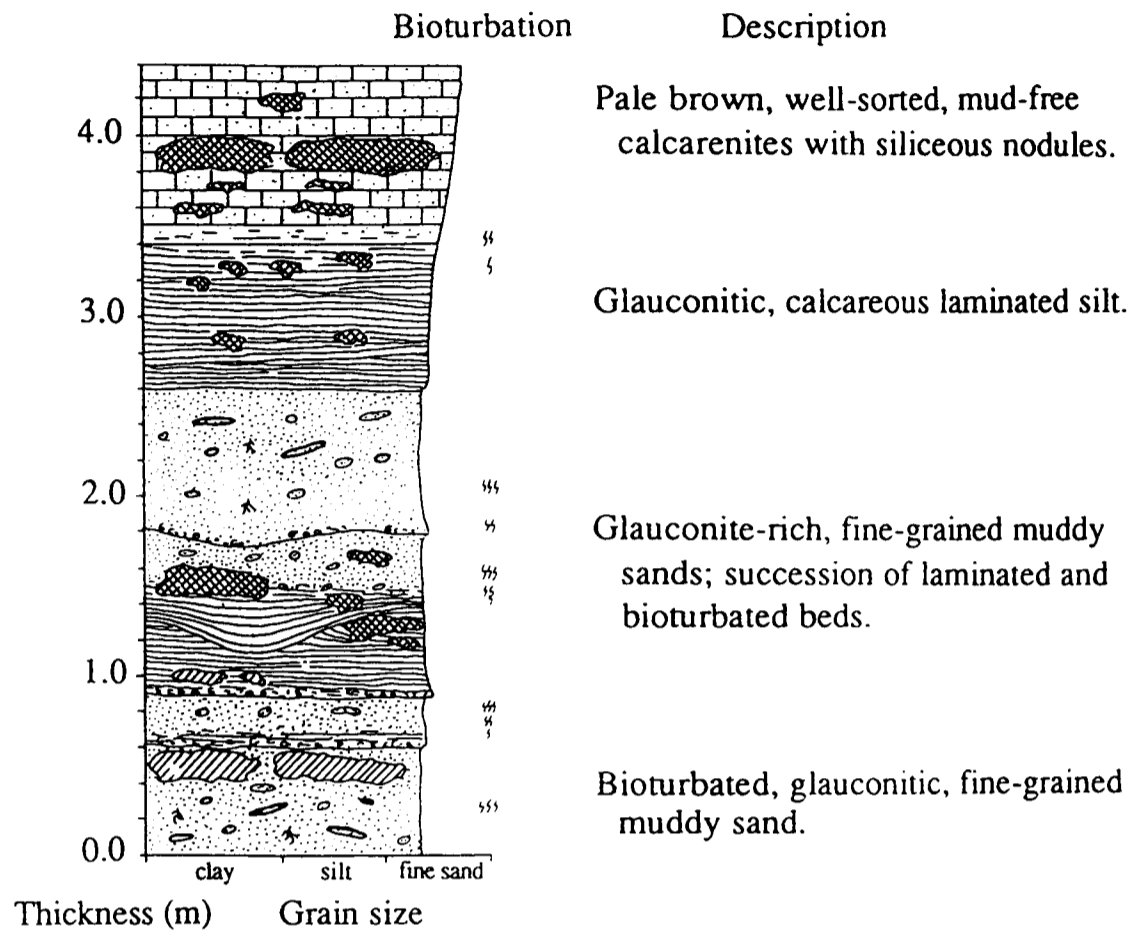


Fig.5: Detailed graphic log of the high *auritus* subzone interval of sedimentary condensation: amalgamated glauconitic storm laminites at the Foxmould-Chert Beds contact, Dunscombe Cliff (SY 153 877), south Devon.



Fig.6: Outcrop of the interval of condensed glauconitic pebble-shell beds in the uppermost Foxmould, Whitecliff, Beer (SY 234 894). Shown graphically in Figure 7.

Description

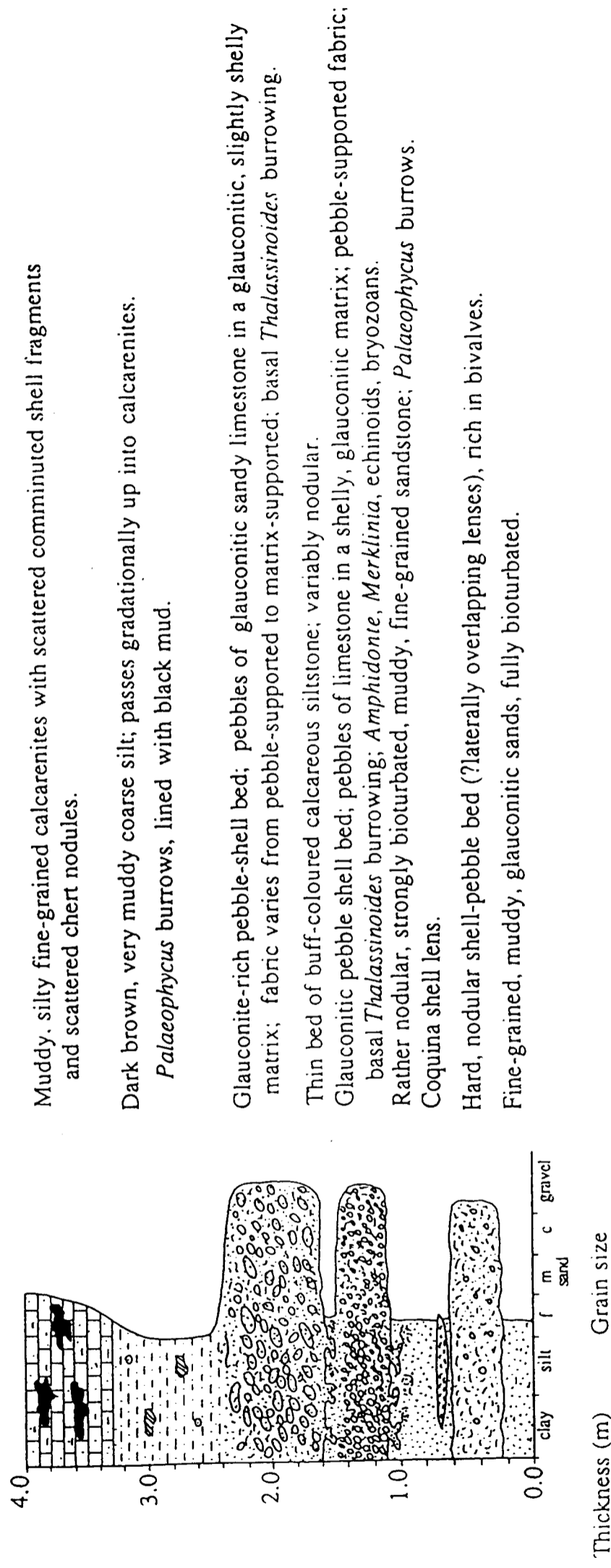


Fig.7: Detailed graphic log of the high *auritus* subzone interval of sedimentary condensation: glauconitic intraformational pebble-shell beds at the Foxmould Chert Beds contact, south-east Devon.



Fig.8: Basal burrowing with glauconitic sediment infill, developed in the glauconitic pebble-shell beds in the uppermost Foxmould, Whitecliff, Beer, south-east Devon (SY 234 894). Middle bed in Fig.7.



Fig.9: Basal burrowing with glauconitic sediment infill, developed in the glauconitic pebble-shell beds in the uppermost Foxmould, Whitecliff, Beer, south-east Devon (SY 234 894). Middle bed in Fig.7.

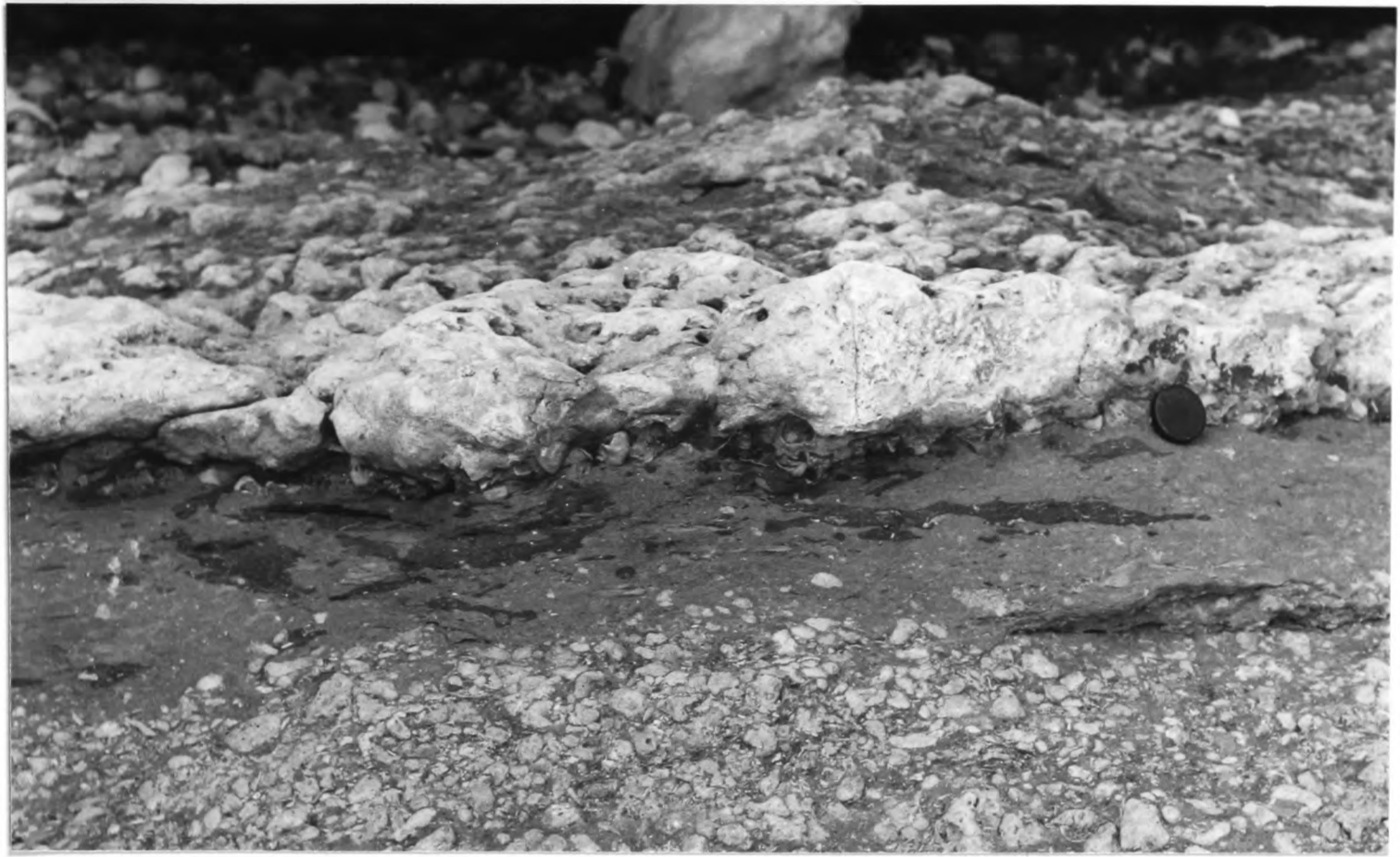


Fig.10: Basal burrowing with glauconitic sediment infill, developed in the glauconitic pebble-shell beds in the uppermost Foxmould, Whitecliff, Beer, south-east Devon (SY 234 894). Upper bed in Fig.7.



Fig.11: Basal burrowing with glauconitic sediment infill, developed in the glauconitic pebble-shell beds in the uppermost Foxmould, Whitecliff, Beer, south-east Devon (SY 234 894). Upper bed in Fig.7.



Fig.12: Two successive nodular horizons developed in the uppermost Foxmould, around Culverhole Point, between Axemouth and Lyme Regis (SY 278 893).



Fig.13: Thick interval of nodular sandstones - pebble beds, section 0.5km east of Corbin Rocks, between Axemouth and Lyme Regis (SY 293 896).



Fig.14: Field outcrop of the lower Chert Beds hardground, Little Beach - Beer Head, south-east Devon (SY 226 879).



Fig.15: Field outcrop of the lower Chert Beds hardground, Little Beach - Beer Head, south-east Devon (SY 226 879).



Fig.16: Thin development of the lower Chert Beds hardground, Whitecliff, Beer (SY 234 894). Note the chert nodules (black) replacing *Thalassinoides* burrows.



Fig.17: Burrowing developed at the base of the lower Chert Beds hardground, Whitecliff, Beer (SY 234 894).

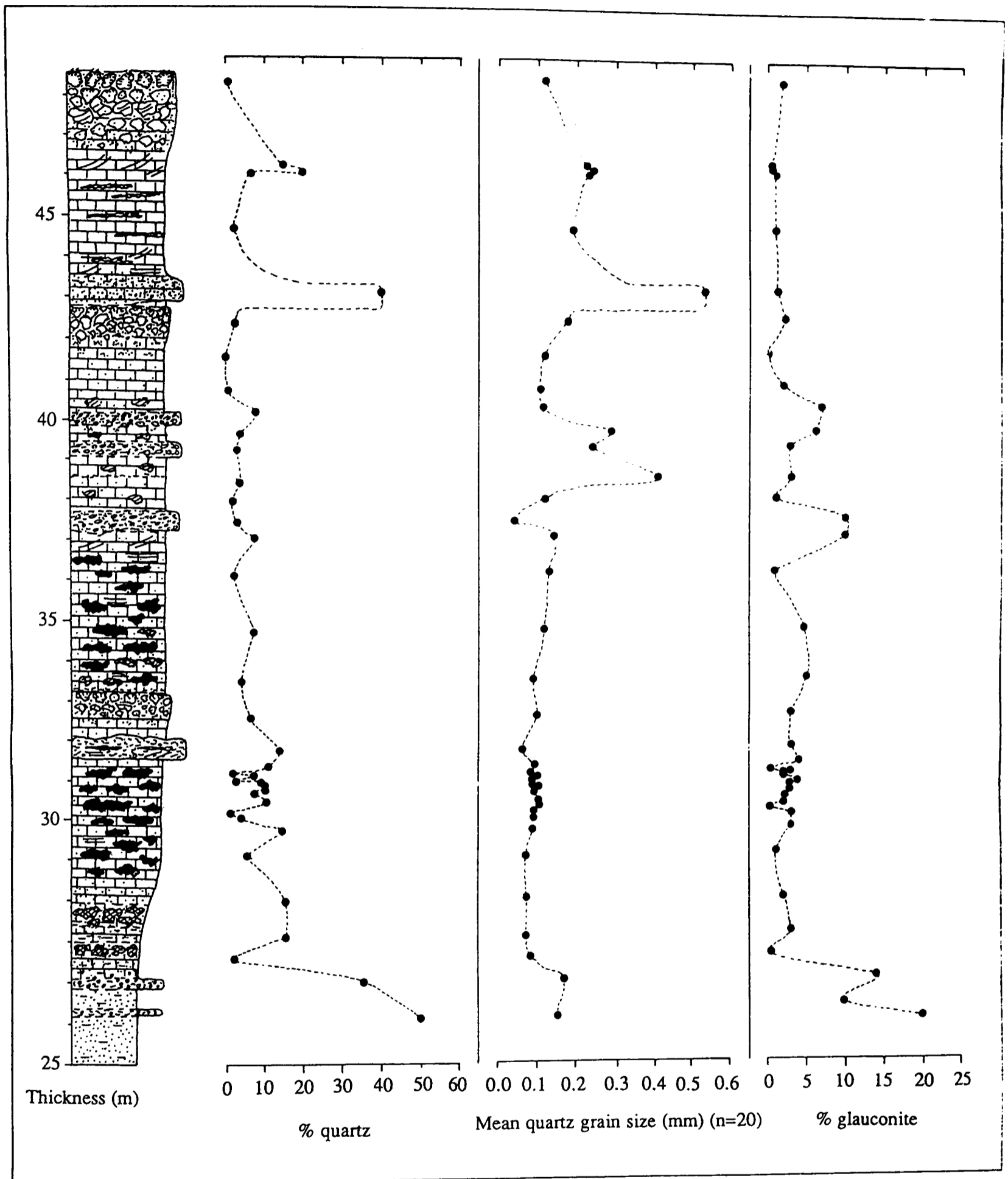


Fig.18: Vertical profile through the uppermost Foxmould, Chert Beds and Top Sandstones, Little Beach - Beer Head (SY 226 879). Shows the reduction in quartz concentration passing into the Chert Beds; the high quartz content of the Coarse Band; the increase in quartz grain size in the upper Chert Beds pebble beds and Coarse Band; high glauconite concentrations in the uppermost Foxmould and upper Chert Beds pebble beds.

Fig.19: Detailed correlation of the uppermost Foxmould, Chert Beds and Top Sandstones across south-east Devon, indicating the lateral extent and proposed correlation of individual hardgrounds and pebble-shell beds. A = uppermost Foxmould interval of glauconite-rich sands and intraformational pebble-shell beds; B = lower Chert Beds hardground; C = Brecciated Limestone hardground; D = the Coarse Band; E = the top Upper Greensand hardground.

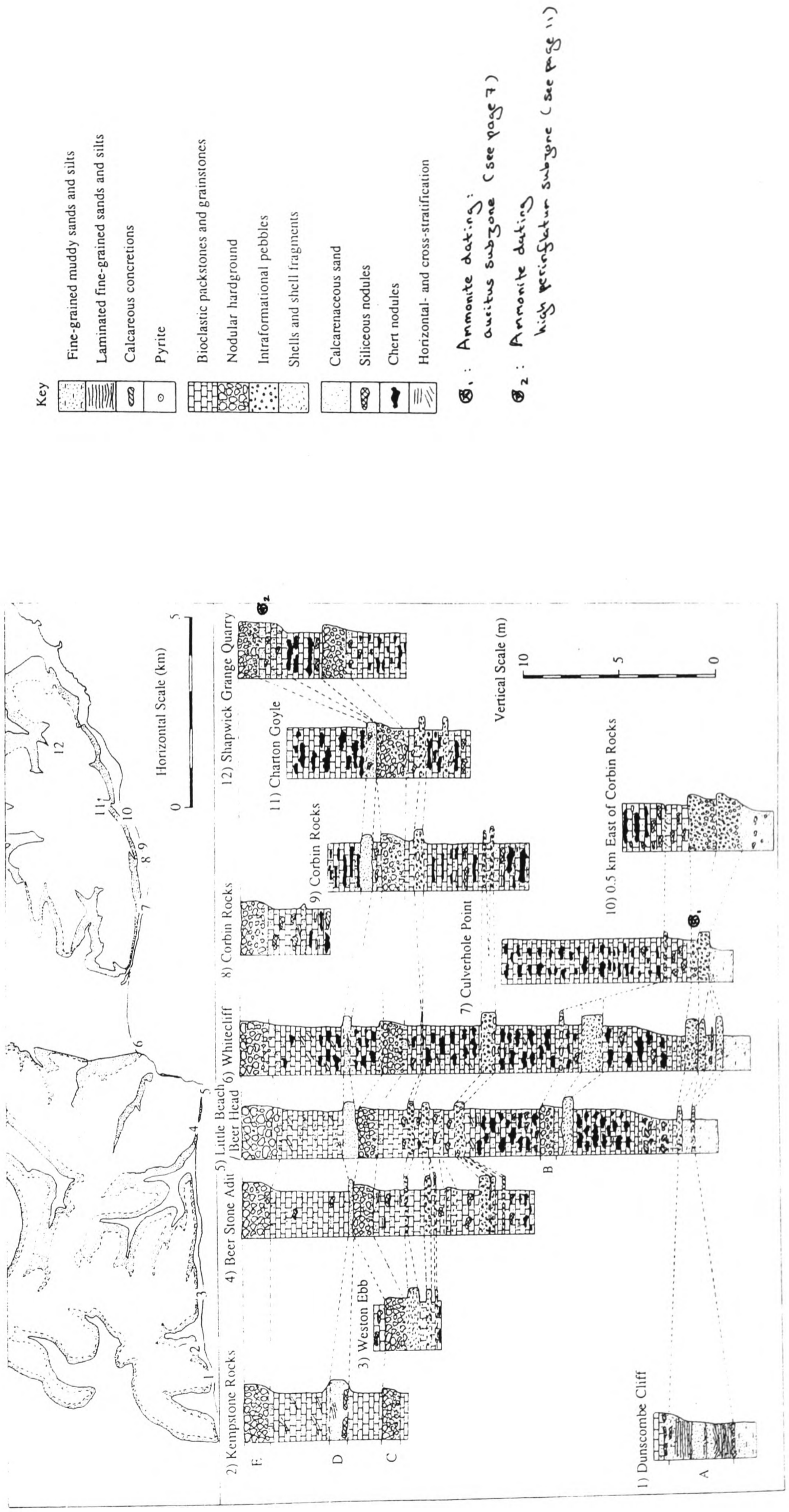




Fig.20: The thick nodular Brecciated Limestone hardground, slipped block, Weston Ebb, west of Branscombe (SY 175 878).



Fig.21: Outcrop of the Brecciated Limestone hardground (lower arrow) and Top Sandstones, Kempstone Rocks, south Devon (SY 161 881). The Coarse Band is developed (upper arrow), weathering back as a notch in the cliffs.



Fig.22: Well-developed rather compacted *Thalassinoides* burrow system, infilled with glauconitic carbonate sand; developed in the lower Top Sandstones, Beer Head (SY 226 879).



Fig.23: Sediment fabric of the Coarse Band, Kempstone Rocks (SY 161 881). Quartz-carbonate sand, rich in coarse rounded quartz grains.



Fig.24: The top Upper Greensand hardground at Whitecliff, Beer (SY 234 894). A well-defined planar surface marks the top of the bed, and a variably-nodular fabric is developed below.



Fig.25: Relict trough cross-bedding preserved in the top Upper Greensand hardground, Beer Head, Beer (SY 226 879).



Fig.26: Small pocket with infill of Beer Head Limestone developed between the uppermost nodules of the top Upper Greensand hardground, Beer Roads, Beer (SY 229 890).



Fig.27: Well-developed rhythmic bedding in the Foxmould, Worbarrow Bay, below Flower's Barrow, south Dorset (SY 866 804).



Fig.28: Close-up view of the rhythmic bedding shown in Fig.27, defined by an increase in the black clay content.



Fig.29: Close-up view of the muddy bed shown in Fig.28; the black mud is redistributed by burrowing activity, often as burrow linings.



Fig.30: Field outcrop of rhythmically-bedded Passage Beds succession at Compton Bay, Isle of Wight (SZ 367 853). Rhythmicity is defined by varying amounts of black mud within pale brown fine-grained siltstones.

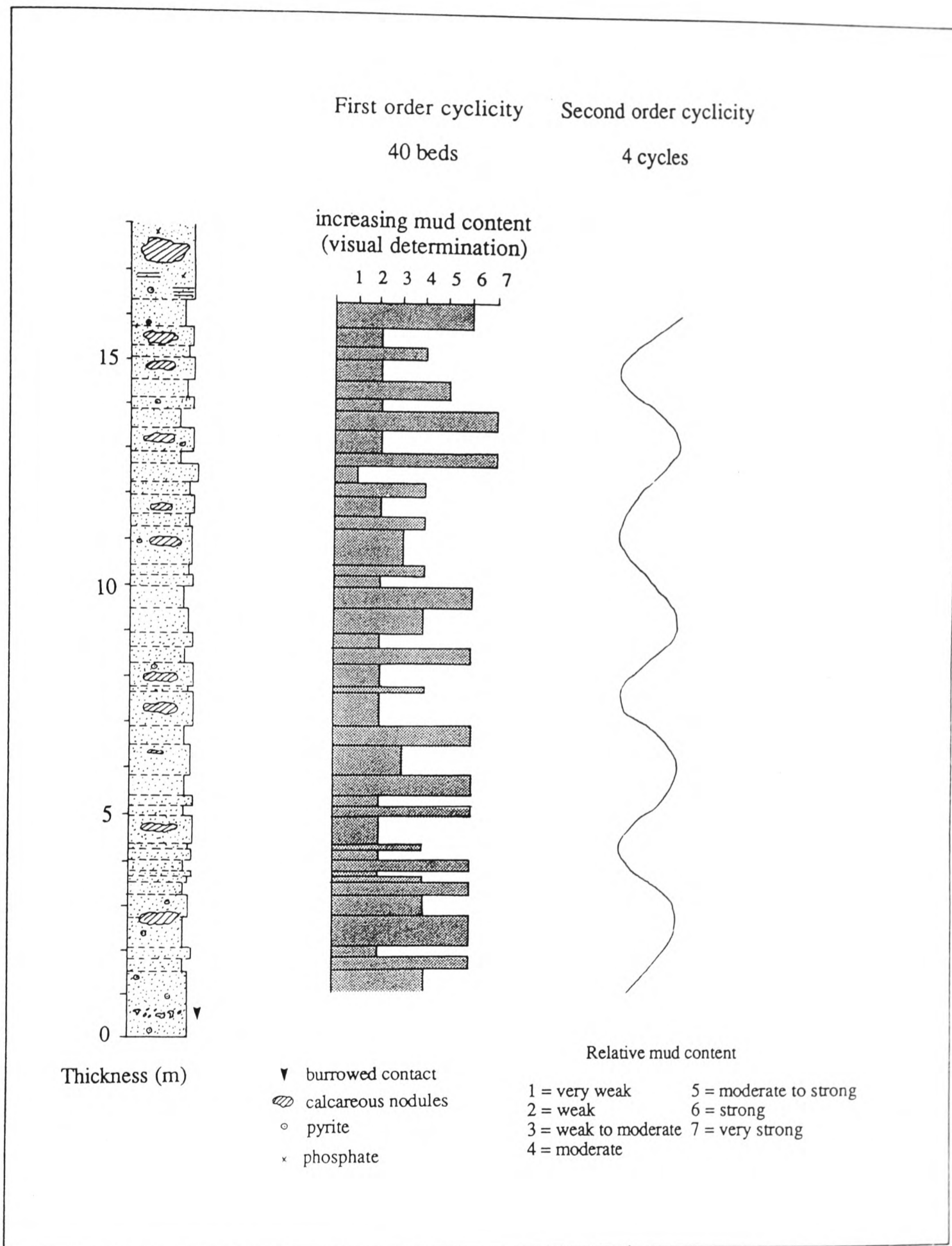


Fig.31: Diagram illustrating the cyclicity developed within the Passage Beds of the Isle of Wight. Bed measurement is accompanied by a visual estimate of the mud concentration (1 = very weak; 7 = very strong); the data are plotted as a simple histogram. The 40 first order cycles group into 4 second order cycles.



Fig.32: Glauconite- and serpulid-rich bed developed in the upper Foxmould, below Flower's Barrow, Worbarrow Bay (SY 866 804).



Fig.33: Close-up view of the concretionary horizon shown in Fig.32, indicating the high serpulid concentrations in the sediment.



Fig.34: The Dispar Zone Ammonite Bed, a phosphatic greensand, slipped blocks west of White Nothe, south Dorset (SY 769 809).

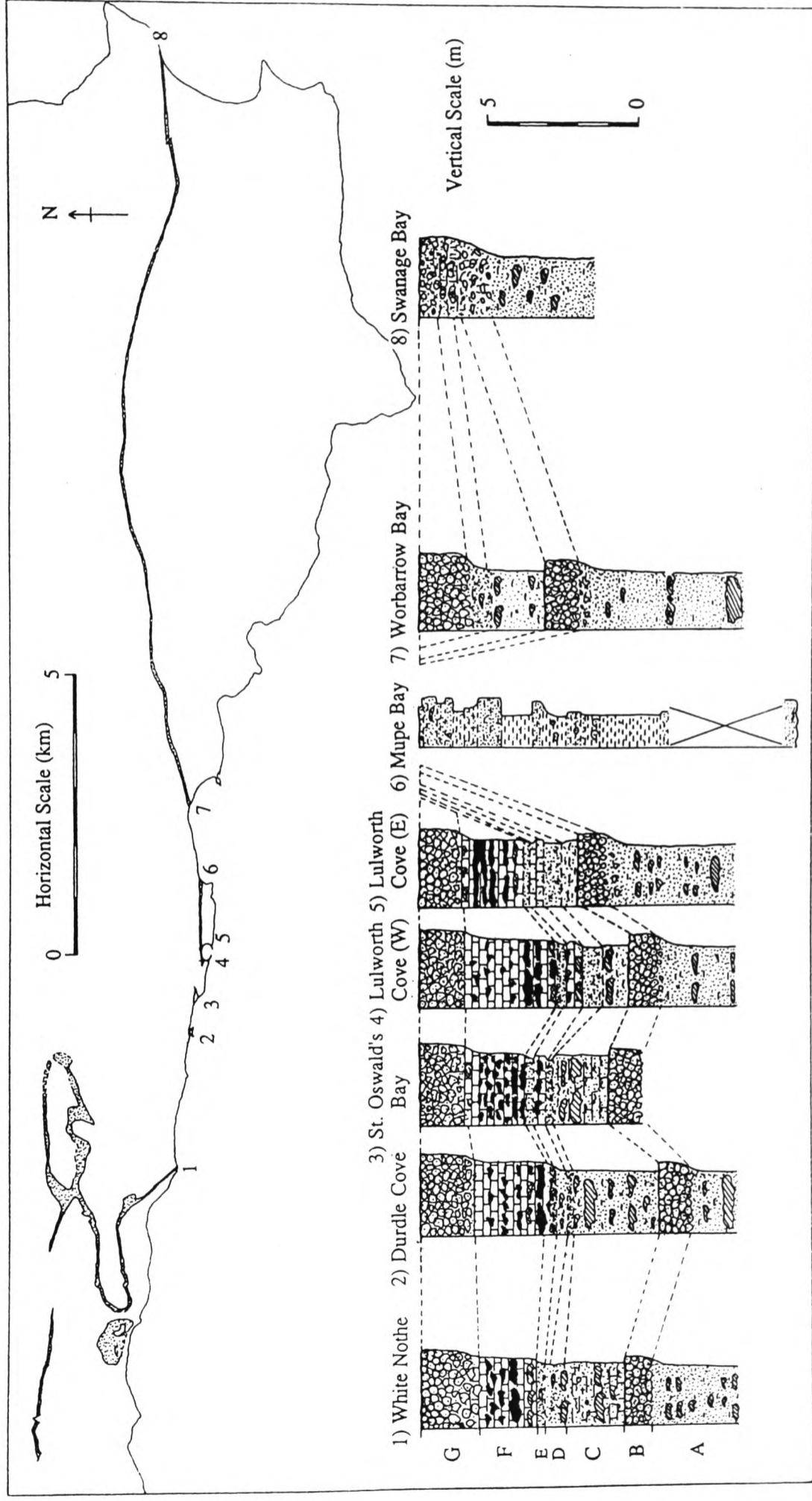


Fig.35: Detailed correlation of the uppermost Foxmould, Exogyra Rock, Dispar Zone Ammonite Beds, Chert Beds and Eggardon Grit across south Dorset. Lower Cenomanian faulting at Mupe Bay results in the Chalk Basement Bed resting directly on the Gault. A = uppermost Foxmould glauconitic marly silts; B = Exogyra Rock; C = glauconitic marls; D = Dispar Zone Ammonite Bed; E = thin glauconite-rich bed above the DZAB; F = Chert Beds; G = Eggardon Grit.



Fig.36: Thin development of the Chert Beds at White Nothe, south Dorset (SY 772 806), lying stratigraphically between the Dispar Zone Ammonite Bed and the Eggardon Grit.



Fig.37: The Eggardon Grit, a thick nodular bed of sandy limestone at the top of the Upper Greensand, Durdle Cove, south Dorset (SY 805 806). Top of the bed is just above the hammer head.

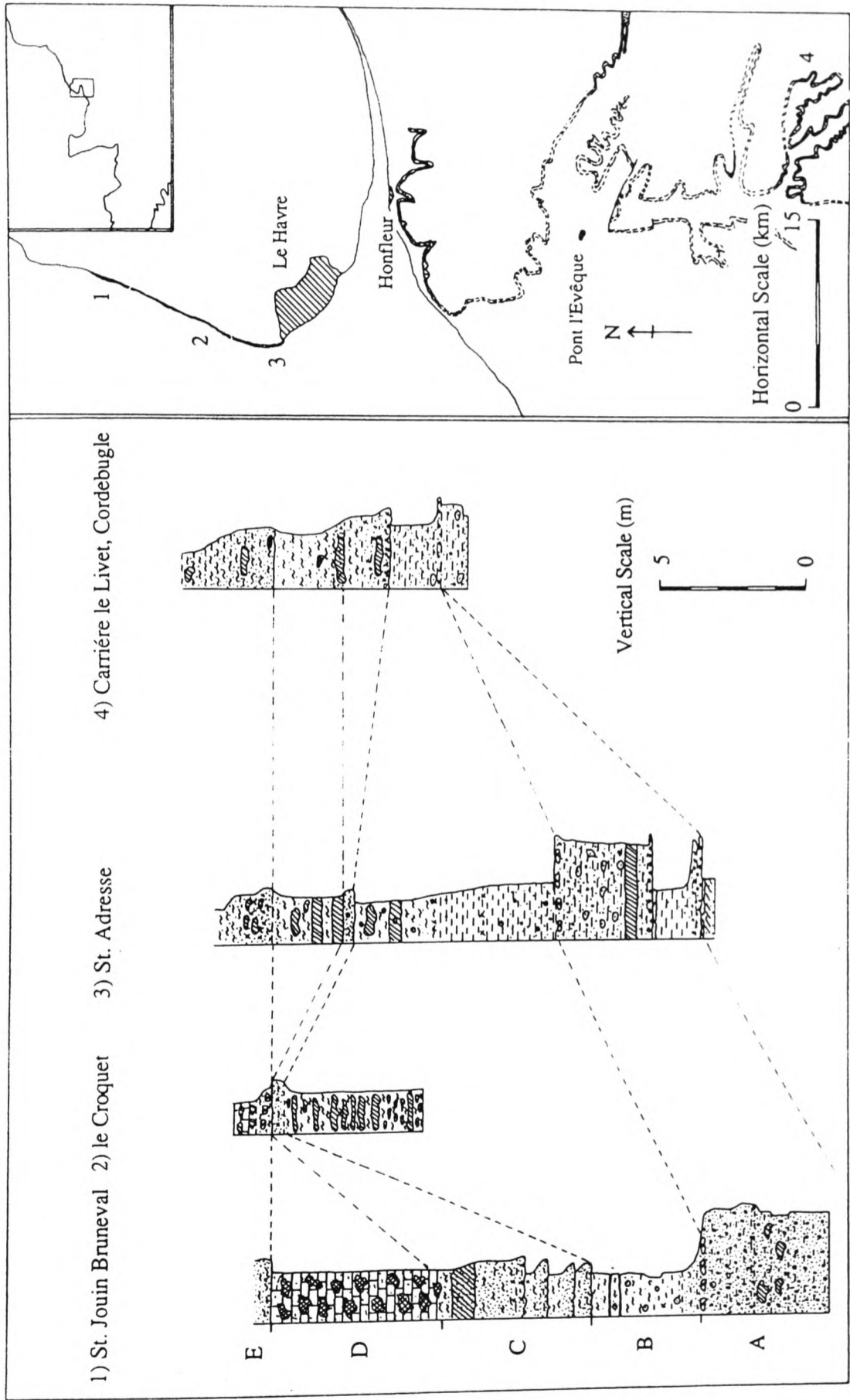


Fig.38: A detailed correlation of selected Middle-Upper Albian sections in Normandy, France. A = Poudingue Ferrugineux; B = Gaize Inférieure; C = high *auritus* subzone greensands, basal contact the surface perforée "Cauville"; D = Craie Glauconieuse, basal contact the surface de ravinement "Octeville".



Fig.39: Glauconitic bed developed in sediments of the high *auritus* subzone, Compton Bay, Isle of Wight (SZ 367 853). Pale brown silts pass up into a bed of green, glauconitic marly silt, with a basal contact marked by a zone of sediment-mixing due to bioturbation.



Fig.40: Close-up of the burrowed basal contact shown in Fig.39.



Fig.41: Field outcrop showing the Upper Greensand succession at Gore Cliff, Isle of Wight (SZ 492 763). The Passage Beds (dark grey) in the lower part of the section pass up into pale brown silts of the Upper Greensand; the top part of the cliff is marked by the development of glauconitic marly silts with prominent chert horizons, the Chert Beds.

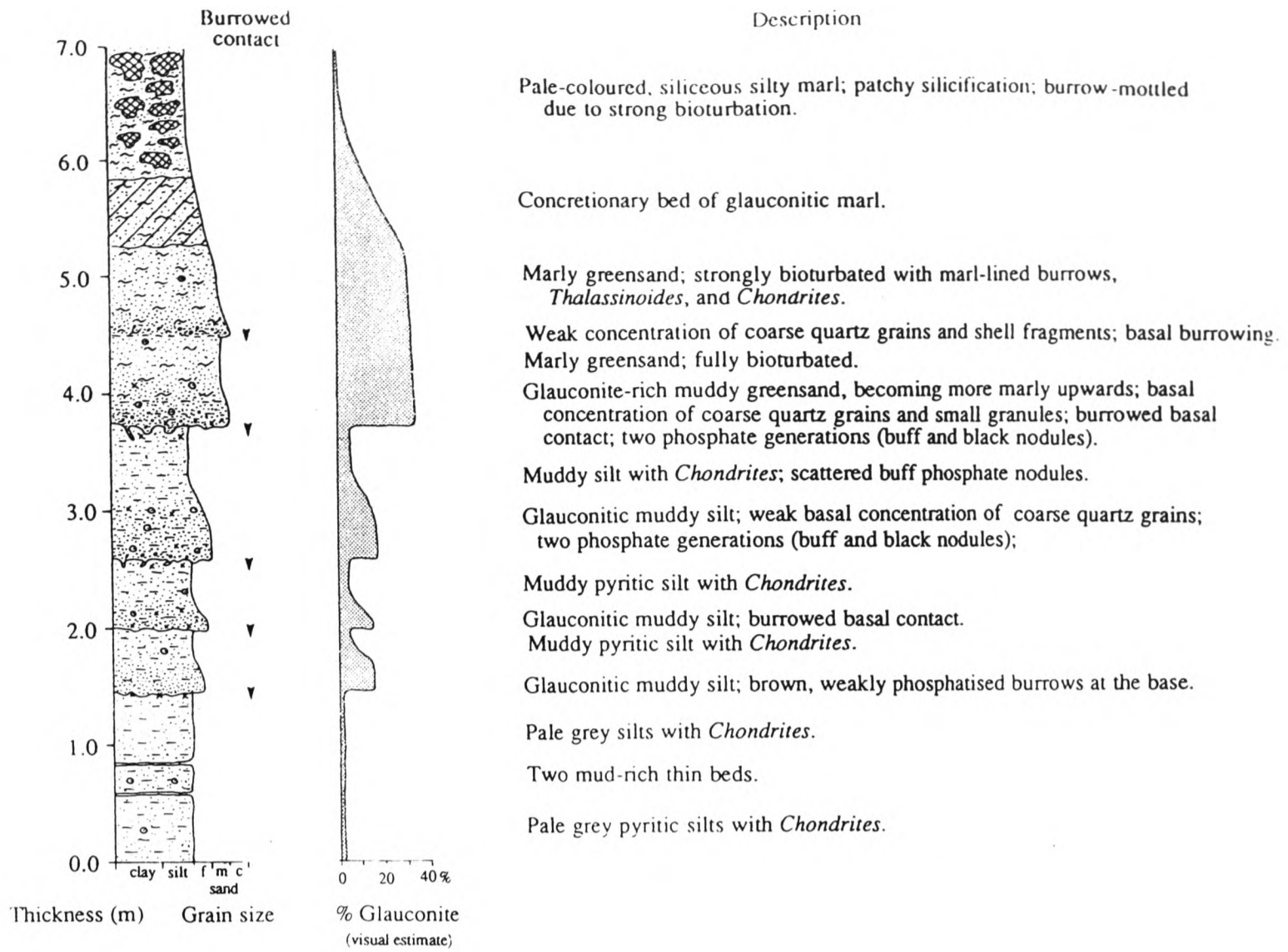


Fig.42: Detailed graphic log of the high *auritus* subzone interval of sedimentary condensation: thin glauconitic cycles at the top of the Gaize Inférieure, St. Jouin-Bruneval, Normandy coast.



Fig.43: Field outcrop showing the high *auritus* subzone sediments, near St. Jouin-Bruneval, Normandy coast; four greensand beds are developed in this interval (the bases of these are arrowed). Field log of the section given in Fig.42.



Fig.44: Field outcrop of three greensand beds developed in a thin Albian sequence on the eastern side of the Armorican Massif, Carrière le Livet, near Cordebugle, Normandy.



Fig.45: The lower greensand bed shown in Fig.44. Facies change is from muddy fine sands to glauconite-rich, muddy fine sands, which become marly immediately above. The base of the greensand bed is marked by an erosion surface with a coarse quartzose lag, and remanié phosphate nodules.



Fig.46: Field outcrop of the lower greensand bed shown in Fig.44. Outcrop is 5m along the section from that shown in Fig.45. The base of the greensand bed is marked by well-developed burrowing.



Fig.47: Field outcrop of erosion surface in the lower Chert Beds, interpreted as the result of Upper Albian synsedimentary faulting, Culverhole Point area (SY 278 893). The erosion surface is marked by a glauconitic, clayey pebble bed.

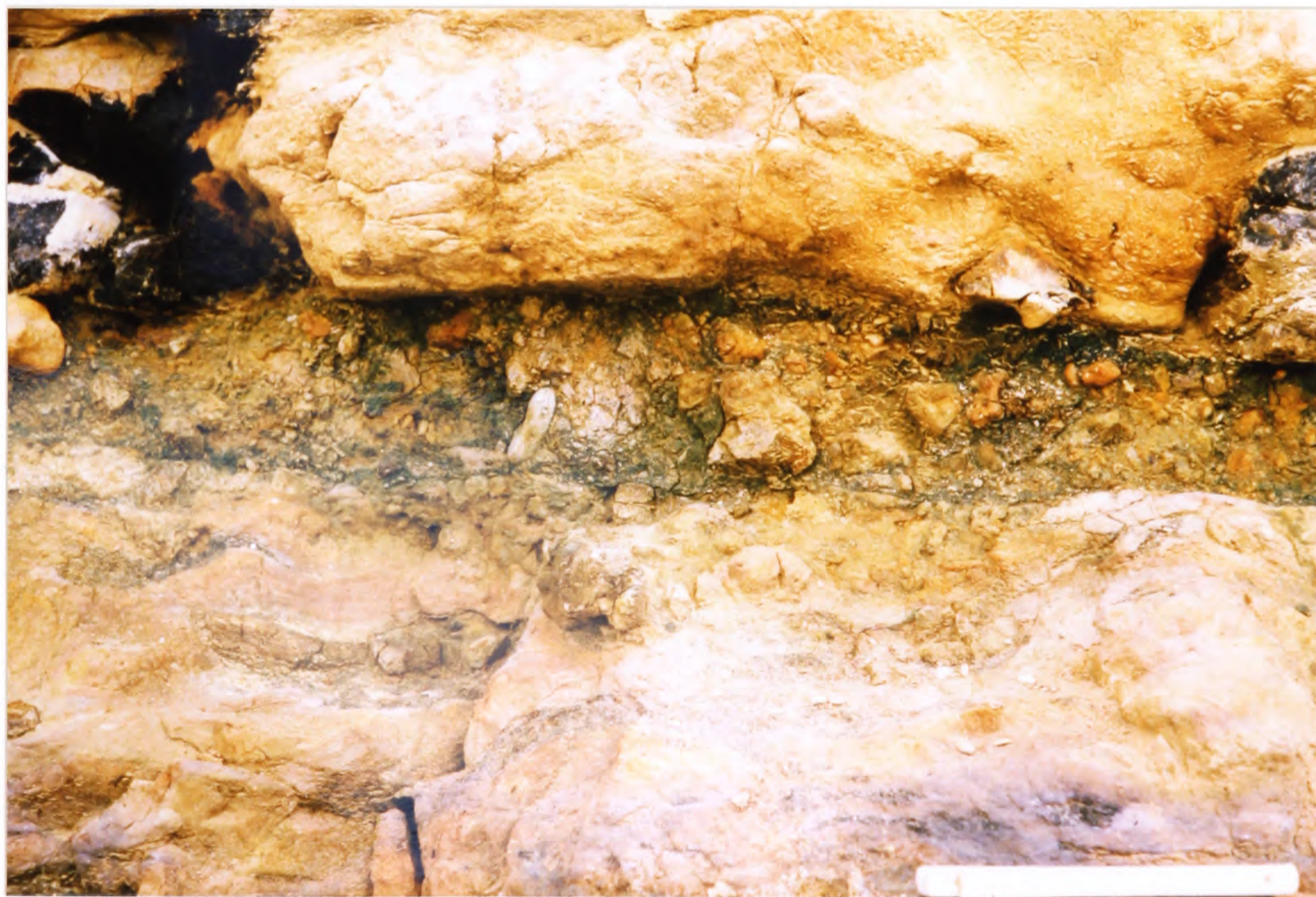


Fig.48: Close-up of the bed shown in Fig.47. Note the burrowed basal contact to the glauconitic pebble bed.



Fig.49: Top of the Eggardon Grit, slipped block below Flower's Barrow, Worbarrow Bay (SY 866 804). Note the erosive nature of the contact, with truncation of the nodules highlighted by the nodule-margin (burrow-wall) glaucopitization.



Fig.50: Top of the Eggardon Grit, slipped block below Flower's Barrow, Worbarrow Bay (SY 866 804). Erosion of the bed has proceeded to a lower level than in Figure 49, with only traces of burrow-wall glaucopitization preserved.



Fig.51: Sipped block of the Upper Greensand below Flower's Barrow, Worbarrow Bay (SY 866 804). Shows a mixed eroded-nodule assemblage, with pale nodules of the Eggardon Grit and smaller glauconitic sandstone nodules of Exogyra Rock lithology.



Fig.52: Field outcrop of the Chalk Basement Bed at Cow Corner, resting on the Exogyra Rock, as a result of Lower Cenomanian synsedimentary faulting.

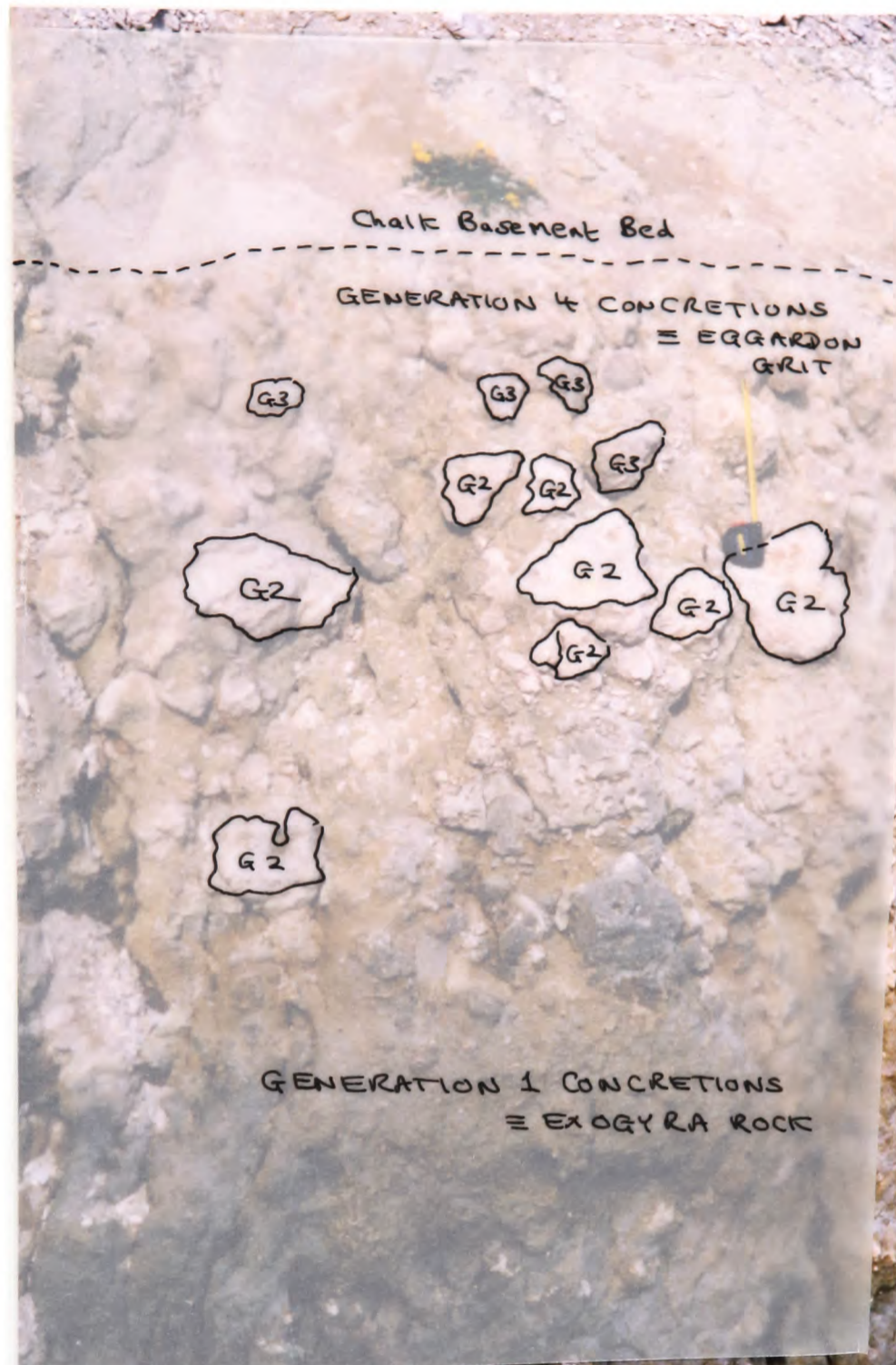


Fig.53: Complex condensation horizon at the top of the Upper Greensand, Swanage Bay, south Dorset (SY 044 811). 1.2 metres of sediment contain four concretion generations, and represent the equivalent of the Chert Beds and Top Sandstones of south-east Devon (around 23 metres in thickness).

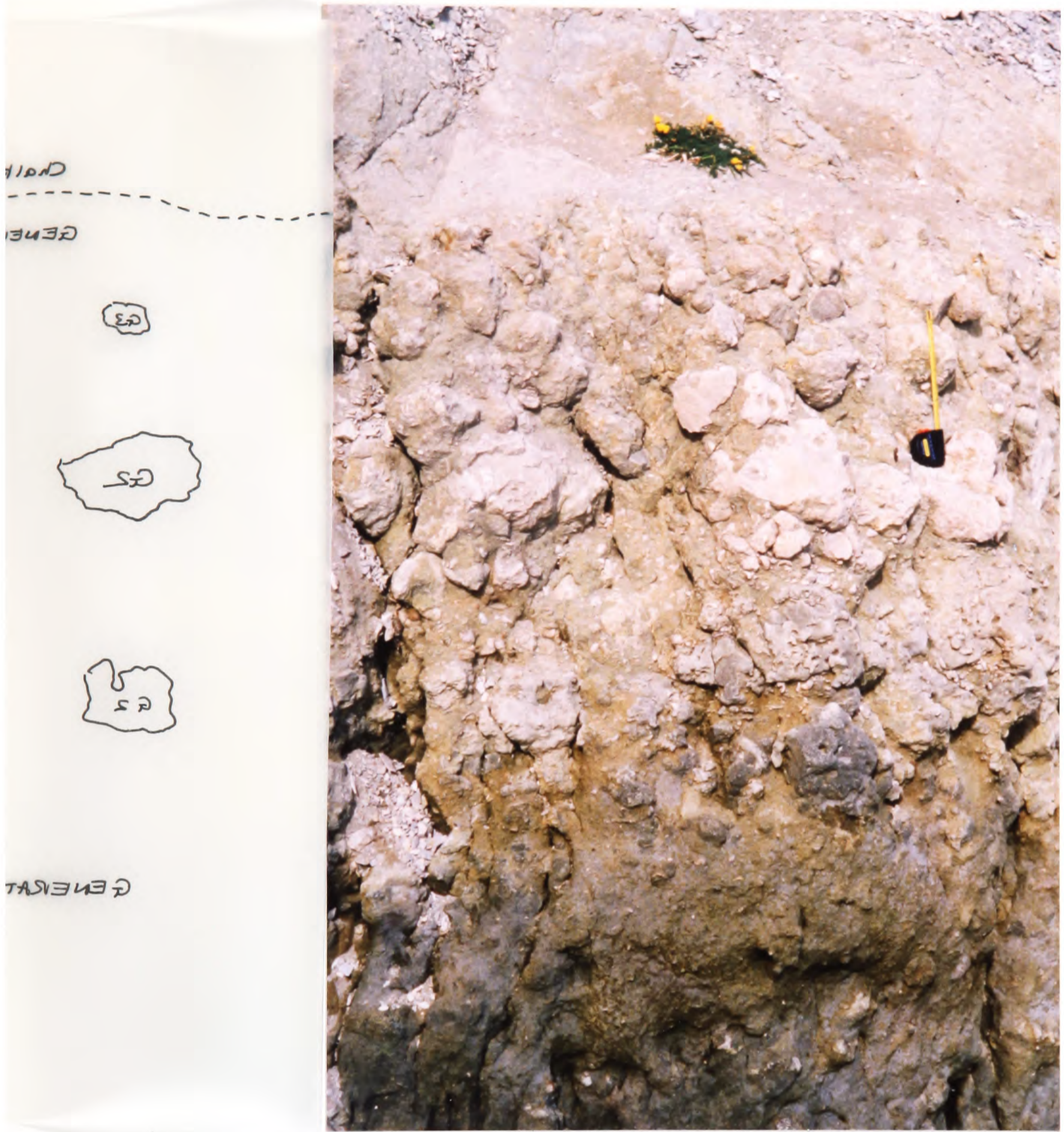


Fig.53: Complex condensation horizon at the top of the Upper Greensand, Swanage Bay, south Dorset (SY 044 811). 1.2 metres of sediment contain four concretion generations, and represent the equivalent of the Chert Beds and Top Sandstones of south-east Devon (around 23 metres in thickness).



Fig.54: Generation 2 nodules in the complex condensation horizon shown in Figure 53. Pale brown concretions represent the Chert Beds lithology, and preserve burrows filled with glauconitic sediment.



Fig.55: Generation 3 nodules in the complex condensation horizon shown in Figure 53. The phosphatic concretions correlate with the Dispar Zone Ammonite Bed.



Fig.56: Thin Chert Beds Member, at Compton Bay, Isle of Wight (SZ 367 853). Well-developed concretionary horizons are present, but chert is not developed. The top of the Upper Greensand occurs at a level marked by the top of the scale rule; the beds are overlain by the Glauconitic Marl. The Chert Beds expand and become more siliceous towards the south of the island (Fig.41).

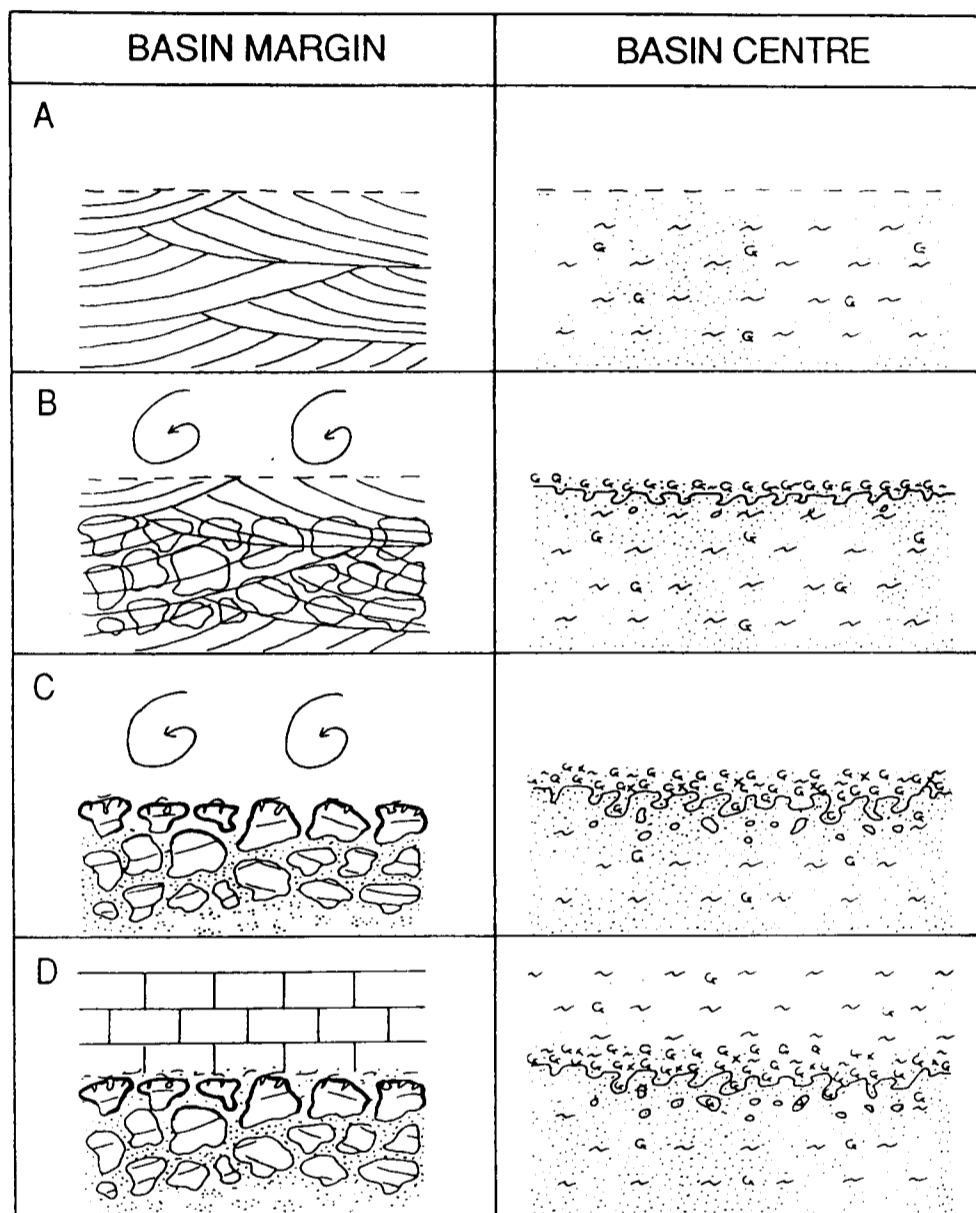


Fig.57: Cartoon illustrating the genetic relationship between nodular hardgrounds and phosphoritic greensands.

A: Halt in sedimentation above cross-stratified bioclastic grainstones, and deeper-water marly silts.

B: Development of nodularity within carbonates; glauconite concentration in deeper settings.

C: Nodules are exposed due to winnowing of the overlying sediment; an often long and complex cycle, which includes nodule boring, encrustation, glauconitization and phosphatisation occurs; increased concentrations of glauconite-rich sediment accumulate in deeper settings, a basal zone of strong burrowing and sediment mixing develops, and phosphate nodules develop.

D: Under relative transgression, sedimentation recommences, preserving the hardground and phosphoritic greensand below bioclastic packstones and silty marls.

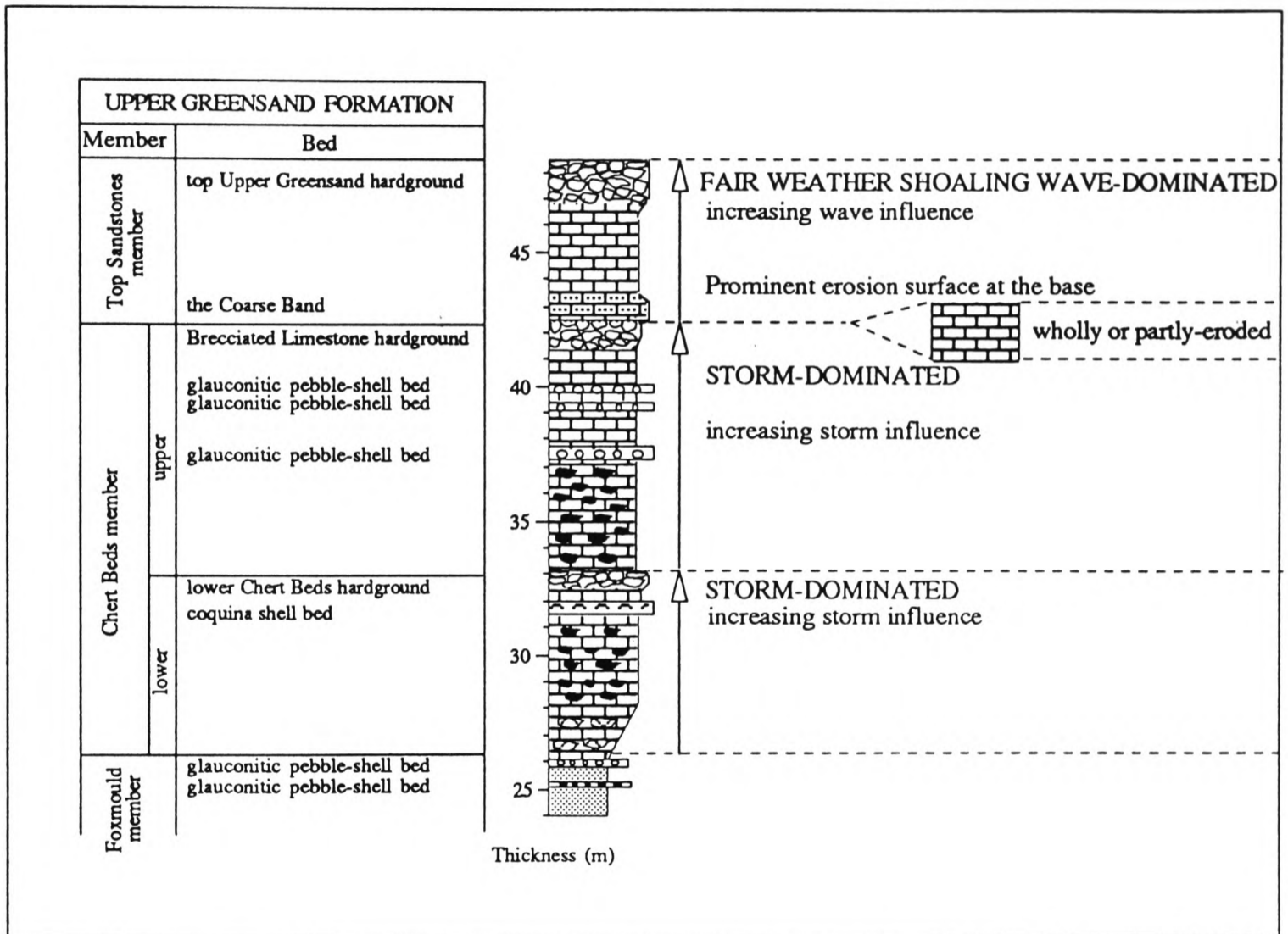


Fig.58: Summary of stratigraphy, cyclicity and sedimentary environments of the Chert Beds and Top Sandstones Members of the Upper Greensand Formation, Beer Head, south-east Devon.



Fig.59: Glauconite-rich greensand bed marking the base of the Upper Greensand south of Eastbourne (TV 610 977). This bed is equivalent to the Coarse Band of south Devon.

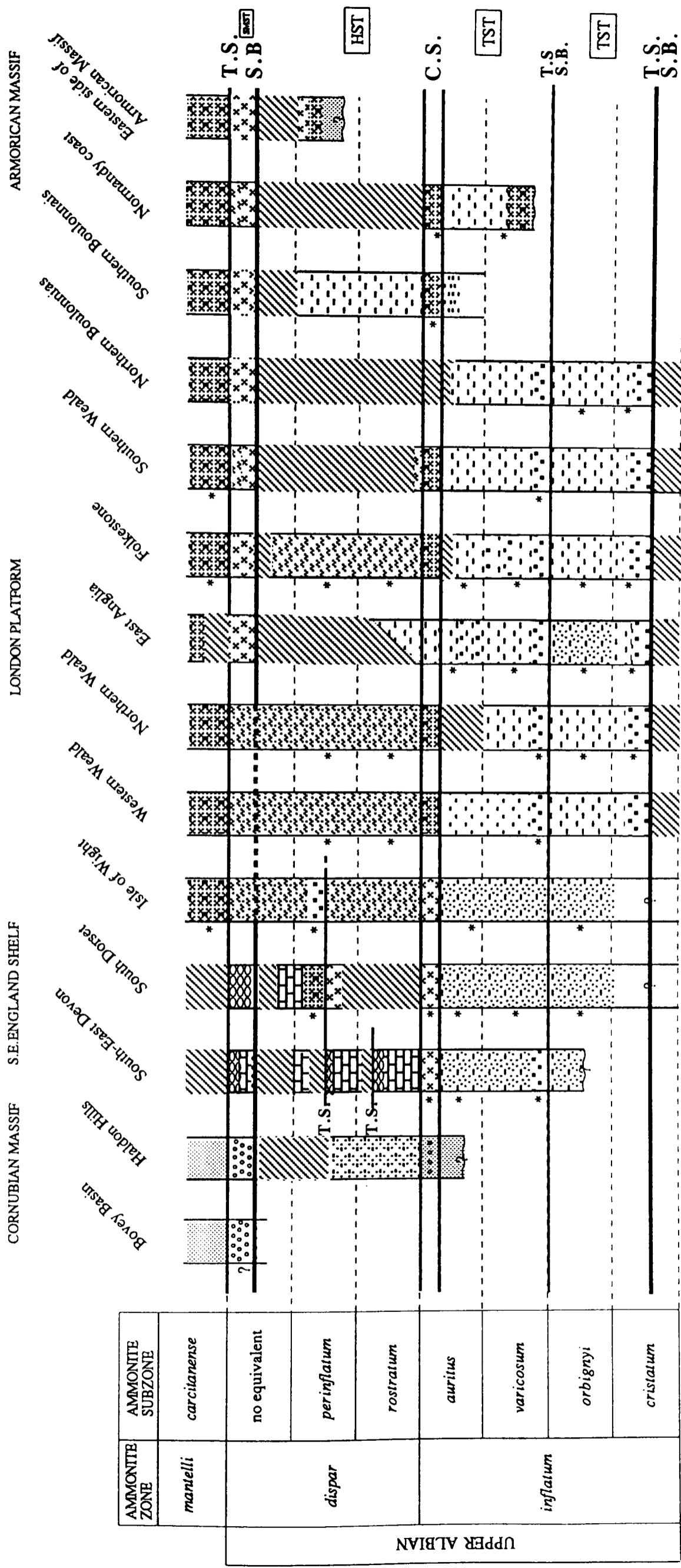


Fig.60: Sequence stratigraphic subdivision of the Upper Albian sediments of the Anglo-Paris Basin, with reference to fourteen designated regional type areas. Ammonite subzonal stratigraphy is plotted as a vertical scale, with proven subzones indicated to the left of each column by a * symbol. Within each column is shown a summary of the sediment composition at a given time interval. Note that no indication of the relative thicknesses is given with this representation. Dotted lines indicate correlative conformities to candidate type II sequence boundaries. Candidate sequential interpretation is given: S.B. = sequence boundary; T.S. = transgressive surface; C.S. = condensed section; TST = transgressive systems tract; HST = highstand systems tract; SMST = shelf margin systems tract. (for key, P.T.O.)

Key to Fig.60

KEY		MUDDY FINE SANDS AND SILTS		SILTY MARLS		COARSE SANDS AND GRAVELS
		GLAUCCONITE-RICH BED		LIMESTONES		NODULAR HARDGROUND
		GLAUCCONITE/PHOSPHATE- RICH BED		CLEAN SANDS		PROVEN AMMONITE SUBZONE
		MARLS		DECALCIFIED LIMESTONES		

TABLE 1 - UPPER ALBIAN CANDIDATE SEQUENCE STRATIGRAPHY OF THE ANGLO-PARIS BASIN

SEQUENCE 3

Transgressive surface. latest Albian/early Cenomanian. The top of the Upper Greensand/base of the Glauconitic Marl across southern England. Marked by a nodular hardground passing basinwards into a phosphoritic greensand.

Shelf margin systems tract. latest *dispar* zone. Comprises a thin shallow-water sequence of sands and gravels, carbonate grainstones (Top Sandstones), sandy limestones and micaceous siltstones.

Sequence boundary (medium). latest *dispar* zone. Placed at the level of the Coarse Band of south-east England and the base of the Upper Greensand at Eastbourne. Marked by an erosion surface with overlying coarse quartzose or glauconite-rich bed.

SEQUENCE 2

Late highstand systems tract. *perinflatum* subzone. In the Chert Beds of south-west England, comprises a thin unit of well-sorted bioclastic grainstones, partially to completely removed by the erosion surface above.

Transgressive surface. *perinflatum* subzone. The Brecciated Limestone hardground of south-west England, a nodular hardground which passes basinwards into a phosphatic greensand, the Dispar Zone Ammonite Bed.

Middle highstand systems tract. *rostratum* subzone. In the Chert Beds of south-west England, comprises a unit of variably-siliceous and glauconitic carbonate packstones and grainstones, shallowing upwards, with several minor transgressive surfaces represented by glauconitic pebble beds.

Transgressive surface. *rostratum* subzone. The lower Chert Beds hardground of south-west England, a nodular hardground.

Early highstand systems tract. *rostratum* subzone. In the Chert Beds of south-west England, comprise siliceous carbonate packstones and grainstones, shallowing upwards.

Condensed interval. high *auritus* subzone. A thin, geographically very widespread glauconitic and phosphatic interval.

Transgressive systems tract. *varicosum* and lower-middle *auritus* subzones. Glauconitic, muddy fine sands and clays.

Sequence Boundary (minor). basal *varicosum* subzone. Represented by the *varicosum* phosphatic nodule bed, with a weak basal erosion surface.

SEQUENCE 1

Transgressive systems tract. middle *cristatum* to *orbigny* subzones. Very thin deposits of clays and glauconitic muddy silts.

Sequence boundary (major). Lower *cristatum* age. Represented by the *cristatum* nodule bed, and marked by a basin-wide erosion surface.

	AMMONITE ZONE	AMMONITE SUBZONE	ANGLO-PARIS BASIN, THIS STUDY	GLOBAL CYCLE CHART OF HAQ ET AL. (1988)
UPPER ALBIAN	<i>dispar</i>	no equivalent	← MEDIUM	← TYPE II, 96.5MA, MINOR
		<i>perinflatum</i>	←--- MINOR	
		<i>rostratum</i>	←--- MINOR	← 97MA, MEDIUM
	<i>inflatum</i>	<i>auritus</i>	← MAJOR	← TYPE I, 98MA, MAJOR
		<i>varicosum</i>	← MINOR	← 98.25MA, MAJOR
		<i>orbigny</i>		
		<i>cristatum</i>	← MAJOR	← TYPE II, 99MA, MEDIUM

Fig.61: Comparison between the sequence stratigraphy proposed for the Anglo-Paris Basin as a result of this study, and the global cycle chart of Haq *et al.* (1988). Shows candidate sequence boundaries (filled arrows), condensed sections (open arrows), and additional minor flooding surfaces (dotted arrows).

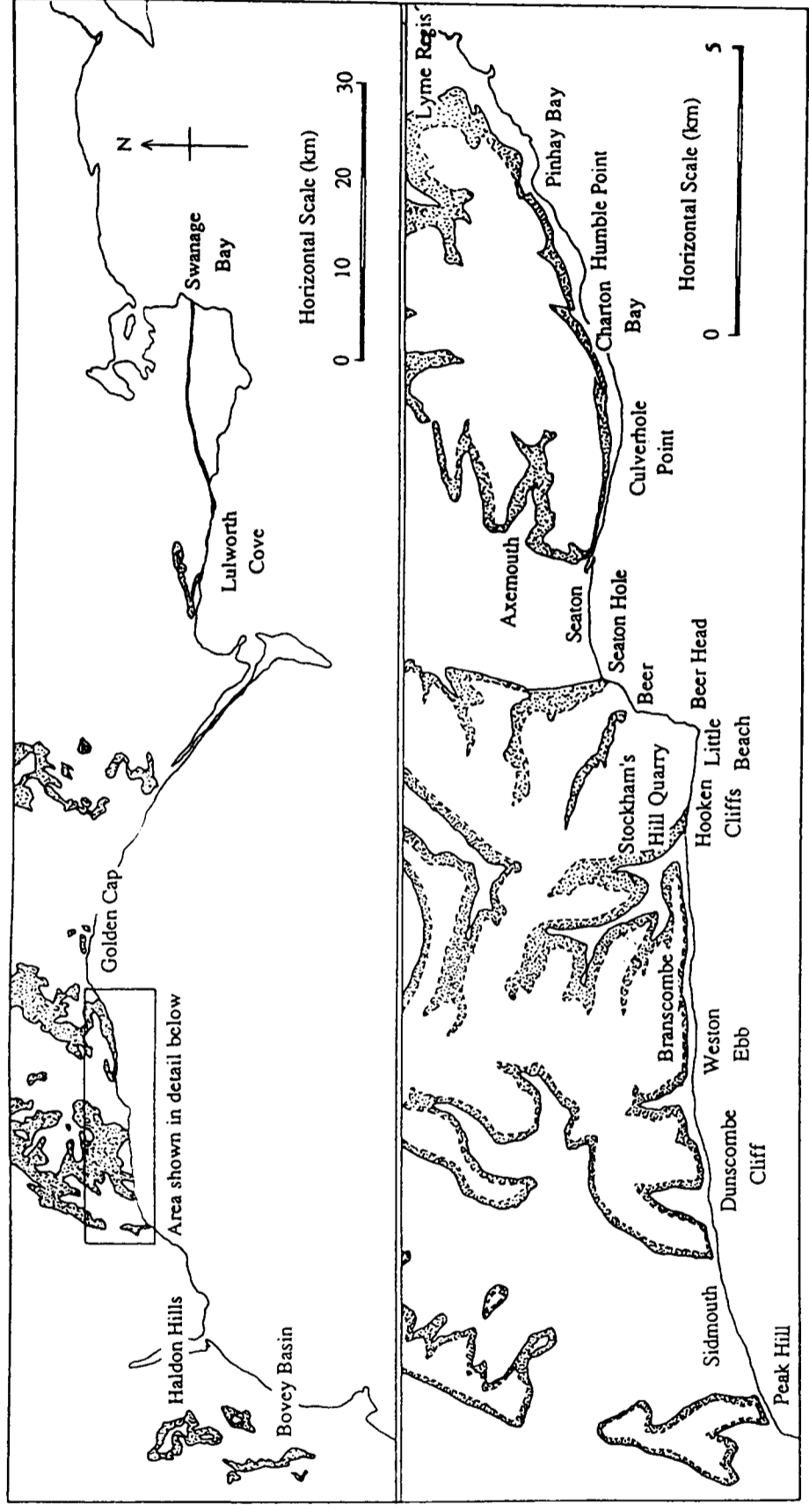


Fig.62: Location map showing the outcrop of the Upper Greensand and Gault across south-west England, and the localities mentioned in the text.

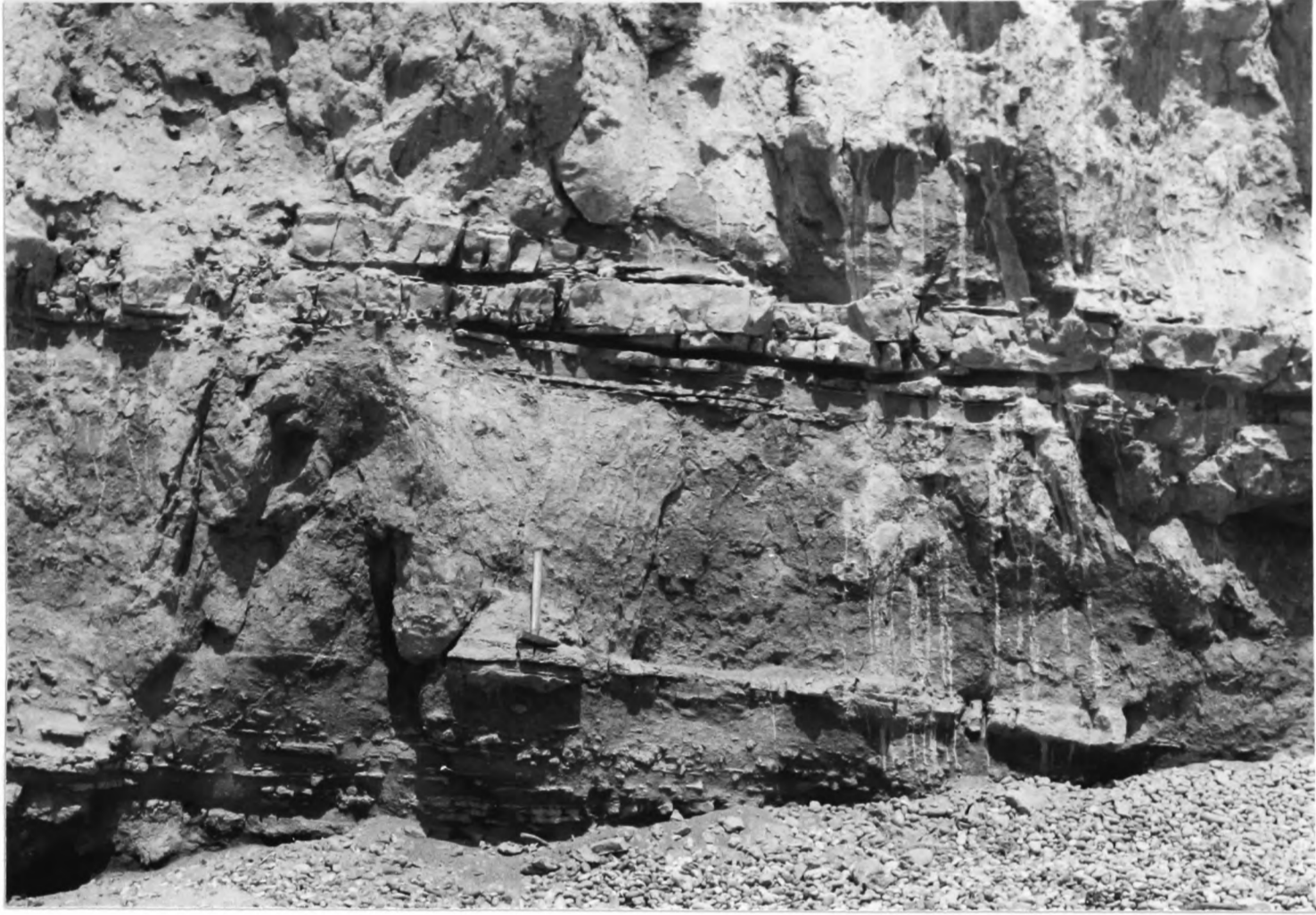


Fig.63: Distal storm laminites, interbedded with fully-bioturbated sediment. Two laminite beds visible, with associated calcareous concretions. Hooken Cliffs, near Beer.

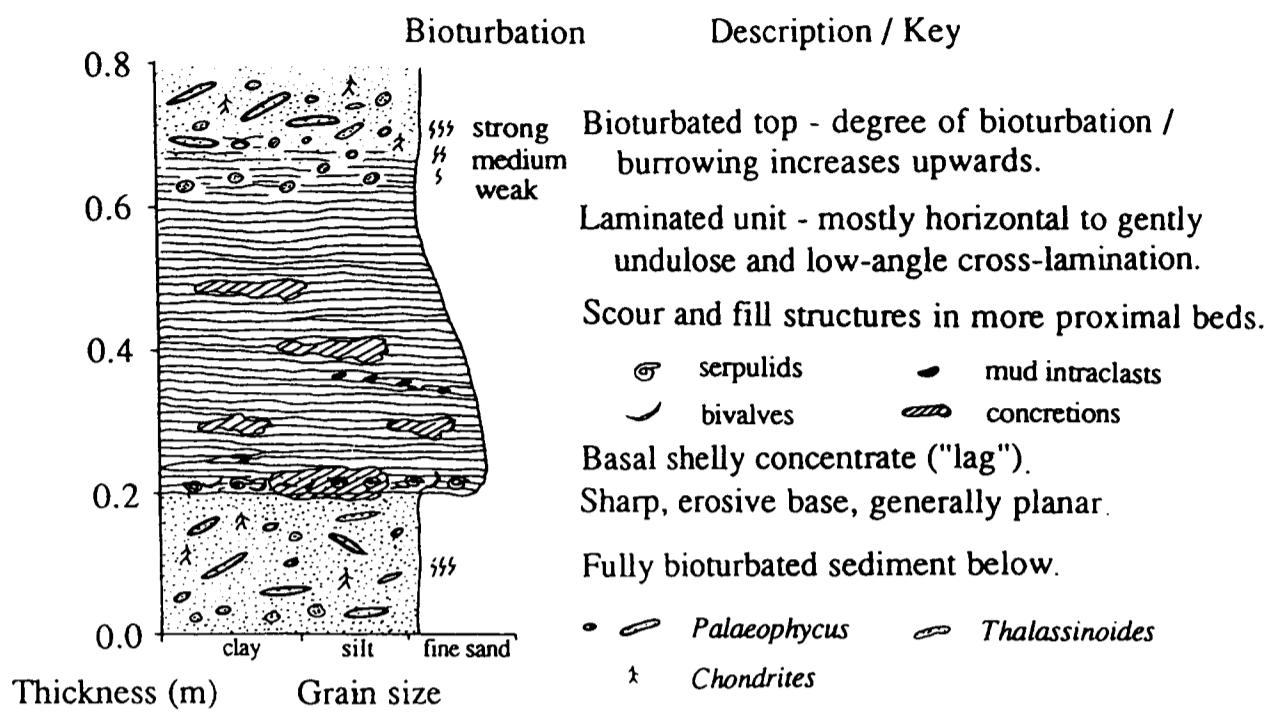


Fig.64: Summary of the typical sedimentological features of a Foxmould member storm laminite bed.

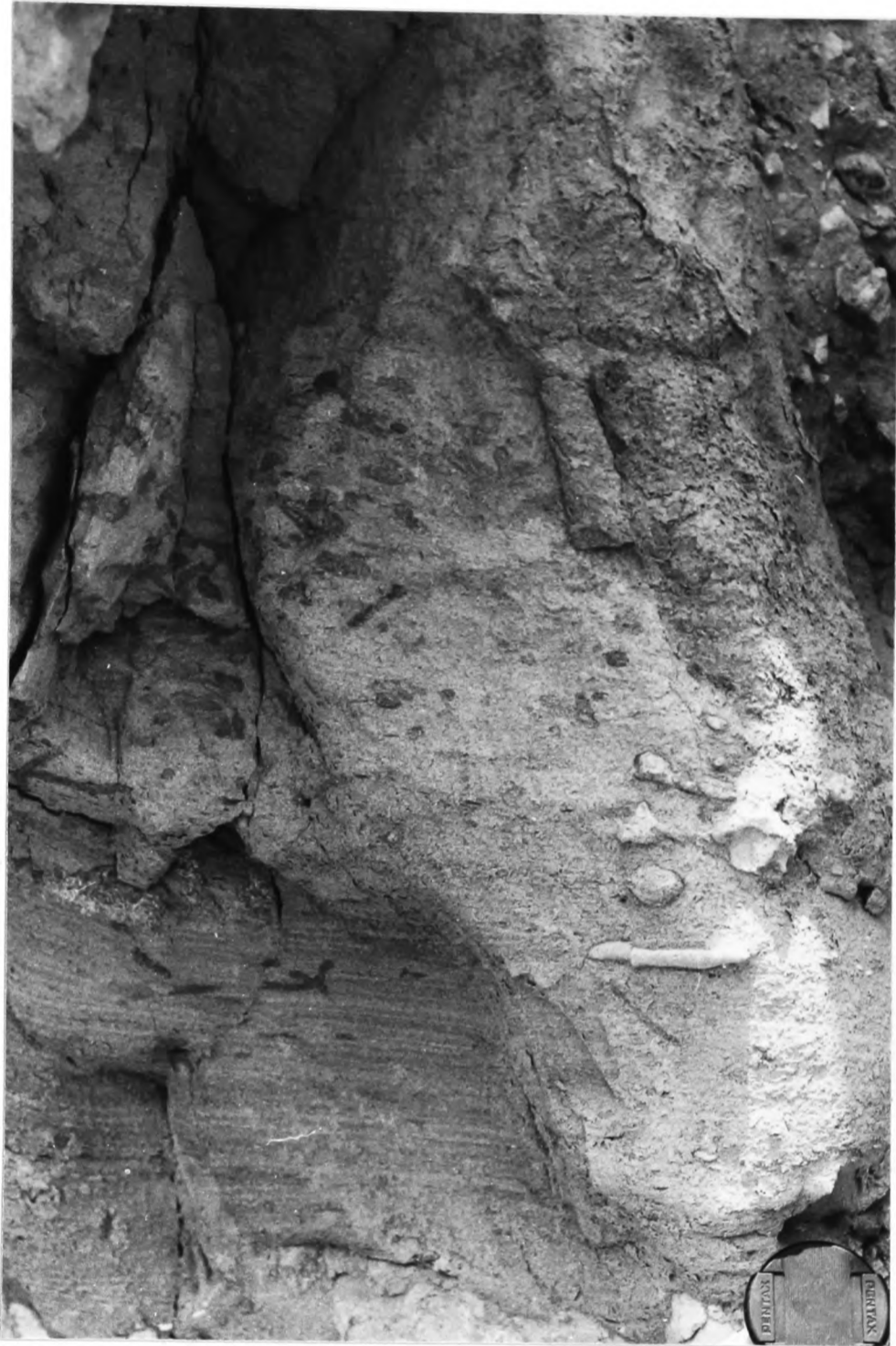


Fig.65: Bioturbated top of a storm laminite bed. Hooken Cliffs, Beer.

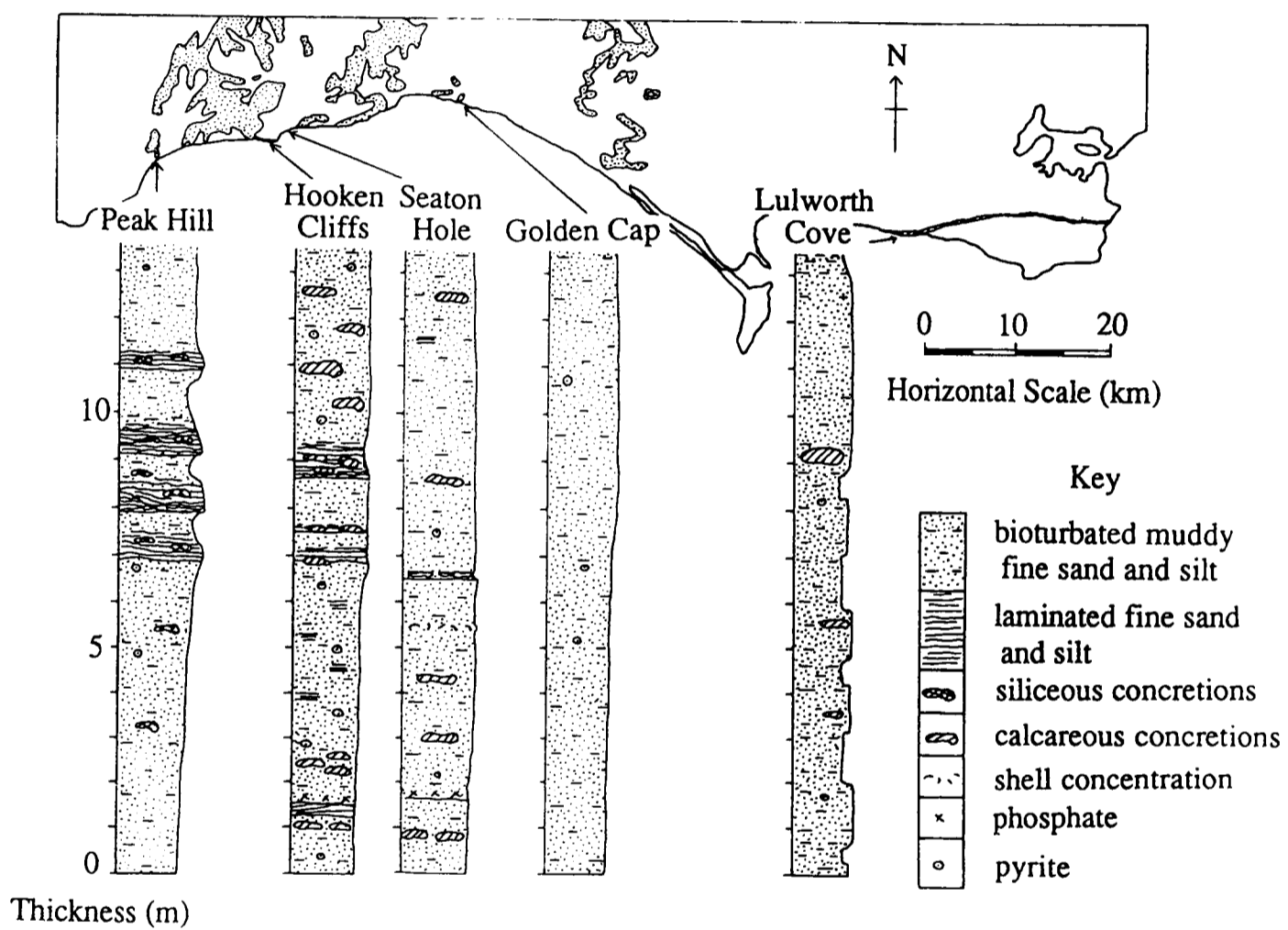


Fig.66: Graphic logs of a selected part of the Foxmould member, demonstrating the west-east trend of thinning, fining and disappearance of storm laminite beds. Peak Hill: muddy fine sands with interbedded laminites ; Hooken Cliffs: muddy fine sands with fewer and thinner laminites ; Seaton Hole: muddy fine sands with traces of lamination ; Golden Cap: homogeneous and fully bioturbated muddy silts ; Lulworth Cove: rhythmically-bedded muddy silts (variations in silt : clay).



Fig.67: Thick, proximal storm laminite bed, with a sharp base and bioturbated top. Peak Hill, near Sidmouth.



Fig.68: Large scour at the base of a proximal storm bed, cutting down through thin, amalgamated laminite beds to the top of an underlying thick bed. Peak Hill, near Sidmouth.

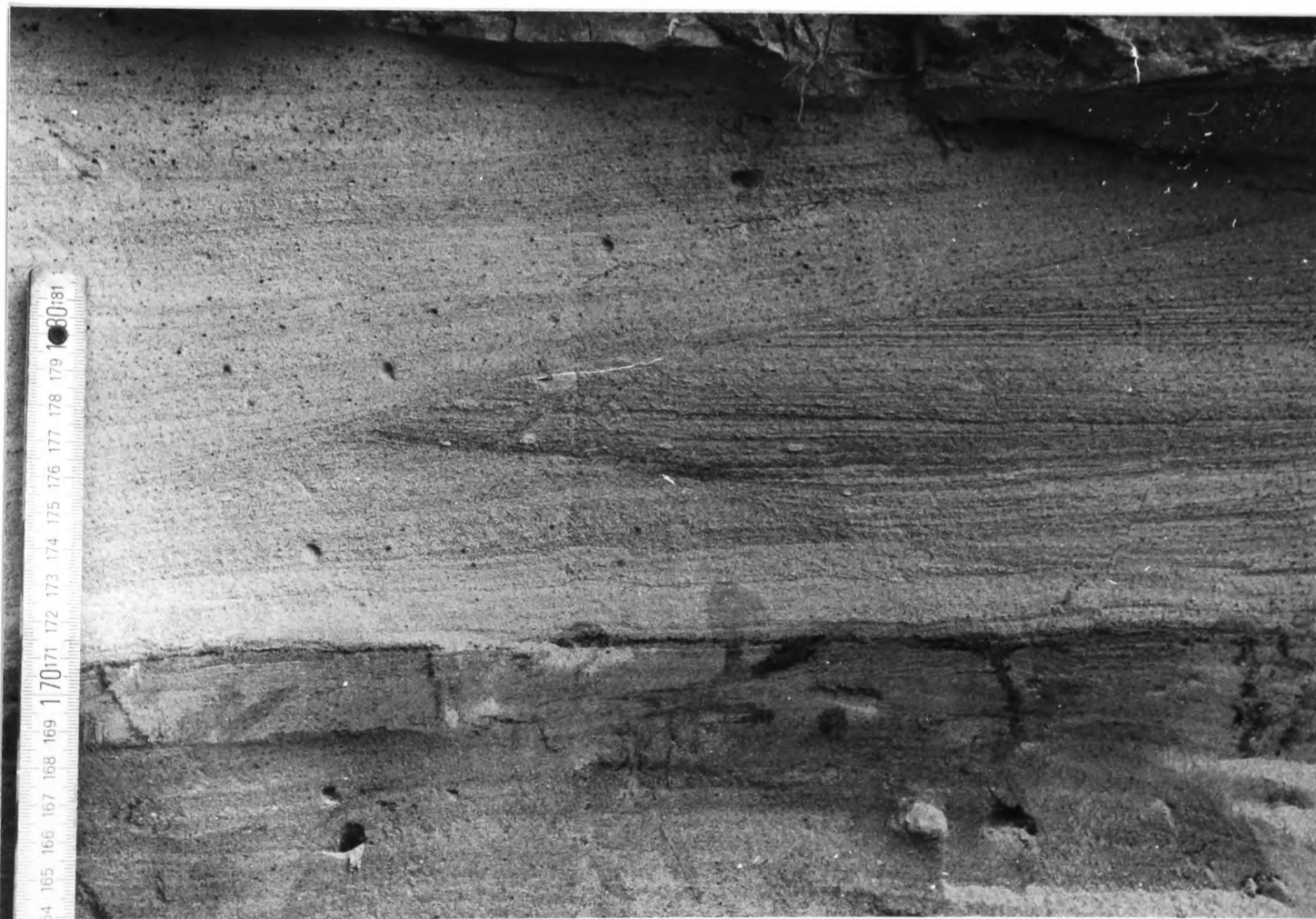


Fig.69: Horizontal and low-angle cross-lamination, developed within a thick proximal laminite bed. Peak Hill, near Sidmouth.

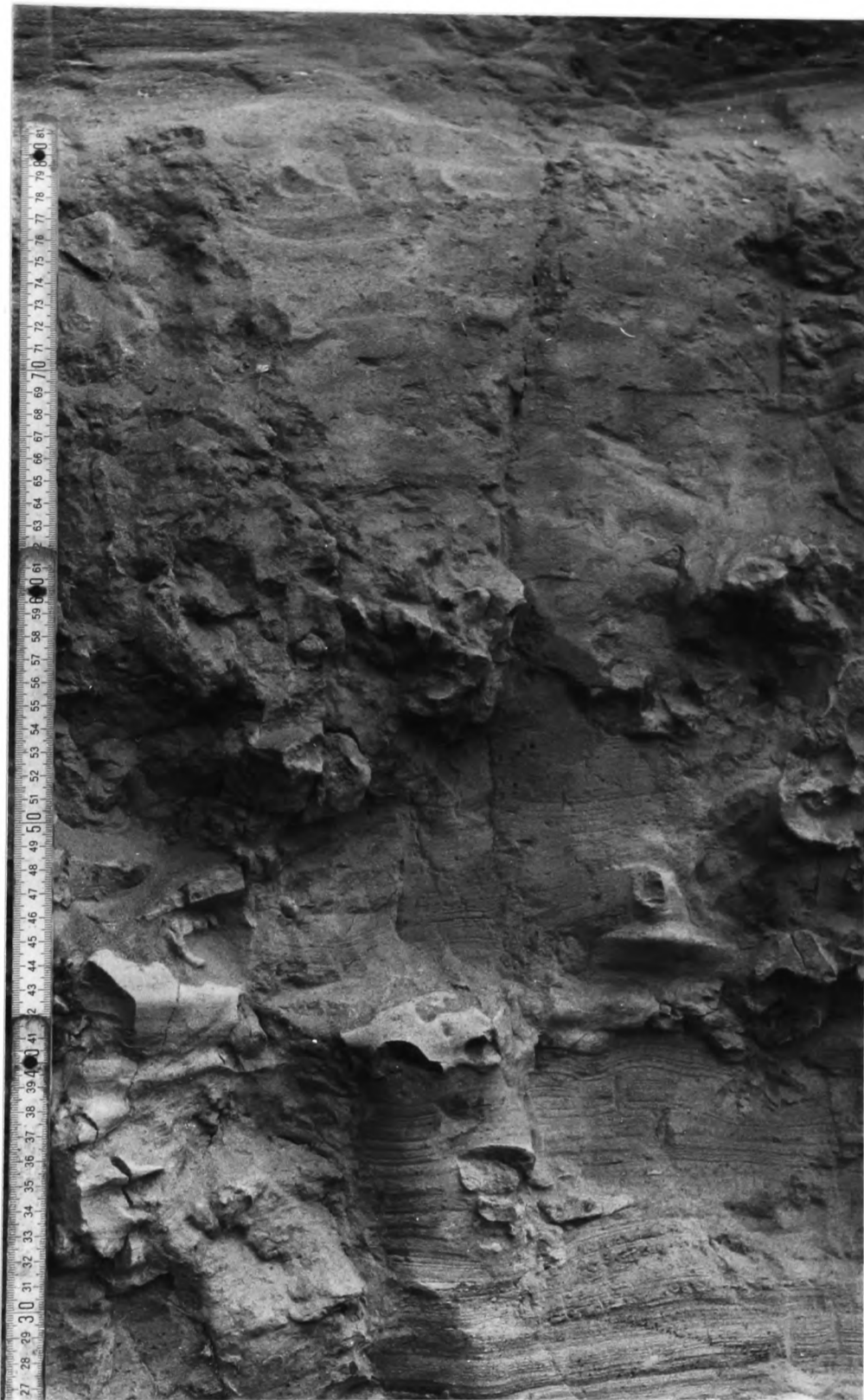


Fig.70: Bioturbated top of the bed seen in Fig.67, showing the progression from horizontally-laminated to structureless bioturbated silt.

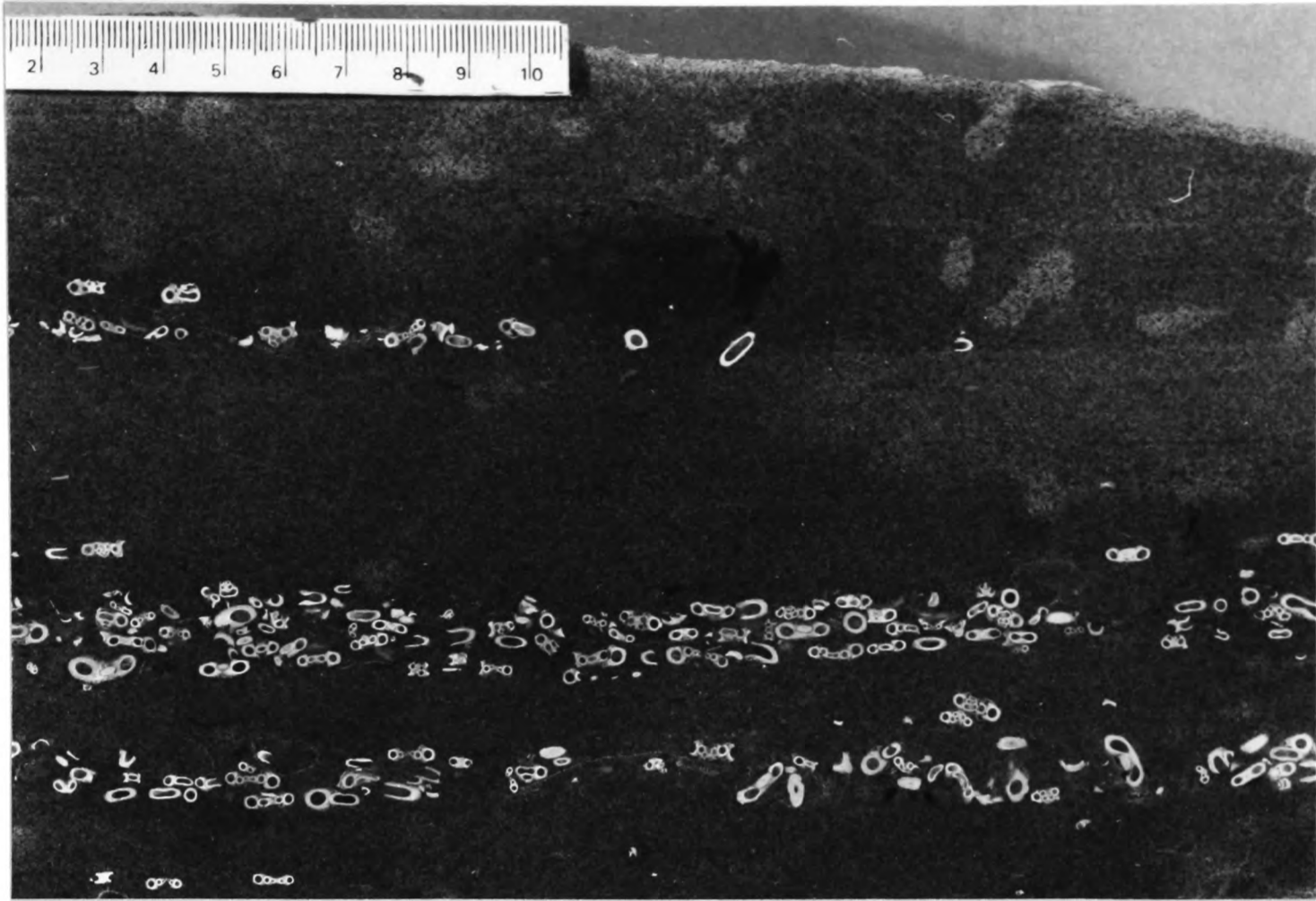


Fig.71: Amalgamated thin storm laminite beds, preserved within a late diagenetic calcareous concretion, Hooken Cliffs, Beer. Each bed has a concentration of serpulid-rich sediment at the base. Note the burrows in the upper part of the top laminite bed.

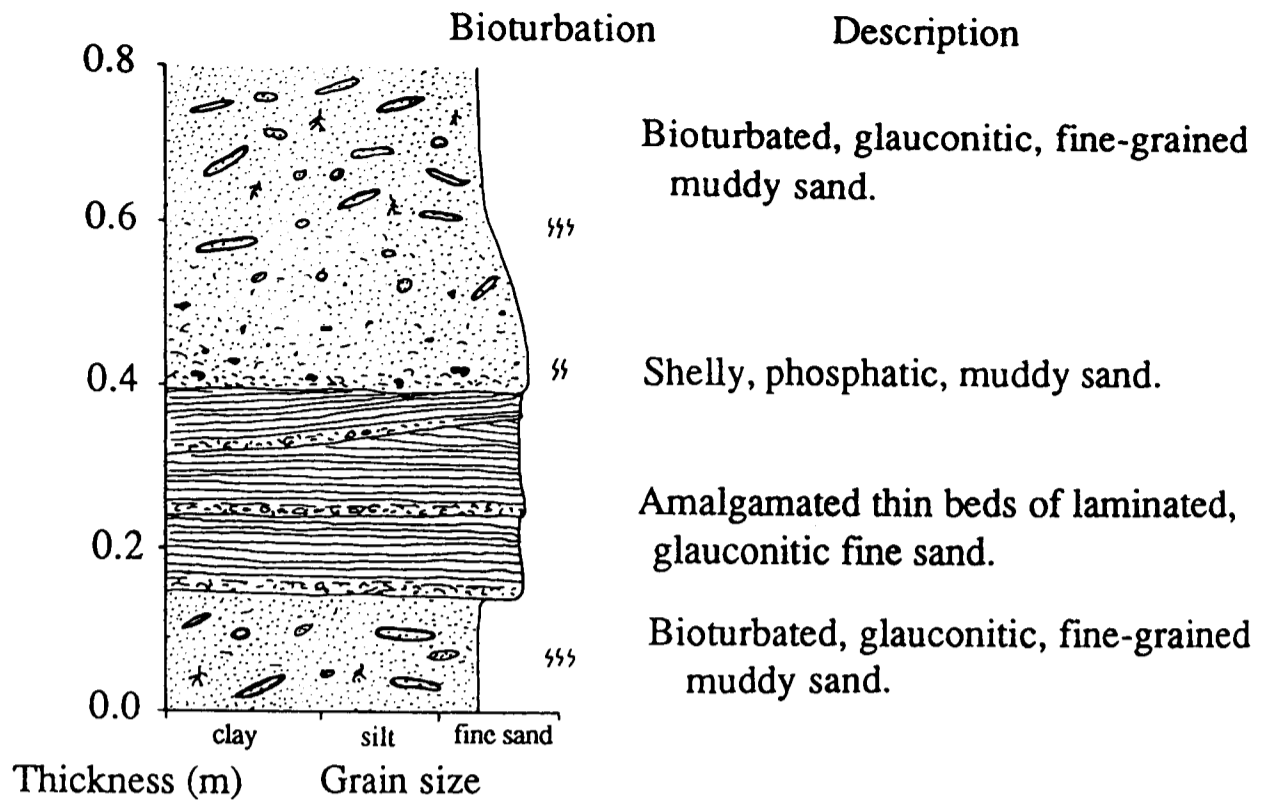


Fig.72: Graphic log of amalgamated thin storm laminites and storm-reworked phosphate horizon, from the Foxmould member, Hooken Cliffs, Beer.



Fig.73: Field outcrop of a lens of tabular cross-lamination preserved in the Foxmould Member, Whitecliff, Beer (SY 234 893).

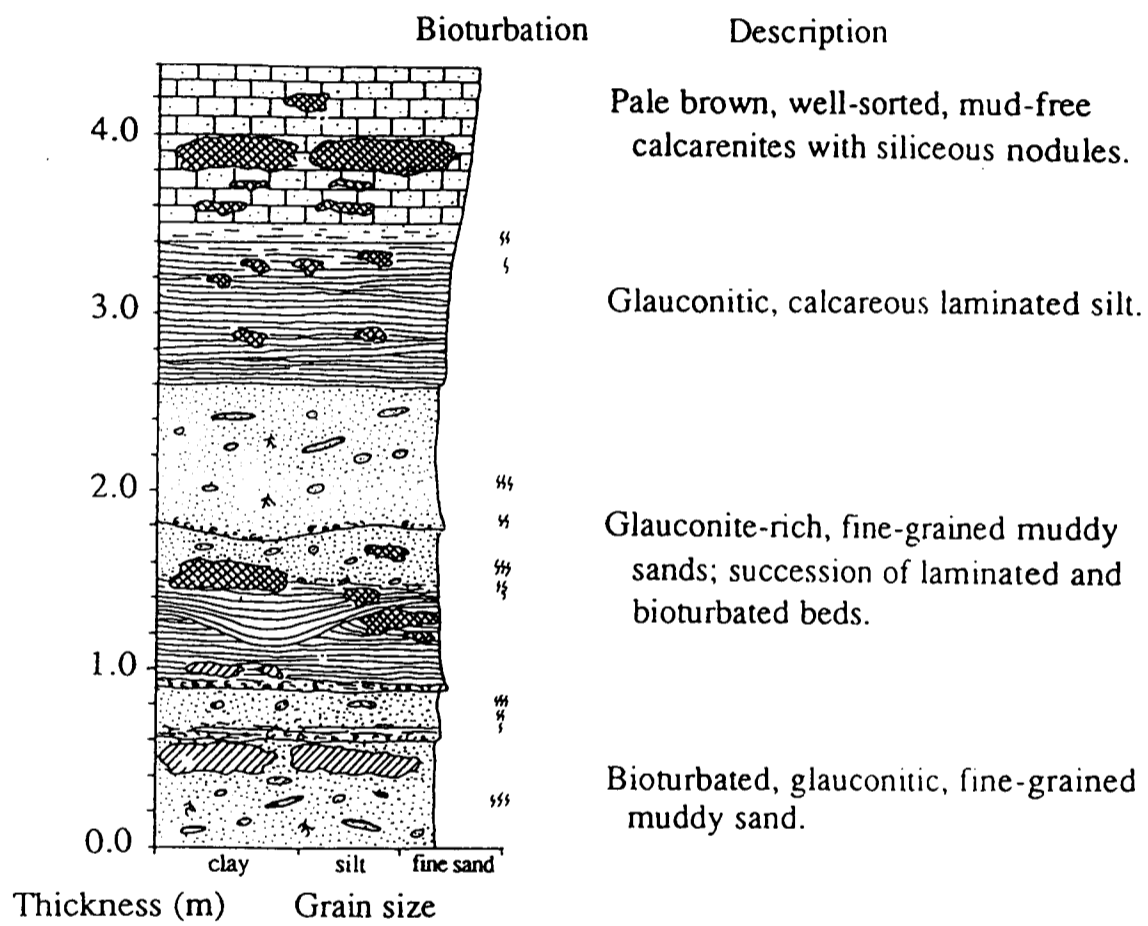


Fig.74: Graphic log of variably-amalgamated, glauconite-rich, thin storm laminites at the Foxmould-Chert Beds contact, Dunscombe Cliff. Correlates with interval shown in Fig.77 and Fig.78.

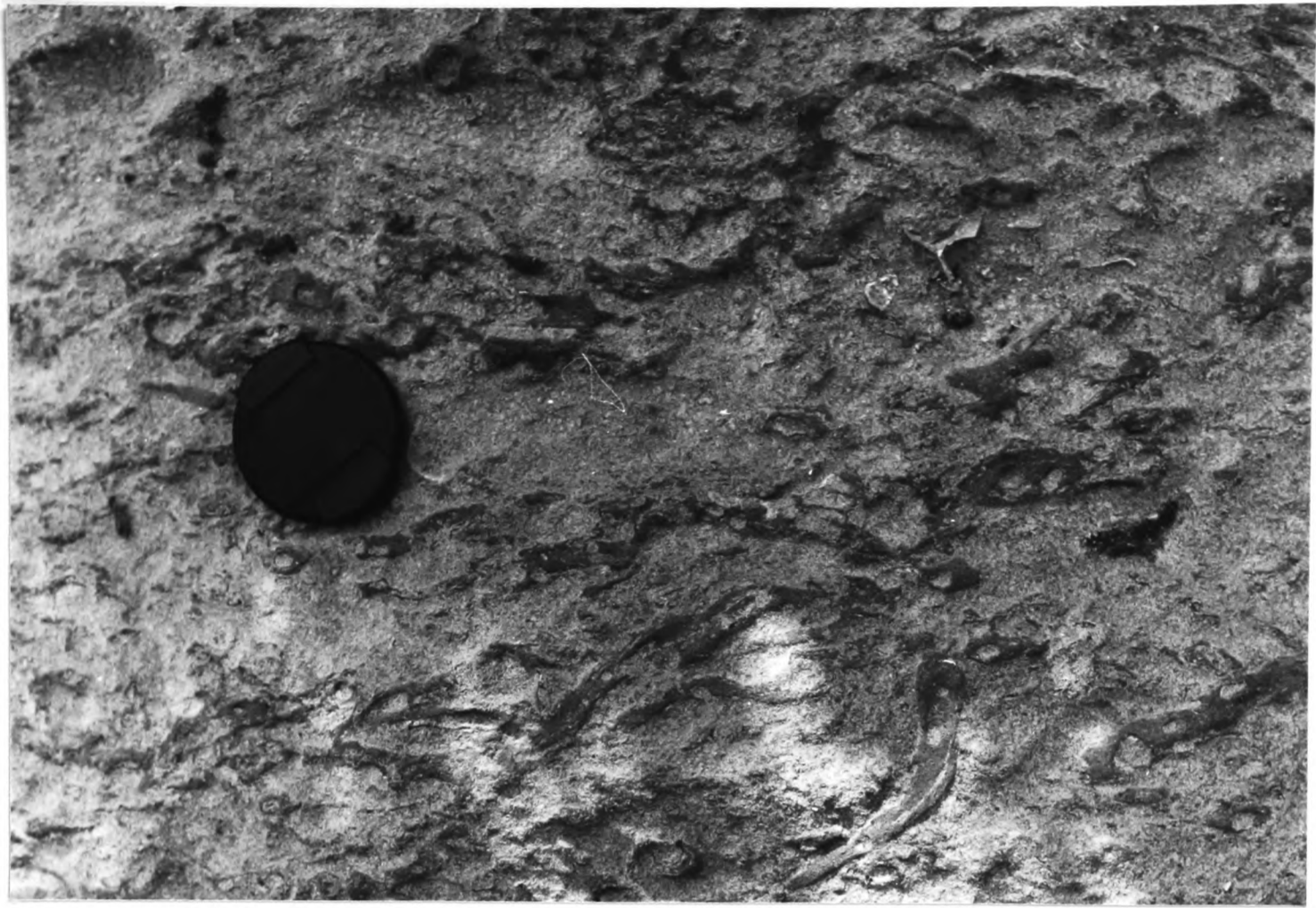


Fig.75: Fully-bioturbated lithofacies, with very abundant black mud-lined *Palaeophycus* burrows. Little Beach, near Beer.

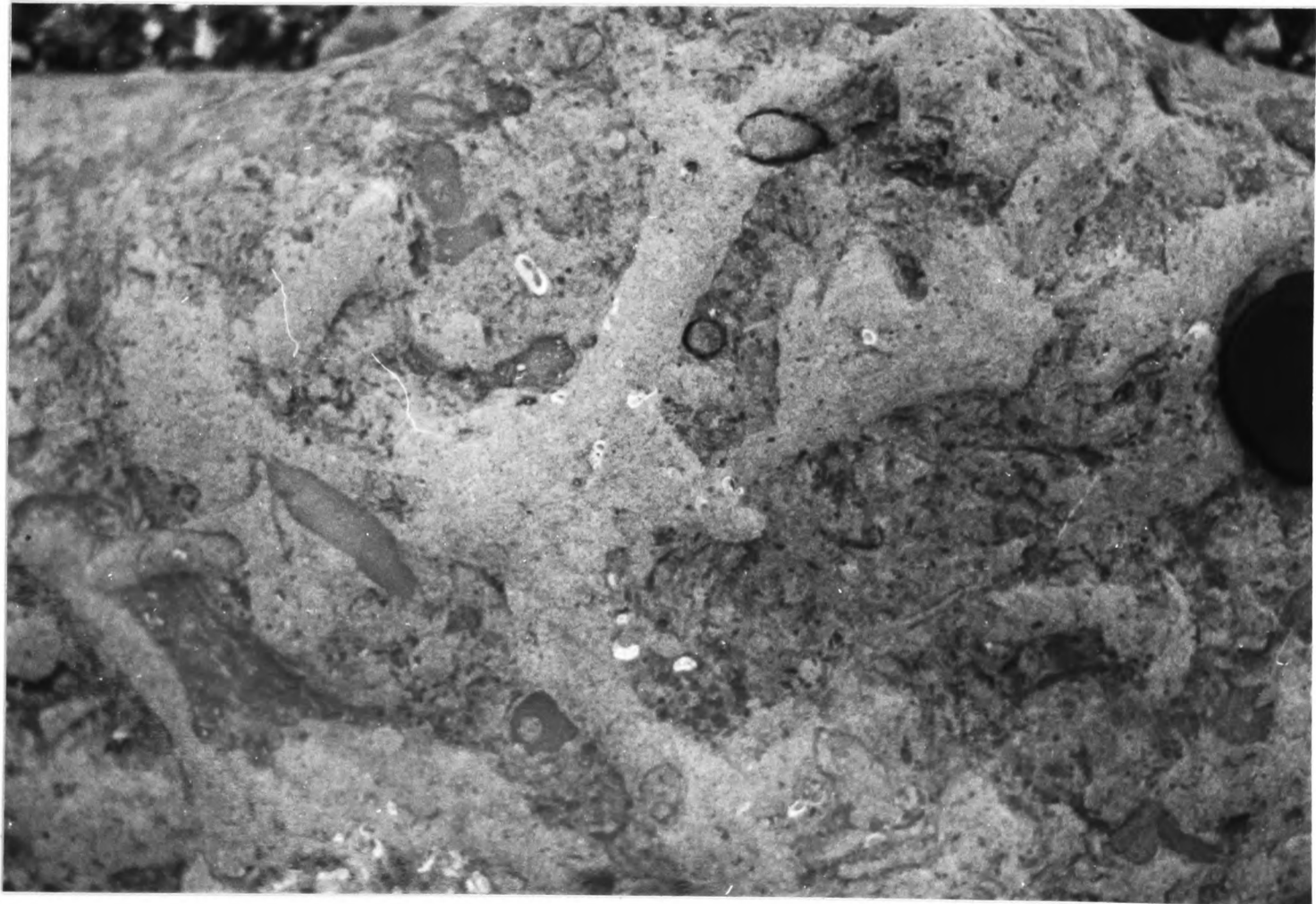


Fig.76: Fully-bioturbated lithofacies showing the *Thalassinoides-Palaeophycus* trace fossil association, preserved within a concretion. Foreshore east of Axemouth.



Fig.77: Pebble-shell beds and coquina lenses in the uppermost Foxmould, with the Chert Beds Member carbonates above. Whitecliff, Beer.

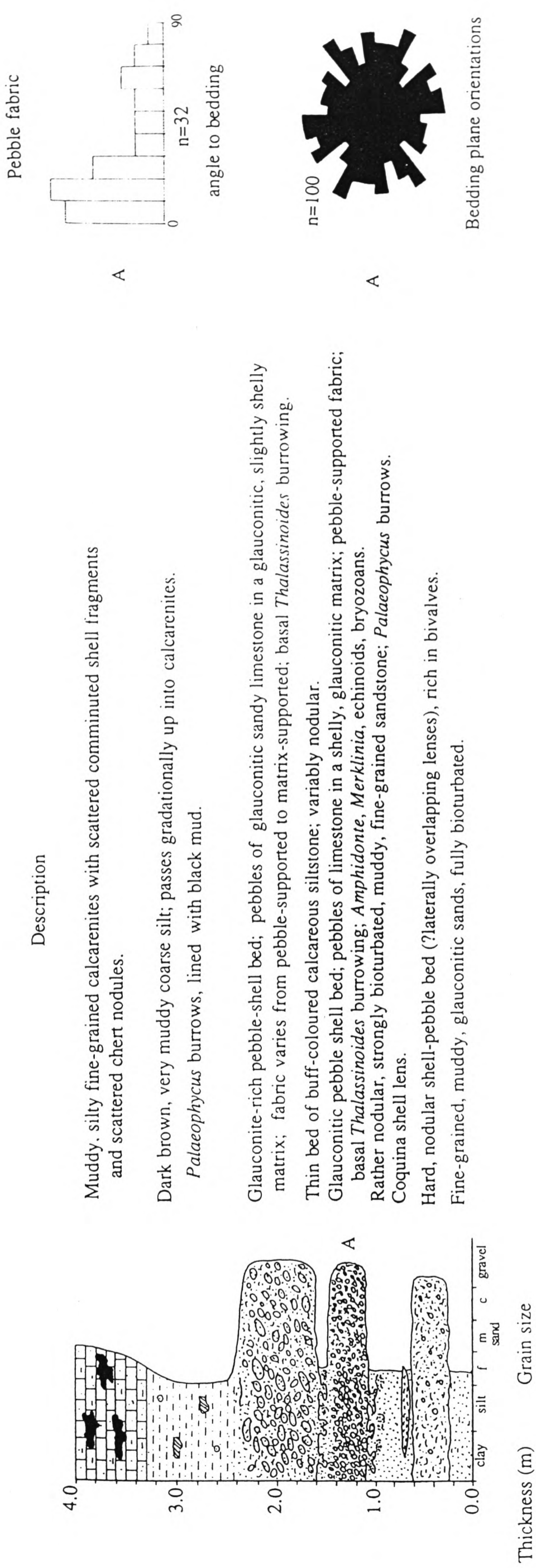


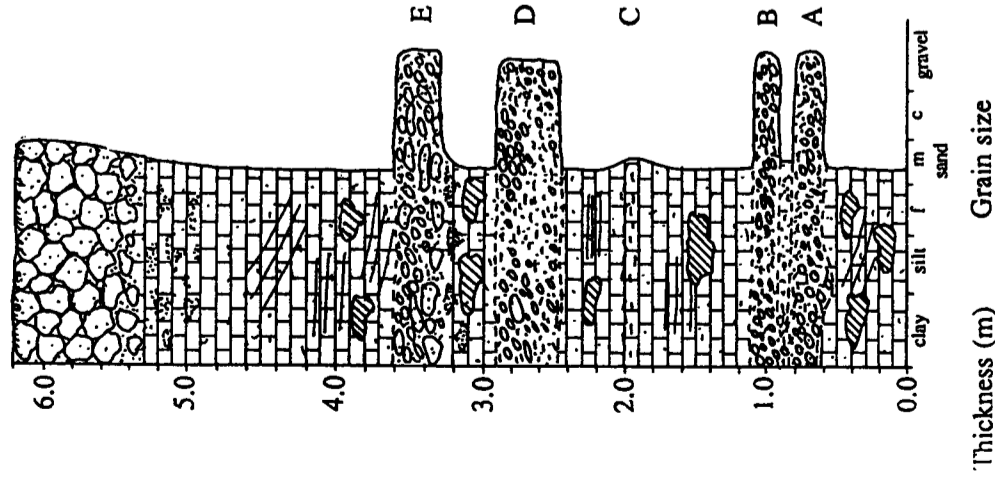
Fig.78: Graphic log and fabric data from the uppermost Foxmould pebble/shell beds seen in Figure 77, Whitecliff, Beer. Fabric data taken on pebble long axes (pebbles with >2:1 length:width ratio). Correlates with interval shown in Figure 74.



Fig.79: Detailed view of the coquina shell lens seen in Figure 77.



Fig.80: Detailed view of the upper two pebble-shell beds shown in Figure 77, showing the sediment fabric, which has a tendency towards bedding-parallel orientations of the pebble long axes.



Description

The Brecciated Limestone hardground, a well-cemented nodular limestone; *Thalassinoides* burrowing between the nodules; upper nodules glauconitised.

Thalassinoides burrows, filled with coarse, glauconitic sand.

Well-sorted calcarenites with fine shell fragments; glauconite-rich /poor lamination and low-angle to trough cross-bedding.

Complex pebble-shell bed; limestone pebbles in a shelly, glauconitic calcarenite matrix.

Thalassinoides-burrowed calcarenites, burrows penetrating down from base of bed above.

Shell-pebble bed; limestone pebbles and *Amphidonte* shells and shell fragments in a glauconitic calcarenite matrix.

Calcarenites with finely-broken shell fragments and faint horizontal lamination.

Calcarenites with poorly-defined weak concentration of large oyster shells.

Calcarenites with finely-broken shell fragments.

Amalgamated pebble-shell beds, separated by a thin sandy layer in some sections; limestone pebbles and oyster shells, occasional basal scour.

Calcarenites with weak low-angle cross-lamination.

Shell fabrics **Pebble fabrics**

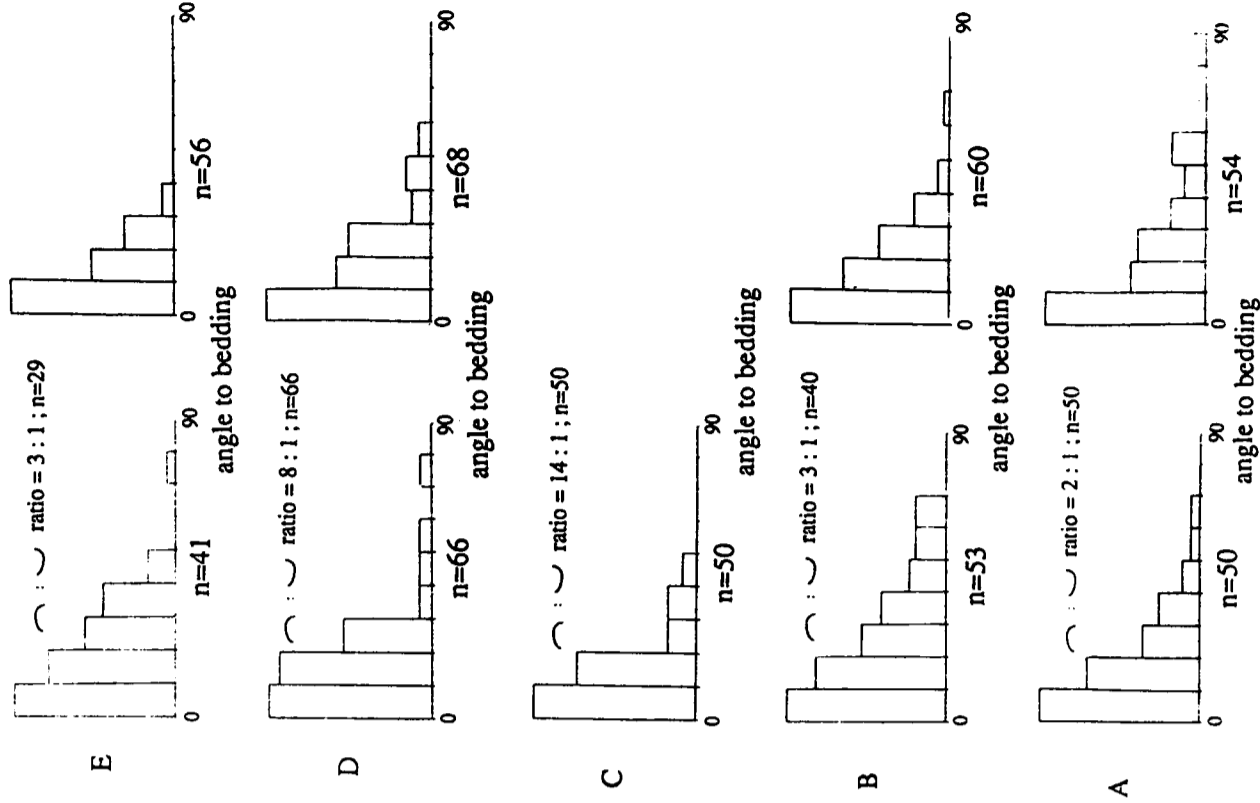


Fig.81: Graphic log and fabric data from the upper Chert Beds pebble-shell beds at Beer Head. Fabric data taken on shell and pebble long axes (pebbles with >2:1 length:width ratio) and on shell convexity orientations.

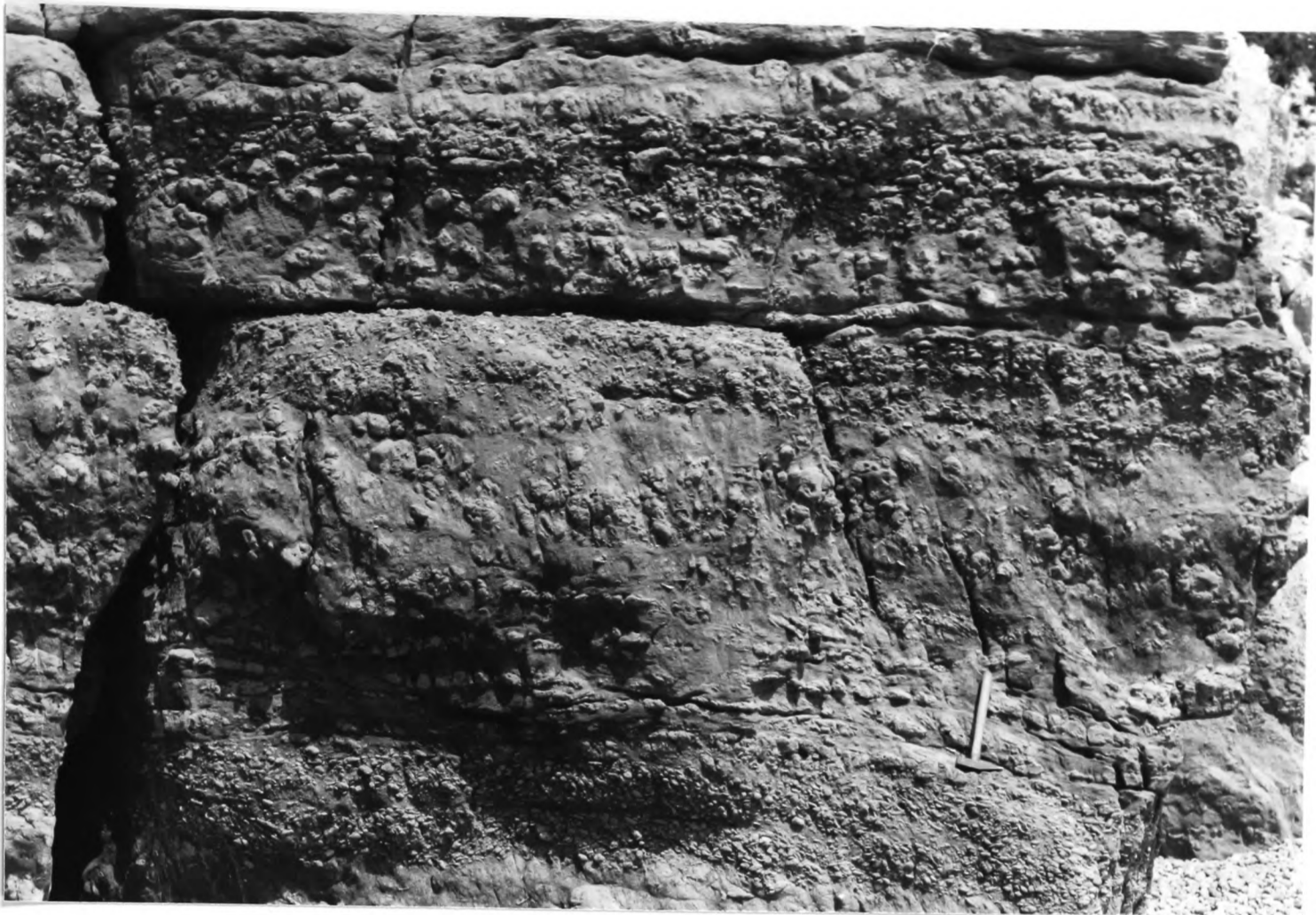


Fig.82: Interbedded carbonate packstones/grainstones and coarse pebble-shell beds, upper Chert Beds, Beer Head (shown graphically in Figure 81).

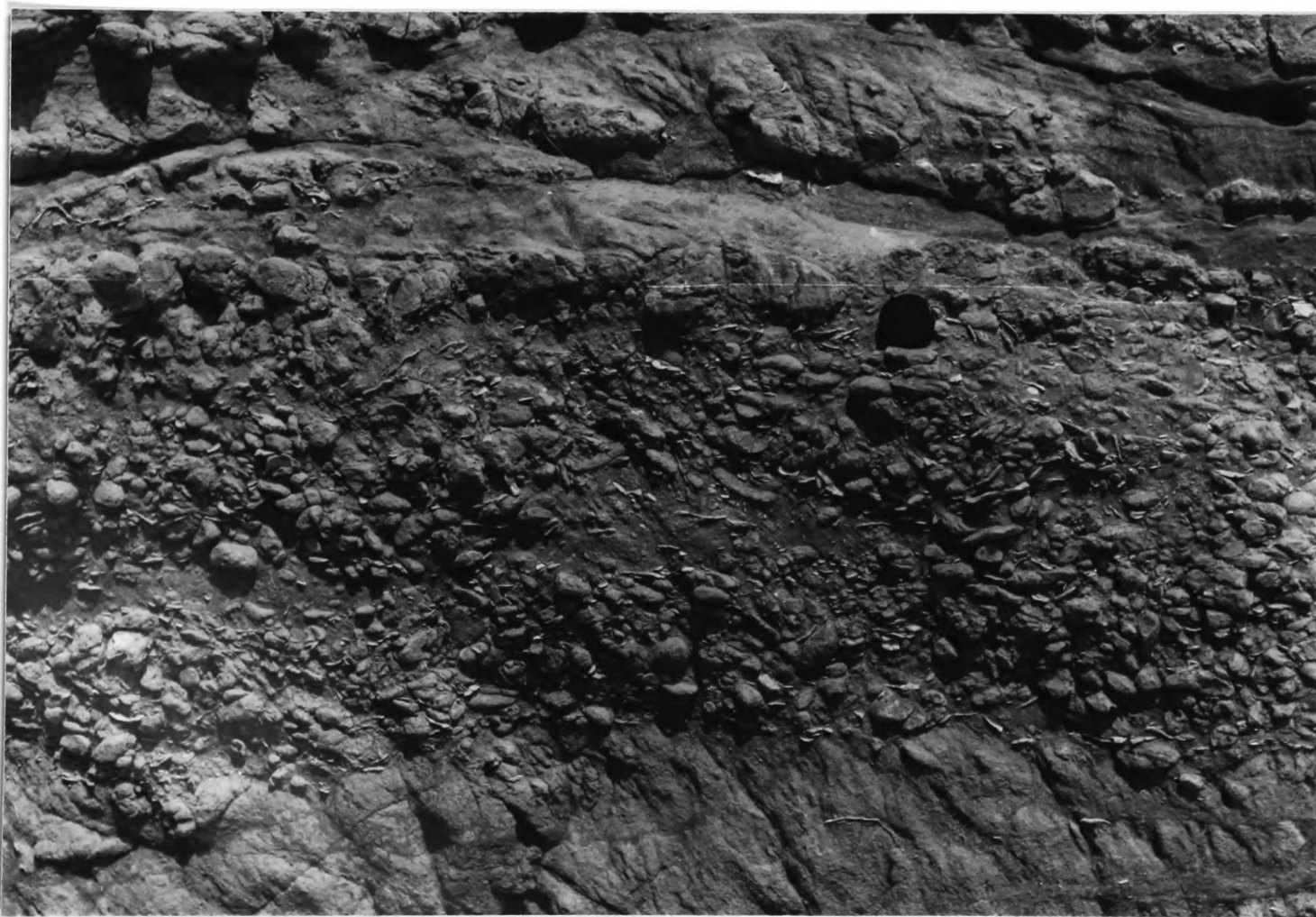


Fig.84: Pebble-shell bed fabric. Shows the predominantly horizontal alignment of the pebble and shell material. An internal sandy lens suggests amalgamation of two beds. A shallow scour at the base of the bed, infilled with pebbles and shells, is present on the left of the picture. Lower pebble-shell bed in upper Chert Beds, Beer Head.

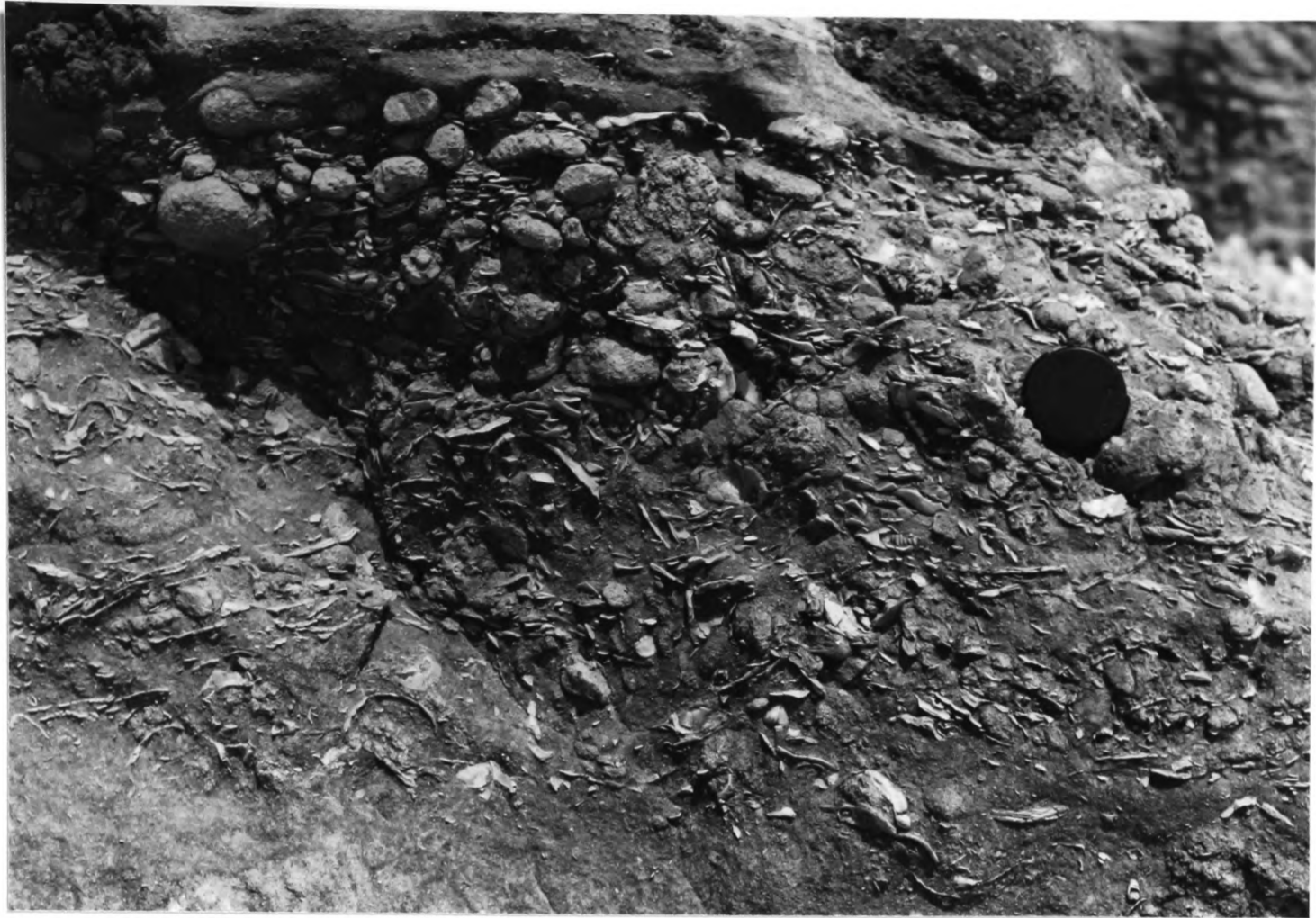


Fig.83: Pebble-shell bed fabric. Shows a patch of pebble-rich sediment in the upper part, probably infilling a small scour. Shell material is predominantly horizontally-oriented, with a patch of imbricated shells on the left of the picture. Lower pebble-shell bed in upper Chert Beds, Beer Head.



Fig.85: Coquina shell bed in the lower Chert Beds, showing sharp base, lower shelly layer, internal sandy lens, and overlying shelly layer with mounded top. Implies amalgamation of at least two discrete events. Little Beach, Beer.

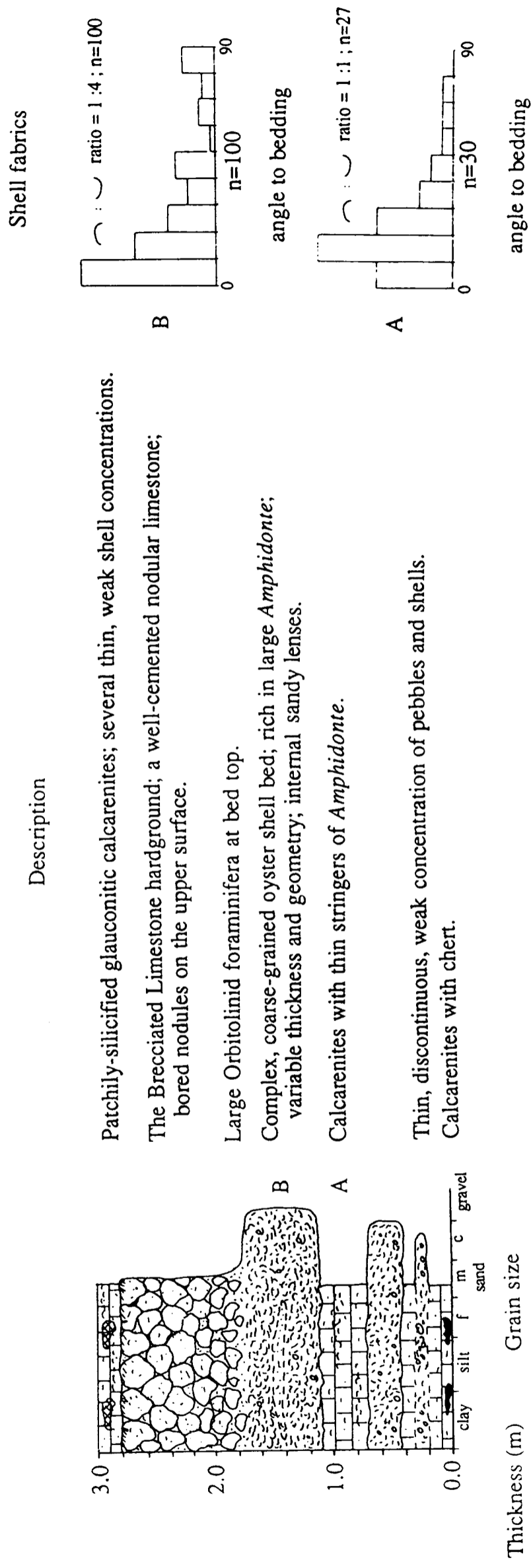


Fig. 86: Graphic log and fabric data from complex proximal shell-pebble beds, Weston Ebb. Fabric data taken on shell long axes and convexity orientations.



Fig.87: Complex proximal shell-pebble beds, upper Chert Beds, just below the Brecciated Limestone hardground, Weston Ebb (shown graphically in Figure 86). Note the internal calcarenite lenses within the uppermost coquina, and thin shell stringers in the sediment immediately below.

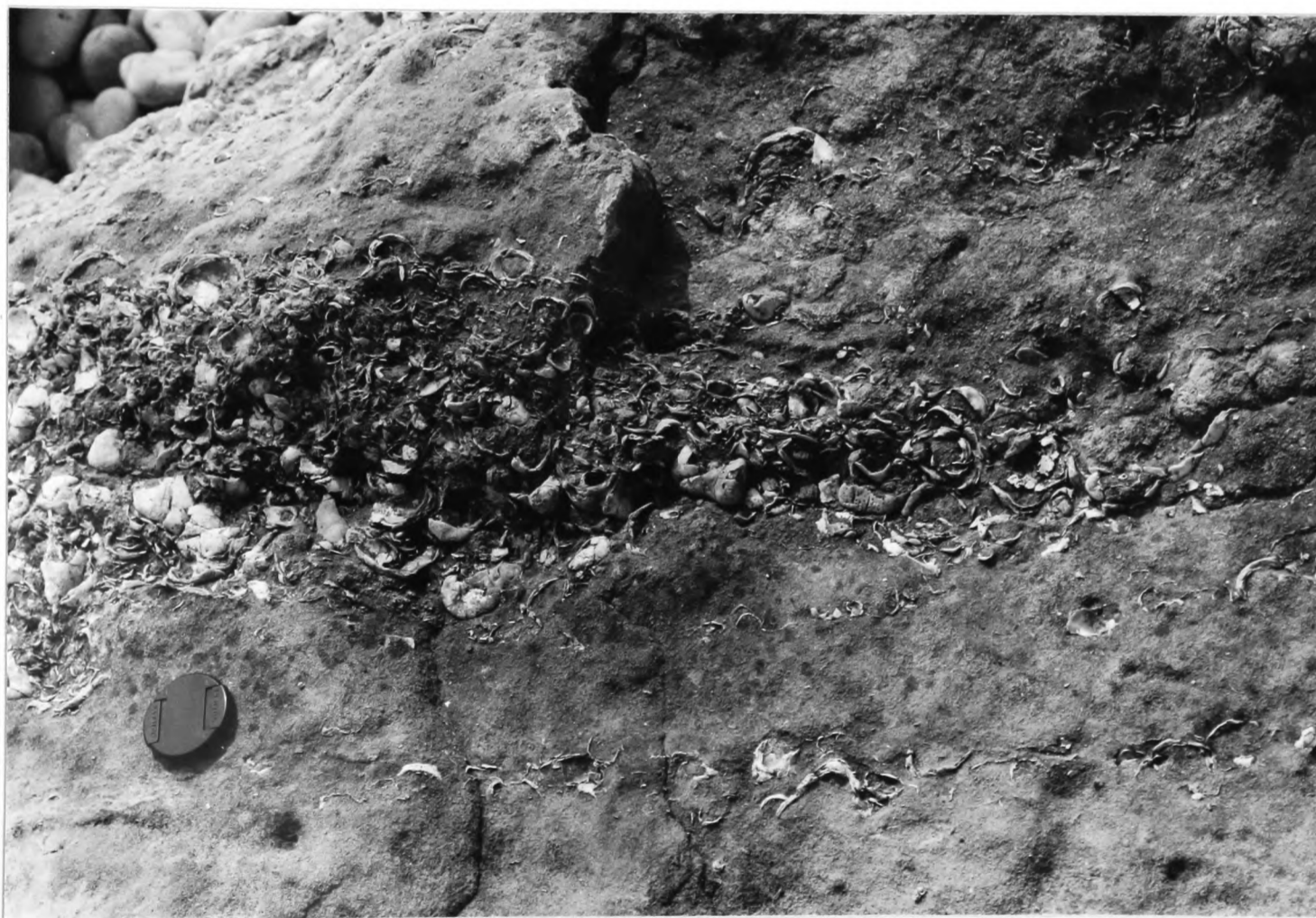


Fig.88: Coarse-grained coquina lens and thin shell stringers, upper Chert Beds, Weston Ebb. Note the predominantly convex-down shell stacking in the main part of the coquina lens, and the predominantly convex-up alignments at the top of the lens, and in the shell stringer below.



Fig.89: Fabric of thin pebble layer, finer-grained shell-pebble bed, and coarse shell stringer, upper Chert Beds, Weston Ebb.



Fig.90: Bedding plane view of shell bed from the Beer Head Limestone (Cenomanian), Weston Ebb. Shows the different shell assemblage to the Upper Greensand shell beds, with variably-fragmented *Merklinia* and *Amphidonte* bivalves.



Fig.91: Fabric of coarse-grained complex, proximal coquina bed, upper Chert Beds, Weston Ebb. Note the close shell stacking in predominantly convex-down orientations. Scattered patches of sediment show imbrication, and orientations up to vertical to bedding. Small intraformational pebbles are present at low concentrations throughout.



Fig.92: Gutter infilled with shell-rich sediment, developed at the base of a coarse-grained, complex, proximal coquina bed, Weston Ebb.



Fig.93: Complex pebble-shell bed, showing evidence for amalgamation of three separate pebble and shell concentrations, upper Chert Beds, Beer Head.

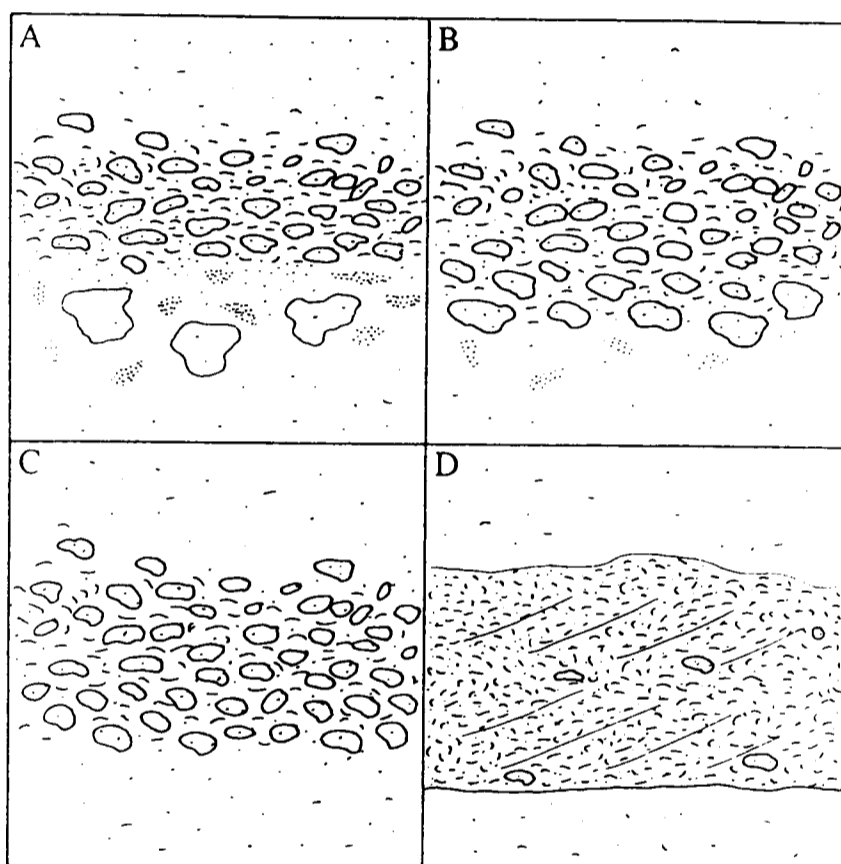


Fig.94: Cartoon showing the different types of basal contact to the pebble/shell beds in the Chert Beds calcarenites. (A) basal firmground burrowing and *in situ* nodules ; (B) basal firmground burrowing, all nodules reworked ; (C) no firmground burrowing, all nodules reworked ; (D) sharp base, overlain by a shell-rich bed, sometimes cross-stratified.

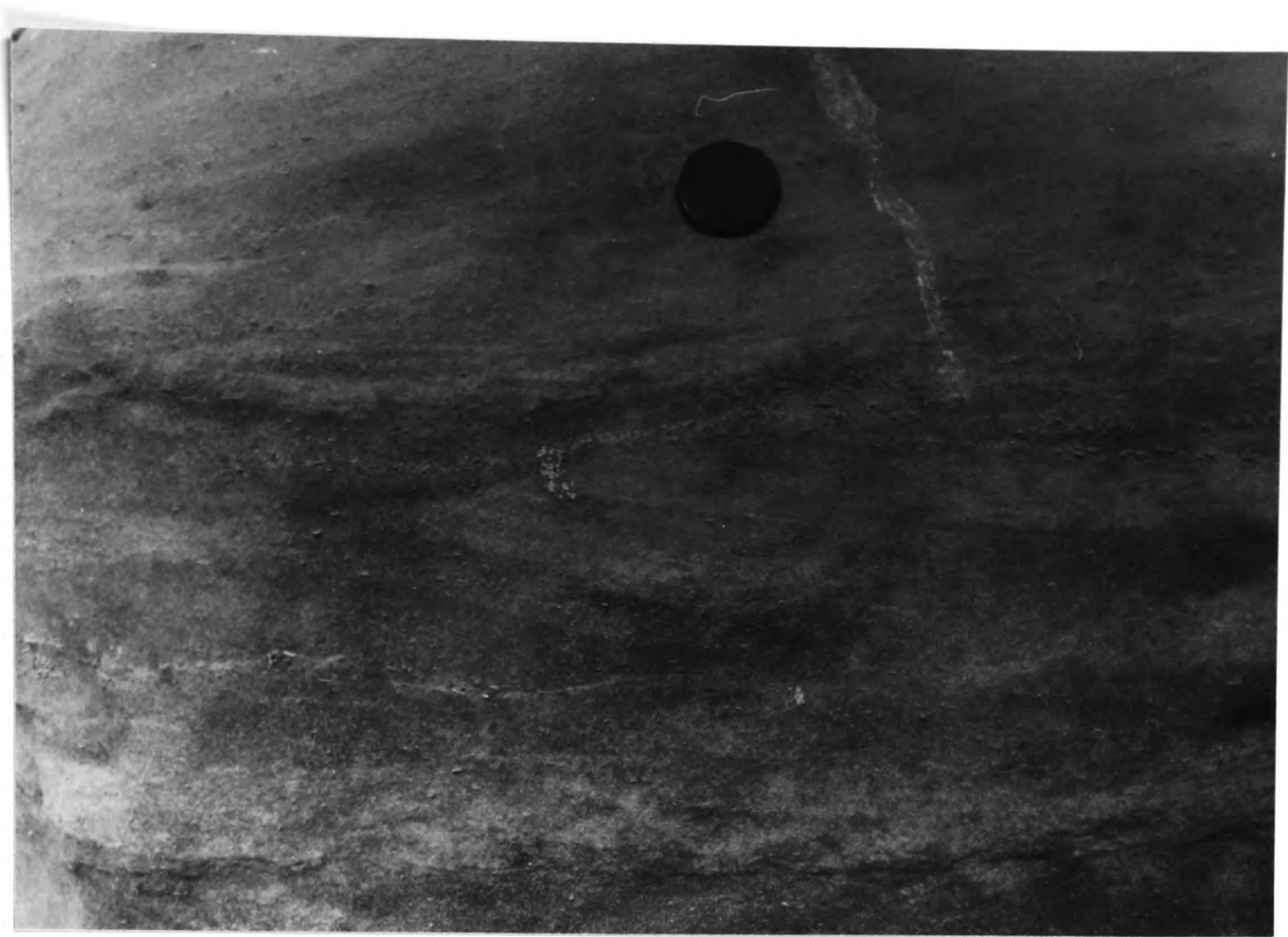


Fig.95: Horizontal and undulose to low-angle cross-lamination, the Chert Beds. Wave-polished block, Culverhole Point.

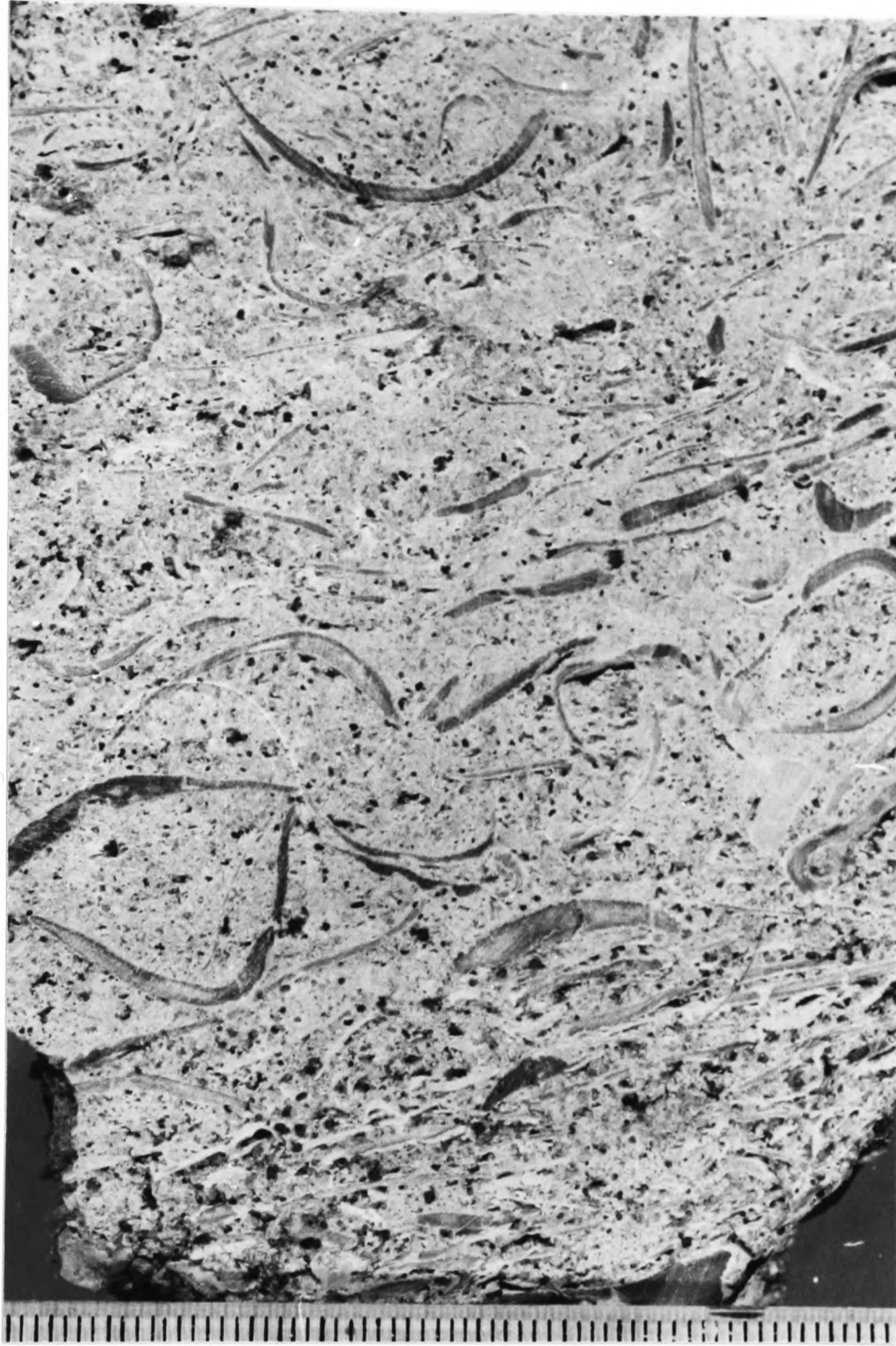


Fig.96: Polished slab from coquina bed, lower Chert Beds, showing the shell fabric. Predominantly horizontal shell orientations, with occasional larger shells up to vertical to the bedding. Note the stratification present within the sample; at least four thin beds are developed, differing in grain size and shell orientation. Little Beach, Beer.

	AMMONITE ZONE	AMMONITE SUBZONE	SOUTH-EAST DEVON		
UPPER ALBIAN	<i>dispar</i>	<i>perinflatum</i>	Upper Greensand Formation	Top Sandstones Member	
		<i>rostratum</i>		Chert Beds Member	
	<i>inflatum</i>	<i>auritus</i>	Upper Greensand Formation	Foxmould Member	
		<i>varicosum</i>			
		<i>orbigny</i>			
		<i>cristatum</i>			
					basal unconformity

Fig.97: Subdivision of the Upper Greensand Formation of south-east Devon, with corresponding ammonite biostratigraphy. Ammonite zonation scheme based on Owen (1976).

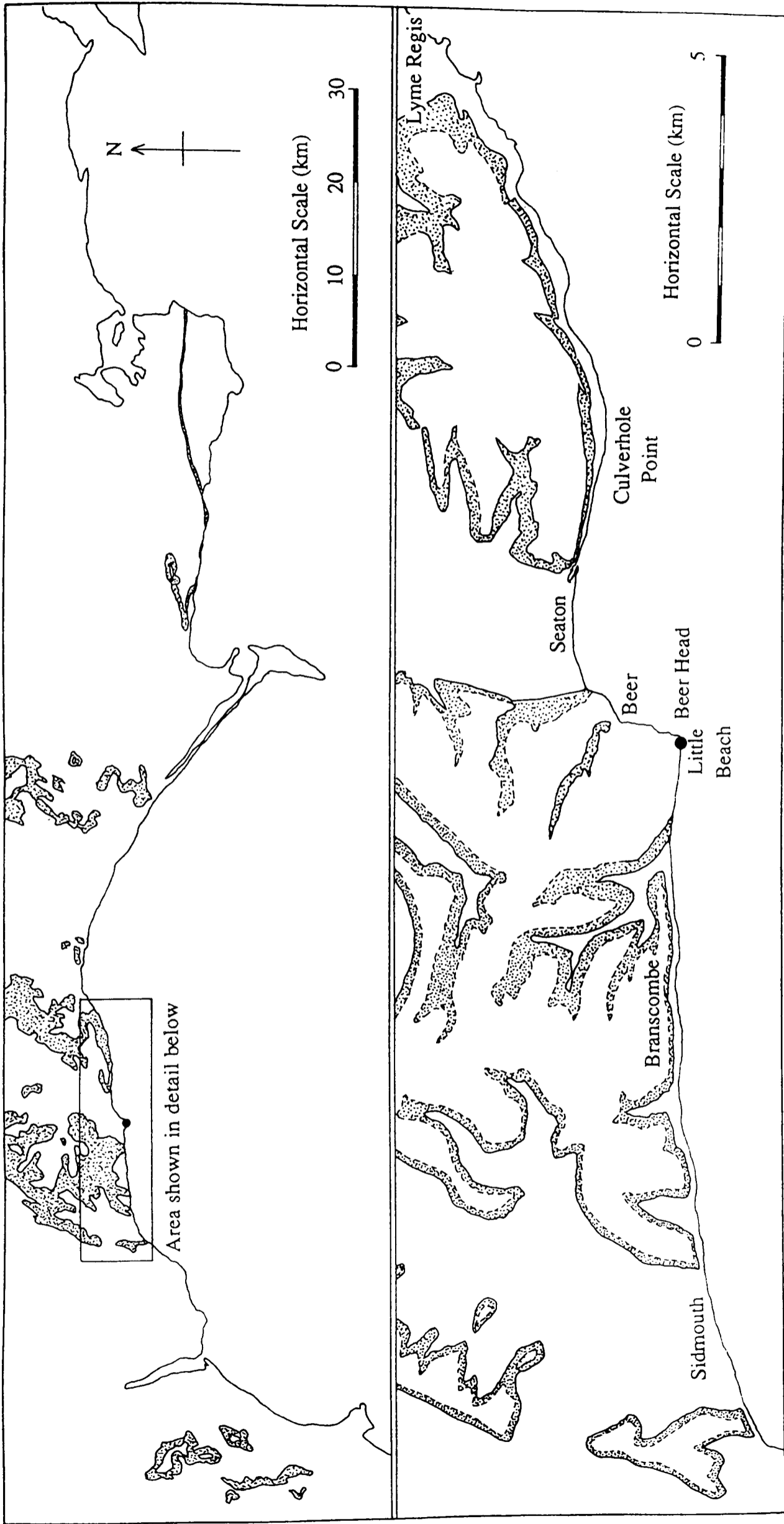


Fig.98: Map showing the Upper Greensand and Gault outcrop across south-west England, and the location of the section sampled, at Little Beach - Beer Head.

Stratigraphy	Sample Number	Sample posn.	Log plot posn.	$\delta^{13}C$	$\delta^{13}C$ 3pt. av.	$\delta^{18}O$	$\delta^{18}O$ 3pt.av.	Cemtn. Index.	$\delta^{13}C$ normd.	$\delta^{18}O$ normd.
B.HEAD LST.	A90/4184	48.72	48.72	3.188		-1.820		4		
UGS-Top Ssts.	A90/4178	47.62	47.62	3.098	3.111	-2.585	-1.924	4	3.478	-1.484
	A90/1362	46.20-46.30	46.25	3.046	3.046	-1.821	-2.148	1	3.162	-1.484
	A90/1365	46.05-46.15	46.10	2.994	3.011	-2.038	-1.960	3	3.185	-1.484
	A90/1369	45.97-46.05	46.01	2.993	2.903	-2.021	-2.095	1	3.178	-1.484
	A90/1368	44.61-44.69	44.65	2.722	2.876	-2.227	-2.252	1	2.978	-1.484
	A90/4168	43.42	43.42	2.913	2.903	-2.509	-2.181	3	3.267	-1.484
	A90/4169	43.12	43.12	3.075	2.908	-1.808	-2.231	1	3.187	-1.484
U.Chert Beds	A90/1372	41.57-41.67	41.62	2.735	2.796	-2.375	-2.157	1	3.042	-1.484
	A90/1367	40.68-40.80	40.74	2.579	2.656	-2.287	-2.120	2	2.856	-1.484
	A90/1386	40.12-41.37	40.20	2.653	2.628	-1.697	-1.968	1	2.726	-1.484
	A90/1385	39.42-39.82	39.67	2.651	2.652	-1.919	-1.785	2	2.801	-1.484
	A90/1389	38.99-39.42	39.20	2.653	2.637	-1.740	-2.006	4	2.741	-1.484
	A90/1400	38.45	38.45	2.608	2.655	-2.360	-2.071	1	2.910	-1.484
	A90/1358	37.95	37.95	2.703	2.701	-2.114	-1.986	2	2.920	-1.484
	A90/1394	37.15-37.65	37.40	2.792	2.659	-1.484	-1.991	2	2.792	-1.484
	A90/1359	37.05	37.05	2.481	2.596	-2.374	-2.117	2	2.788	-1.484
	A90/1395	36.15	36.15	2.516	2.436	-2.494	-2.560	3	2.864	-1.484
	A90/4495*	35.15	35.15	2.311	2.398	-2.813	-2.476	4	2.770	-1.484
	A90/1361	34.75	34.75	2.367	2.399	-2.120	-2.573	3	2.586	-1.484
	A90/4504*	34.75	34.75	2.519	2.478	-2.785	-2.428	3	2.968	-1.484
	A90/1392	33.55	33.55	2.548	2.246	-2.380	-2.880	4	2.857	-1.484
L.Chert Beds	A90/1363	32.50-32.60	32.55	1.672	1.949	-3.474	-3.339	3	2.360	-1.484
	A90/1397	31.75-32.15	31.95	1.627	1.652	-4.163	-4.011	3	2.551	-1.484
	A90/1402	31.75	31.75	1.656	1.661	-4.396	-3.694	4	2.661	-1.484
	A90/1375	31.28-31.35	31.31	1.700	1.662	-2.524	-3.498	4	2.059	-1.484
	A90/1384	31.15-31.20	31.18	1.631	1.612	-3.573	-2.071	5	2.352	-1.484
	A90/1373	31.04-31.15	31.09	1.505	1.586	-3.116	-3.114	2	2.068	-1.484
	A90/1382	30.97-31.02	31.00	1.621	1.635	-2.654	-2.668	3	2.025	-1.484
	A90/1371	30.90-30.98	30.94	1.778	1.781	-2.235	-2.370	3	2.037	-1.484
	A90/1381	30.80-30.85	30.82	1.945	1.890	-2.222	-2.101	5	2.200	-1.484
	A90/1374	30.76-30.80	30.78	1.946	1.853	-1.847	-2.113	2	2.071	-1.484
	A90/1376	30.66-30.72	30.69	1.667	1.778	-2.270	-2.199	4	1.938	-1.484
	A90/1377	30.39-30.51	30.45	1.720	1.697	-2.481	-2.567	4	2.064	-1.484
	A90/1383	30.29-30.37	30.32	1.705	1.608	-2.950	-2.996	2	2.211	-1.484
	A90/1380	30.11-30.19	30.15	1.400	1.419	-3.557	-3.469	5	2.115	-1.484
	A90/1379	29.99-30.03	30.01	1.151	1.431	-3.899	-3.368		1.984	-1.484
	A90/1378	29.65-29.70	29.68	1.741	1.452	-2.649	-2.867	4	2.143	-1.484
	A90/1364	29.05	29.05	1.463	1.621	-2.052	-2.562	3	1.659	-1.484
	A90/1360	27.95	27.95	1.659	1.625	-2.985	-2.244	2	2.177	-1.484
	A90/1366	27.10	27.10	1.754	1.699	-1.696	-2.293	3	1.827	-1.484
	A90/1403	26.55	26.55	1.684	1.926	-2.198	-2.117	2	1.930	-1.484
Foxmould	A90/1393	25.80-26.05	25.93	2.339	1.825	-2.456	-2.499	2	2.674	-1.484
	A90/1398	25.15-25.35	25.25	1.452	1.961	-2.843	-2.382	4	1.921	-1.484
	A90/1401	24.99-25.15	25.07	2.093		-1.848		4	2.219	-1.484

Table 2: Carbon- and oxygen-isotopic data from Little Beach - Beer Head, south-east Devon. Data are from whole rock samples, generated by crushing, except for the two samples marked *, which were generated by drilling a small amount of powder from fresh specimen surfaces. Normalised data reflect modification to remove postulated silica diagenesis; data normalised to the lowest $\delta^{18}O$ value.

Sample Number	Sample posn.	Log plot posn.	$\delta^{13}\text{C}$	$\delta^{18}\text{O}$	Cemtn. Index	$\delta^{13}\text{C}$ normd.	$\delta^{18}\text{O}$ norm.
A90/1375	31 28-31.35	31.31	1.700	-2.524	4	1.934	-1.847
A90/1384	31 15-31.20	31.18	1.631	-3.573	5	2.226	-1.847
A90/1373	31.04-31.15	31.09	1.505	-3.116	2	1.943	-1.847
A90/1382	30 97-31.02	31.00	1.621	-2.654	3	1.899	-1.847
A90/1371	30 90-30.98	30.94	1.778	-2.235	3	1.912	-1.847
A90/1381	30 80-30.85	30.82	1.945	-2.222	5	2.074	-1.847
A90/1374	30 76-30.80	30.78	1.946	-1.847	2	1.946	-1.847
A90/1376	30 66-30.72	30.69	1.667	-2.270	4	1.813	-1.847
A90/1377	30 39-30.51	30.45	1.720	-2.481	4	1.938	-1.847
A90/1383	30 29-30.37	30.32	1.705	-2.950	2	2.086	-1.847
A90/1380	30 11-30.19	30.15	1.400	-3.557	5	1.990	-1.847
A90/1379	29 99-30.03	30.01	1.151	-3.899		1.859	-1.847
A90/1378	29 65-29.70	29.68	1.741	-2.649	4	2.018	-1.847

Table 3: Detailed sample set extracted from Table 2, with corresponding normalised values.

Sample Number	Sample type	$\delta^{13}\text{C}$	$\delta^{18}\text{O}$
A90/4509	matrix	2.828	-2.232
A90/4510	edge sil.nod.	1.596	-4.000
A90/4511	centre sil. nod	1.889	-3.584
A90/4512	oyster	2.381	-3.064
A90/4513	matrix	2.375	-1.903
A90/4514	weak sil.nod.	2.659	-2.065

Table 4: Isotopic data from repeated drillings of a single hand specimen showing patchy silicification, collected from the top glauconitic pebble-shell bed in the uppermost Foxmould at Whitecliff, Beer (SY 234 893).

Sample Number	Oyster posn.	$\delta^{13}\text{C}$	$\delta^{18}\text{O}$	$\delta^{13}\text{C}$ normd.	$\delta^{18}\text{O}$ normd.
A90/4508	48.68	3.530	-2.507		
A90/4192	48.67	2.810	-1.785	3.153	-1.319
A90/4496	48.62	2.991	-1.830	3.367	-1.319
A90/4196	44.02	2.823	-2.025	3.343	-1.319
A90/4506	41.62	2.499	-2.542	3.399	-1.319
A90/4498	40.72	2.918	-1.319	2.918	-1.319
A90/4507	40.05	3.062	-1.708	3.348	-1.319
A90/1457	39.20	2.903	-1.475	3.018	-1.319
A90/4199	38.57	0.814	-2.646	1.791	-1.319
A90/1456	37.40	2.583	-2.131	3.181	-1.319
A90/4493	36.50	2.953	-1.910	3.388	-1.319
A90/1453	36.15	2.149	-2.511	3.026	-1.319
A90/4194	35.85	1.813	-2.225	2.480	-1.319
A90/4200	35.40	1.096	-2.860	2.230	-1.319
A90/4494	35.15	1.596	-3.774	3.403	-1.319
A90/4193	34.70	1.797	-2.823	2.904	-1.319
A90/4503	34.65	2.484	-3.148	3.830	-1.319
A90/4502	34.15	1.990	-3.814	3.826	-1.319
A90/4195	34.00	2.052	-2.426	2.867	-1.319
A90/4505	33.45	2.179	-3.120	3.505	-1.319
A90/4198	33.15	2.220	-2.265	2.916	-1.319
A90/4197	32.30	2.825	-1.733	3.129	-1.319
A90/4499	32.10	1.544	-4.320	3.753	-1.319
A90/1458	31.95	1.486	-3.932	3.409	-1.319
A90/4190	31.50	2.220	-3.345	3.711	-1.319
A90/4501	31.00	1.351	-4.237	3.499	-1.319
A90/4497	30.45	2.819	-2.947	4.017	-1.319
A90/4500	26.50	2.352	-1.924	2.797	-1.319
A90/4191	26.00	4.050	-2.987		
A90/1459	25.25	1.143	-2.755		

Table 5: Carbon- and oxygen-isotopic data from oysters collected throughout the Little Beach - Beer Head section. Normalised data reflects modification to remove postulated silica diagenesis.

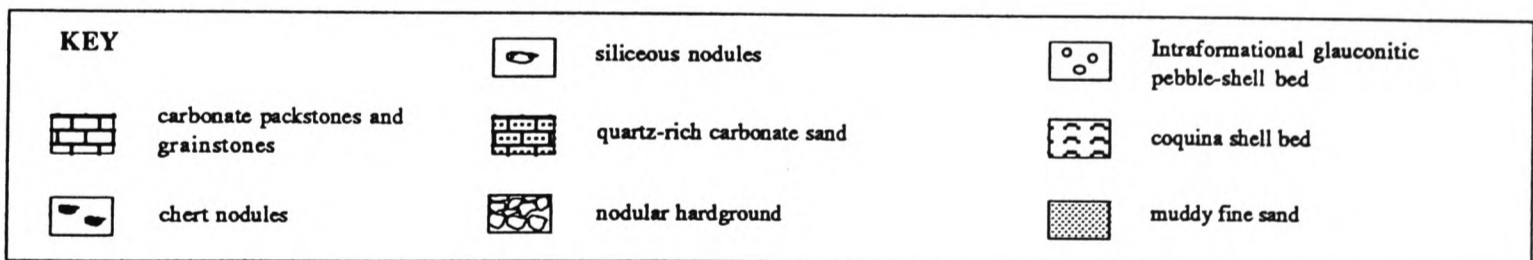
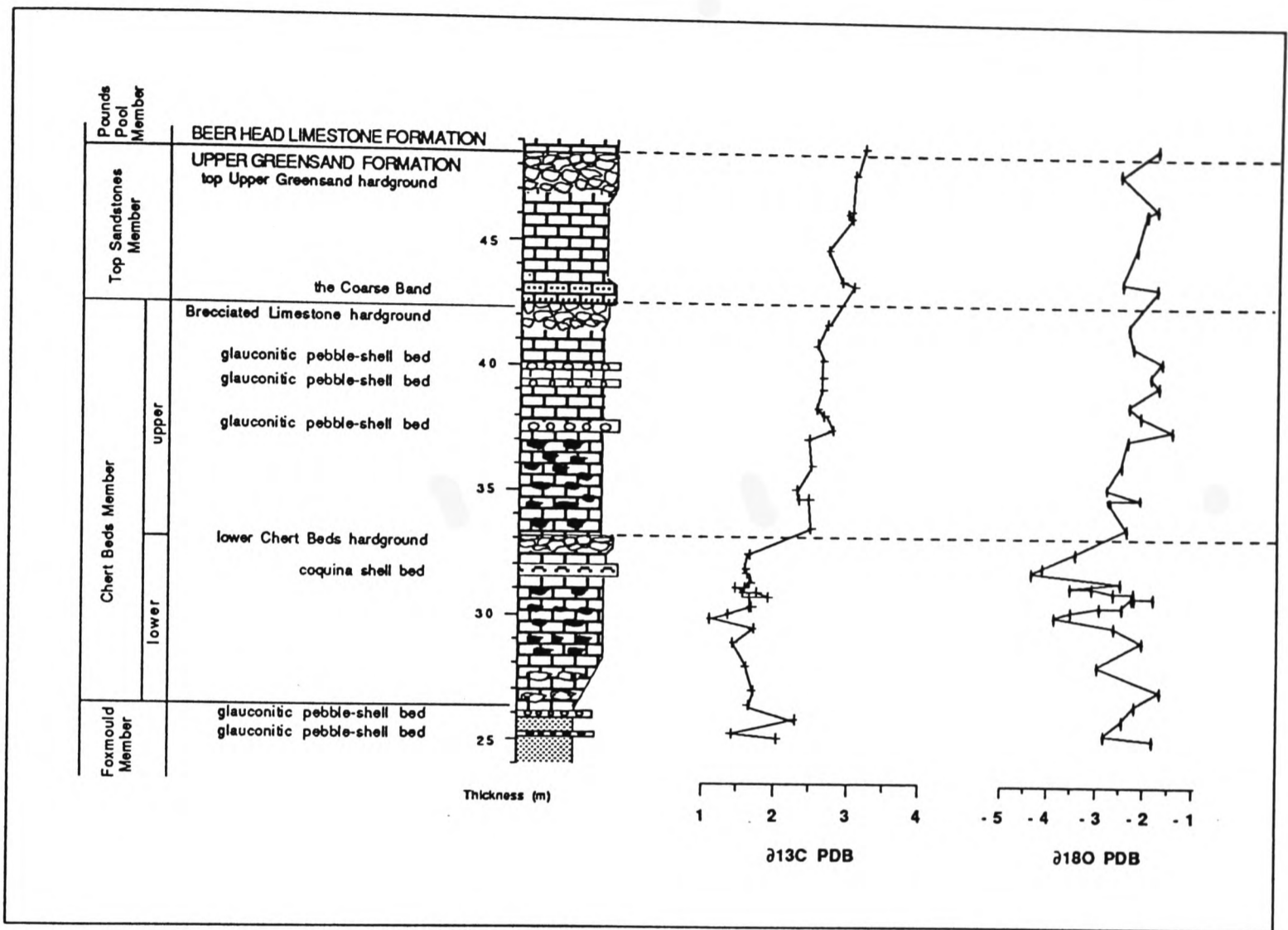


Fig.99: Carbon- and oxygen-stable isotope stratigraphy of the Upper Greensand (Chert Beds and Top Sandstones Members), Little Beach - Beer Head, south-east Devon. The $\delta^{13}\text{C}$ and $\delta^{18}\text{O}$ values are measured from whole-rock carbonate samples. The accompanying lithostratigraphy shows the subdivision of the Upper Greensand in south-east Devon.

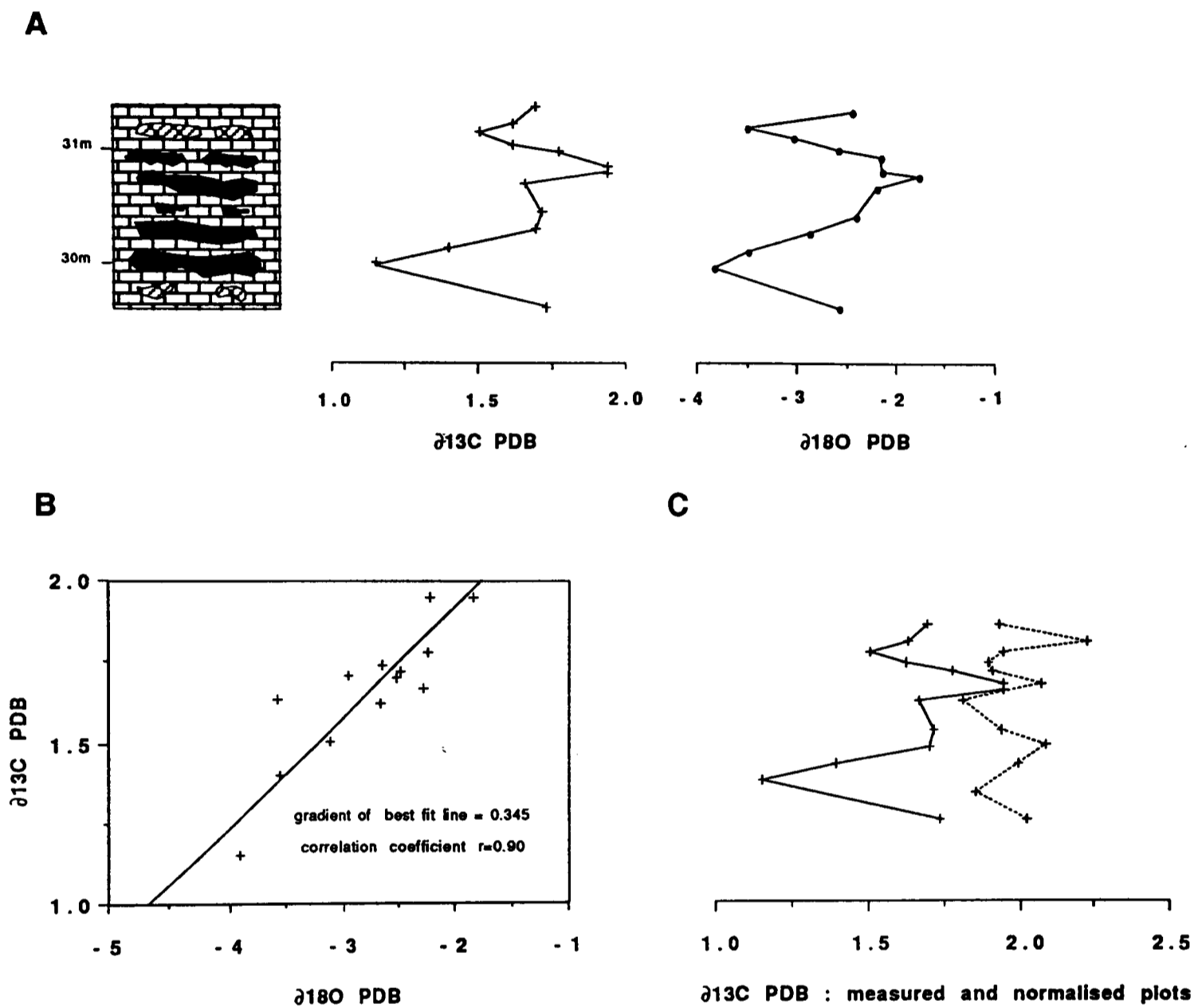


Fig.100: Investigation of the isotopic modification resulting from silica diagenesis.

Fig.100A: the isotopic changes across 1.63m of the lower Chert Beds, showing the positions of prominent chert nodules and nodules of siliceous limestone.

Fig.100B: plot of $\delta^{13}\text{C}$ vs $\delta^{18}\text{O}$, showing the good positive correlation, and the best fit line, the gradient of which represents the isotopic changes caused by silicification.

Fig.100C: original carbon-isotope plot and normalised plot (dotted), removing the effects of silicification.

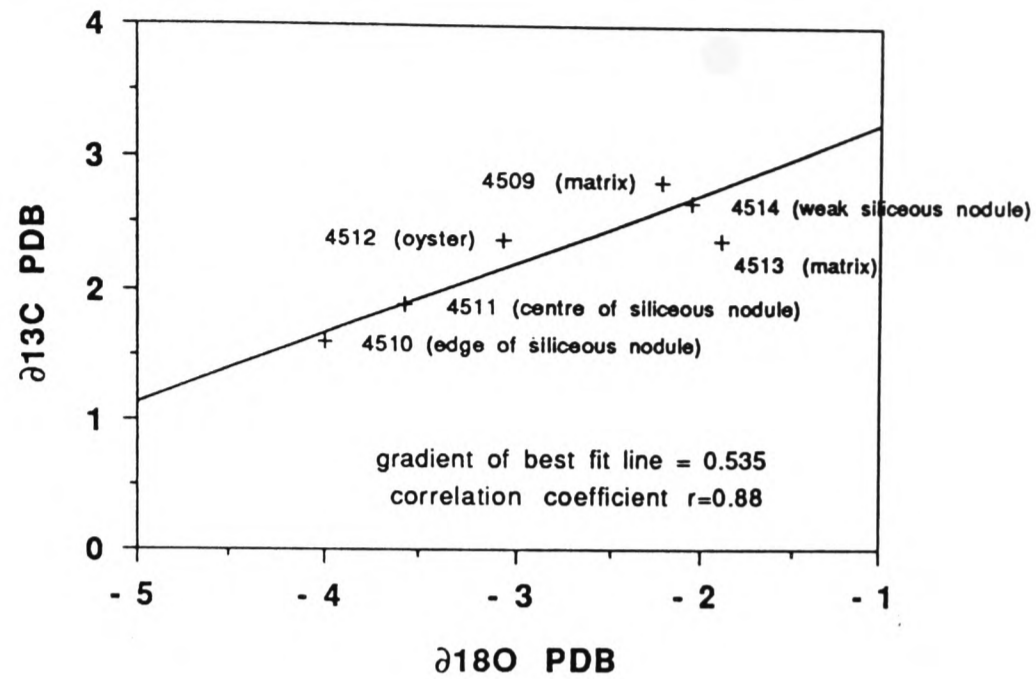


Fig.101: Plot of $\delta^{13}\text{C}$ vs $\delta^{18}\text{O}$ values recorded from repeated drillings of a single hand specimen showing patchy silicification, collected from the top glauconitic pebble-shell bed of the uppermost Foxmould at Whitecliff, Beer (SY 234 893).

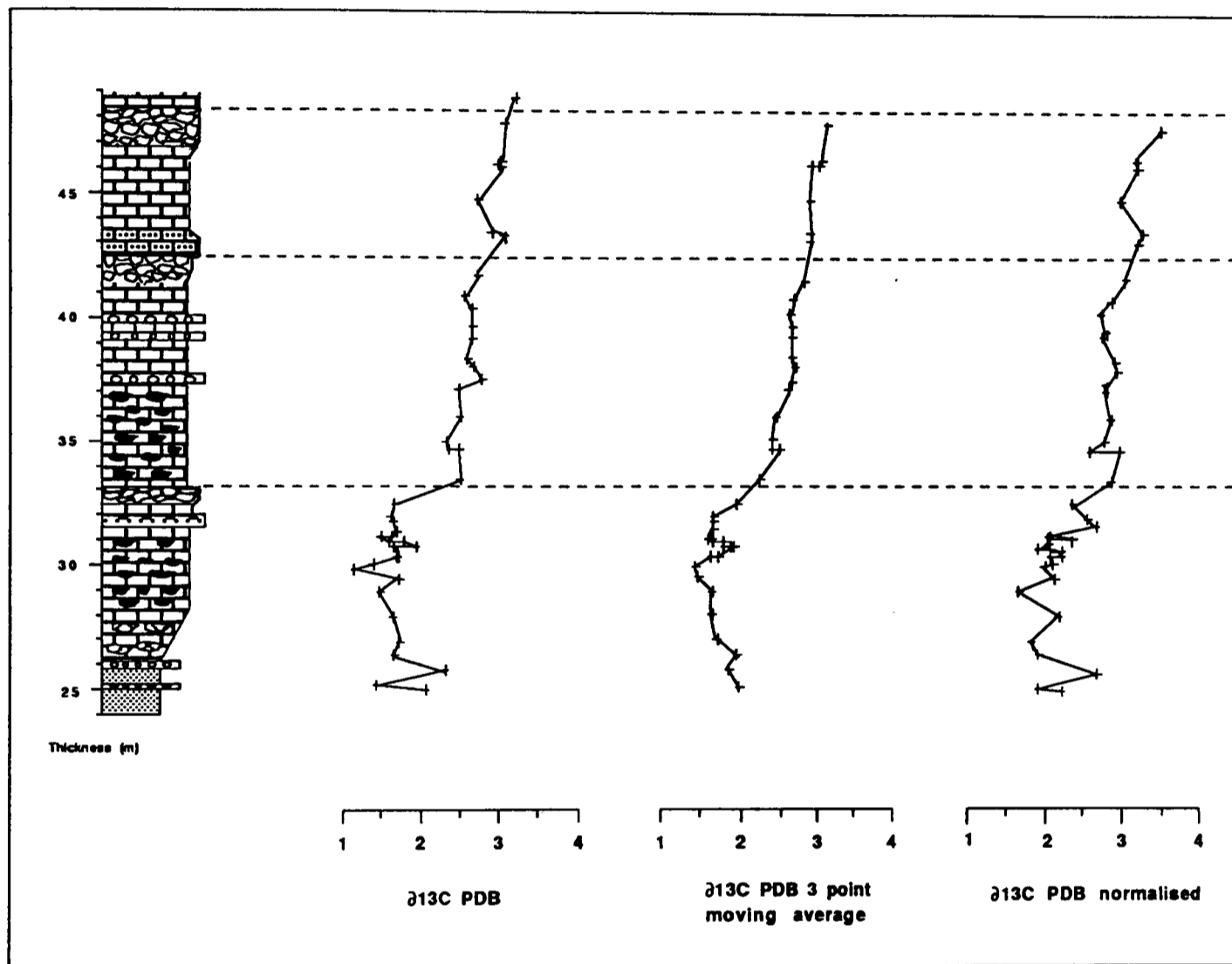


Fig.102: Carbon-isotope stratigraphy of the Upper Greensand (Chert Beds and Top Sandstones), Beer Head - Little Beach. The three plots show measured $\delta^{13}\text{C}$ values, three point moving average of measured $\delta^{13}\text{C}$ values, and $\delta^{13}\text{C}$ values normalised to remove the variations assumed to represent changes due to silicification.

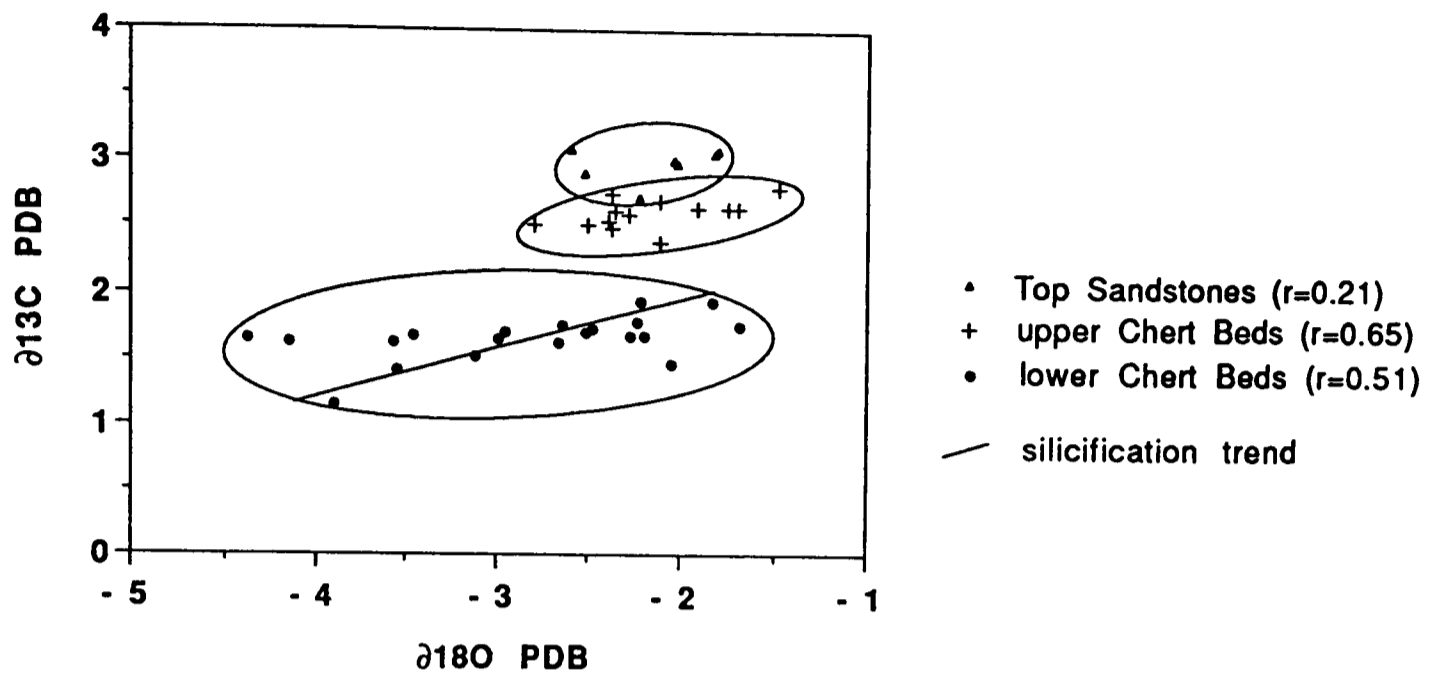


Fig.103: Plot of $\delta^{13}\text{C}$ vs $\delta^{18}\text{O}$ values for the whole rock data set (Little Beach - Beer Head section). Data from the lower Chert Beds, upper Chert Beds and the Top Sandstones plot as three distinct groups, with little or no overlap. The silicification trend established in Figure 5B is shown for the lower Chert Beds. Data from the upper Chert Beds, and possibly the Top Sandstones, also show a scatter of values inferring that a major control on recorded $\delta^{13}\text{C}$ values (low variability within each group) was silica diagenesis. The plot clearly displays the abrupt positive shift between the lower and upper Chert Beds, and shows that it is not caused by silicification.

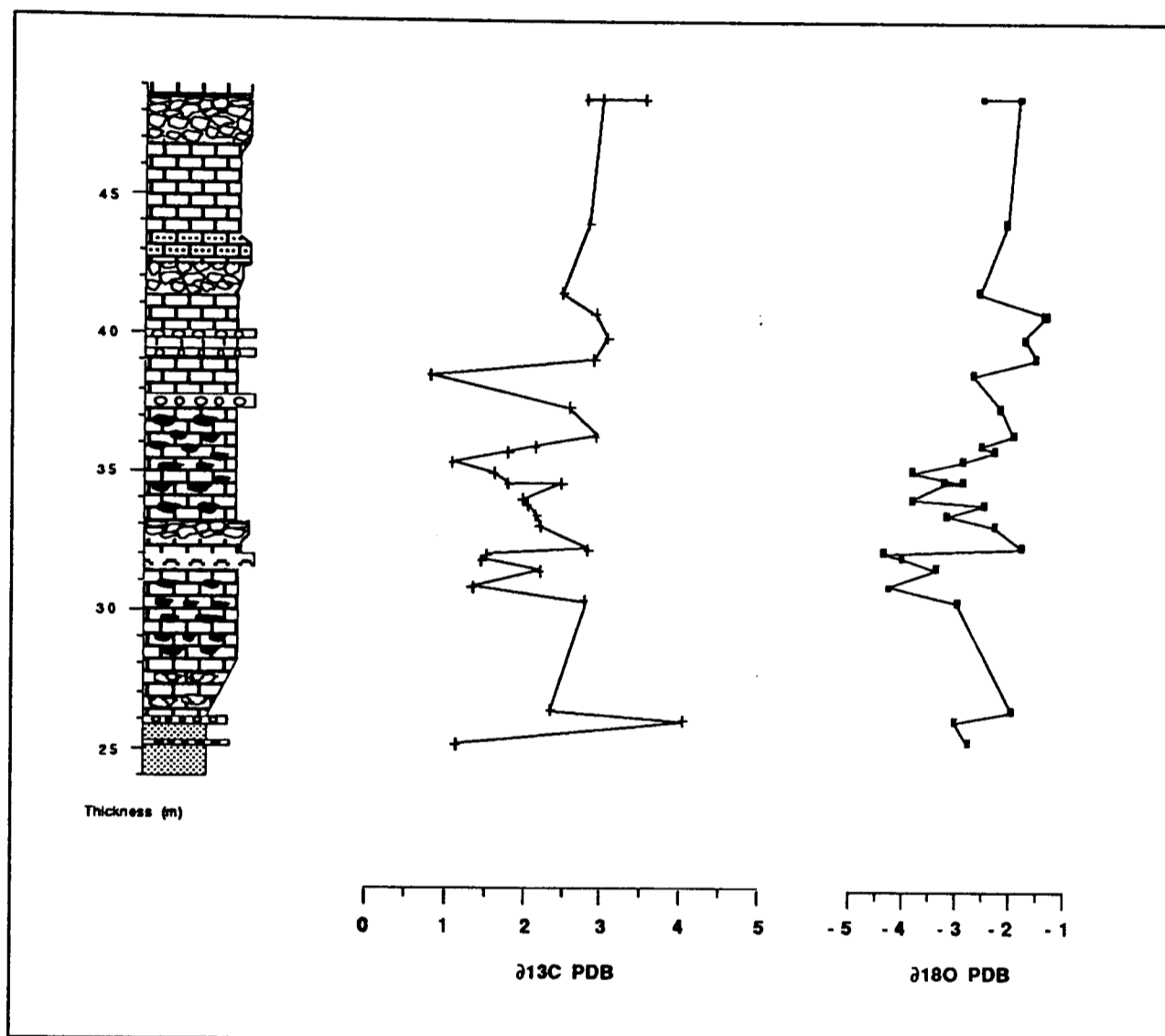


Fig.104: Carbon- and oxygen-isotope stratigraphy of the Upper Greensand (Little Beach - Beer Head). The isotopic values are from oysters collected throughout the succession.

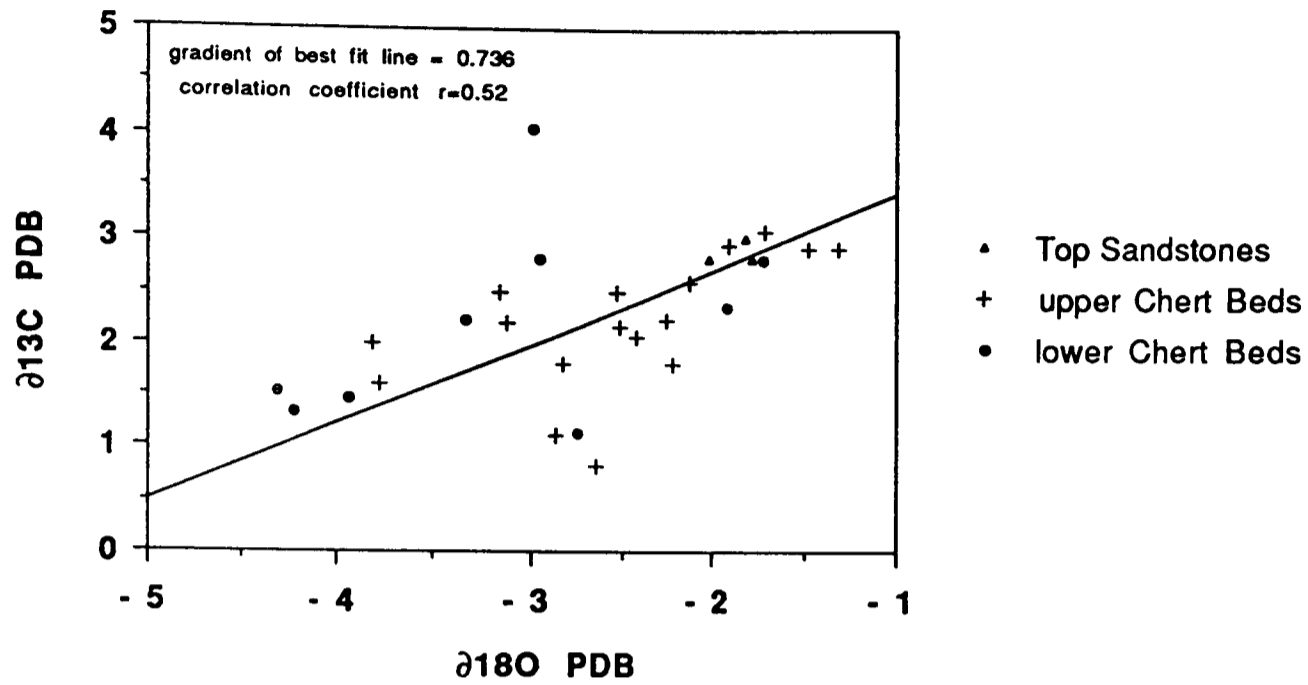


Fig.105: Plot of $\delta^{13}\text{C}$ vs $\delta^{18}\text{O}$ values for the oyster data set (Little Beach - Beer Head section). Data from the lower Chert Beds, upper Chert Beds and Top Sandstones plotted separately. A high degree of scatter is shown, with little indication of any secular changes. Some degree of correlation establishes a tentative silicification modification trend.

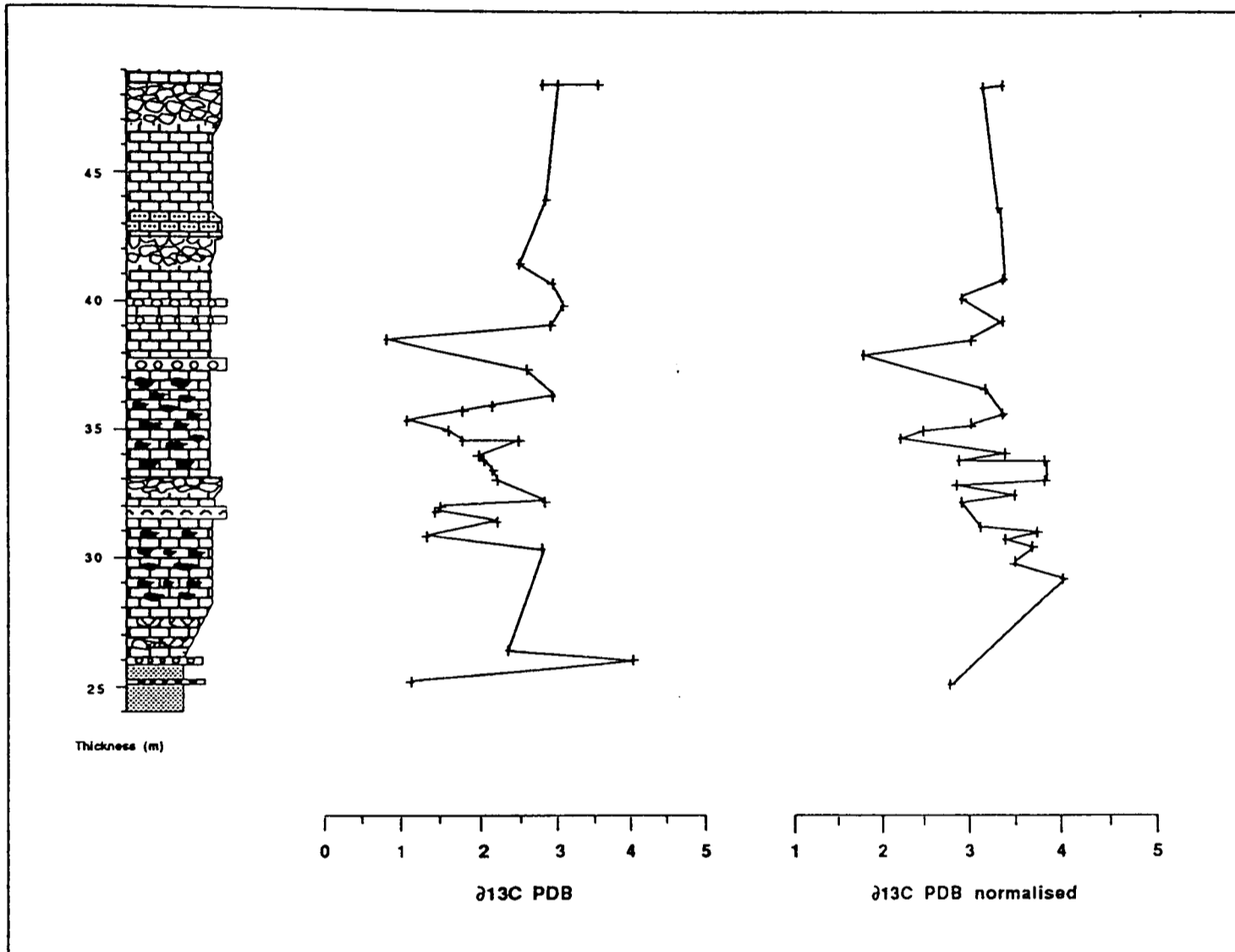


Fig.106: Carbon-isotope stratigraphy from oyster samples (Little Beach - Beer Head section). The two plots show measured $\delta^{13}\text{C}$ values, and $\delta^{13}\text{C}$ values normalised to remove the variations interpreted as due to silicification.

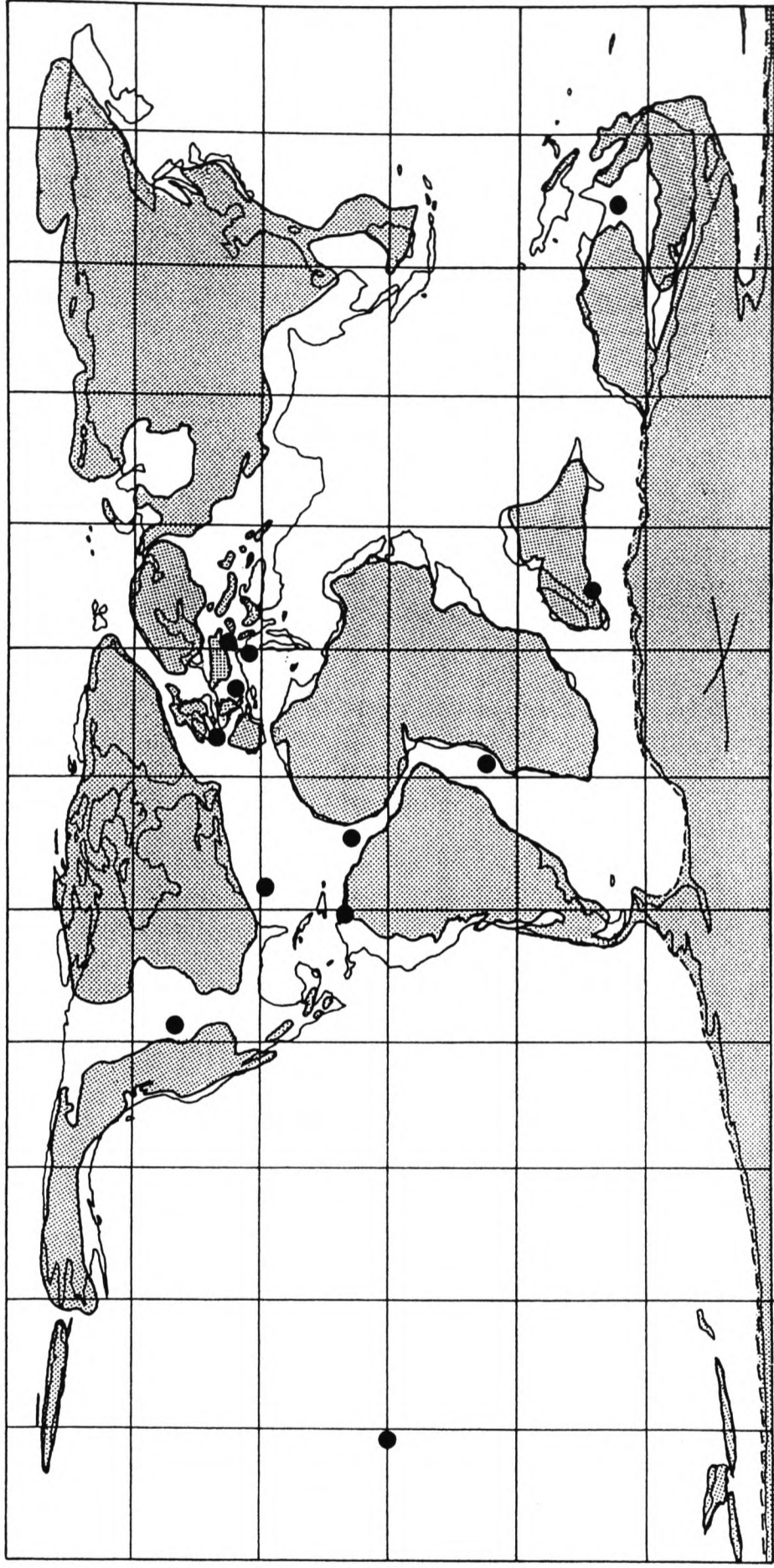


Fig.107: Global distribution of Upper Albian black shales (discussed in the text), plotted on an Albian (105Ma) palaeogeographic reconstruction of Funnel (1990).

MICROPROBE CHEMICAL ANALYSES OF GLAUCONITIC GRAINS

TABLE 6. Microprobe chemical analyses of glauconitic grains from the Foxmould Member, Upper Greensand Formation, Beer, south-east Devon.

Total iron is given as Fe₂O₃ in the analyses of this and the following tables.

wt%	F1	F2	F3	F4	F5	F6	F7	F8	F9	F10	F11	F12	F13	F14	F15	AV.F1-15
SiO ₂	53.73	51.24	52.63	52.71	53.52	51.86	53.67	48.09	46.06	52.33	53.64	46.03	42.41	25.99	48.39	48.81
K ₂ O	8.15	8.30	8.66	6.81	8.21	8.60	8.15	8.19	7.52	8.49	8.28	8.11	4.47	3.27	8.28	7.57
Fe ₂ O ₃	19.83	25.35	20.84	20.44	21.83	21.01	19.87	20.16	18.94	21.98	20.12	11.22	21.42	20.96	17.13	20.07
Al ₂ O ₃	8.26	7.27	7.70	8.97	7.96	7.74	9.34	6.85	7.51	7.86	9.79	20.37	12.63	5.09	15.27	9.51
MgO	4.07	3.47	4.00	3.45	3.82	4.01	3.87	3.66	3.28	3.63	3.57	2.12	6.34	1.87	2.79	3.60
CaO	0.36	0.34	0.26	0.83	0.43	0.19	0.50	0.30	0.30	0.26	0.42	0.36	0.64	0.74	0.43	0.42
Na ₂ O	0.09	0.09	0.02	0.11	0.09	0.09	0.11	0.02	0.09	0.07	0.07	0.22	0.13	0.14	0.18	0.10
MnO ₂	0.05	0.01	0.05	0.09	0.01	0.03	0.04	0.01	0.03	0.04	0.01	0.04	0.16	0.08	0.01	0.04
TiO ₂	0.07	0.05	0.04	0.11	0.04	0.05	0.07	0.05	0.04	0.04	0.09	0.24	0.27	31.20*	0.16	0.09
P ₂ O ₅	0.00	0.12	0.03	0.03	0.03	0.09	0.03	0.06	0.06	0.06	0.00	0.18	0.03	0.03	0.06	0.05
Total	94.77	94.24	94.23	93.55	95.94	93.67	95.65	87.39	83.83	94.76	95.99	88.89	88.50	89.37	92.70	92.23

TABLE 7. Microprobe chemical analyses of glauconitic grains from the uppermost Foxmould member, Upper Greensand Formation, Beer, south-east

Devon.

wt%	TF1	TF2	TF3	TF4	TF5	TF6	TF7	TF8	TF9	TF10	TF11	TF12	TF13	TF14	TF15	TF16	TF17	AV.TF1-17
SiO ₂	51.02	52.65	51.45	51.19	51.05	52.13	51.92	52.56	51.93	48.68	50.60	50.79	51.12	48.90	51.93	54.07	50.64	51.32
K ₂ O	7.12	8.20	8.10	7.37	7.30	7.41	8.09	6.74	7.48	7.17	7.19	7.30	7.46	6.66	7.92	7.95	7.50	7.47
Fe ₂ O ₃	17.02	21.31	20.59	16.38	15.81	17.10	20.04	16.53	17.95	15.17	16.03	16.32	16.63	16.96	18.57	18.24	19.43	17.65
Al ₂ O ₃	7.83	7.26	6.88	7.91	7.88	8.88	7.40	10.08	8.30	10.56	7.92	7.84	7.83	7.90	8.04	8.44	7.23	8.13
MgO	4.04	3.71	3.97	4.35	4.59	3.88	3.86	4.23	3.96	4.12	4.28	4.37	4.50	3.51	3.83	4.31	3.91	4.08
CaO	0.34	0.60	0.33	0.53	0.88	0.49	0.36	0.93	0.40	0.67	0.36	0.46	0.47	0.40	0.40	0.66	0.34	0.51
Na ₂ O	0.13	0.00	0.07	0.34	0.35	0.05	0.05	0.09	0.09	0.11	0.09	0.12	0.07	0.05	0.11	0.02	0.13	0.11
MnO ₂	0.03	0.01	0.00	0.03	0.01	0.04	0.05	0.04	0.04	0.04	0.00	0.00	0.01	0.00	0.03	0.04	0.05	0.02
TiO ₂	0.09	0.07	0.05	0.09	0.05	0.07	0.04	0.07	0.07	0.07	0.07	0.07	0.07	0.11	0.07	0.05	0.09	0.07
P ₂ O ₅	0.00	0.12	0.00	0.03	0.03	0.03	0.00	0.06	0.03	0.09	0.03	0.03	0.00	0.00	0.03	0.09	0.00	0.03
Total(%)	87.62	93.93	91.44	88.22	87.95	90.08	91.81	91.33	90.25	86.68	86.57	87.30	88.16	84.49	90.93	93.87	89.32	89.35

TABLE 8. Microprobe chemical analyses of glauconitic grains from the Chert Beds, Upper Greensand Formation, Beer, south-east Devon.

wt%	CB1	CB2	CB3	CB4	CB5	CB6	CB7	CB8	CB9	CB10	CB11	AV.CB1-11
SiO ₂	49.65	50.78	51.14	51.67	46.55	51.29	51.60	51.09	51.12	50.88	38.79	49.51
K ₂ O	7.63	7.40	6.99	8.01	7.64	8.42	8.48	7.64	7.52	8.46	5.92	7.65
Fe ₂ O ₃	16.54	20.82	19.18	19.06	19.15	21.22	21.87	20.22	17.88	21.15	12.10	19.02
Al ₂ O ₃	9.38	8.18	8.37	8.91	6.99	7.48	7.49	7.81	9.62	7.62	11.07	8.45
MgO	4.45	4.06	4.60	4.24	3.80	4.13	4.01	3.91	4.56	3.98	2.51	4.02
CaO	1.71	0.50	0.21	0.43	0.51	0.34	0.52	0.54	0.67	0.36	0.49	0.57
Na ₂ O	0.09	0.06	0.05	0.04	0.07	0.02	0.02	0.02	0.09	0.06	0.14	0.06
MnO ₂	0.03	0.00	0.03	0.00	0.00	0.01	0.01	0.03	0.04	0.01	0.01	0.01
TiO ₂	0.14	0.09	0.07	0.09	0.07	0.04	0.05	0.07	0.11	0.04	0.25	0.09
P ₂ O ₅	0.00	0.00	0.00	0.03	0.03	0.03	0.03	0.03	0.00	0.00	0.03	0.02
Total	89.62	91.89	90.64	92.48	84.81	92.98	94.08	91.36	92.61	92.56	71.31	89.49

TABLE 9. Microprobe chemical analyses of glauconitic grains from the Chert Beds, Upper Greensand Formation, Beer, south-east Devon.

wt%	CB12	CB13	CB14	CB15	CB16	CB17	CB18	CB19	CB20	CB21	CB22	Av. CB12-2
SiO ₂	46.81	47.93	46.61	49.03	49.66	40.35	49.29	49.21	51.91	47.42	50.57	48.07
K ₂ O	6.26	6.12	6.31	6.61	6.63	5.44	6.47	7.46	8.24	6.45	8.12	6.74
Fe ₂ O ₃	17.59	17.99	17.53	18.17	18.61	14.62	17.35	19.77	17.32	17.53	21.03	17.96
Al ₂ O ₃	7.66	8.01	8.08	8.66	8.76	6.98	9.30	7.47	9.57	8.26	6.90	8.15
MgO	3.49	3.51	3.54	3.52	3.65	3.32	3.67	3.80	4.08	3.78	3.94	3.66
CaO	0.58	0.77	1.00	0.63	0.61	5.56*	0.96	0.43	0.65	0.43	0.57	0.66
Na ₂ O	0.15	0.20	0.29	0.16	0.04	0.26	0.18	0.11	0.00	0.24	0.07	0.15
MnO ₂	0.07	0.03	0.04	0.01	0.03	0.03	0.07	0.03	0.01	0.03	0.01	0.03
TiO ₂	0.07	0.13	0.25	0.07	0.11	0.07	0.16	0.11	0.07	0.05	0.02	0.10
P ₂ O ₅	0.06	0.06	0.09	0.03	0.03	0.00	0.03	0.03	0.03	0.03	0.03	0.04
Total	82.74	84.75	83.74	86.89	88.13	76.63	87.43	88.42	91.88	84.22	91.26	86.01

TABLE 10. Microprobe chemical analyses of glauconitic grains from the top Upper Greensand hardground, Beer, south-east Devon.

wt%	HG1	HG2	HG3	HG4	HG5	Av. HG1-5
SiO ₂	43.34	44.83	44.85	46.32	34.60	42.79
K ₂ O	5.88	6.33	6.77	4.75	3.86	5.52
Fe ₂ O ₃	14.27	16.26	13.34	11.11	8.80	12.76
Al ₂ O ₃	6.75	6.22	7.61	8.70	7.50	7.36
MgO	3.57	3.58	4.13	4.07	3.48	3.77
CaO	0.64	0.48	0.22	0.77	1.08	0.64
Na ₂ O	0.02	0.09	0.07	0.07	0.05	0.06
MnO ₂	0.01	0.05	0.01	0.04	0.00	0.02
TiO ₂	0.04	0.04	0.02	0.05	0.04	0.04
P ₂ O ₅	0.06	0.06	0.00	0.03	0.03	0.04
Total	74.58	77.94	78.02	75.91	59.44	73.18

TABLE 11. Microprobe chemical analyses of glauconitic grains from the Dispar Zone Ammonite Bed, Durdle Cove, south Dorset.

wt%	DZ1	DZ2	DZ3	DZ4	DZ5	DZ6	DZ7	DZ8	DZ9	DZ10	DZ11	DZ12	DZ13	DZ14	DZ15	DZ16	DZ17	DZ18	DZ19	AV.DZ1-DZ
SiO ₂	37.35	51.42	51.53	51.65	51.18	51.60	52.32	51.96	51.46	51.38	50.19	50.45	50.71	51.52	51.32	50.28	50.59	51.34	51.13	50.55
K ₂ O	5.91	8.01	7.54	7.84	8.34	7.21	8.76	7.82	8.64	8.16	7.62	8.11	7.58	8.02	8.38	8.26	8.13	7.84	8.13	7.91
Fe ₂ O ₃	10.70	18.96	18.70	17.83	19.62	19.06	18.92	19.39	19.61	19.36	20.93	20.65	20.42	19.53	20.50	19.97	19.91	18.53	19.29	19.05
Al ₂ O ₃	11.05	8.19	9.49	10.25	6.78	9.21	6.80	9.28	6.49	8.22	7.25	6.45	7.86	8.56	5.75	6.17	7.45	9.22	6.28	8.03
MgO	2.41	3.92	3.84	3.98	4.10	3.77	4.46	3.70	4.32	3.82	3.64	3.96	3.58	3.80	4.32	4.18	3.87	3.93	4.23	3.89
CaO	0.98	0.40	0.56	0.45	0.29	0.63	0.20	0.46	0.22	0.36	0.49	0.43	0.56	0.50	0.26	1.27	0.59	0.47	0.33	0.50
Na ₂ O	0.16	0.05	0.09	0.05	0.00	0.05	0.04	0.00	0.05	0.05	0.06	0.04	0.02	0.02	0.06	0.06	0.02	0.02	0.00	0.04
MnO ₂	0.00	0.00	0.00	0.03	0.00	0.00	0.05	0.01	0.01	0.01	0.01	0.00	0.01	0.01	0.01	0.03	0.00	0.01	0.00	0.01
TiO ₂	0.22	0.02	0.07	0.05	0.04	0.11	0.04	0.02	0.00	0.05	0.04	0.02	0.07	0.04	0.02	0.04	0.02	0.11	0.04	0.05
P ₂ O ₅	0.08	0.03	0.03	0.06	0.00	0.06	0.00	0.03	0.03	0.03	0.06	0.06	0.00	0.03	0.03	0.61	0.18	0.03	0.03	0.07
Total	68.86	91.00	91.85	92.19	90.35	91.70	91.59	92.76	90.83	91.44	90.29	90.17	90.81	92.03	90.65	90.87	90.76	91.50	89.46	89.95

TABLE 12. Microprobe chemical analyses of glauconitic grains from the Upper Greensand at Gore Cliff, Isle of Wight.

wt%	GC1	GC2	GC3	GC4	GC5	GC6	GC7	GC8	GC9	GC10	GC11	AV.GC1-11
SiO ₂	29.53	37.79	46.72	45.33	46.53	47.10	32.18	46.59	42.46	23.39	42.11	39.98
K ₂ O	2.44	5.67	6.77	6.40	6.84	5.70	4.53	6.41	5.00	3.07	3.92	5.16
Fe ₂ O ₃	8.88	13.39	16.30	16.47	16.07	14.21	9.44	15.33	8.72	7.62	9.92	12.40
Al ₂ O ₃	7.96	6.35	8.44	8.76	8.69	9.26	9.99	8.35	14.54	5.87	9.25	8.86
MgO	2.25	2.69	2.82	2.72	2.86	2.93	2.93	3.15	2.11	1.95	2.50	2.63
CaO	12.03	9.48	1.07	2.17	0.39	0.91	8.84	0.54	1.19	17.71	0.77	5.01
Na ₂ O	0.28	0.00	0.05	0.00	0.11	0.07	0.00	0.07	0.12	0.00	0.31	0.10
MnO ₂	0.05	0.05	0.04	0.00	0.01	0.00	0.05	0.04	0.01	0.01	0.00	0.02
TiO ₂	0.06	0.05	0.09	0.09	0.05	0.05	0.51	0.07	0.04	0.37	0.11	0.14
P ₂ O ₅	7.88	6.06	0.49	0.98	0.06	0.03	5.61	0.03	0.46	12.32	0.17	3.10
Total	71.36	80.53	82.79	82.92	81.61	80.26	74.08	80.58	74.65	72.26	69.06	77.28

TABLE 13. Microprobe chemical analyses of glauconitic grains from the basal Upper Greensand at Eastbourne.

wt%	E1	E2	E3	E4	E5	E6	E7	E8	E9	E10	E11	E12	E13	E14	AV.E1-14
SiO ₂	40.11	45.48	46.40	46.87	45.66	46.97	48.42	46.64	44.68	46.59	47.09	47.02	47.61	46.67	46.16
K ₂ O	5.94	6.40	6.63	6.62	6.59	6.75	6.51	6.84	5.90	6.77	6.65	6.92	7.04	6.98	6.61
Fe ₂ O ₃	11.06	12.47	11.92	10.75	13.60	14.04	12.15	14.56	11.87	13.67	12.23	14.97	13.26	13.16	12.84
Al ₂ O ₃	6.75	8.10	8.53	9.60	6.95	7.19	9.40	6.35	7.77	7.42	8.73	6.88	7.59	7.93	7.80
MgO	3.55	3.73	3.88	4.13	3.68	3.80	4.27	3.89	3.76	3.78	3.98	3.74	4.15	4.09	3.89
CaO	5.21	0.37	0.27	0.33	0.30	0.59	0.27	0.34	3.44	0.34	0.29	0.32	0.27	0.34	0.91
Na ₂ O	0.00	0.02	0.02	0.09	0.09	0.05	0.12	0.00	0.04	0.05	0.07	0.02	0.04	0.04	0.05
MnO ₂	0.03	0.01	0.03	0.01	0.00	0.01	0.00	0.00	0.00	0.00	0.01	0.01	0.01	0.03	0.01
TiO ₂	0.02	0.05	0.04	0.05	0.02	0.04	0.09	0.02	0.04	0.04	0.07	0.02	0.04	0.04	0.04
P ₂ O ₅	3.11	0.03	0.03	0.03	0.03	0.14	0.03	0.03	1.94	0.06	0.03	0.03	0.03	0.03	0.40
Total	75.78	76.66	77.75	78.48	76.92	79.58	81.26	78.67	79.44	78.72	79.15	79.93	80.04	80.31	78.76

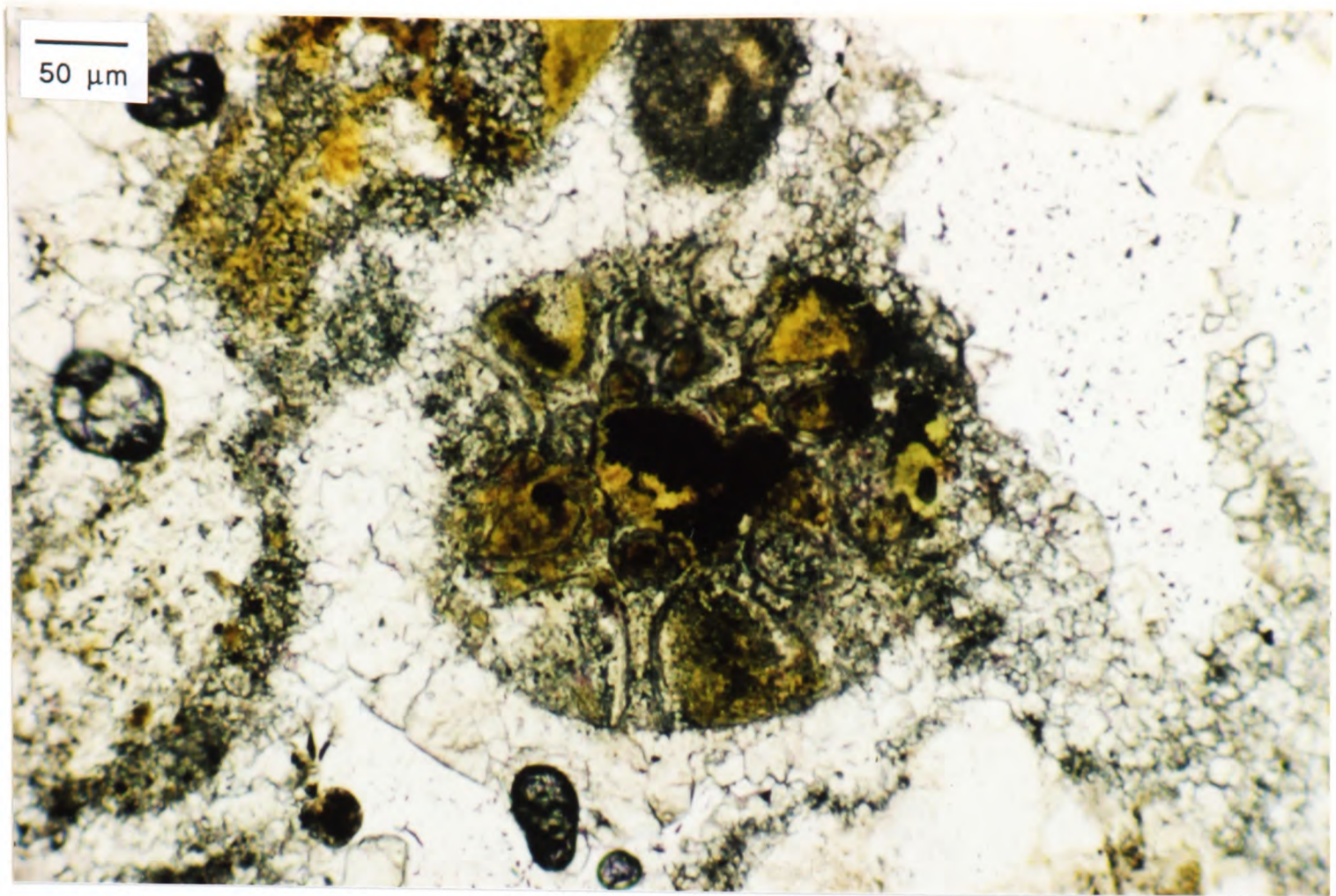


Fig.108: Photomicrograph of glauconite filling the porosity within a bryozoan bioclast: coquina bed in lower Chert Beds Member, Upper Greensand Formation, Little Beach, Beer, south-east Devon.

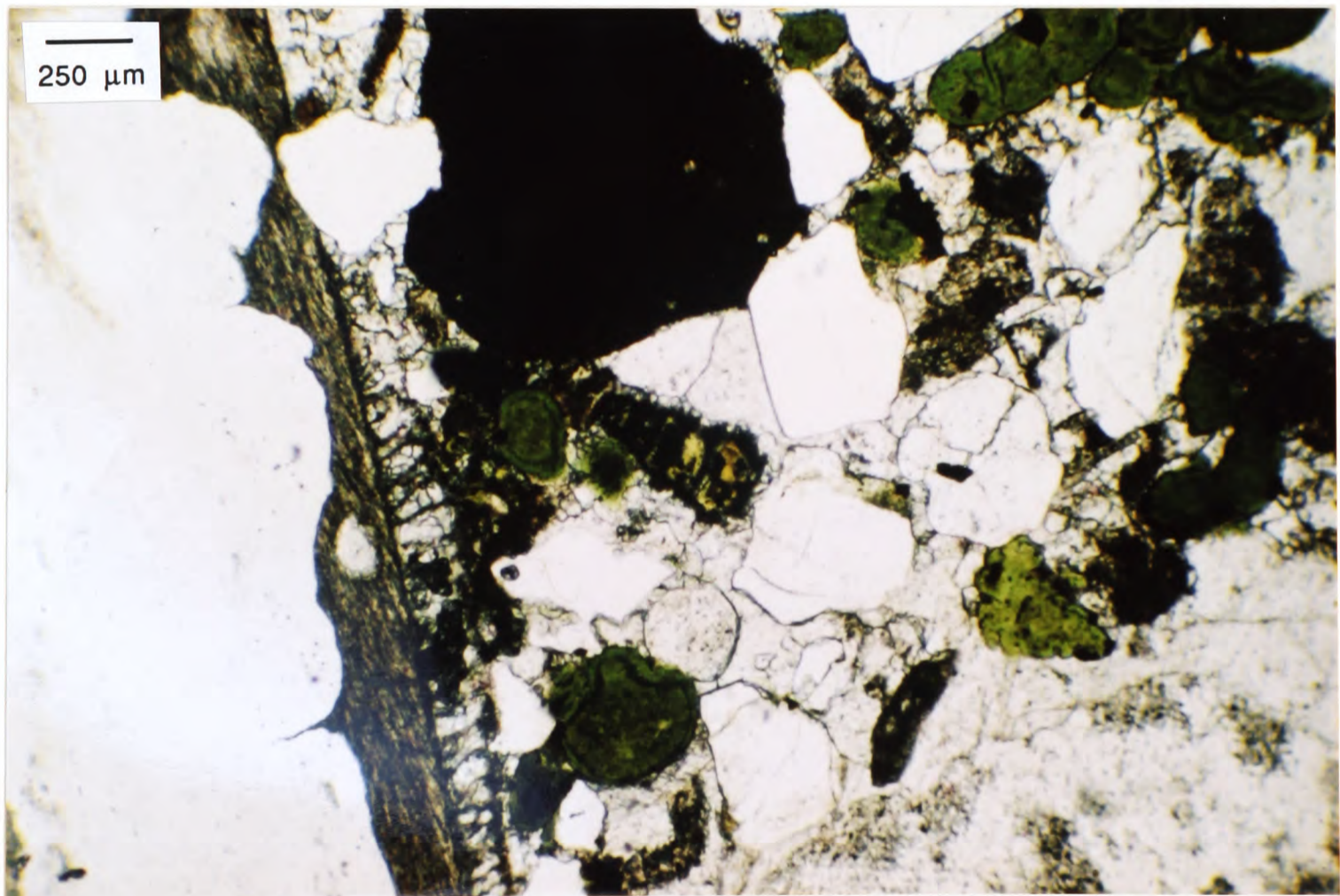


Fig.109: Photomicrograph of glauconite filling the chambers of a foraminifera, and rimmed grains with two accretion phases: middle pebble-shell bed in uppermost Foxmould interval of glauconitic pebble-shell beds, Upper Greensand Formation, Whitecliff, Beer, south-east Devon.

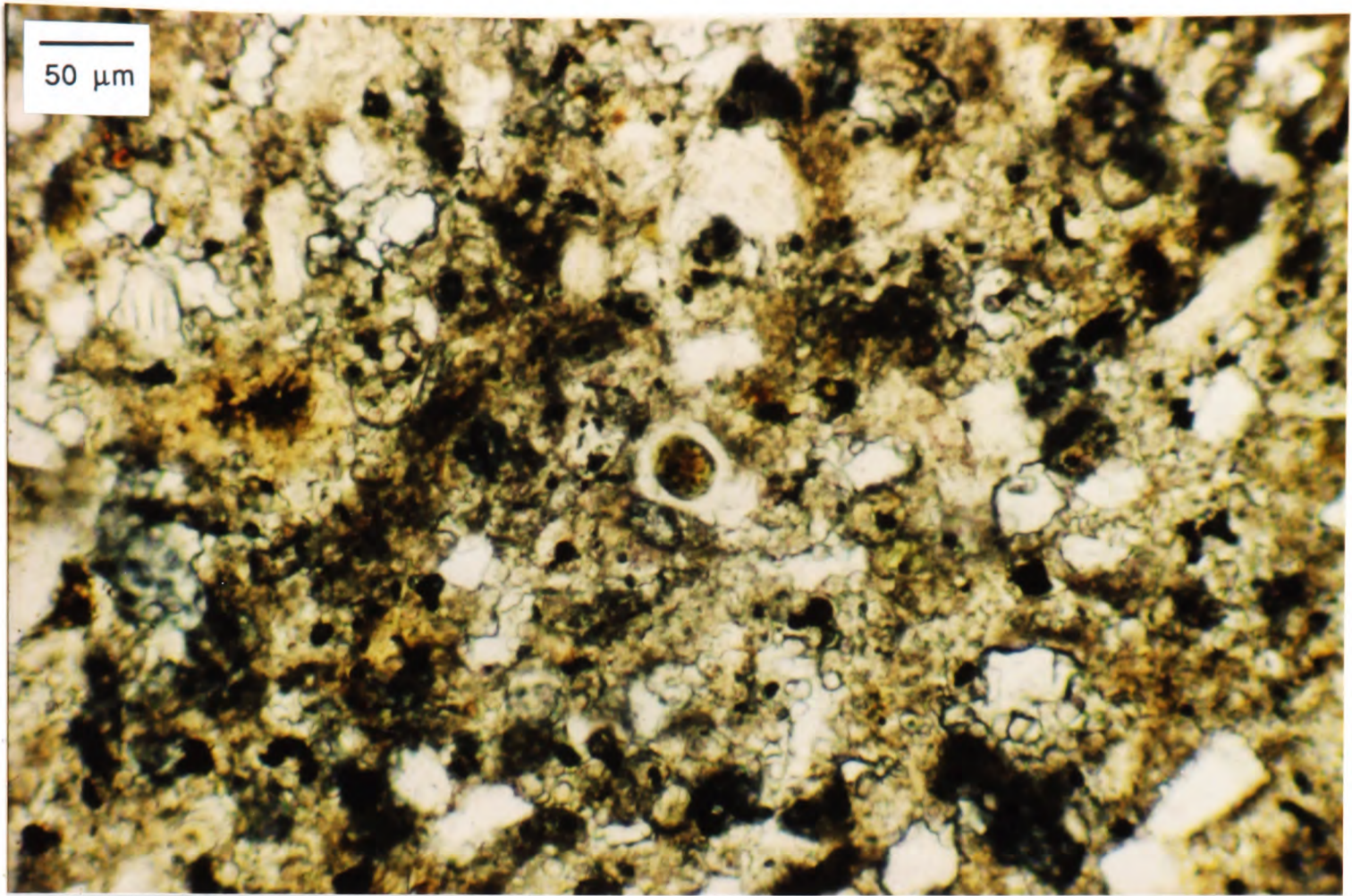


Fig.110: Photomicrograph of glauconite filling the axial canal of a sponge spicule (transverse section): Blue Rag, Upper Greensand, Hollows Lane, Selbourne, western Weald.

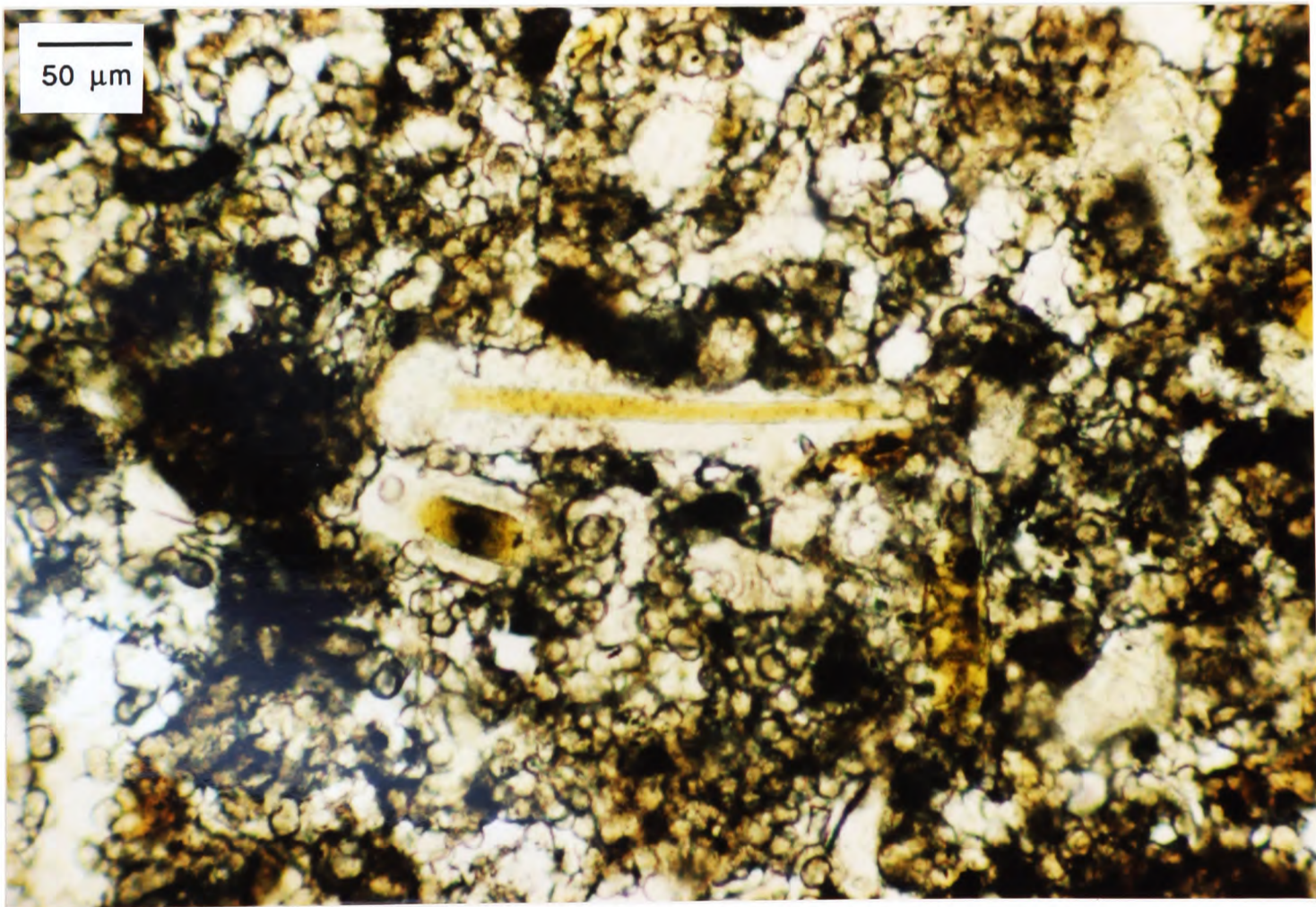


Fig.111: Photomicrograph of glauconite filling the axial canal of a sponge spicule (longitudinal section): Blue Rag, Upper Greensand, Hollows Lane, Selbourne, western Weald.

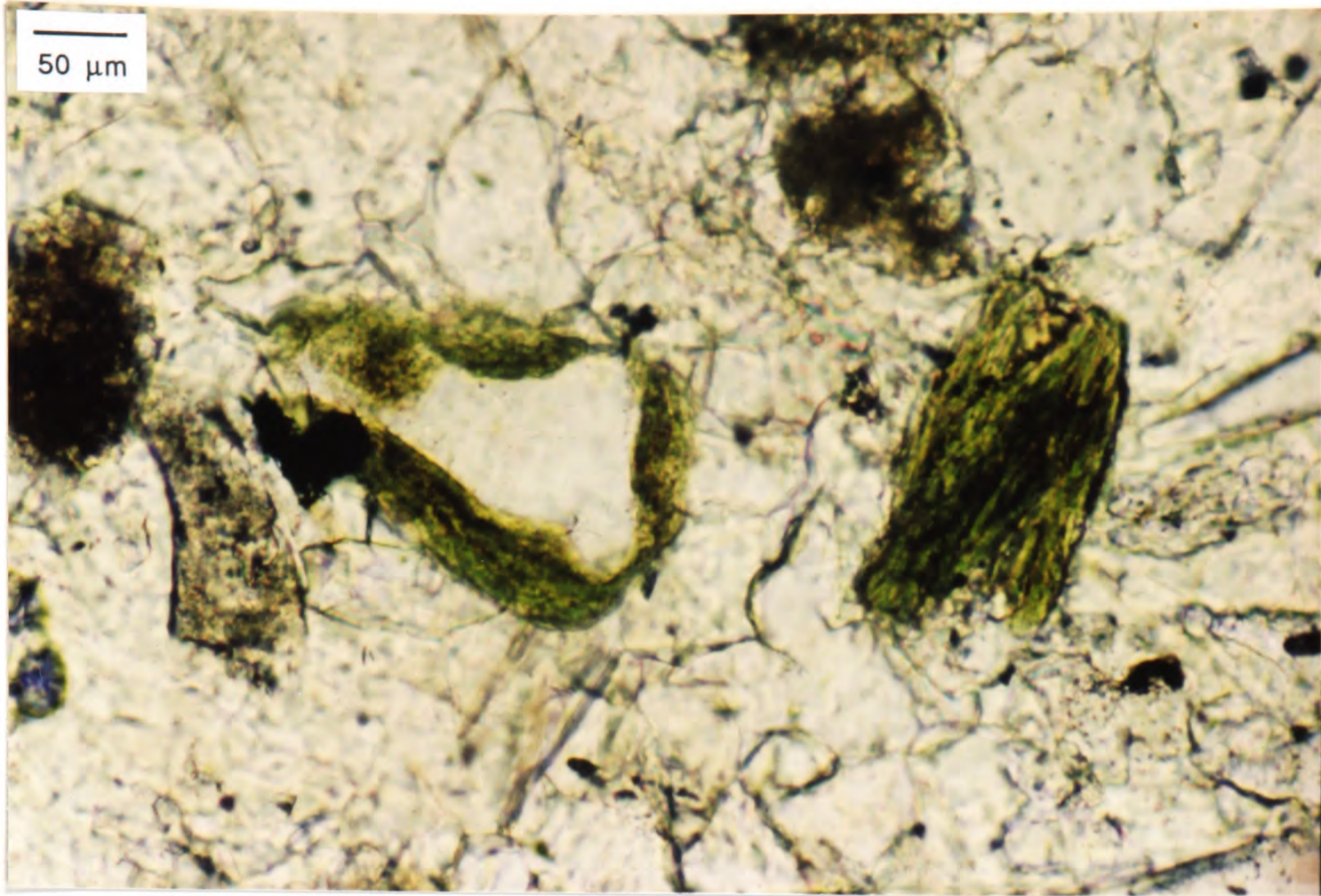


Fig.112: Photomicrograph of glauconite rimming a quartz grain, and a vermicular glauconitic grain: upper thick storm laminite bed, Foxmould Member, Upper Greensand Formation, Hooken Cliffs, Beer, south-east Devon.

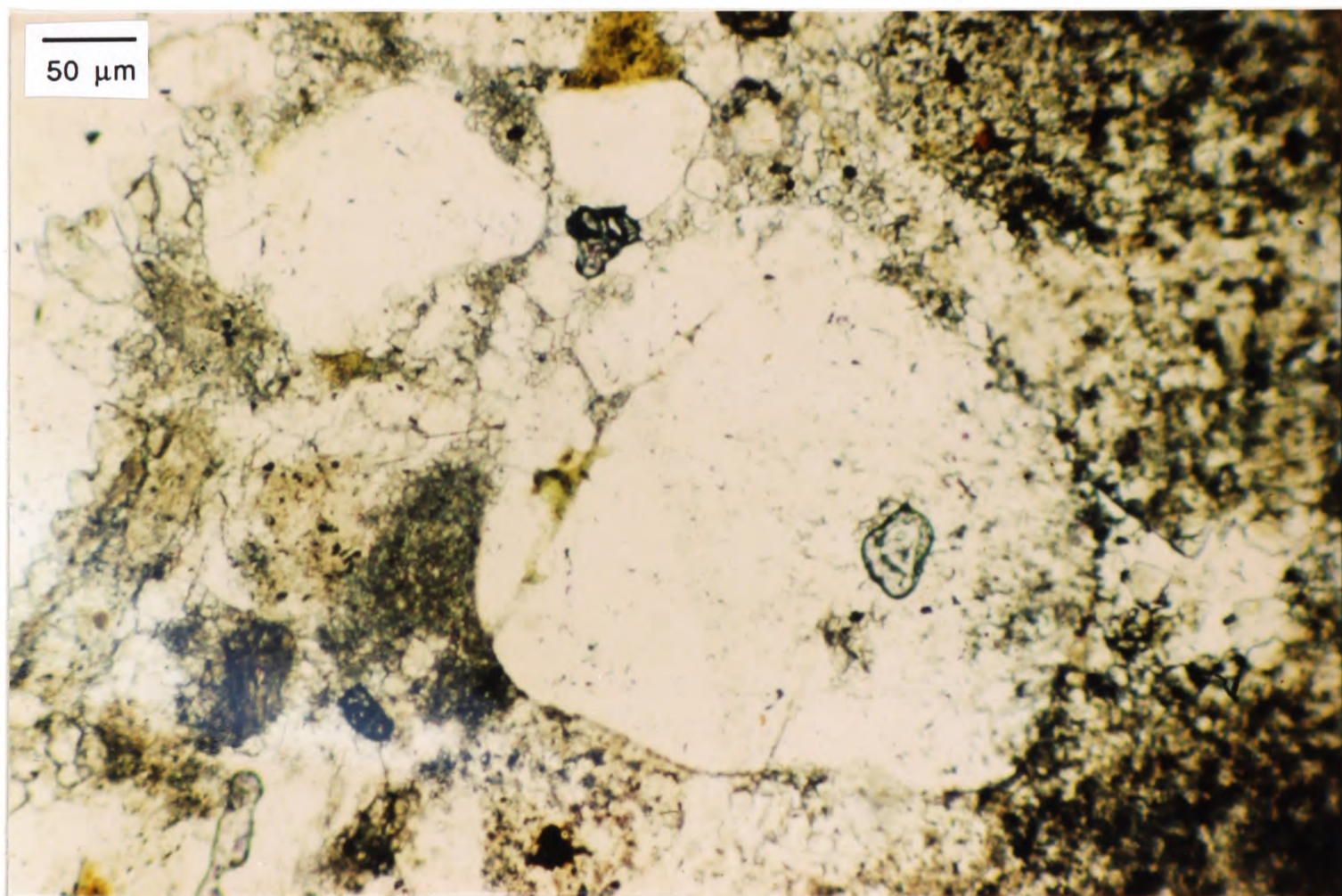


Fig.113: Photomicrograph of glauconite forming along cracks in a quartz grain: coquina bed in lower Chert Beds Member, Upper Greensand Formation, Little Beach, Beer, south-east Devon.

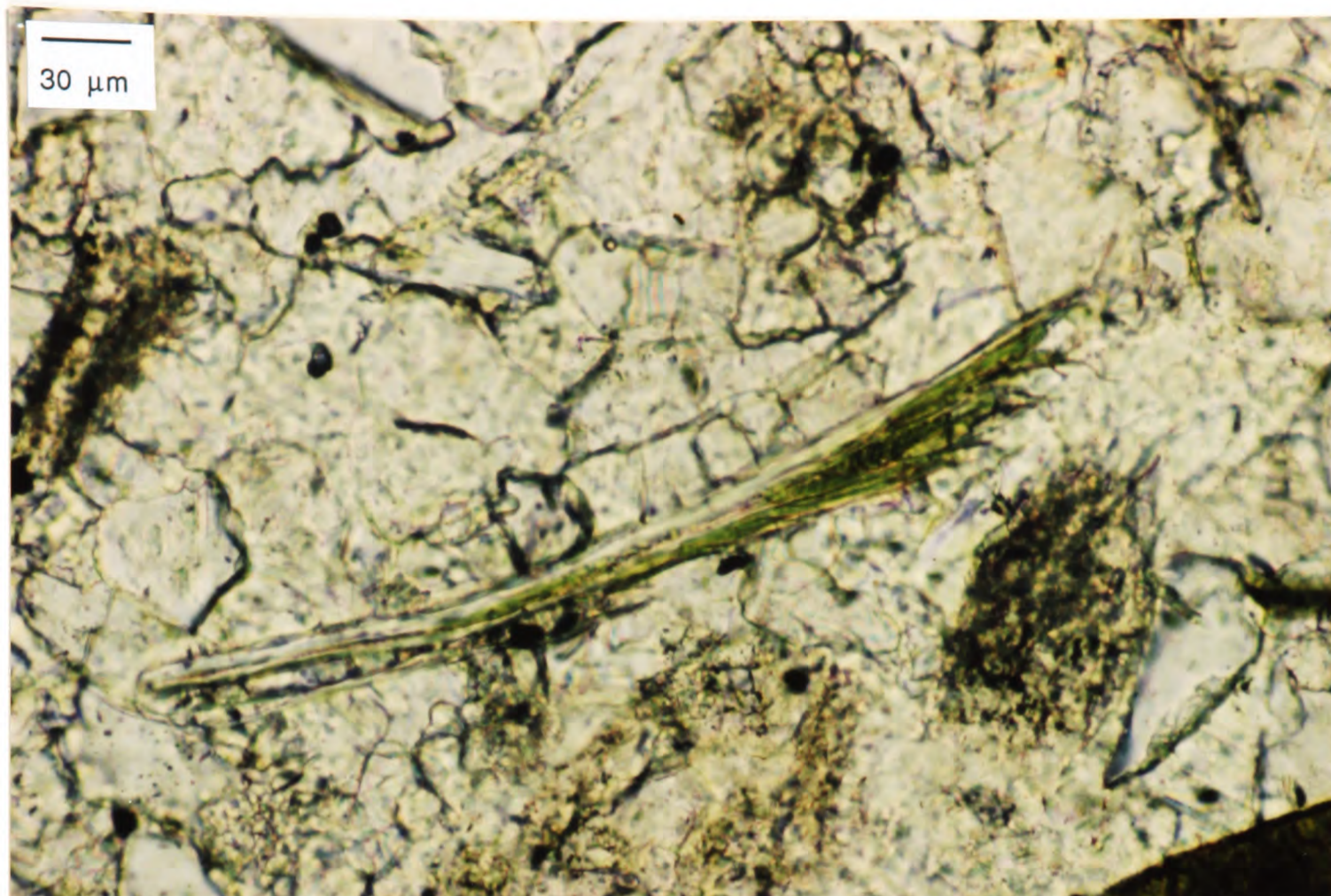


Fig.114: Photomicrograph of glauconite growing within the flakes of a muscovite grain: Foxmould Member (loose sample), Upper Greensand Formation, Hooken Cliffs, south-east Devon.

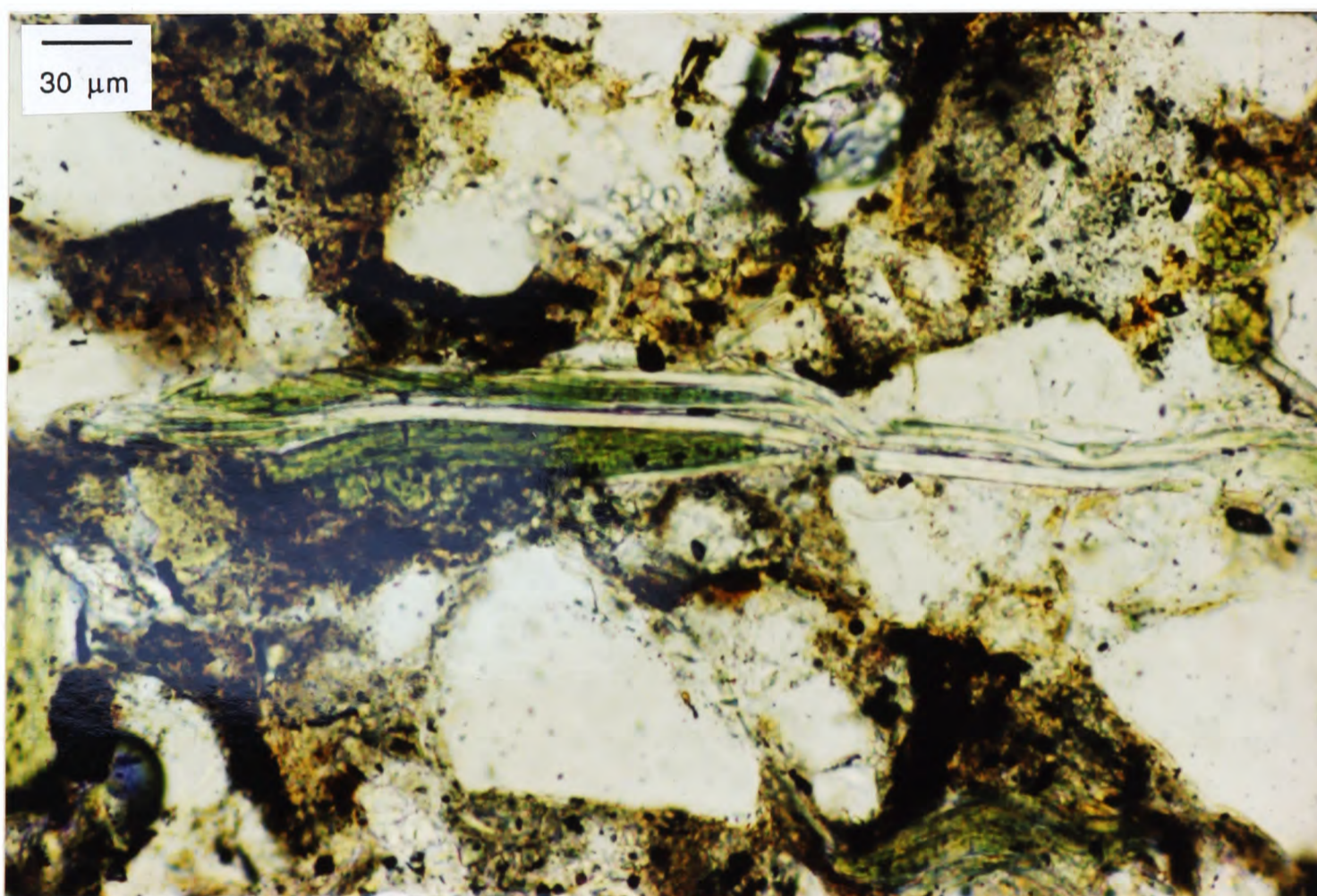


Fig.115: Photomicrograph of glauconite growing within the flakes of a muscovite grain: upper thick storm laminite bed, Foxmould Member, Upper Greensand Formation, Hooken Cliffs, Beer, south-east Devon.

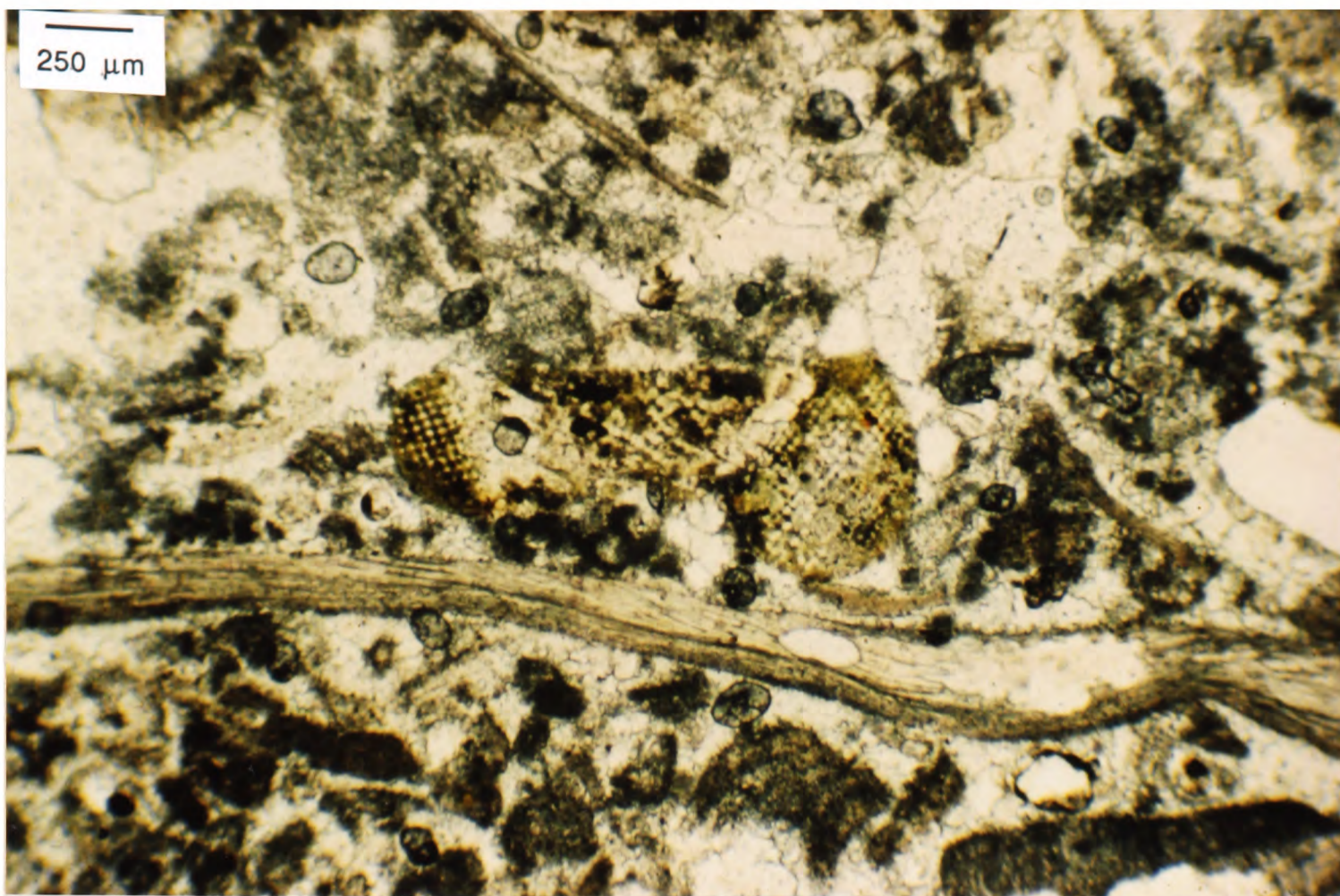


Fig.116: Photomicrograph of glauconitized echinoid bioclast: coquina bed in lower Chert Beds Member, Upper Greensand Formation, Little Beach, Beer, south-east Devon.

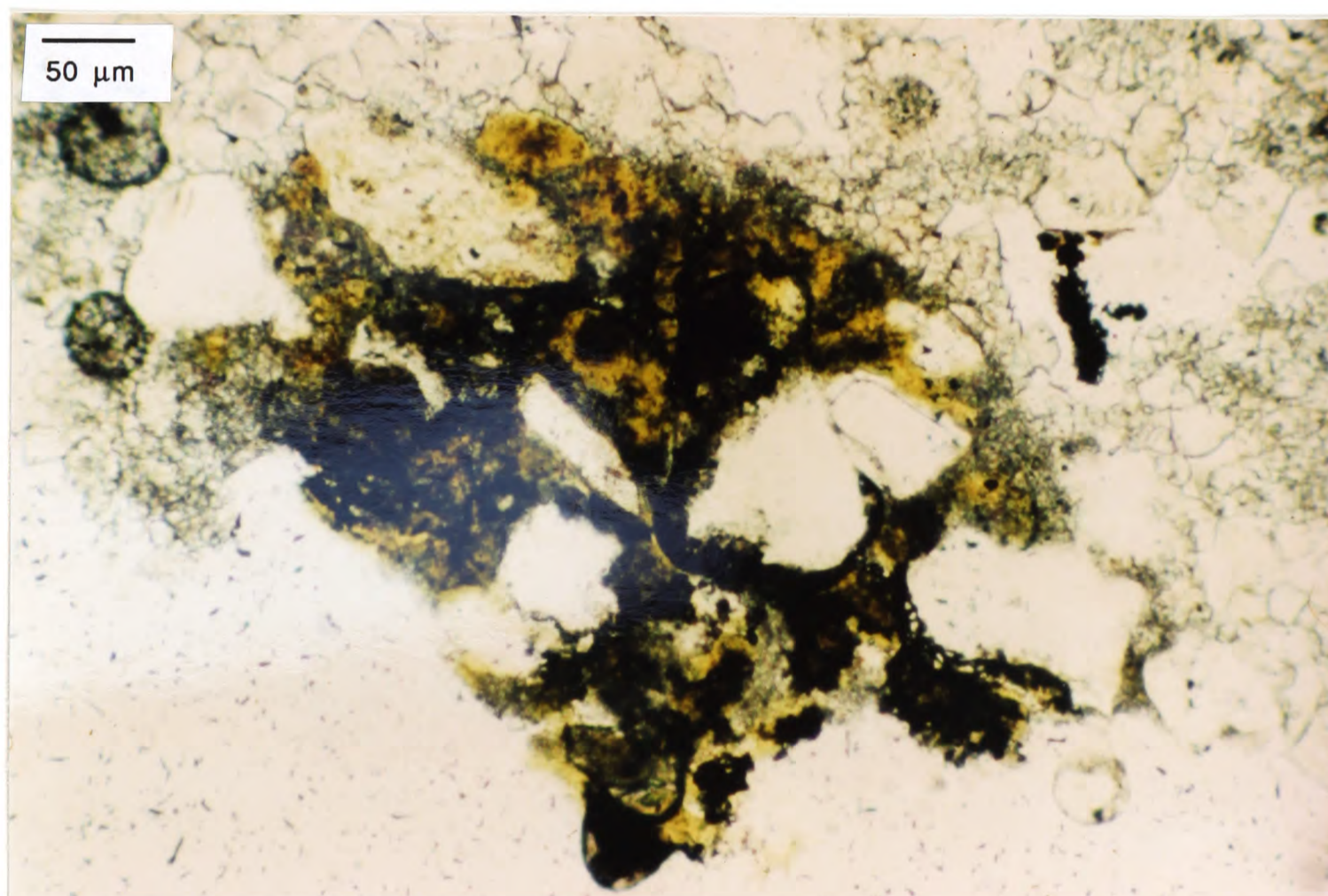


Fig.117: Photomicrograph of glauconite replacing an aggregate of silt-sized quartz grains and mud, interpreted as a faecal pellet: coquina bed in lower Chert Beds Member, Upper Greensand Formation, Little Beach, Beer, south-east Devon.

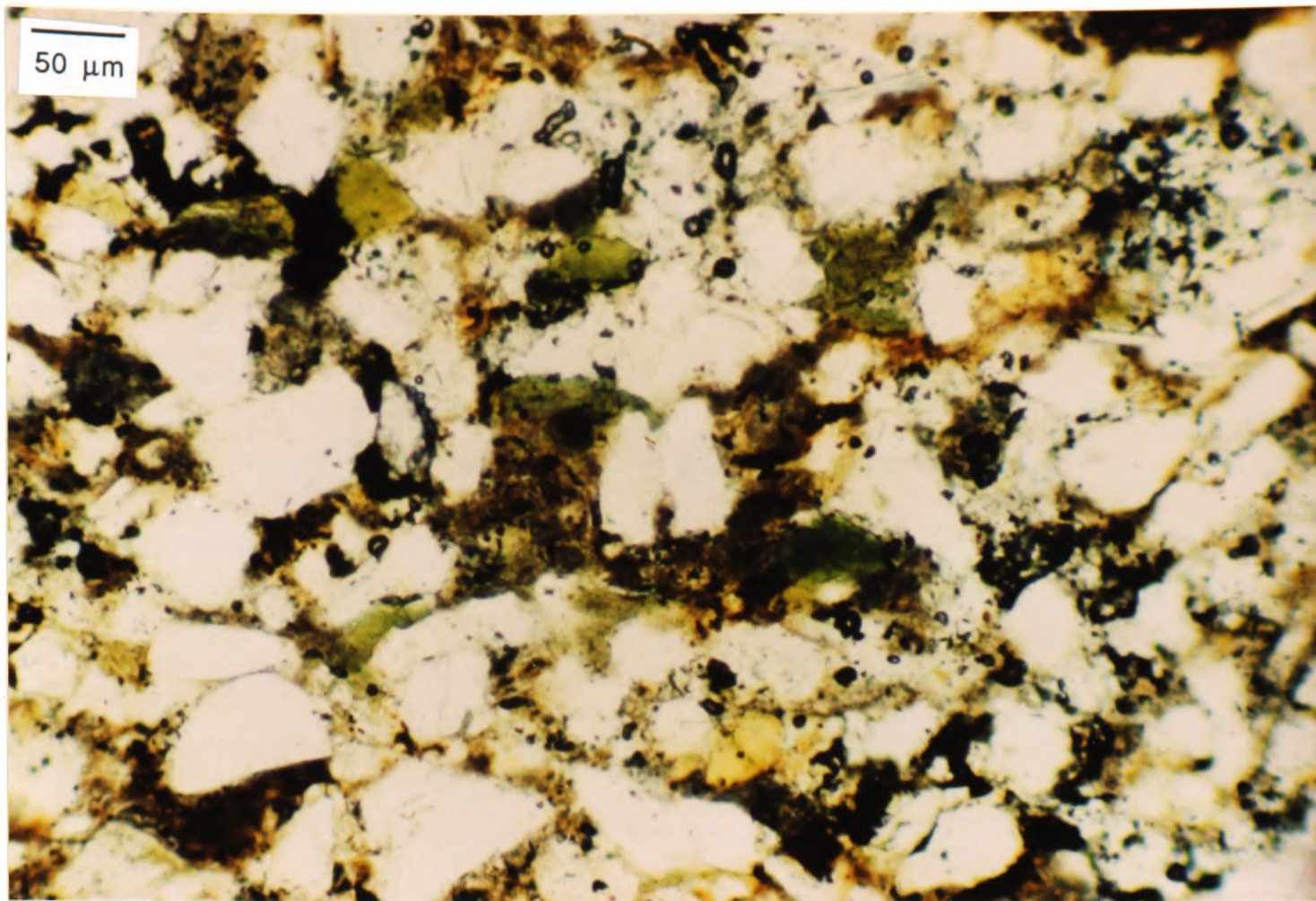
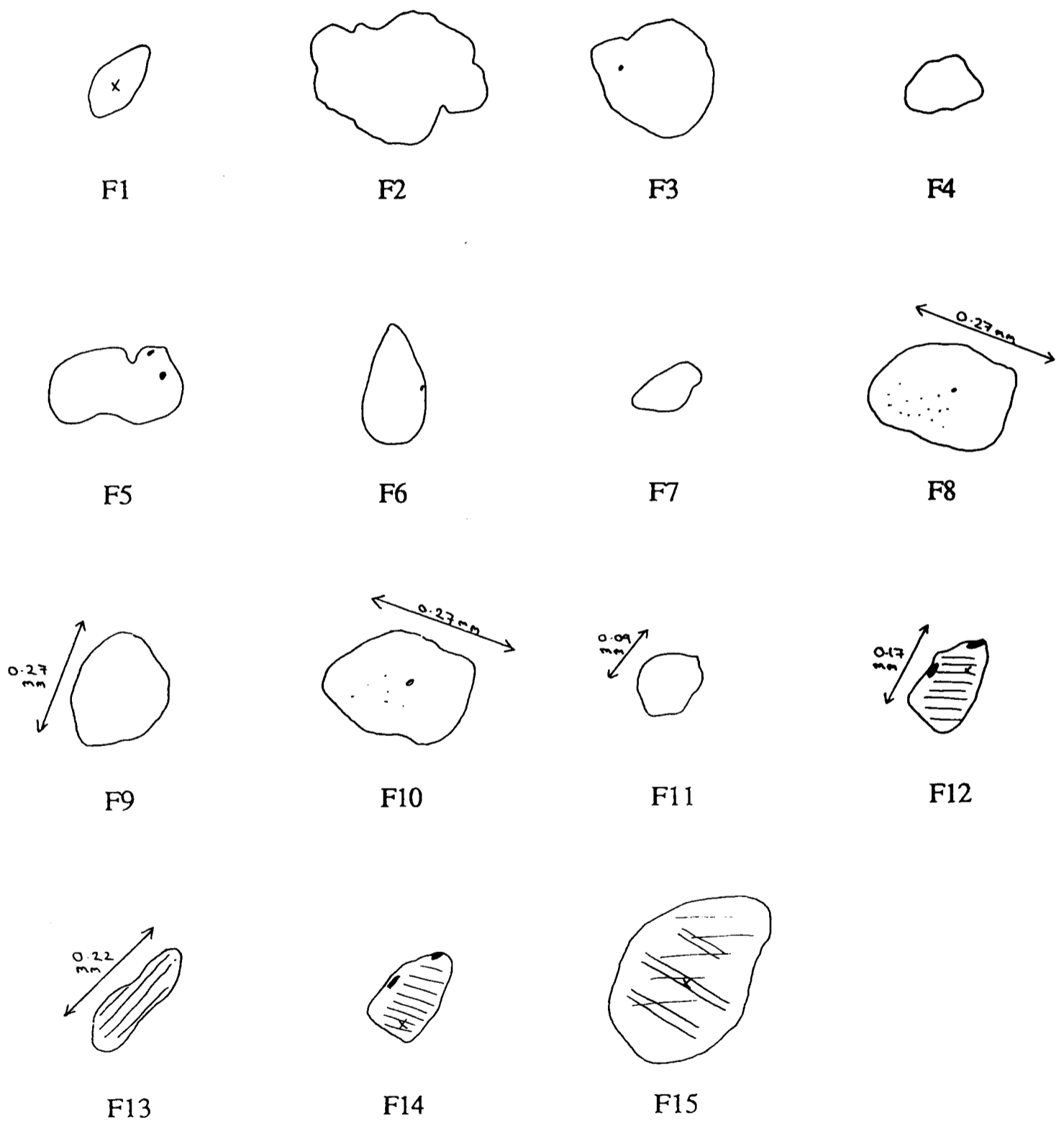


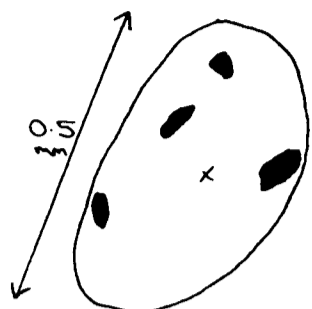
Fig.118: Photomicrograph of glauconite replacing the muddy matrix sediment of fine-grained muddy sand: Foxmould Member (loose sample), Upper Greensand Formation, Hooken Cliffs, Beer, south-east Devon.

Fig.119: Morphologies of glauconitic grains measured by electron microprobe analysis.
 119.1: Foxmould glauconites; 119.2: uppermost Foxmould glauconites; 119.3: upper Chert Beds (lower part) glauconites; 119.4: upper Chert Beds (upper part) glauconites; 119.5: top Upper Greensand glauconites; 119.6: Dispar Zone Ammonite Beds glauconites; 119.7: Upper Greensand, Gore Cliff glauconites; 119.8 Upper Greensand, Eastbourne glauconites.

1) Foxmould



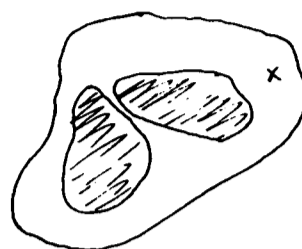
2) uppermost Foxmould



TF1



TF2



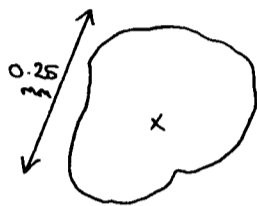
TF3



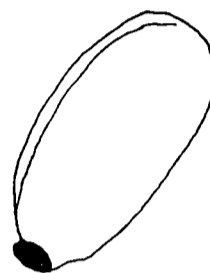
TF4



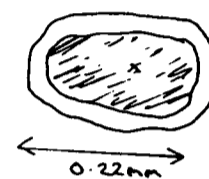
TF5



TF6



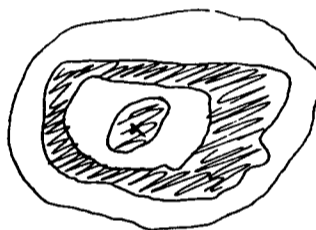
TF7



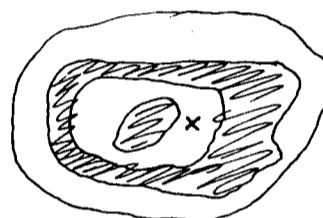
TF8



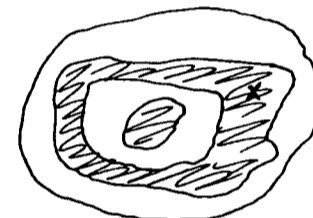
TF9



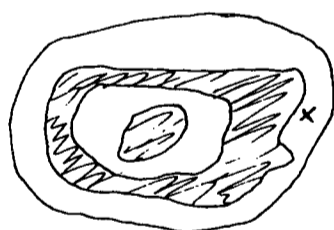
TF10



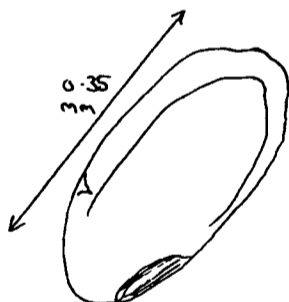
TF11



TF12



TF13



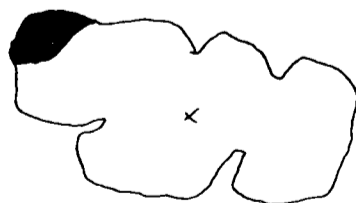
TF14



TF15

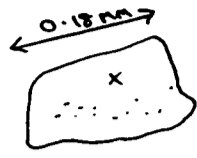


TF16



TF17

3) upper Chert Beds (lower part)



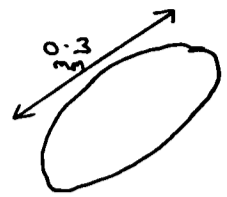
CB1



CB2



CB3



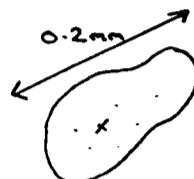
CB4



CB5



CB6



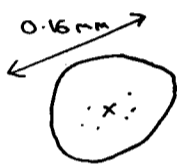
CB7



CB8



CB9



CB10



CB11

4) upper Chert Beds (upper part)



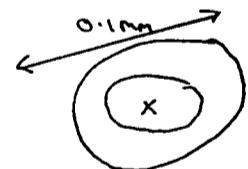
CB12



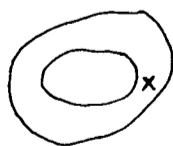
CB13



CB14



CB15



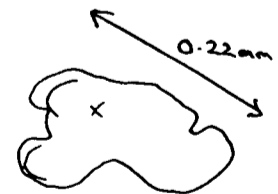
CB16



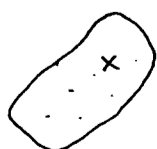
CB17



CB18



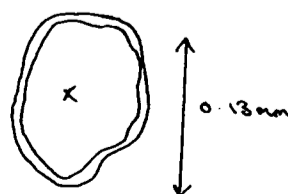
CB19



CB20



CB21



CB22

5) top Upper Greensand hardground



HG1



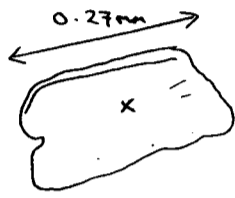
HG2



HG3

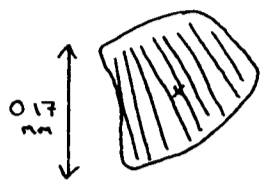


HG4

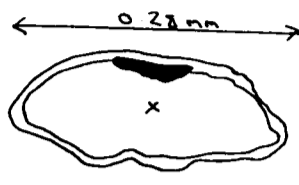


HG5

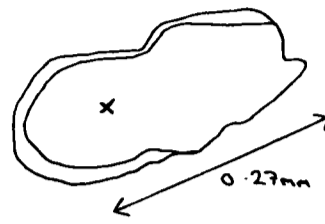
6) Dispar Zone Ammonite Bed



DZ1



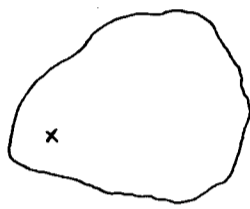
DZ2



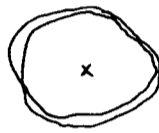
DZ3



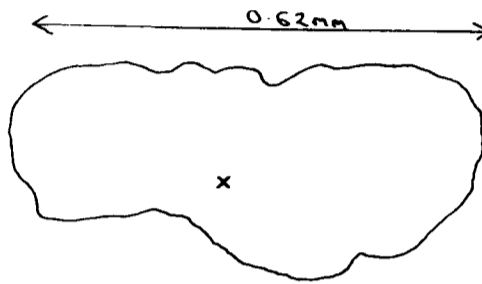
DZ4



DZ5



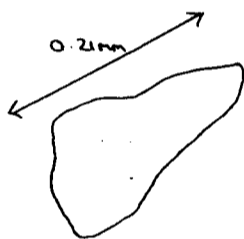
DZ6



DZ7



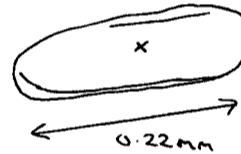
DZ8



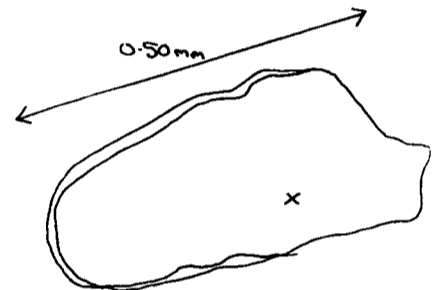
DZ9



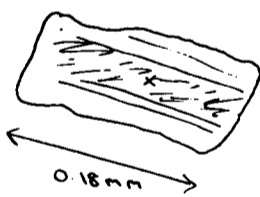
DZ10



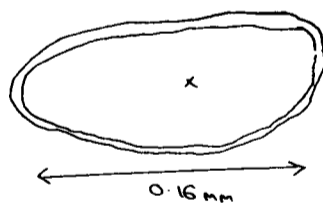
DZ11



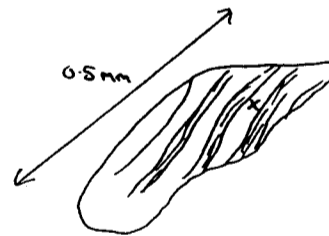
DZ12



DZ13



DZ14



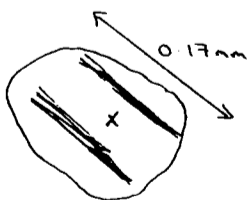
DZ15



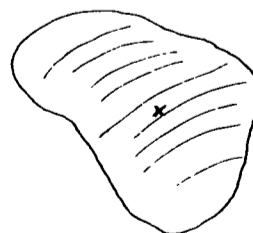
DZ16



DZ17



DZ18

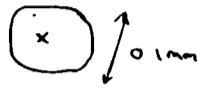


DZ19

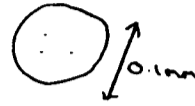
7) Upper Greensand, Gore Cliff



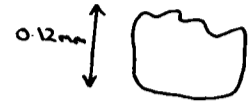
GC1



GC2



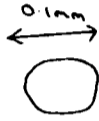
GC3



GC4



GC5



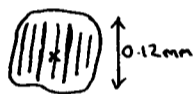
GC6



GC7



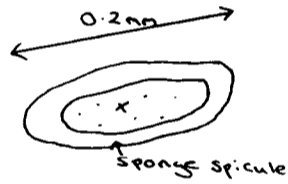
GC8



GC9

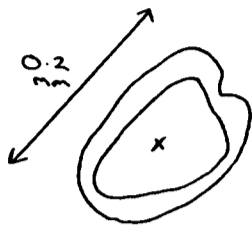


GC10



GC11

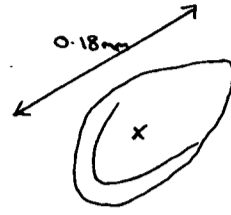
8) Upper Greensand, Eastbourne



E1



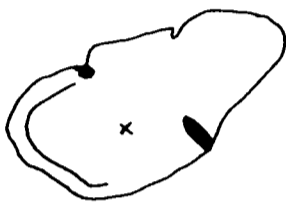
E2



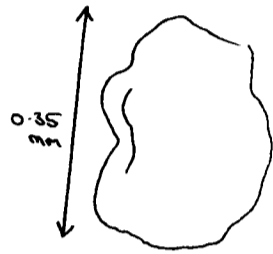
E3



E4



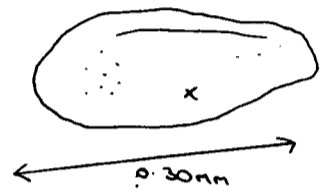
E5



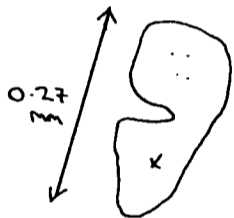
E6



E7



E8



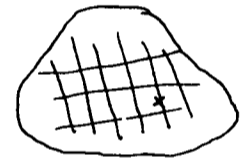
E9



E10



E11



E12



E13



E14

TABLE 14 - SULPHUR-CARBON ANALYSES

Upper Greensand, south-east Devon

	Sample no.	wt% org.C	wt%S
Foxmould, Upper Greensand, Hooken Cliffs, 8.25m	RP1	0.33	0.24
Loose Foxmould, Upper Greensand, Hooken Cliffs	RP39	0.38	0.11
Foxmould, Upper Greensand, Seaton Hole, 10.25m	RP9	0.13	0.03
Foxmould, Upper Greensand, Seaton Hole, 5.80m	RP34	0.06	0.01
Muddy bed, Foxmould, Upper Greensand, Seaton Hole, 5.40m	RP8	0.28	0.08
Foxmould, Upper Greensand, Seaton Hole, 0.50m	RP12	0.07	0.01

Gault and Upper Greensand, south Dorset

Limestone, Chert Beds, Durdle Cove, 43.94-46.34m	RP15	0.72	0.02
Glauconitic limestone, minor hiatus just above DZAB, Durdle Cove, 43.64-43.94m	RP51	0.24	0.06
Dispar Zone Ammonite Bed, Upper Greensand, Durdle Cove, 43.39-43.64m	RP54	0.14	0.02
Marly, glauconitic sand just below DZAB, Durdle Cove, 43.09-43.39m	RP42	0.14	0.04
Marly sand just above Exogyra Rock, Durdle Cove, 40.60-41.34m	RP46	0.24	0.07
Glauconitic marly silt below Exogyra Rock, Durdle Cove, 39.25m	RP19	0.12	0.05
Glauconitic fine sand, Upper Greensand, Durdle Cove, 30m	RP52	0.34	0.02
Glauconitic silts, Upper Greensand, Durdle Cove, 26m	RP2	0.18	0.05
Muddy sand, Upper Greensand, Durdle Cove, 23m	RP17	0.27	0.09
Grey silt, Upper Greensand, Durdle Cove, 17.92m	RP20	0.19	0.01
Iron-rich silty clay (rather weathered), Gault, Durdle Cove, 5m	RP13	1.74	0.22

Glauconitic sand below Exogyra Rock, West side of Lulworth Cove, 18.77-21.87m	RP23	0.16	0.32
Upper Greensand, West side of Lulworth Cove, 16.27-18.47m	RP38	0.16	0.05
Black clay band, Upper Greensand, West side of Lulworth Cove, 16.07-16.27m	RP6	0.38	0.30
Thin clayey seam, Upper Greensand, West side of Lulworth Cove, 14.72m	RP10	0.25	0.09
Upper Greensand, West side of Lulworth Cove, 12.67m	RP47	0.23	0.31
Muddy sand, Upper Greensand, West side of Lulworth Cove, 9.2m	RP18	0.37	0.29
Glauconitic clayey silt, West side of Lulworth Cove, 3.15m	RP21	0.27	0.07

Dispar Zone Ammonite Bed, Upper Greensand, excavated section below Flower's Barrow, Worbarrow Bay, 60m	RP4	0.18	0.03
Dispar Zone Ammonite Bed, Upper Greensand, below Flower's Barrow, Worbarrow Bay, 60m	RP22	0.03	0.01
Glauconitic fine sand above Exogyra Rock, Upper Greensand, below Flower's Barrow, Worbarrow Bay, 57.92-59.42m	RP11	0.00	0.02
Glauconitic fine sand below Exogyra Rock, below Flower's Barrow, Worbarrow Bay, 54.00-56.42m	RP48	0.07	0.02
Glauconitic serpulid limestone, below Flower's Barrow, Worbarrow Bay, 54m	RP49	0.00	0.01
Fine sand, Upper Greensand, below Flower's Barrow, Worbarrow Bay, 52.82-53.67m	RP14	0.00	0.01
Black clay band, Upper Greensand, below Flower's Barrow, Worbarrow Bay, 49.37-49.52m	RP7	0.21	0.04
Fine sands, Upper Greensand, below Flower's Barrow, Worbarrow Bay, 45.42-45.0m	RP5	0.02	0.04
Rhythmically-bedded silt, Upper Greensand, below Flower's Barrow, Worbarrow Bay, 37.92m	RP37	0.06	0.01
Rhythmically-bedded silt, Upper Greensand, below Flower's Barrow, Worbarrow Bay, 37.62m	RP24	0.22	0.04
Rhythmically-bedded silt, Upper Greensand, below Flower's Barrow, Worbarrow Bay, 37.17m	RP3	0.10	0.02
Uppermost Gault, below Flower's Barrow, Worbarrow Bay, 34.08m	RP36	0.26	0.08
Gault clay, below Flower's Barrow, Worbarrow Bay, 29.88m	RP16	0.29	0.10
Gault clay, below Flower's Barrow, Worbarrow Bay, 14.7m	RP35	0.59	0.04

Passage Beds and Upper Greensand, Isle of Wight

Chert Beds equivalent, Upper Greensand, Compton Bay, Isle of Wight, 37.88m	RP50	0.41	0.33
Upper Greensand, Compton Bay, Isle of Wight, 34.13m	RP43	0.18	0.23
Upper Greensand, Compton Bay, Isle of Wight, 23.13m	RP26	1.10	0.10
Upper Greensand, Compton Bay, Isle of Wight, 21.13m	RP45	0.00	0.54
Passage Beds, Compton Bay, Isle of Wight, 14.54-14.74m	RP32	0.16	0.22
Weakly to moderately muddy silt, Passage Beds, Compton Bay, Isle of Wight, 14.14-14.54m	RP40	0.16	0.08
Weakly muddy silt, Passage Beds, Compton Bay, Isle of Wight, 13.89-14.14m	RP33	0.23	0.11
Strongly muddy silt, Passage Beds, Compton Bay, Isle of Wight, 13.45-13.89m	RP28	0.17	0.12
Weakly muddy silt, Passage Beds, Compton Bay, Isle of Wight, 13.32-13.45m	RP29	0.14	0.09
Strongly muddy silt, Passage beds, Compton Bay, Isle of Wight, 12.64-12.92m	RP31	0.15	0.11
Passage Beds, Compton Bay, Isle of Wight, 5.58m	RP27	0.50	0.21
Glauconitic silt, basal Passage Beds, Compton Bay, Isle of Wight, 0.5m	RP44	0.59	0.33
Uppermost Gault/Passage Beds, Compton Bay, Isle of Wight, 0.02m	RP25	0.51	0.31

Gault clay, Folkstone

Clay 1m above <i>cristatum</i> nodule bed, basal Upper Gault, Copt Point Folkstone	RP30	0.69	0.25
Clay 0.6m below <i>cristatum</i> nodule bed, upper Lower Gault, Copt Point, Folkstone	RP41	0.80	0.46
Clay 1m above base of the Gault, <i>spathi</i> subzone, Lower Gault, Copt Point, Folkstone	RP53	0.43	0.19

Fig.120: sulphur/carbon data - the Foxmould Member, Upper Greensand, south-east Devon

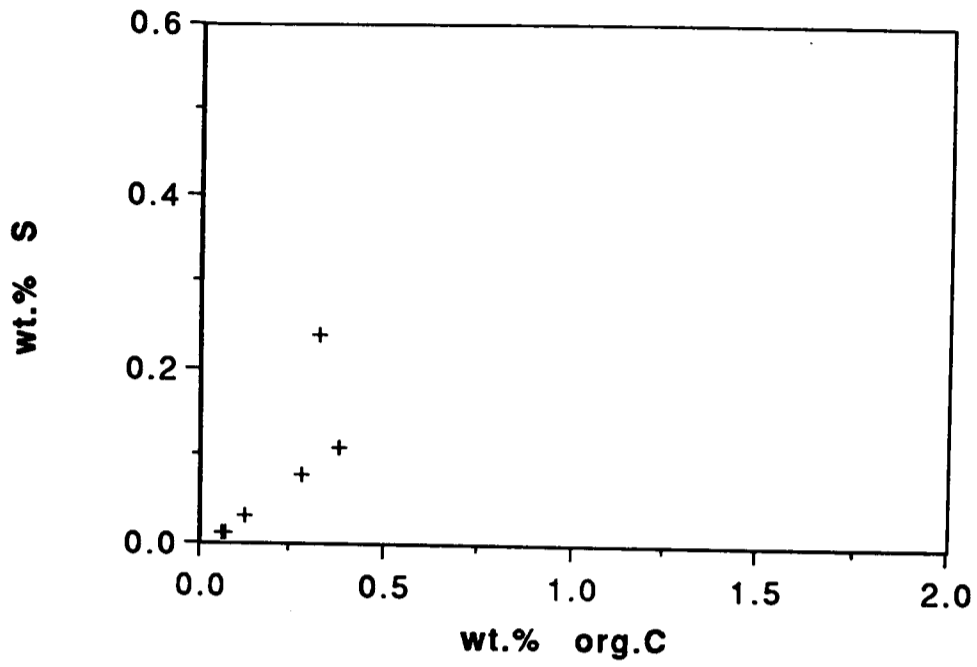


Fig. 121: sulphur/carbon data - the Upper Greensand and Gault of south Dorset

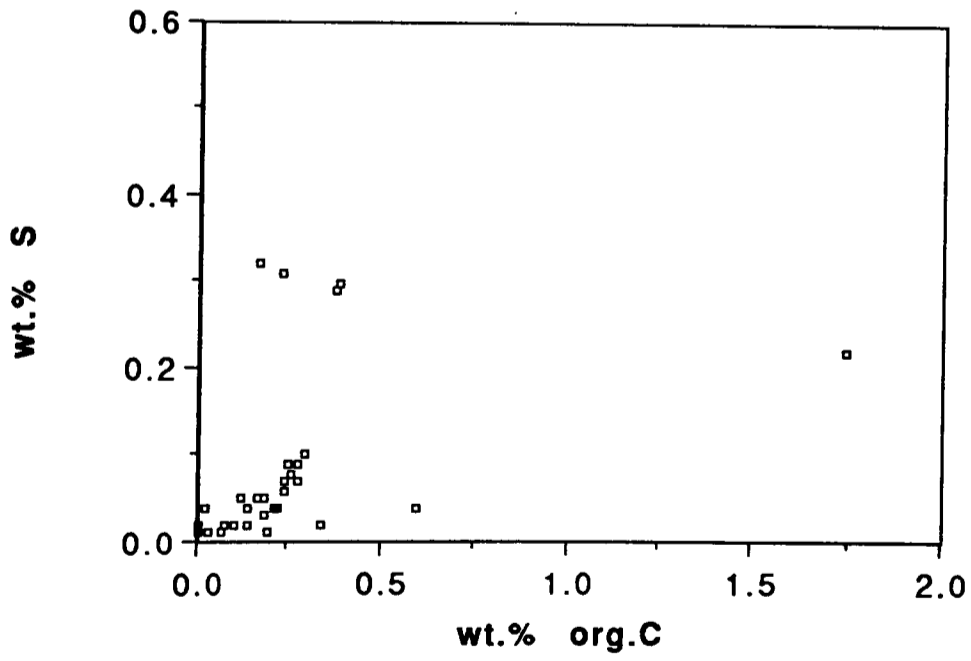


Fig. 122: sulphur/carbon data - Passage Beds and Upper Greensand, Compton Bay, Isle of Wight

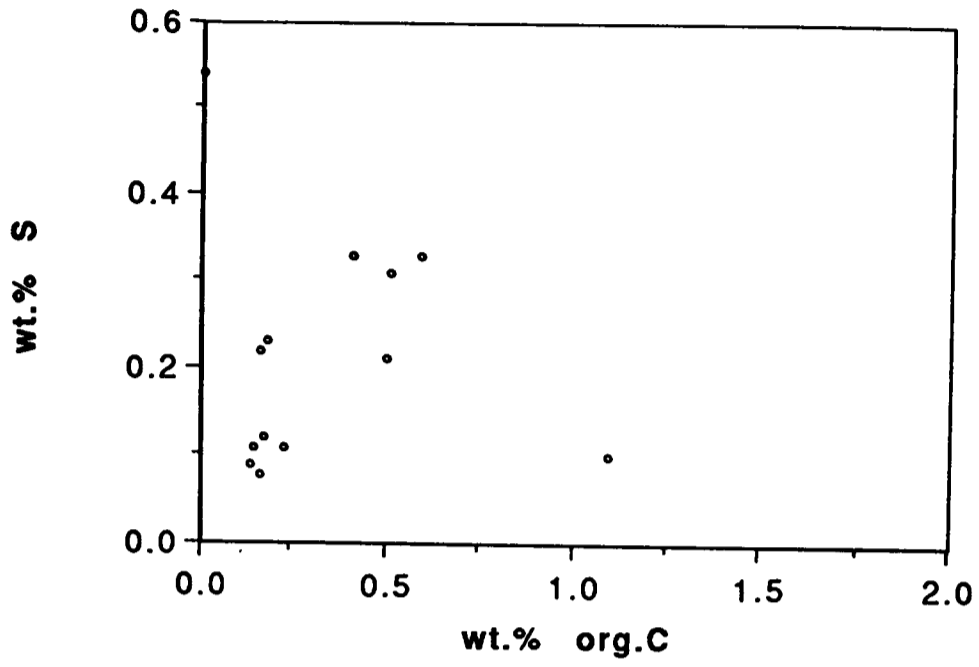
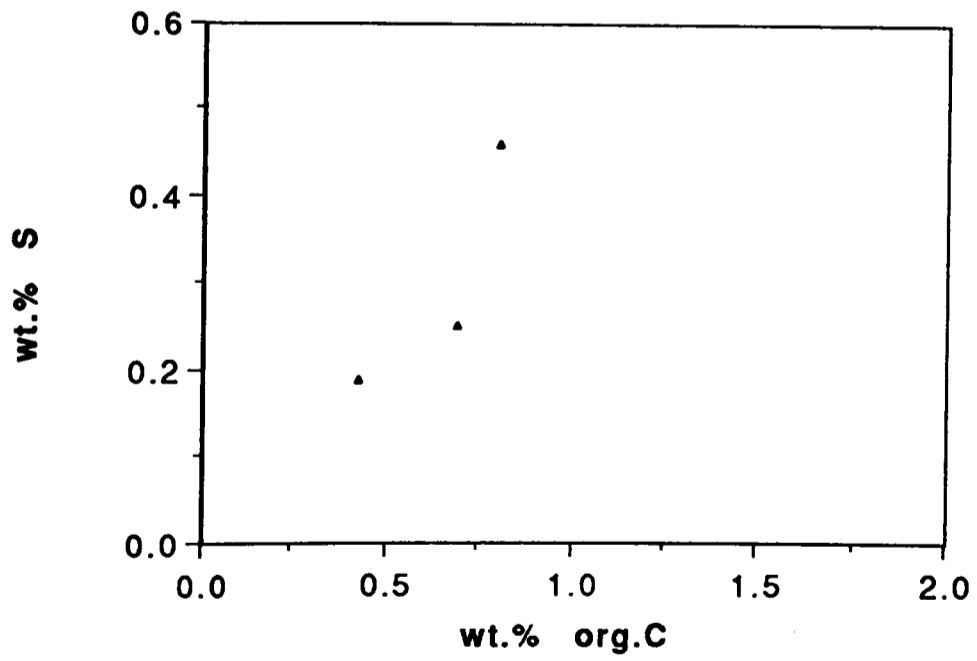


Fig.123: sulphur/carbon data - Gault clay, Folkstone



RYAZANIAN

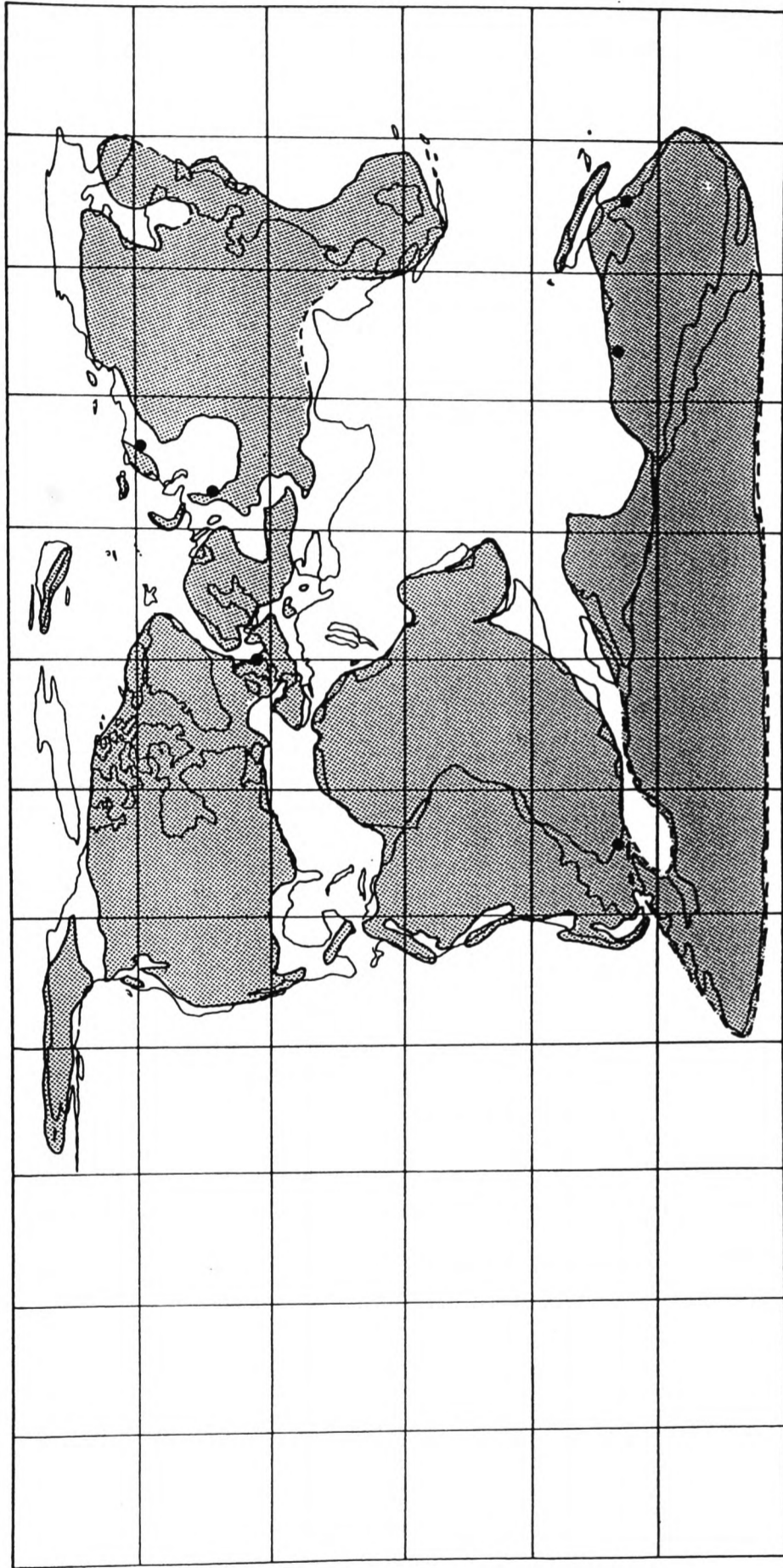


Fig.124: World-wide distribution of glauconitic facies during the Ryazanian, plotted on a palaeogeographic reconstruction of Funnel (1990).

VALANGINIAN

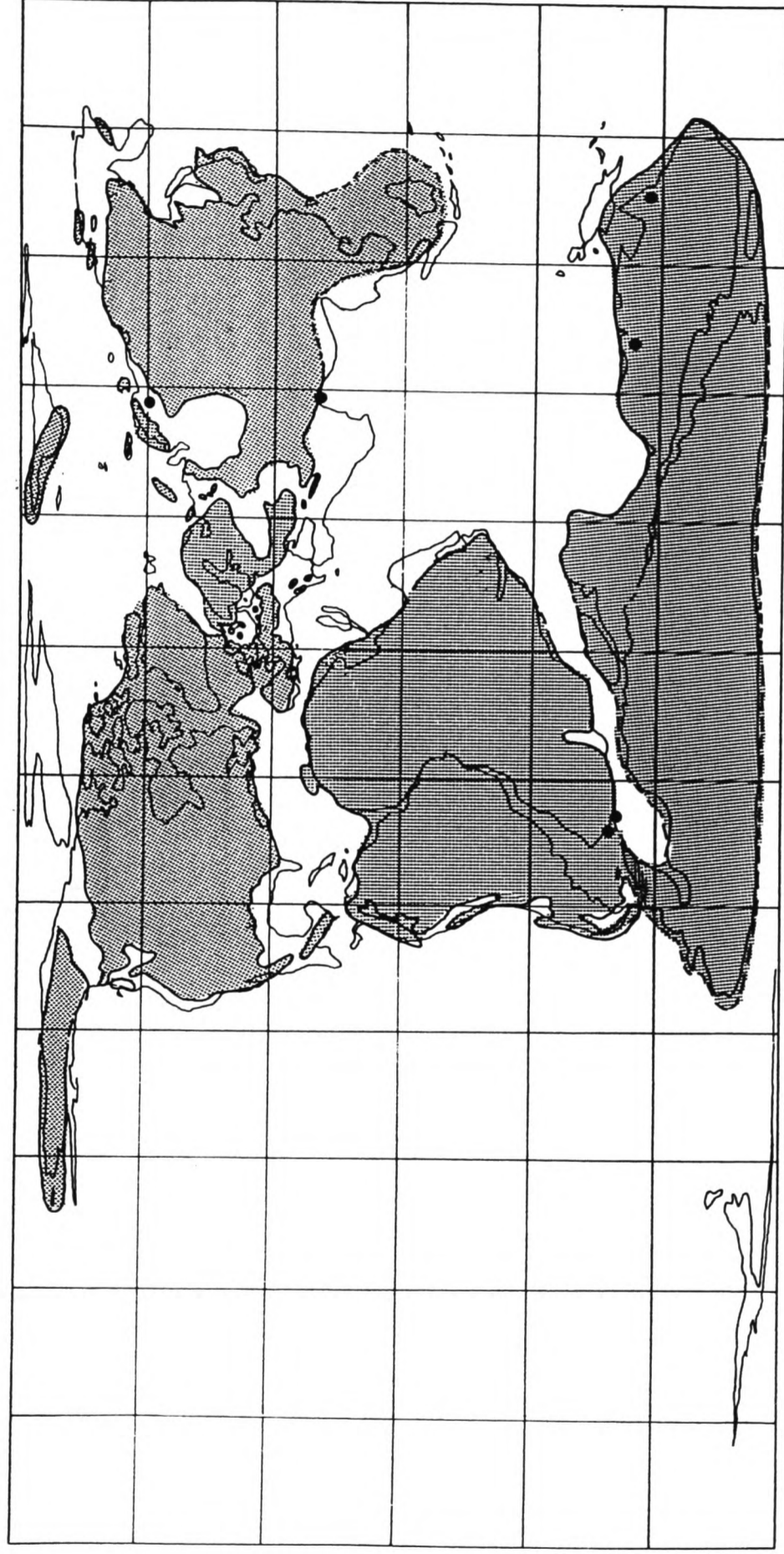


Fig.125: World-wide distribution of glauconitic facies during the Valanginian, plotted on a palaeogeographic reconstruction of Funnel (1990).

HAUTERIVIAN

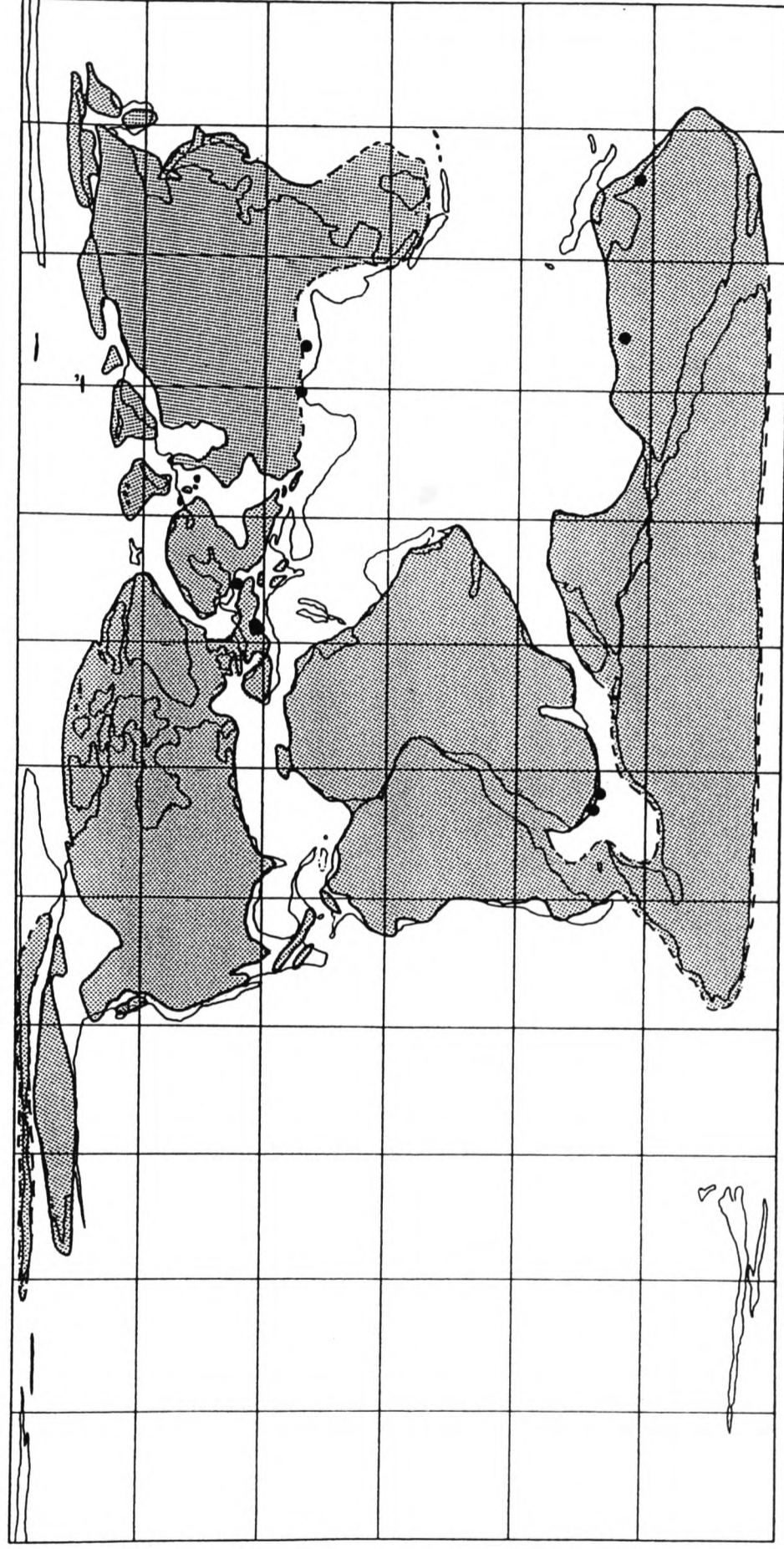


Fig.126: World-wide distribution of glauconitic facies during the Hauterivian, plotted on a palaeogeographic reconstruction of Funnel (1990).

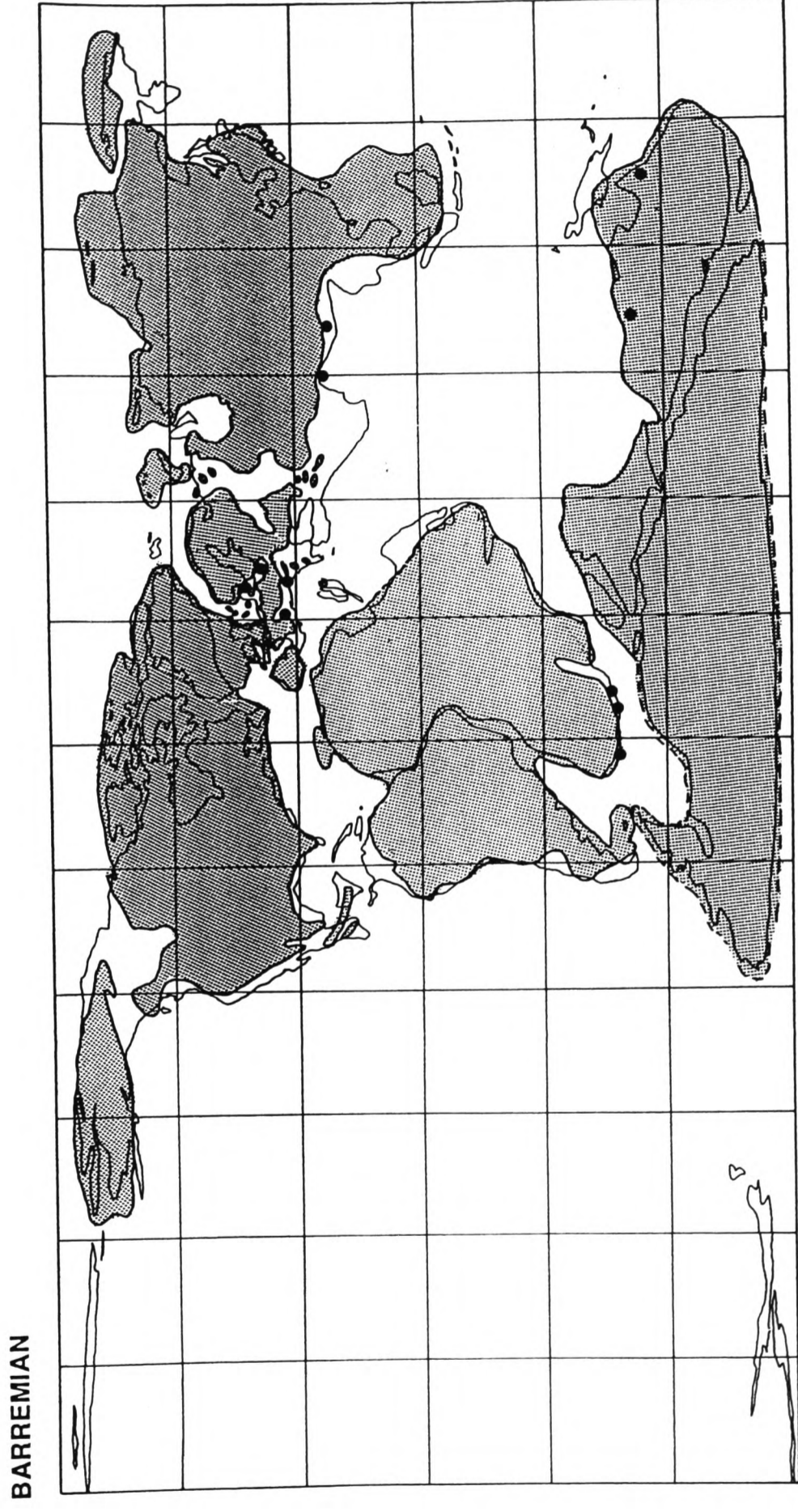


Fig.127: World-wide distribution of glauconitic facies during the Barremian, plotted on a palaeogeographic reconstruction of Funnel (1990).

APTIAN

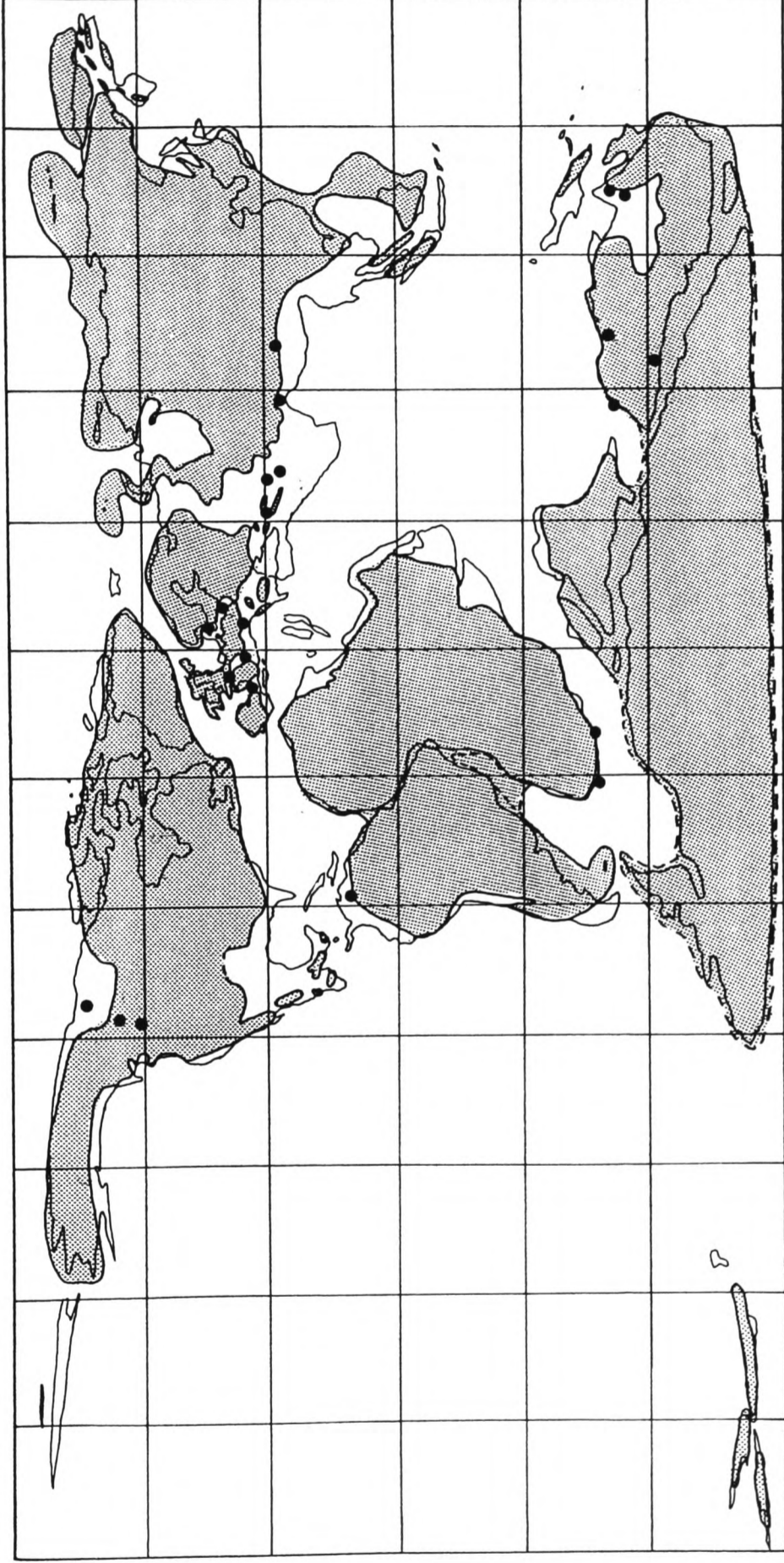


Fig.128: World-wide distribution of glauconitic facies during the Aptian, plotted on a palaeogeographic reconstruction of Funnel (1990).

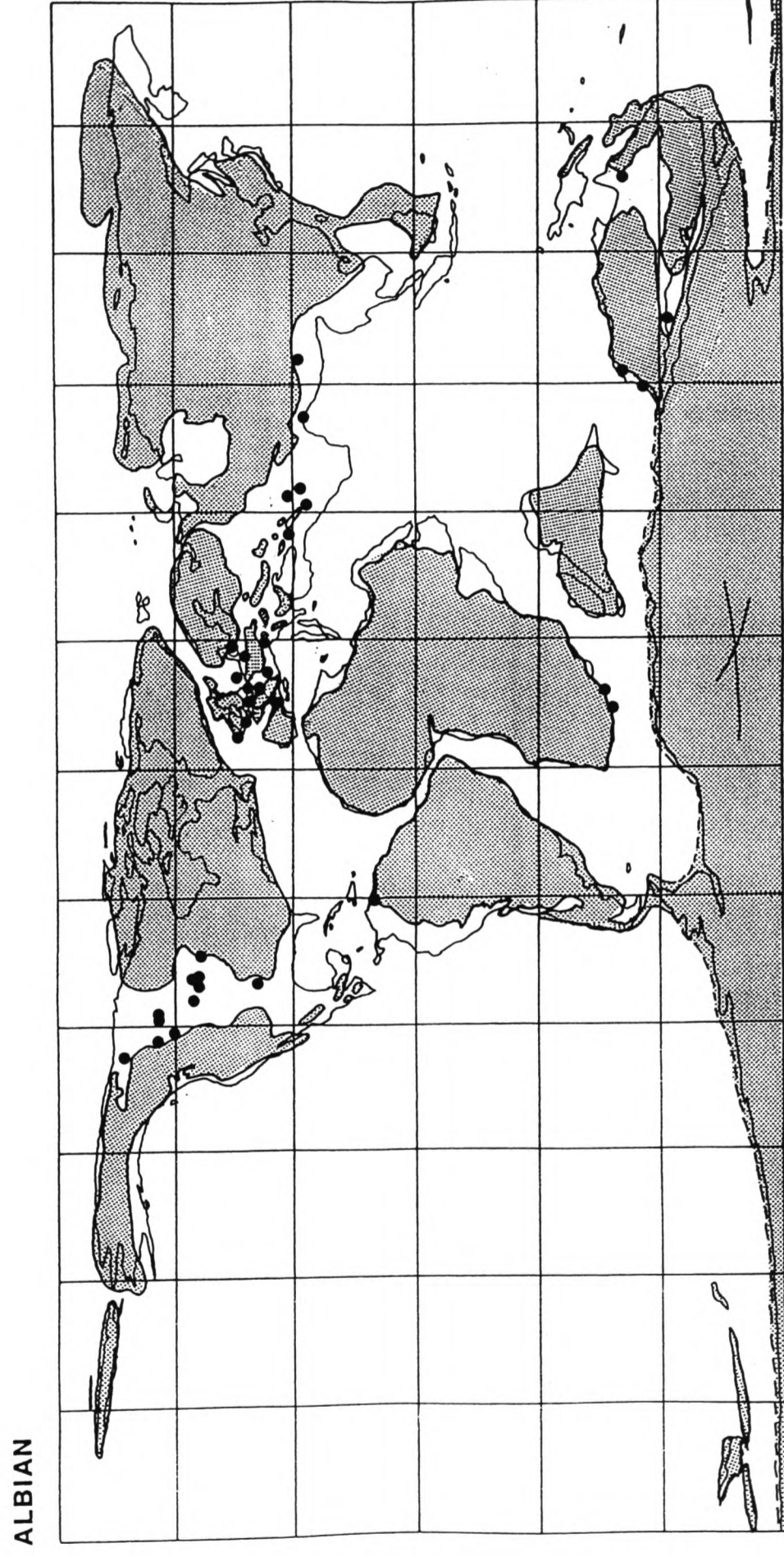


Fig.129: World-wide distribution of glauconitic facies during the Albian, plotted on a palaeogeographic reconstruction of Funnel (1990).

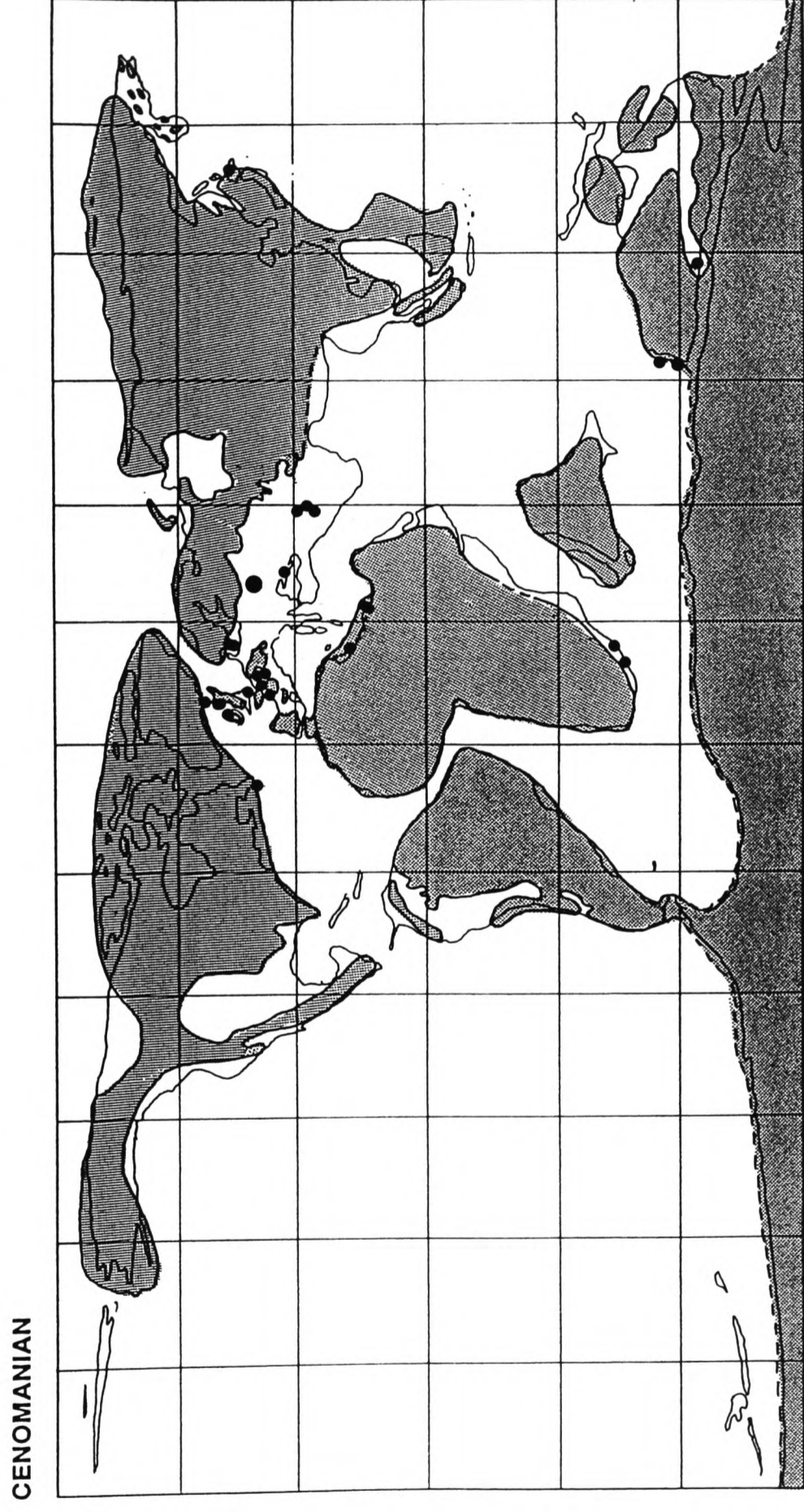


Fig.130: World-wide distribution of glauconitic facies during the Cenomanian, plotted on a palaeogeographic reconstruction of Funnel (1990).

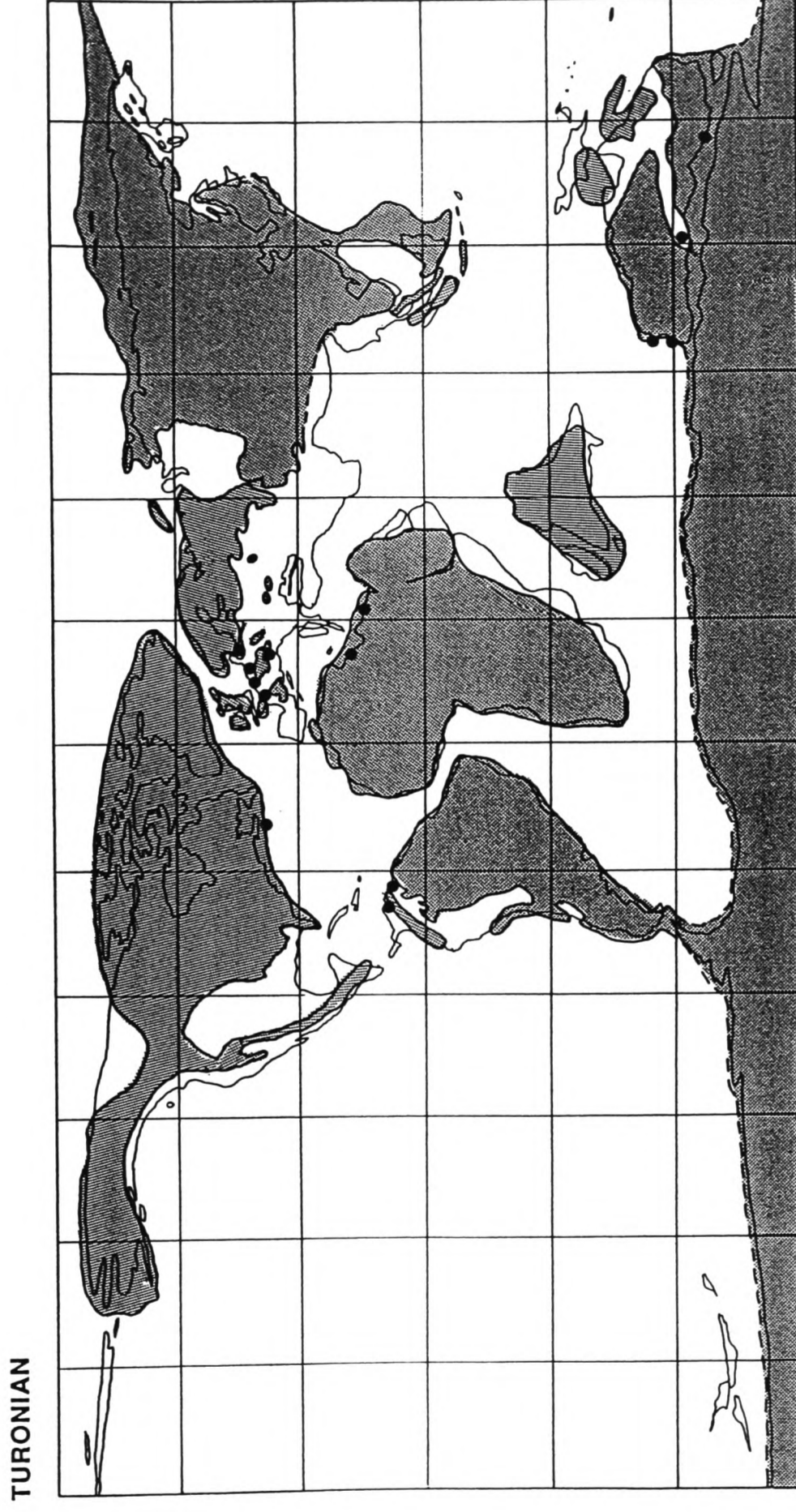


Fig.131: World-wide distribution of glauconitic facies during the Turonian, plotted on a palaeogeographic reconstruction of Funnel (1990).

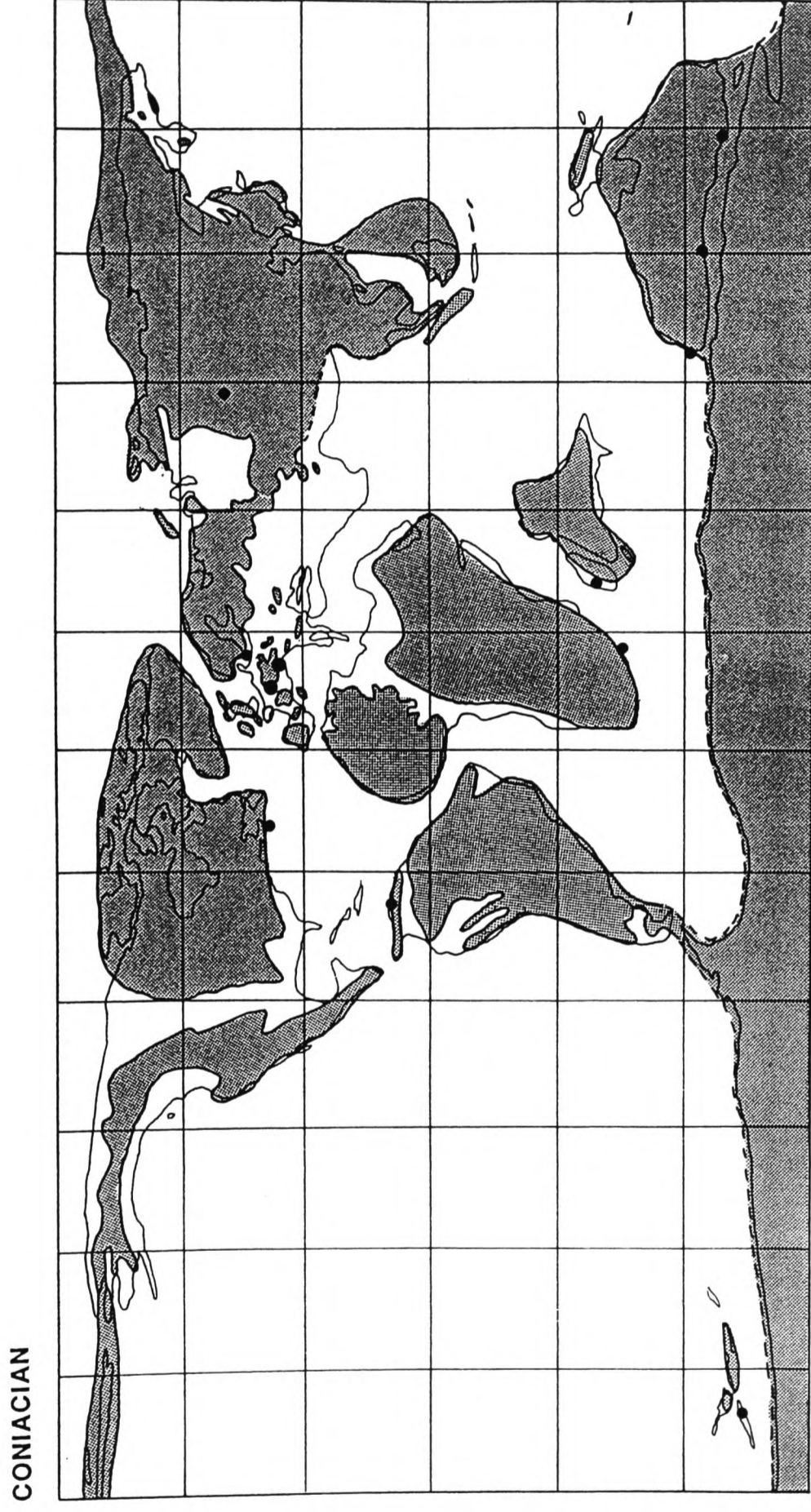


Fig.132: World-wide distribution of glauconitic facies during the Coniacian, plotted on a palaeogeographic reconstruction of Funnel (1990).

SANTONIAN



Fig.133: World-wide distribution of glauconitic facies during the Santonian, plotted on a palaeogeographic reconstruction of Funnel (1990).

CAMPANIAN

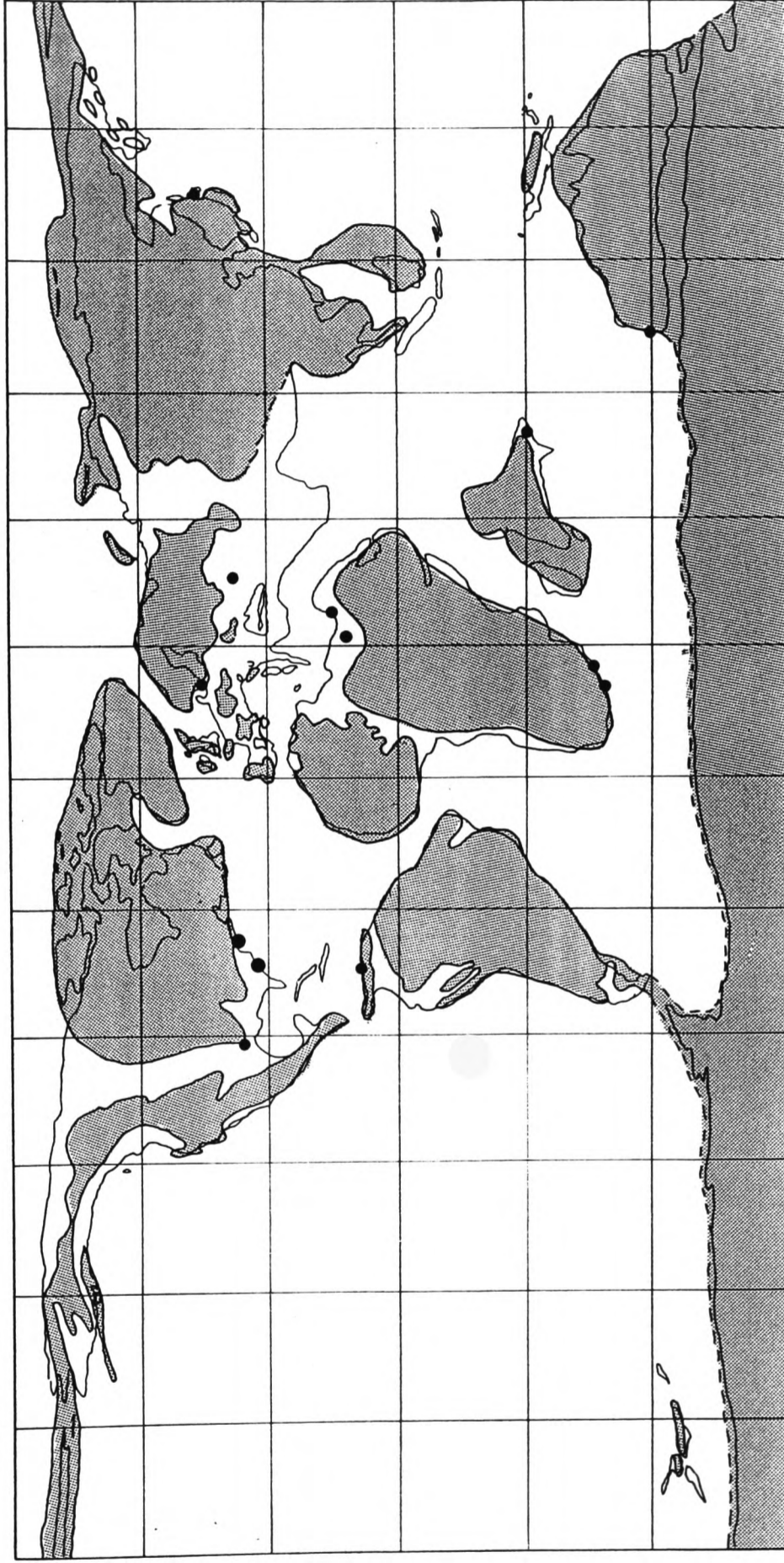


Fig.134: World-wide distribution of glauconitic facies during the Campanian, plotted on a palaeogeographic reconstruction of Funnel (1990).

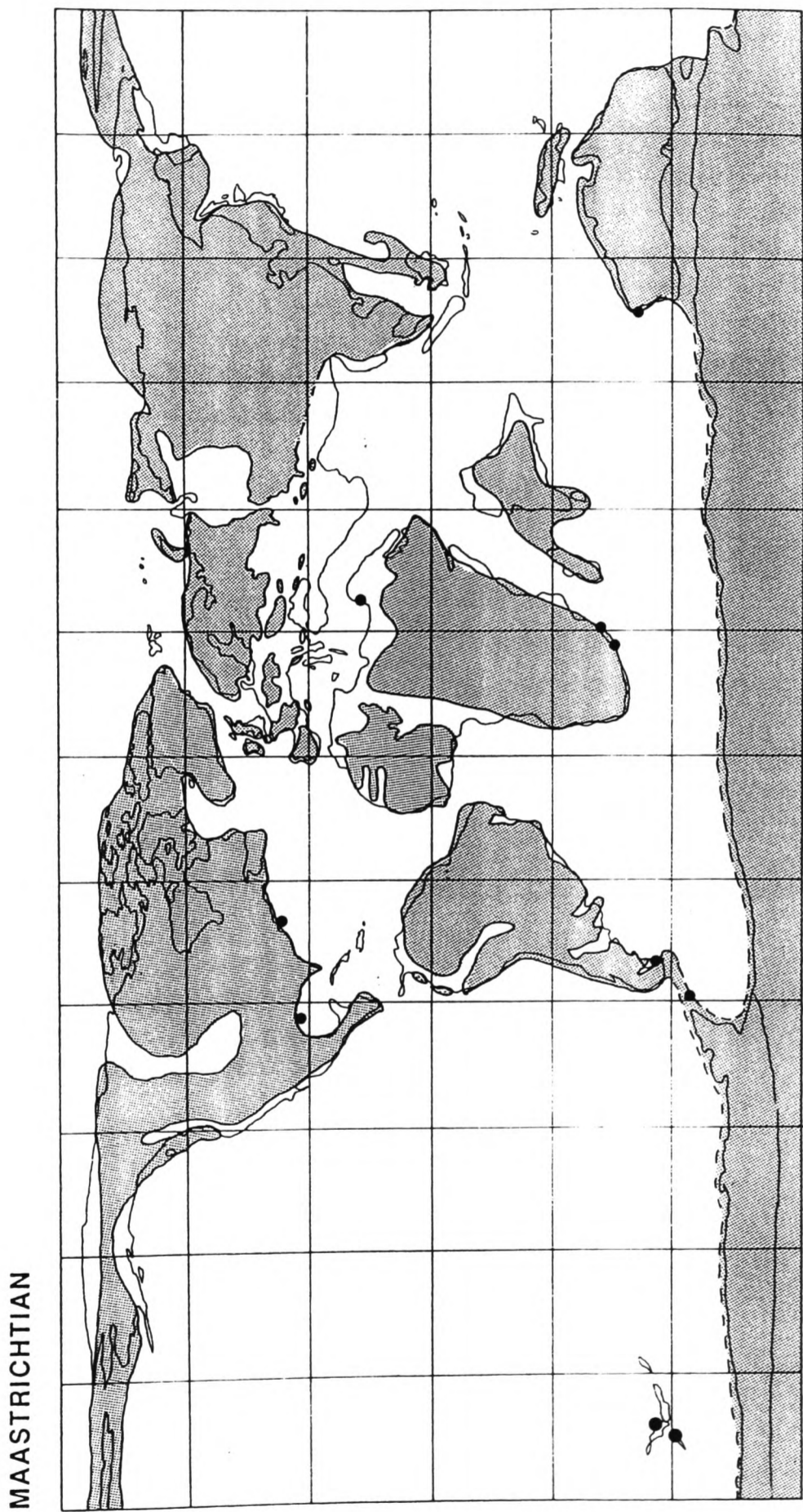


Fig.135: World-wide distribution of glauconitic facies during the Maastrichtian, plotted on a palaeogeographic reconstruction of Funnel (1990).

GLAUCONITE PRODUCTION RATE (KM³/MA)

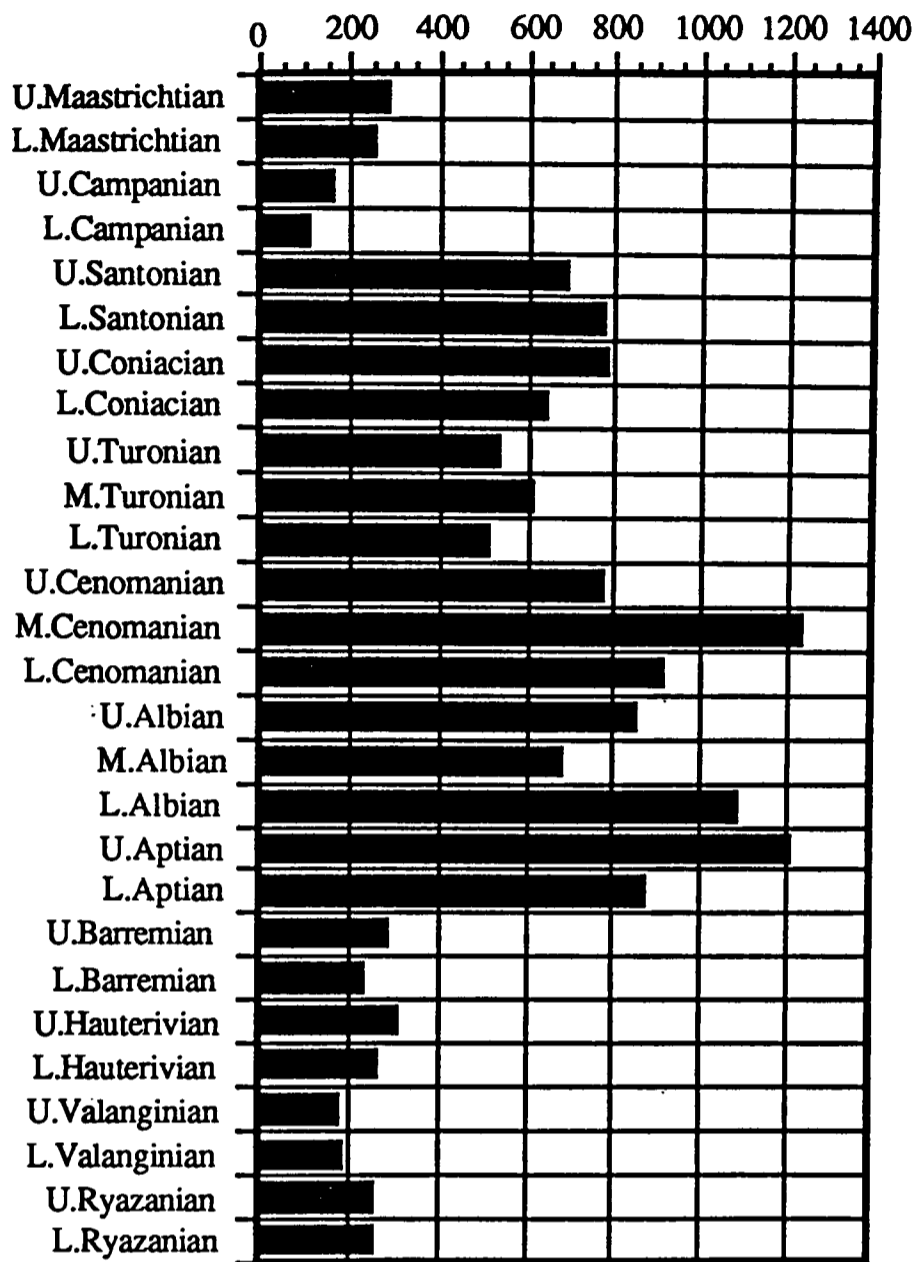


Fig.136: Diagram showing glauconite production rates (measured in km³ per Ma) for each substage of the Cretaceous, derived from volumetric calculations for a large data set of Cretaceous glauconitic facies.

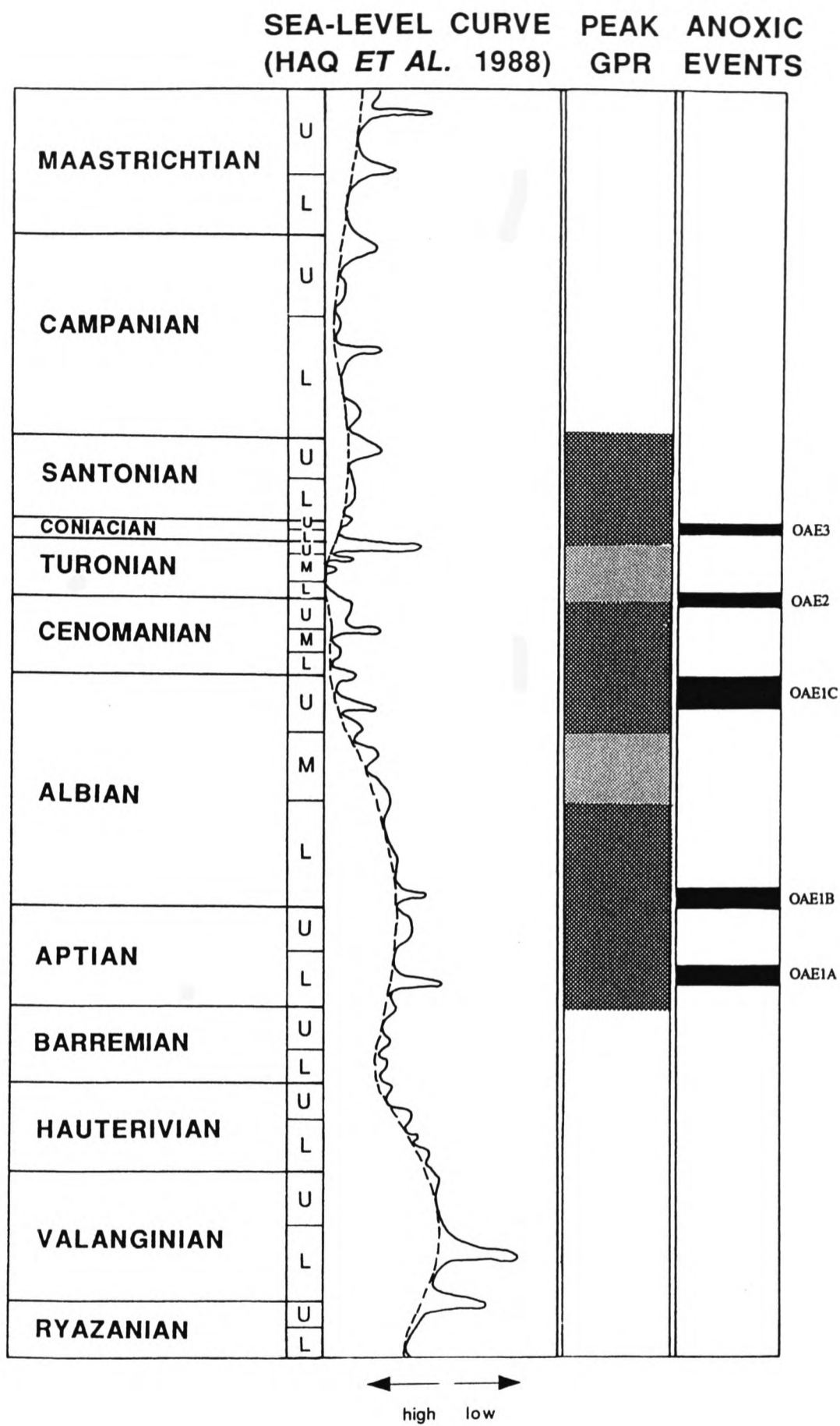


Fig.137: Diagram showing the correlation between the Cretaceous sea-level of Haq *et al.* (1990), peak glauconite production rates (GPR), and the oceanic anoxic events/subevents of Jenkyns (1980), Schlanger *et al.* (1987), Arthur *et al.* (1990) and Jenkyns (1991). Stippled area indicates a middle-Upper Cretaceous interval of high GPR; heavy stipple indicates the three main peaks in GPR during the interval.

GRAPHIC LOGS

A series of 48 graphic logs is presented, covering sections discussed in the text. These are catalogued from west to east across southern England, followed by French examples. All thicknesses are in metres.

- 1 BABCOMBE COPSE 1 (SX 868 762)
- 2 BABCOMBE COPSE 2 (SX 868 762)
- 3 PEAK HILL (SY 109 866)
- 4 DUNSCOMBE CLIFF (SY 153 877)
- 5 KEMPSTONE ROCKS (SY 161 881)
- 6 WESTON EBB (SY 175 878)
- 7 BEER STONE ADIT (SY 220 881)
- 8 HOOKEN CLIFFS - LITTLE BEACH - BEER HEAD 1 (SY 220 879) TO (SY 227 879)
- 9 HOOKEN CLIFFS - LITTLE BEACH - BEER HEAD 2 (SY 220 879) TO (SY 227 879)
- 10 WHITECLIFF, BEER 1 (SY 234 893)
- 11 WHITECLIFF, BEER 2 (SY 234 893)
- 12 CULVERHOLE 1 (SY 272 895)
- 13 CULVERHOLE 2 (SY 272 895)
- 14 CORBIN ROCKS 1 (SY 285 893)
- 15 CORBIN ROCKS 2 (SY 285 893)
- 16 CORBIN ROCKS 3 (SY 284 893)
- 17 EAST OF CORBIN ROCKS (SY 293 896)
- 18 HUMBLE POINT (SY 305 899)
- 19 CHARTON GOYLE (SY 296 903)
- 20 SHAPWICK GRANGE QUARRY (SY 312 918)
- 21 STONEBARROW HILL (SY 378 929)
- 22 GOLDEN CAP - BASAL GAULT (SY 405 920)
- 23 GOLDEN CAP 1 (SY 405 920)
- 24 GOLDEN CAP 2 (SY 405 920)
- 25 EGGARDON HILL (SY 939 948)
- 26 STANDER'S MILL PLANTATION (SY 588 975)
- 27 SLIPPED BLOCK WEST OF WHITE NOTHE (SY 769 809)
- 28 SECTION BELOW HOLWORTH HOUSE (SY 764 814)
- 29 DURDLE COVE 1 (SY 805 806)
- 30 DURDLE COVE 2 (SY 805 806)
- 31 ST. OSWALD'S BAY (SY 815 800)
- 32 LULWORTH COVE, WEST SIDE (SY 825 800)
- 33 LULWORTH COVE, EAST SIDE (SY 828 800)
- 34 MUPE BAY (SY 843 800)
- 35 WORBARROW BAY, BELOW FLOWER'S BARROW - BASAL GAULT (SY 866 804)
- 36 WORBARROW BAY, BELOW FLOWER'S BARROW 1 (SY 866 804)
- 37 WORBARROW BAY, BELOW FLOWER'S BARROW 2 (SY 866 804)
- 38 SWANAGE BAY (SZ 044 811)
- 39 COMPTON BAY, ISLE OF WIGHT 1 (SZ 367 853)
- 40 COMPTON BAY, ISLE OF WIGHT 2 (SZ 367 853)
- 41 NATIONAL TRUST CAR PARK, NEAR BLACKGANG CHINE,
ISLE OF WIGHT (SZ 491 767)
- 42 GORE CLIFF, ISLE OF WIGHT 1 (SZ 492 763)
- 43 GORE CLIFF, ISLE OF WIGHT 2 (SZ 492 763)
- 44 SOUTH OF EASTBOURNE (TV 610 977)
- 45 ST. JOUIN-BRUNEVAL
- 46 LE CROQUET (SLIPPED BLOCK)
- 47 ST. ADRESSE
- 48 CARRIERE LE LIVET, NEAR CORDEBUGLE

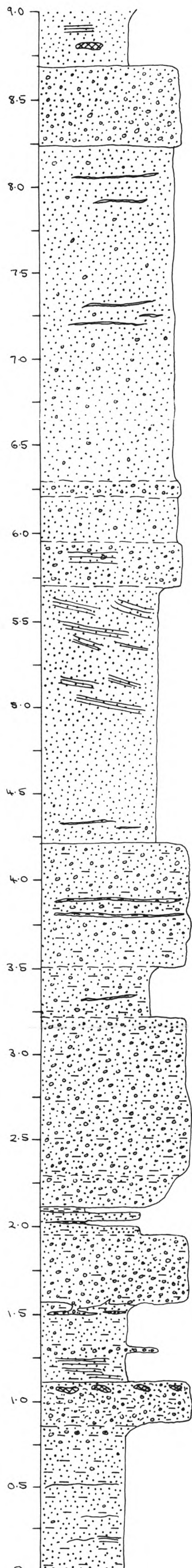
KEY TO GRAPHIC LOGS

	clay
	marl
	muddy silt
	fine-grained muddy sand and silt
	laminated fine sand and silt
	gravelly sand and sandy gravel
	bioclastic packstones and grainstones
	intraformational pebbles and shells
	shell fragments
	calcareenaceous sand
	nodular hardground
	burrowed basal contact; arrow to lowest level of burrowing
	pyrite
	phosphate
	calcareous concretions
	siliceous nodules
	chert nodules
	horizontal stratification
	cross-stratification
	<i>Thalassinoides</i>
	<i>Palaeopycus</i> , black mud lining
	<i>Palaeopycus</i> , buff marl lining
	<i>Planolites</i>
	<i>Chondrites</i>
	bivalve (whole)
	fragmentary fossils
	gastropod
	ammonite
	brachiopod
	serpulid
	echinoid
	bryozoan
	shark tooth
	fossil wood

BABCOMBE COPSE 1 (SX 868 762)

1

PALAEOCURRENT DATA	% GLAUCONITE					TRACE FOSSILS	FOSSILS	DESCRIPTION / NOTES
	0	25	50	75	100			
9.0								
8.5						-		Grey-brown sandy gravel; abundant small granules; granule-supported; almost mud-free.
8.0						-		
7.5						-		Pale brown, moderately well-sorted (clay-free), coarse, slightly gravelly sand; granules of quartz and feldspar; thin, horizontally-oriented clay laminac (drapes).
7.0						-		
6.5								
6.0								
5.5								Pale greenish-brown, moderately-sorted sandy gravel; clay-poor; horizontal lamination; strong iron staining
5.0								
4.5								Pale greenish-brown, soft, medium to coarse-grained, soft sands; heavy mineral-rich, and mud-poor; well-developed horizontal and planar cross-bedding; scattered small granules and clay drapes in basal part.
4.0								
3.5								Brown, poorly-sorted, sandy, muddy gravel; quartz and feldspar-rich; thin horizontal iron-rich seams (?mineralised clay drapes).
3.0								
2.5								Brown, poorly-sorted, pebbly, medium-grained, slightly muddy sand; thin, impersistent, internal clay seam.
2.0								
1.5								
1.0								
0.5								
0								

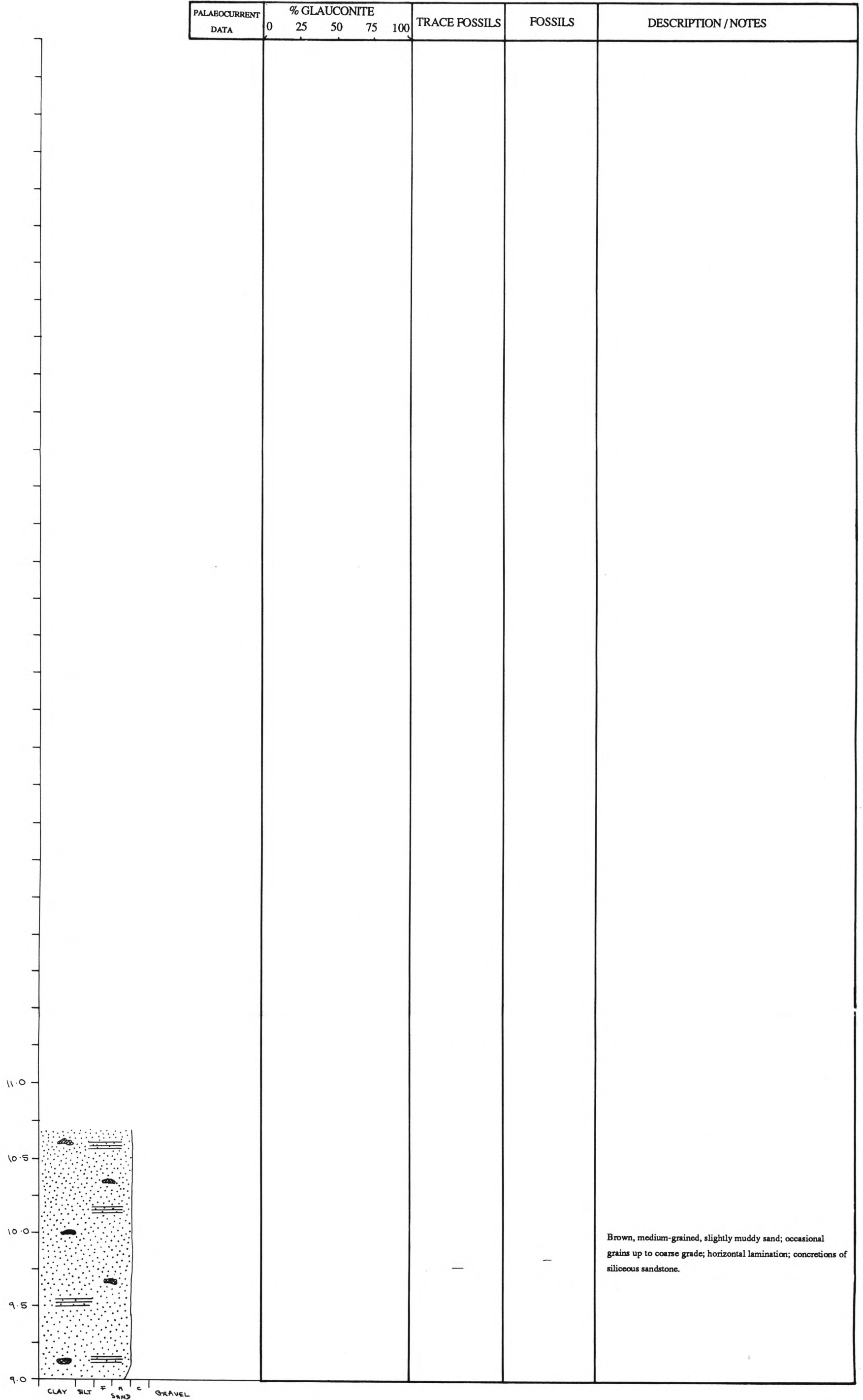


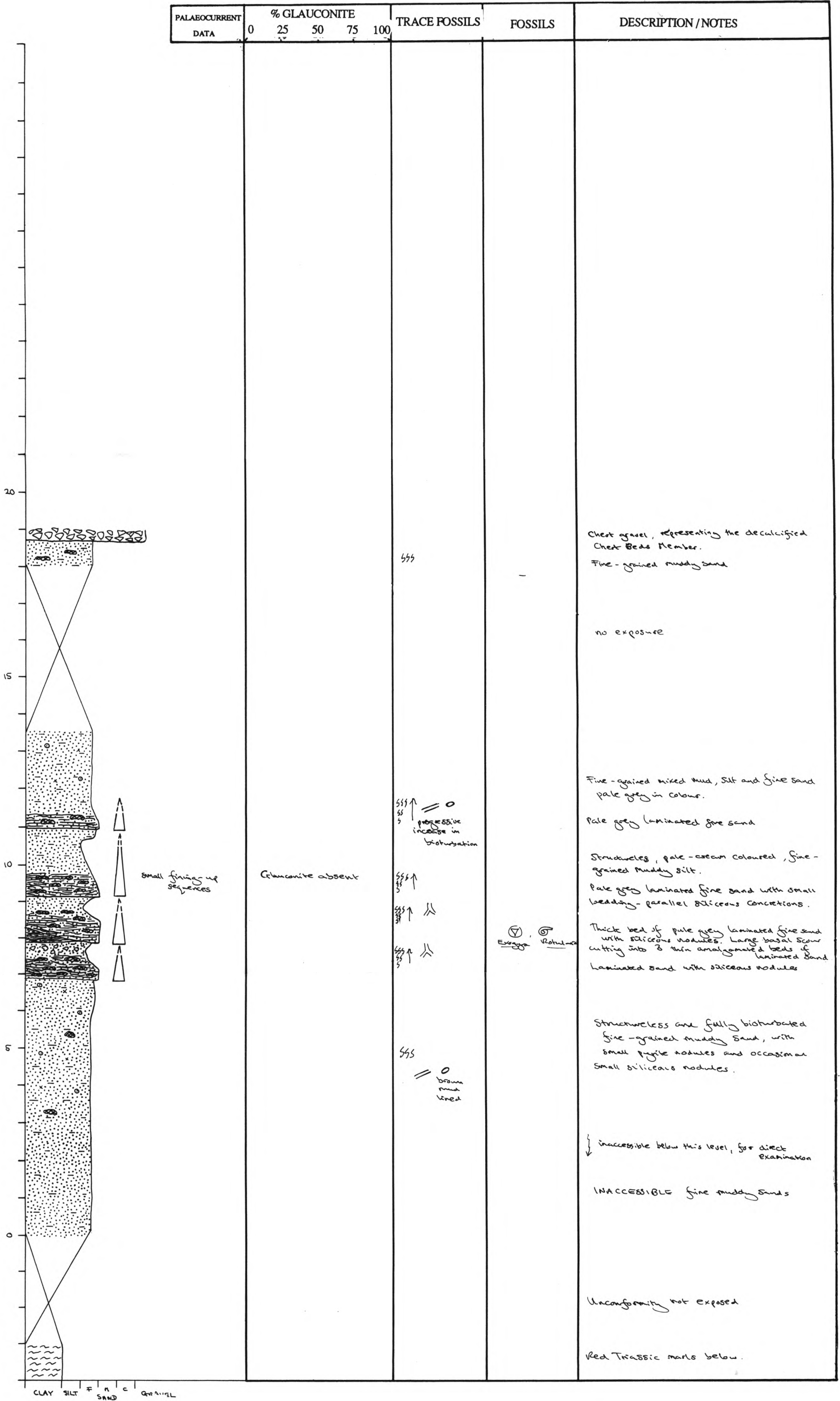
CLAY SILT F M C GRAVEL

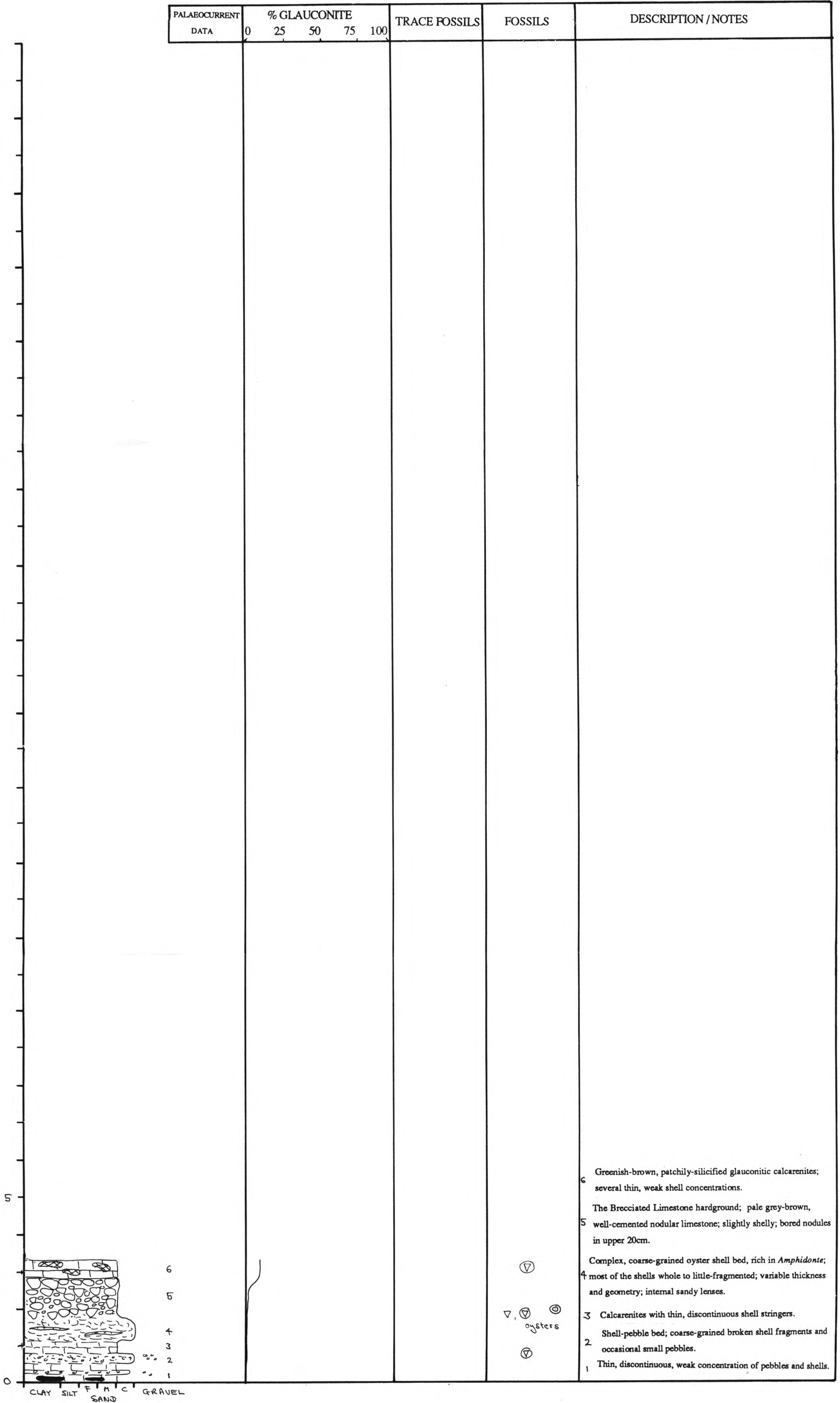
rare (V)

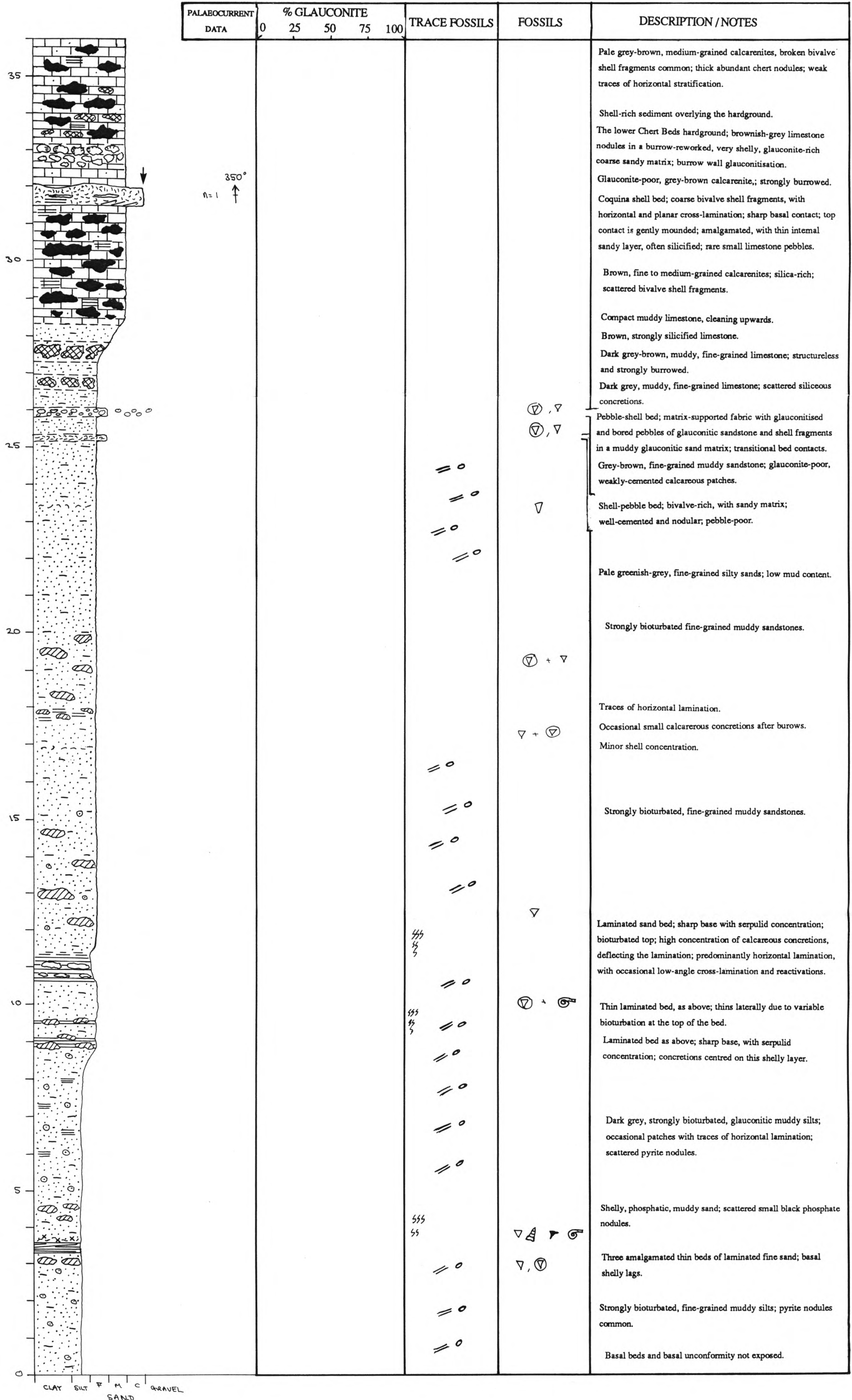
(V) Amphidonte

BABCOMBE COPSE 2 (SX 868 762)

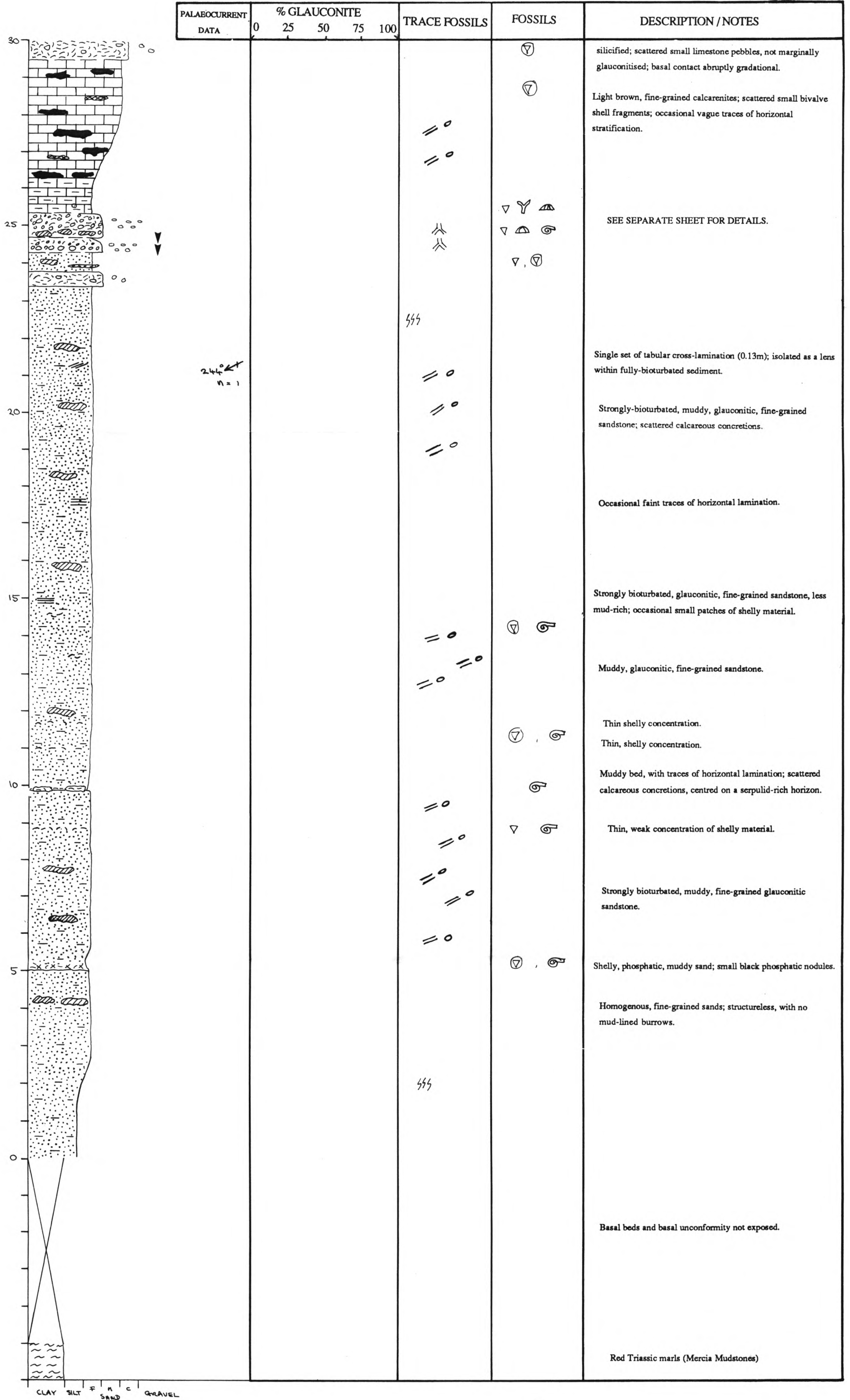






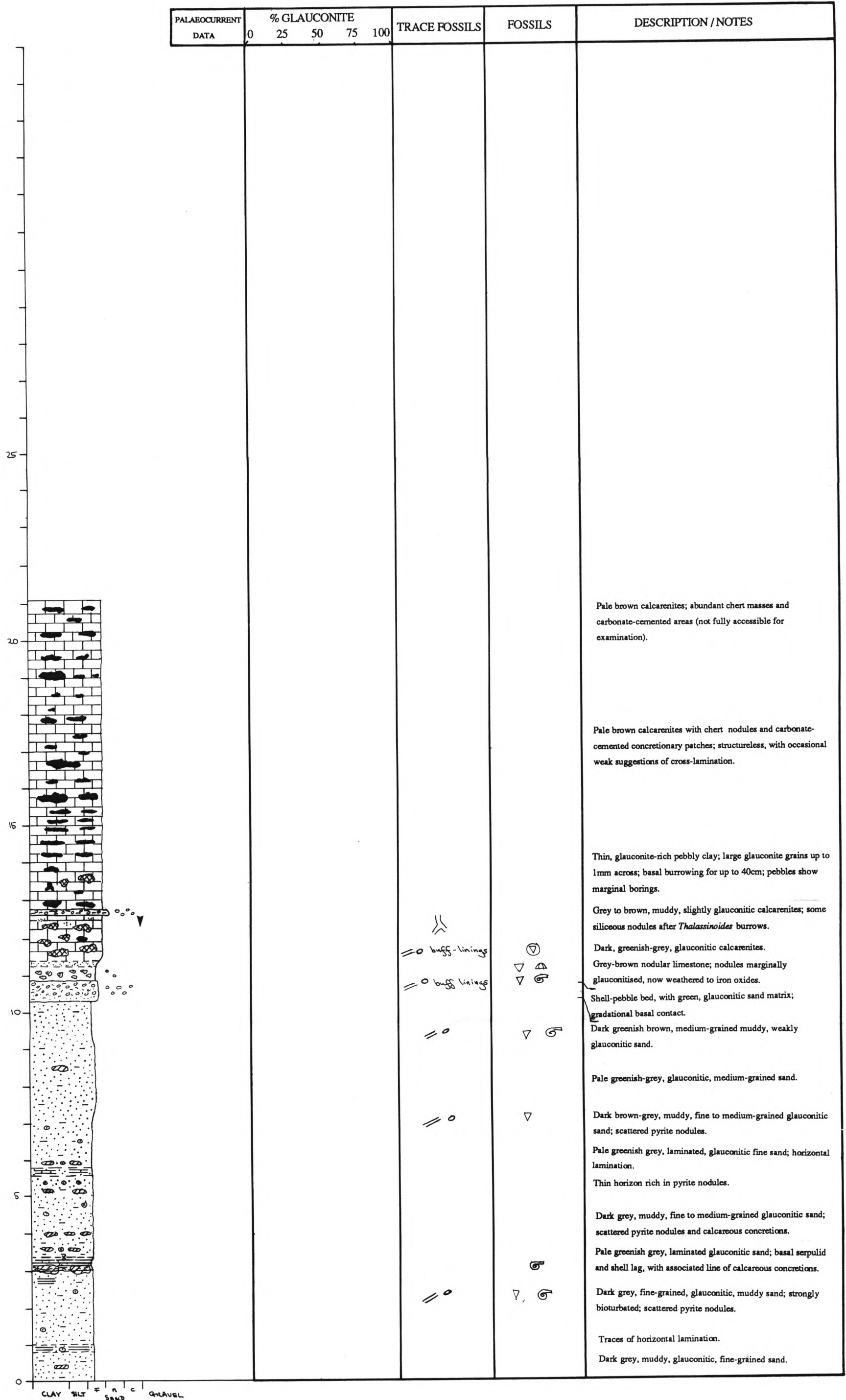


CLAY SILT F M C GRAVEL SAND



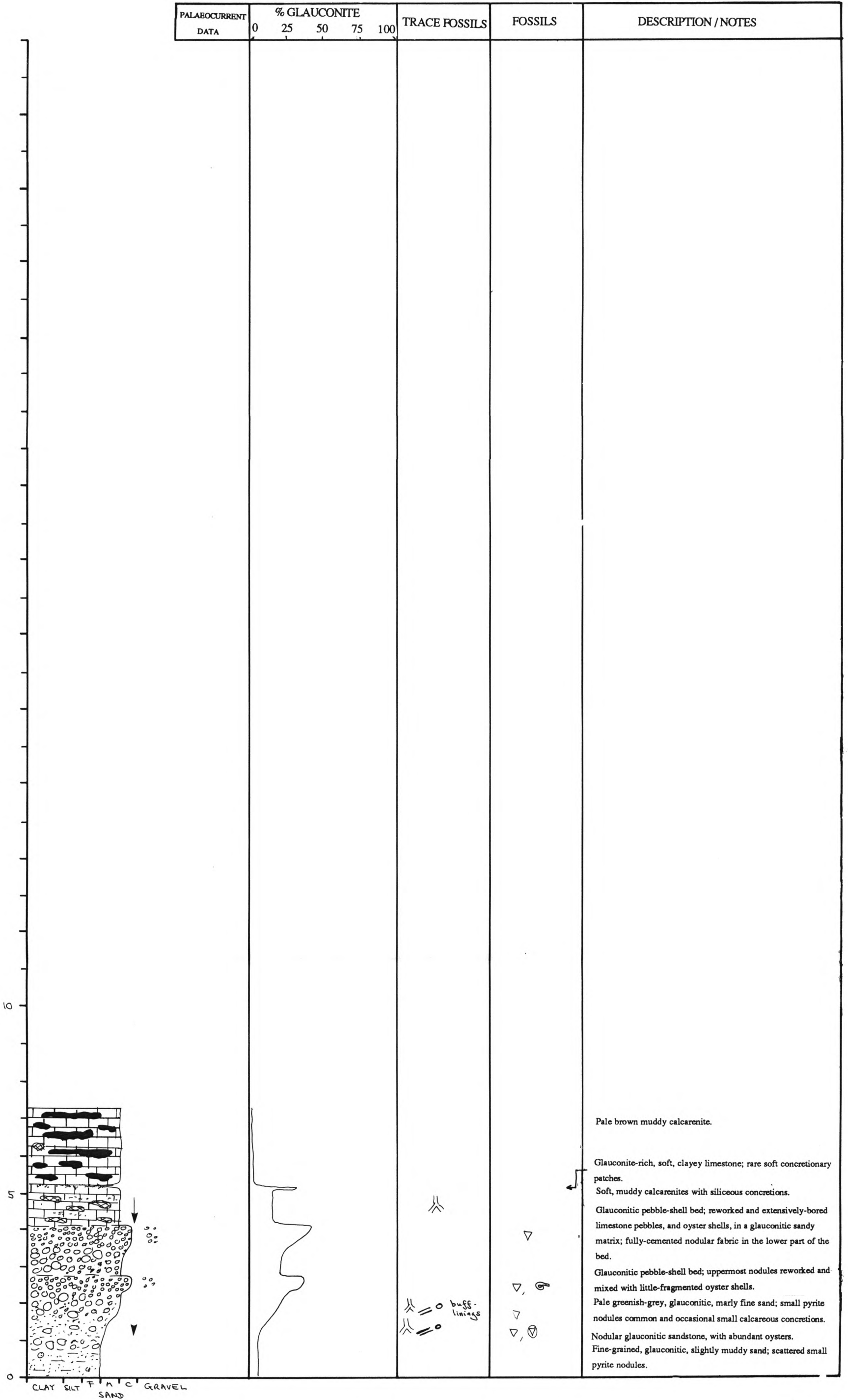
WHITECLIFF, BEER 2 (SY 234 893)

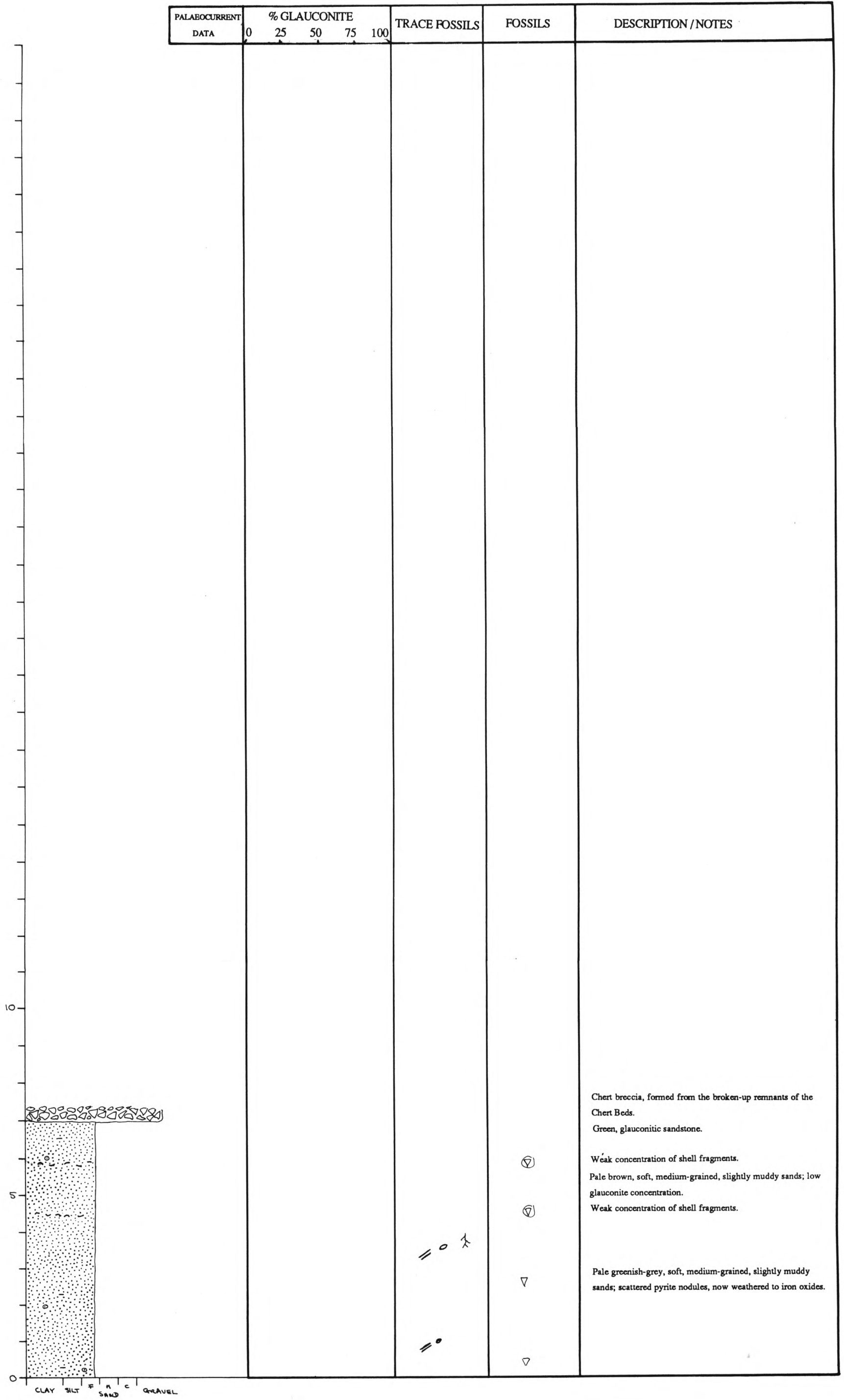
PALAEOCURRENT DATA	% GLAUCONITE					TRACE FOSSILS	FOSSILS	DESCRIPTION / NOTES
	0	25	50	75	100			
								<p>The top Upper Greensand hardground. Greyish-brown nodular limestone; scattered medium to coarse quartz grains, rare small granules; variable degree of nodularity laterally; sediment in between the nodules burrow-reworked; relict trough cross-stratification and burrowing in the nodules; nodule margin glauconitisation in the upper part and upper surface phosphatisation.</p>
						↘	⊖	<p>Brown, well-sorted calcarenites; abundant, glauconitic sediment-filled <i>Thalassinoides</i> burrows; traces of trough cross-bedding; becomes nodular passing upwards.</p>
							⊖	<p>Brown, well-sorted medium to coarse-grained calcarenites; traces of trough cross-bedding; chert nodules common.</p>
							rare ⊖	<p>The Coarse Band. Greenish-brown, quartz-rich calcarenaceous sand; well-rounded quartz grains; mostly structureless, but traces of horizontal to low-angle planar cross-lamination; planar but burrowed basal contact, with piping down of sediment into the bed below; gradational upper contact.</p>
						↘		<p>Cream-coloured, very pure calcarenites.</p>
							⊖-rich, ⊕	<p>Cream-coloured, very shell-rich, coarse, quartzose carbonate sand, rich in bivalve shell fragments.</p>
							⊖, ⊕	<p>The Brecciated Limestone hardground; a mass of calcareous nodules in a burrow-reworked, glauconitic, shelly matrix; little glauconitisation, no phosphatisation; relict cross-stratification; rare upper surface borings.</p>
							⊖	<p>Thin, weak concentration of bored limestone pebbles and shell fragments.</p>
							⊖, ⊕	<p>Glauconitic, quartzose calcarenites; abundant bivalve shell fragments; traces of trough cross-bedding.</p>
							⊖	<p>Shell-pebble bed; shell-rich, glauconitic carbonate sand; shells in upper part horizontally aligned; glauconitised limestone pebbles; gradational base.</p>
								<p>Brown, fine-grained calcarenites; low quartz content; occasional traces of horizontal and low-angle cross-bedding. Muddy in the basal part.</p>
							⊖	<p>Nodular bed; calcareous nodules and smaller glauconitised and bored pebbles; burrowing between the nodules.</p>
							⊖	<p>Brown, glauconite-poor calcarenites; scattered small bivalve shell fragments.</p>
							⊖-rich	<p>Shell-pebble bed, rich in fine shell fragments, now strongly</p>



PALAEOCURRENT DATA	% GLAUCONITE					TRACE FOSSILS	FOSSILS	DESCRIPTION / NOTES
	0	25	50	75	100			
								Strongly-silicified cherty limestone, with rare patches of unsilicified pale brown calcarenite; occasional traces of horizontal lamination.
							rare	Weakly glauconitic, slightly shelly, pale brown cherty limestone.
								Pebble (-shell) bed; horizon of limonitised, bored calcareous concretions in a glauconitic calcarenite matrix; basal burrowing.
								Slightly shelly, soft, pale brown glauconitic calcarenite; patchy calcareous cementation.
							Pebble-shell bed; strongly bored, small limonitised pebbles and oyster shells in a glauconitic calcarenite matrix; passes up into glauconite-rich calcarenite.	

PALAEOCURRENT DATA	% GLAUCONITE					TRACE FOSSILS	FOSSILS	DESCRIPTION / NOTES
	0	25	50	75	100			
<p>CLAY SILT F A C SAND GRAVEL</p>								<p>top Upper Greensand hardground; nodular limestone with patchily phosphatised upper surface and occasional serpulid encrusters; piping down of overlying Cenomanian sandy limestone between the nodules; nodules in upper part marginally glauconitised.</p> <p>Medium to coarse, slightly shelly calcarenite; patchily silicified; horizontally-aligned concentration of thin-shelled oysters.</p> <p>Patchily-silicified quartzose calcarenite; quartz of medium to coarse grade; low angle tabular cross sets and burrowed basal contact.</p> <p>Pale brown, strongly silicified, weakly glauconitic calcarenites, with horizontal glauconite-rich/poor lamination.</p>





10

5

0

CLAY SILT F SAND C GRAVEL

Chert breccia, formed from the broken-up remnants of the Chert Beds.

Green, glauconitic sandstone.

Weak concentration of shell fragments.

Pale brown, soft, medium-grained, slightly muddy sands; low glauconite concentration.

Weak concentration of shell fragments.

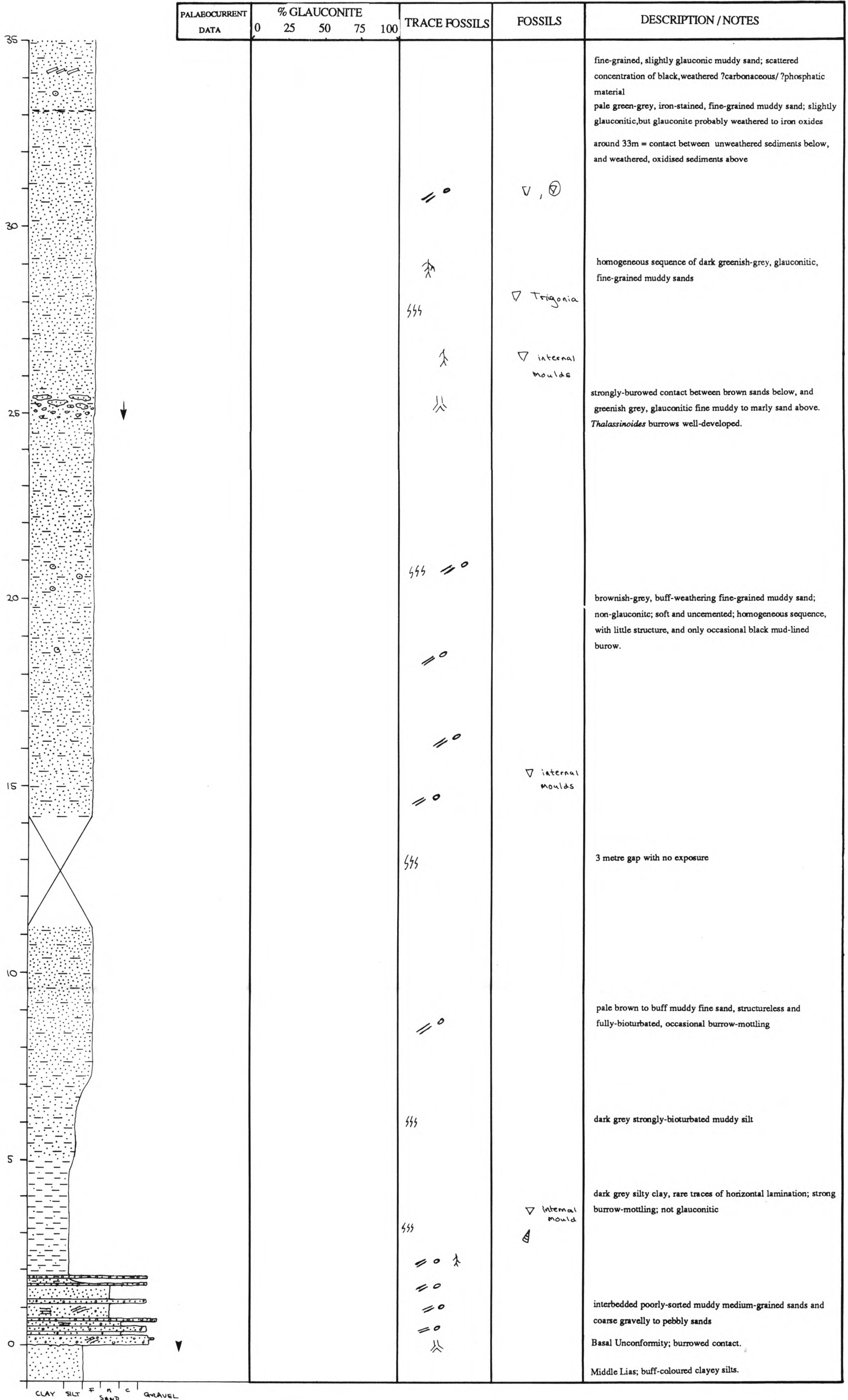
Pale greenish-grey, soft, medium-grained, slightly muddy sands; scattered pyrite nodules, now weathered to iron oxides.

⊖

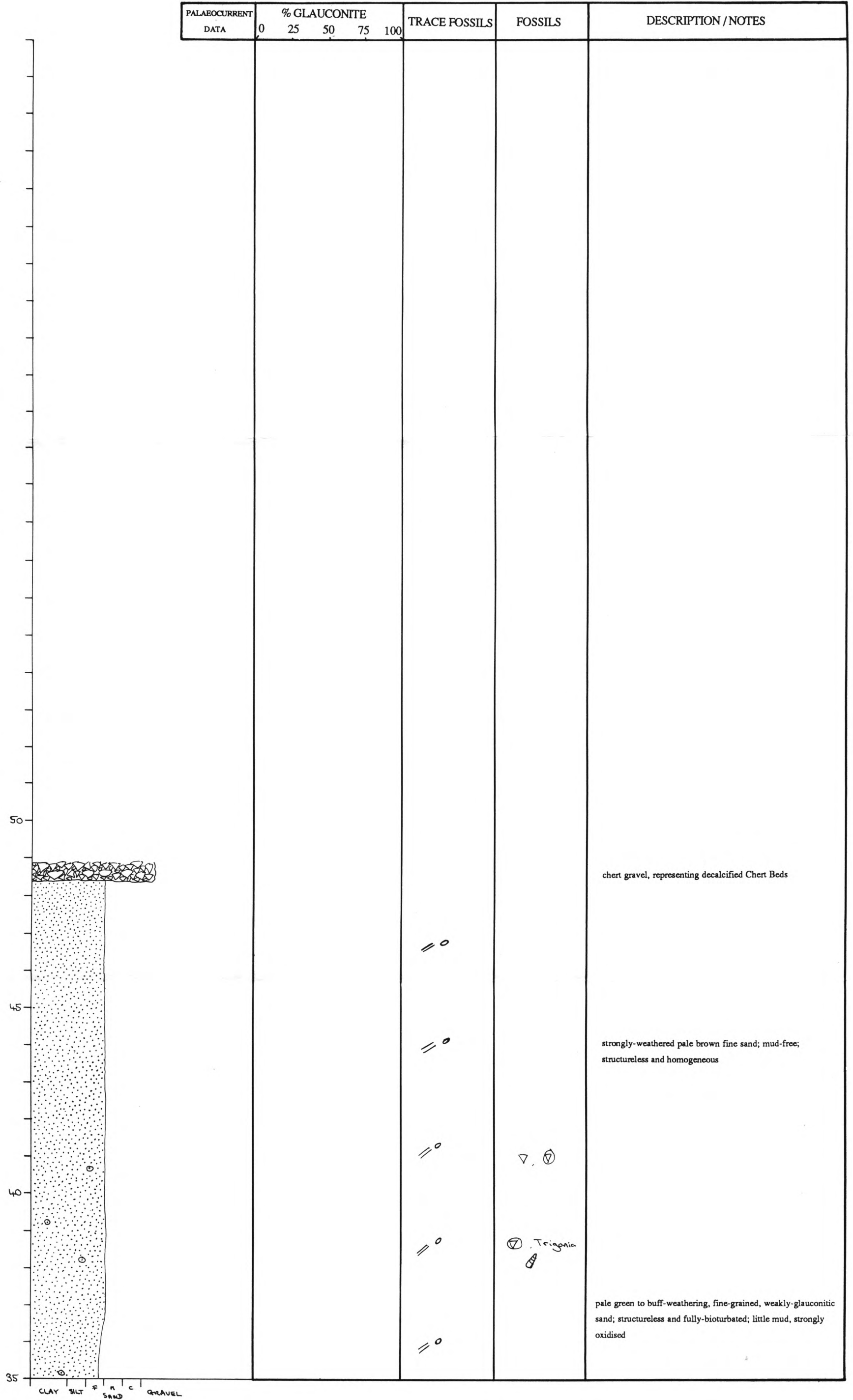
⊖

⊖

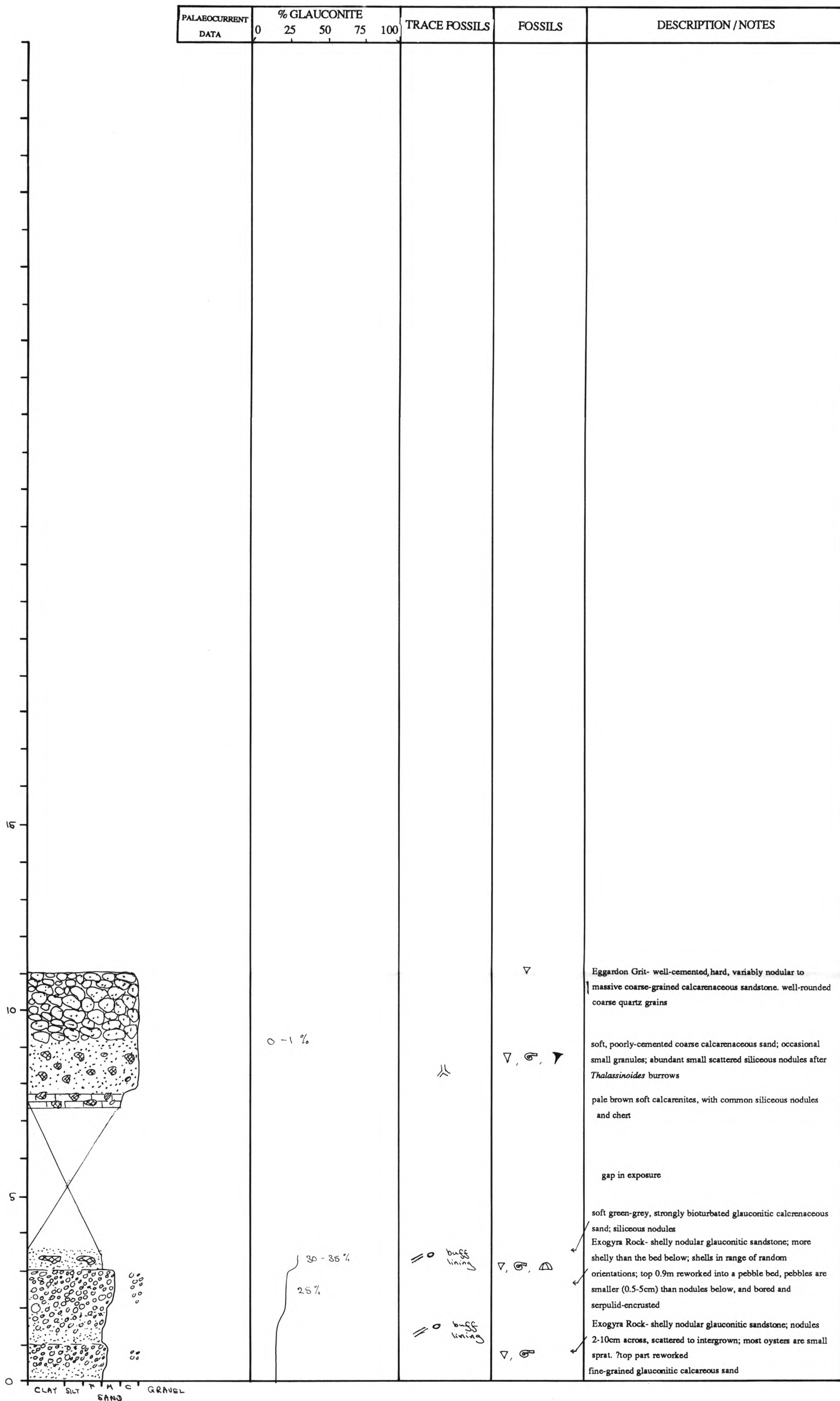
⊖

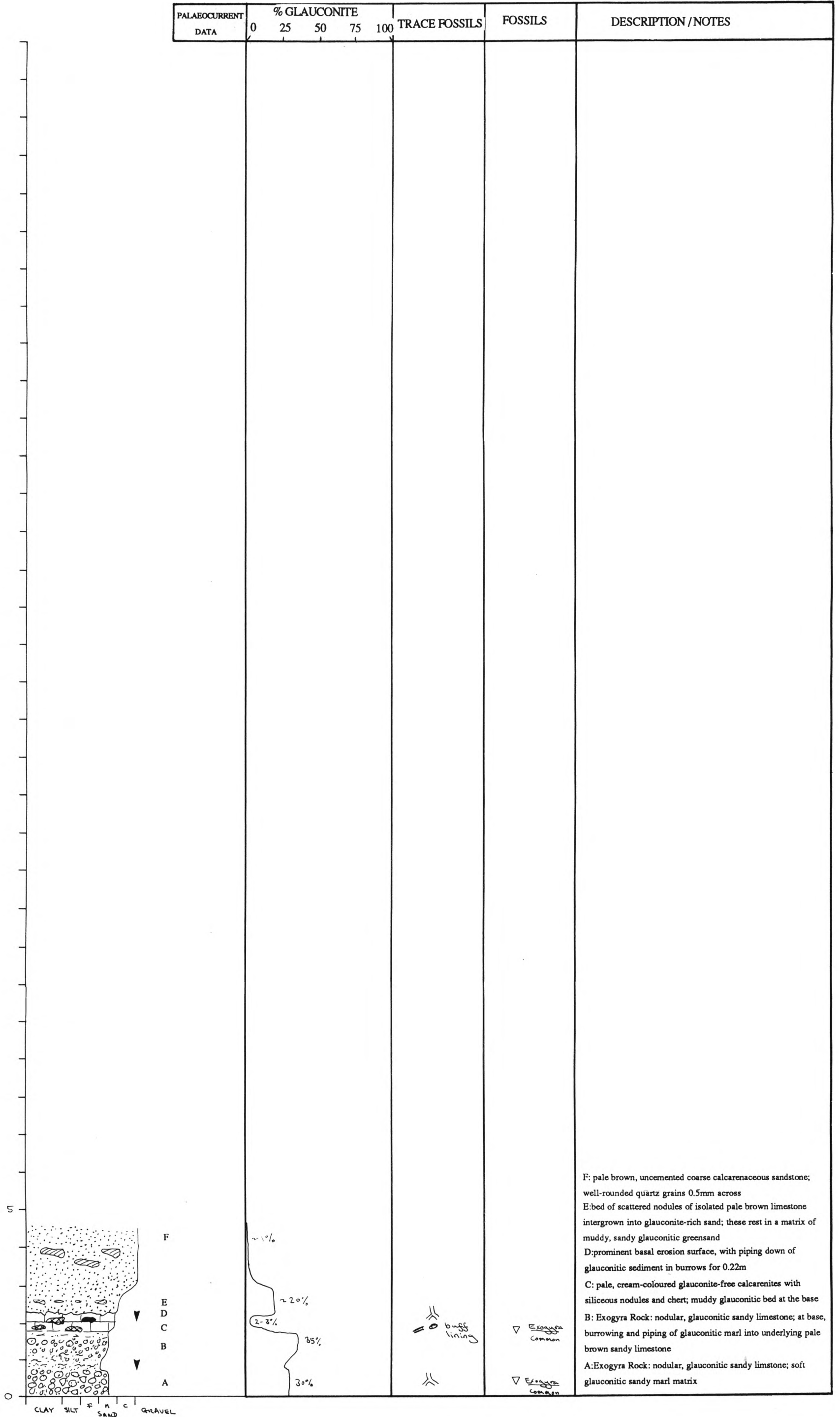


CLAY SILT F SAND C GRAVEL



EGGARDON HILL (SY 939 948)

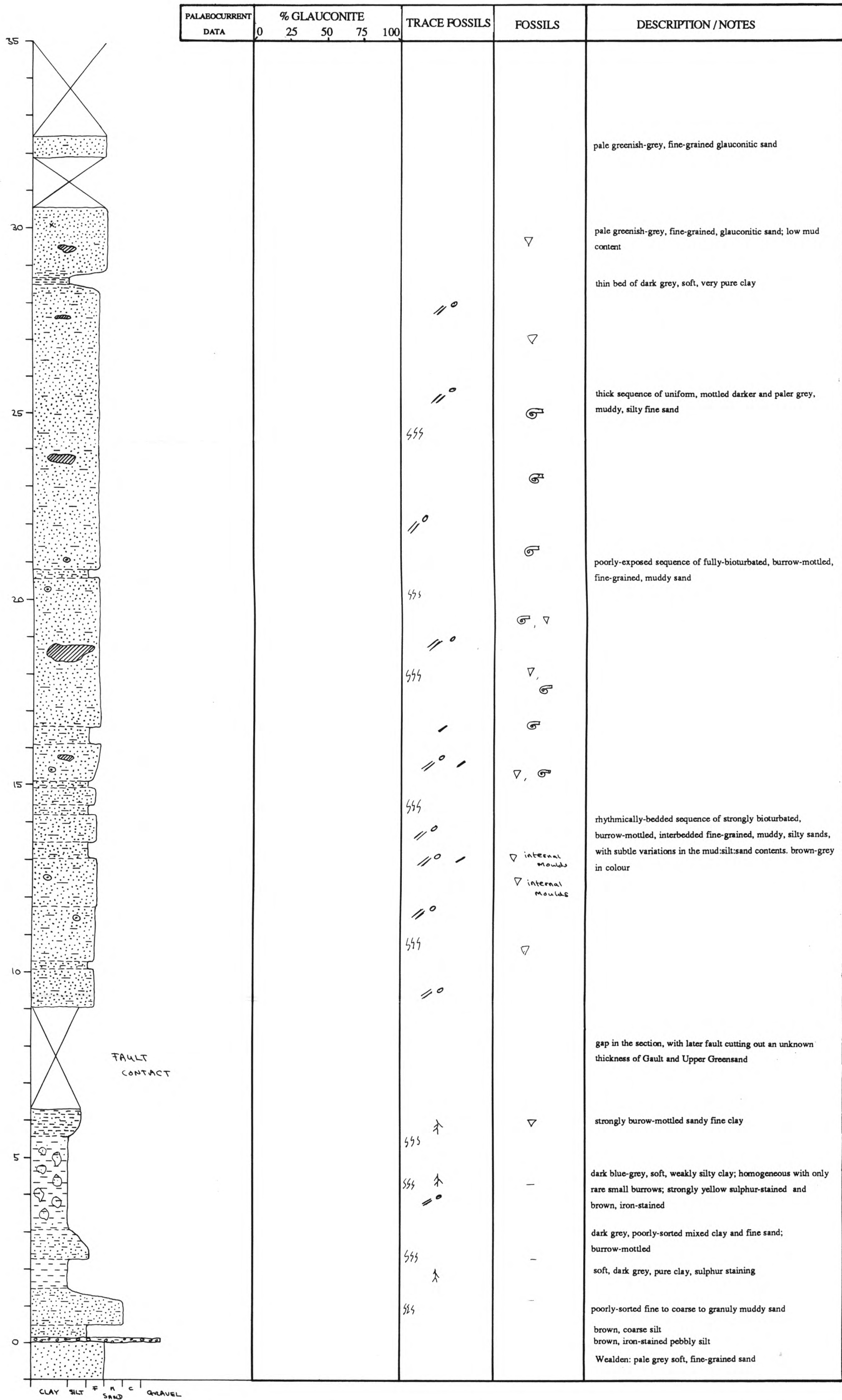




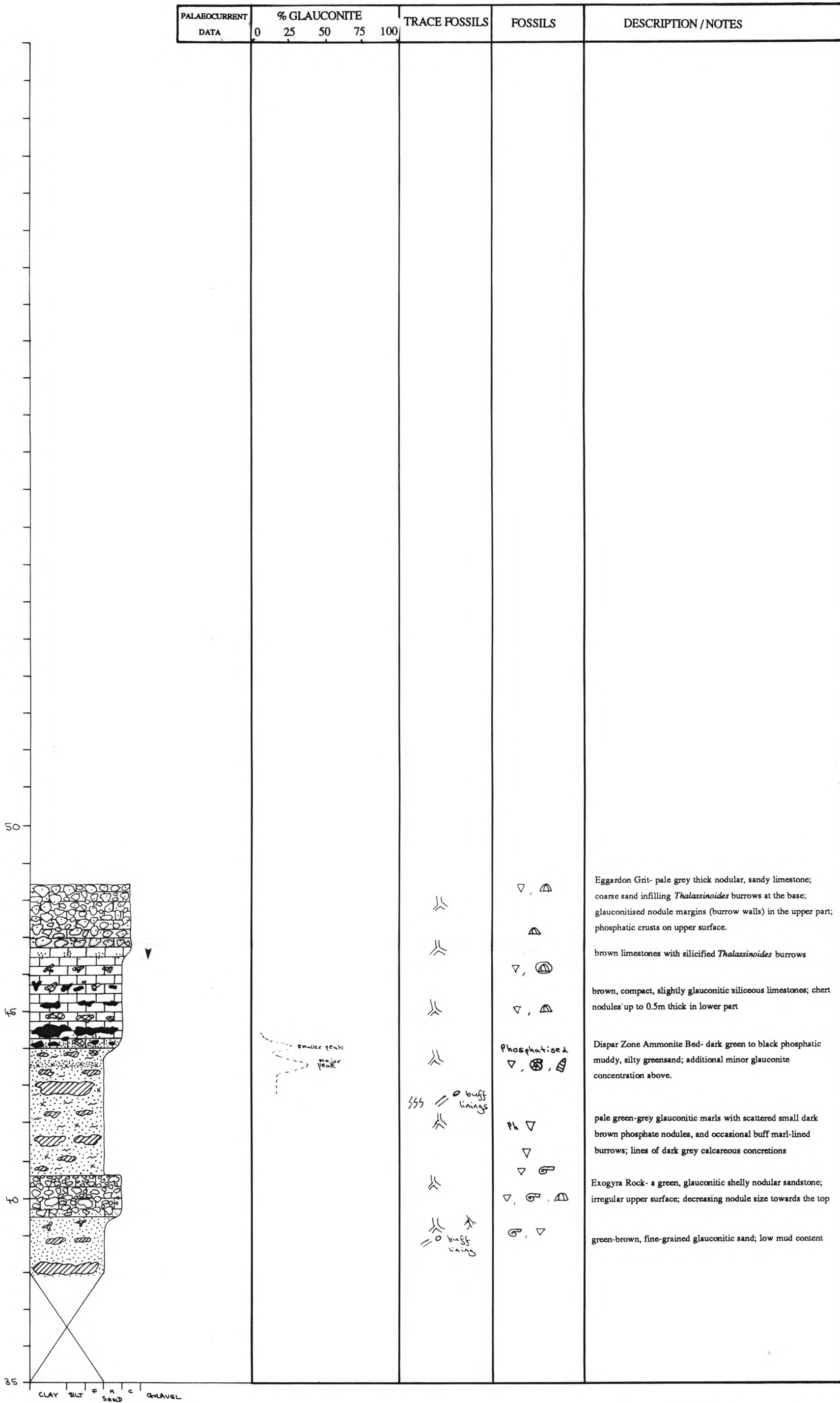
SECTION BELOW HOLWORTH HOUSE (SY 764 814)

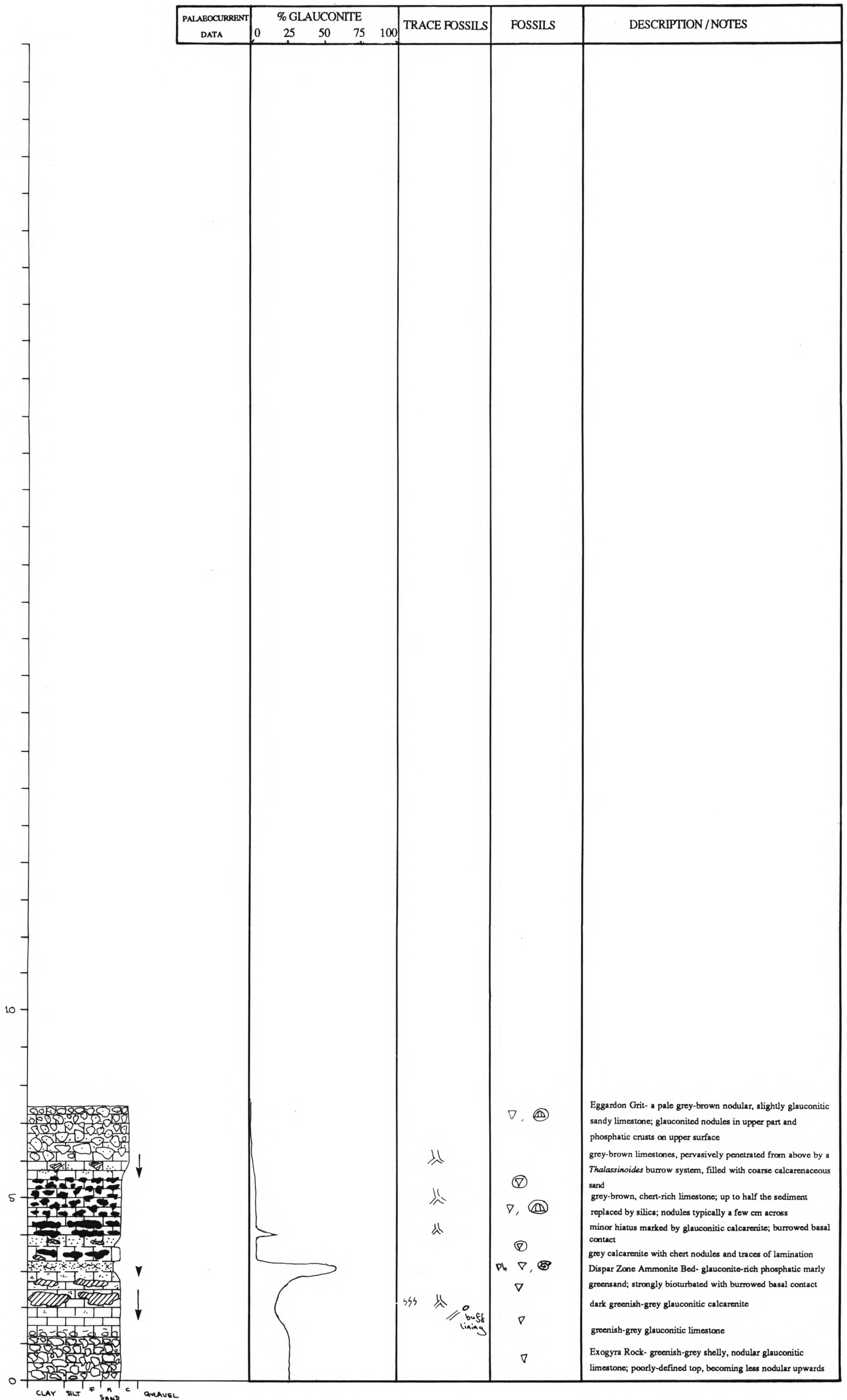
PALAEOCURRENT DATA	% GLAUCONITE					TRACE FOSSILS	FOSSILS	DESCRIPTION / NOTES
	0	25	50	75	100			
						<p>sss o //</p> <p>pale grey silt-filled</p> <p>sss grey ss, occasional</p> <p>pale grey silt-filled ss 1cm diam.</p> <p>pale grey silt-filled ~1mm diameters</p> <p>sss</p> <p>sss</p> <p>sss pale grey silt-filled common</p>	<p>▽, <i>Exogyra</i></p> <p>▽ <i>Entolium</i></p> <p>⊕</p> <p>fossils not common</p> <p>rare ▽, <i>Entolium</i></p> <p>▽, <i>Entolium</i> large + small</p> <p>▽ <i>Entolium</i></p> <p>-</p> <p>-</p> <p>-</p> <p>-</p>	<p>Mottled grey, very muddy fine sand</p> <p>Dark grey, compact, silty clay scattered pyritic nodules.</p> <p>Dark grey-brown soft, silty clay</p> <p>Dark grey, compact, slightly silty clay occasional small calcareous concretions.</p> <p>Pale-weathered muddy fine sand, &d upper and lower contacts.</p> <p>Compact, dark grey clay, fairly pure + silt-free, scattered pyrite nodules</p> <p>Soft, silty, slightly sandy clay. Mottled dark grey + paler greenish grey.</p> <p>Thin bed of soft weakly silty clay.</p> <p>Mottled greenish-brown and grey, silty, sandy clay</p> <p>Interbedded weakly silty and moderately silty clays (rhythmic bedding - weakly defined) Mottled dark grey + paler grey-brown in colour.</p> <p>Grey silty clay</p> <p>Large gap in the section; basal unconformity not exposed.</p> <p>Kimberidge Clay exposed below</p>
	0% (-2%)							
	slightly glauconitic, ~2%							

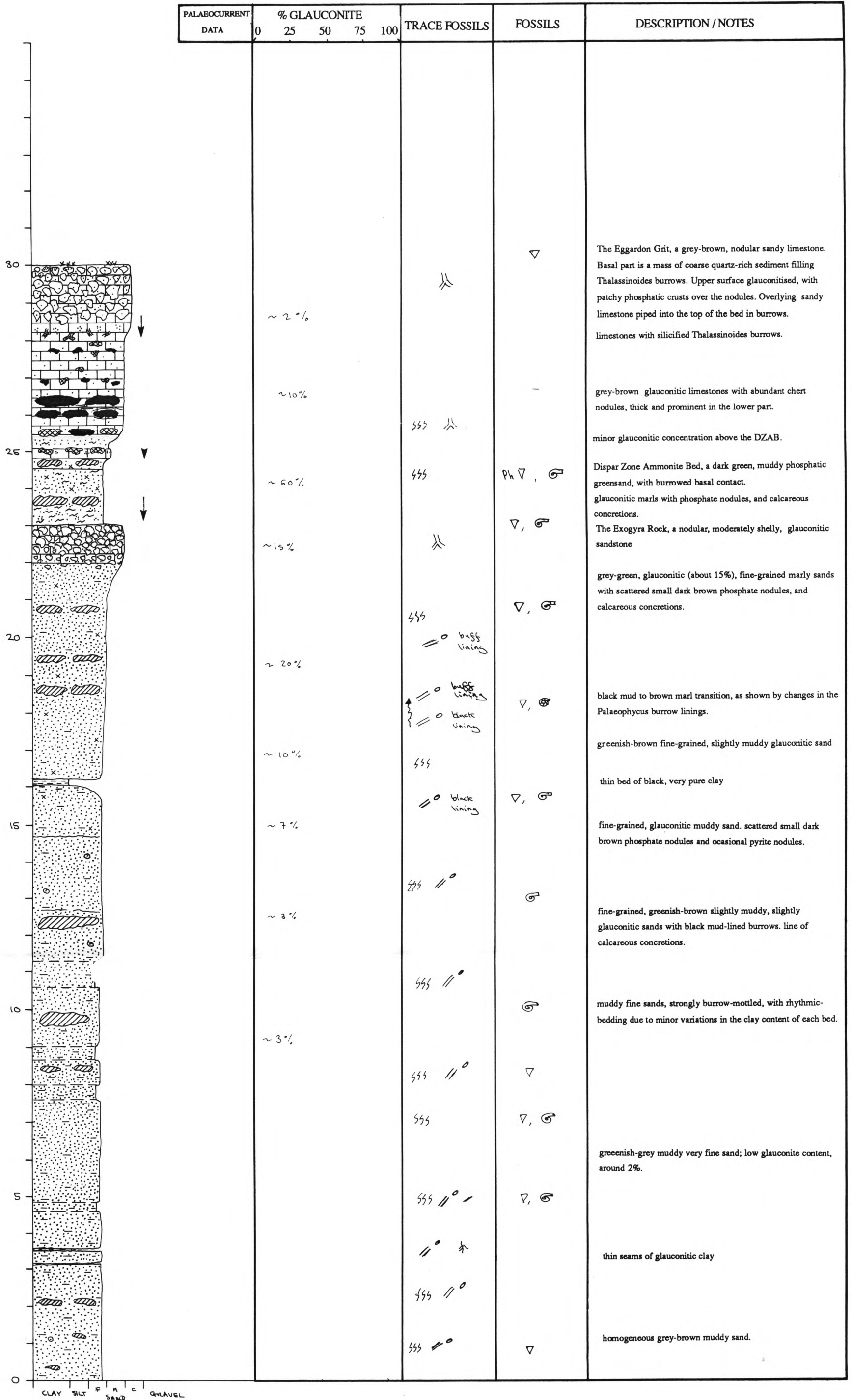
CLAY SILT F M C SAND GRAVEL



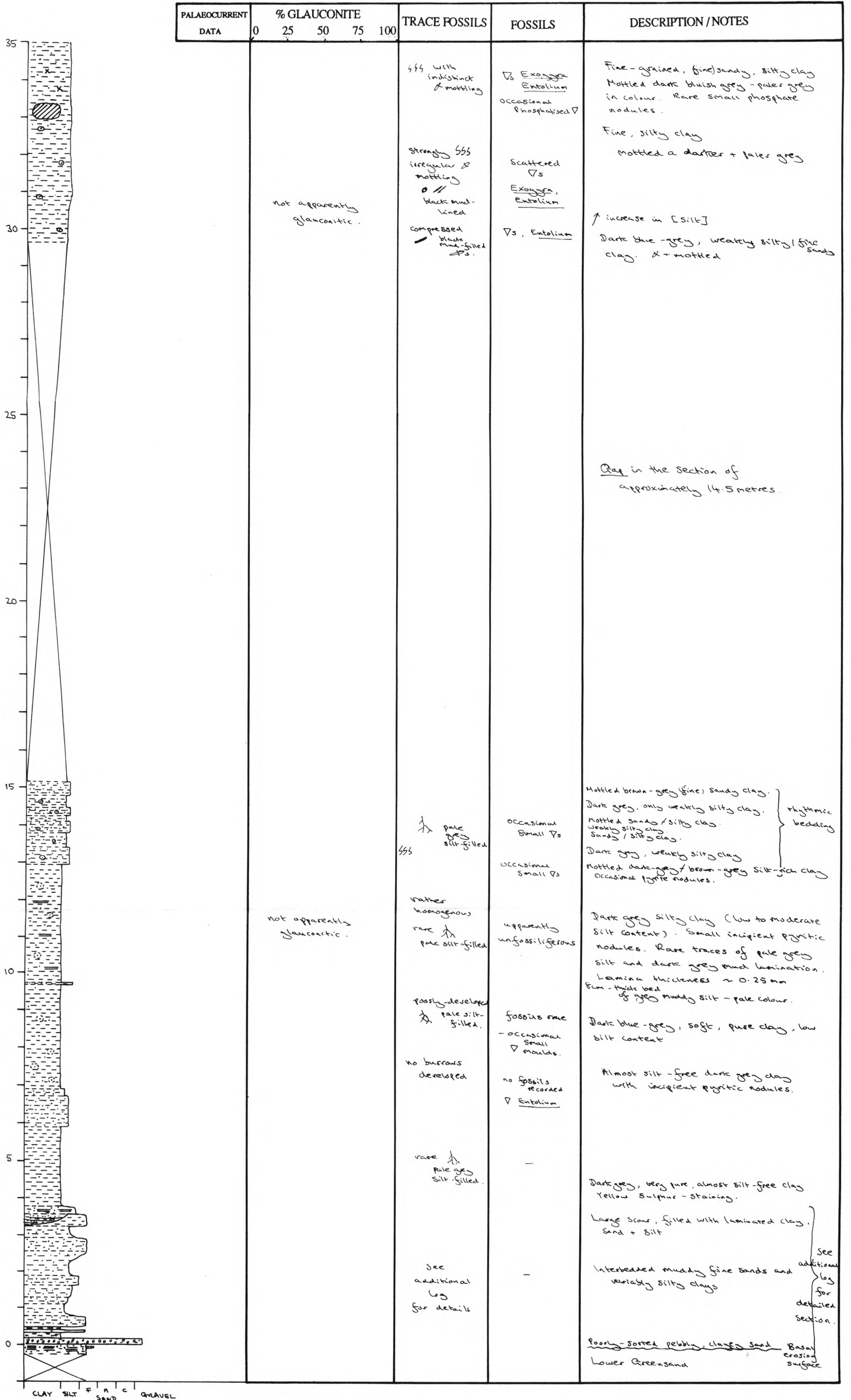
CLAY SILT SAND GRAVEL



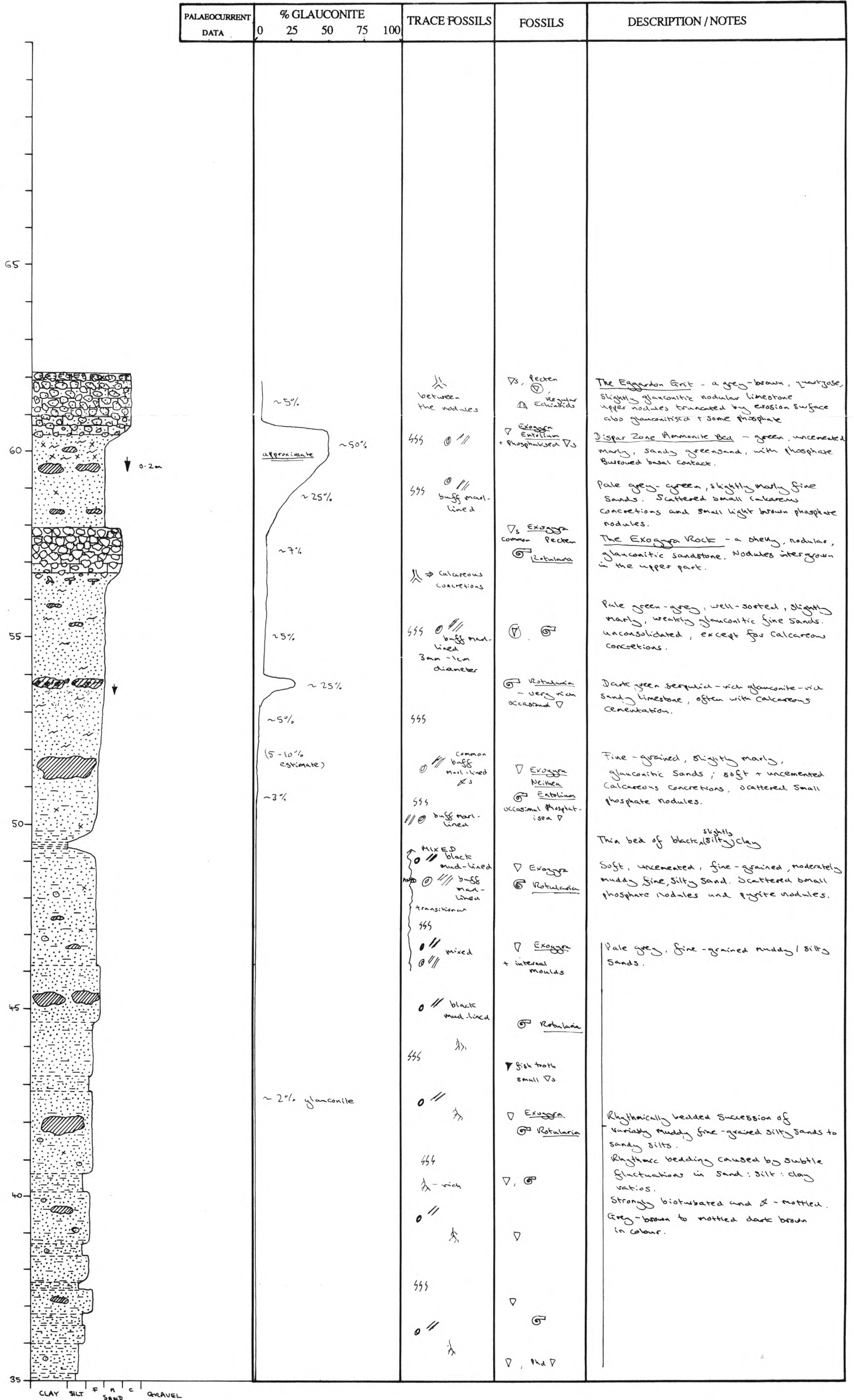




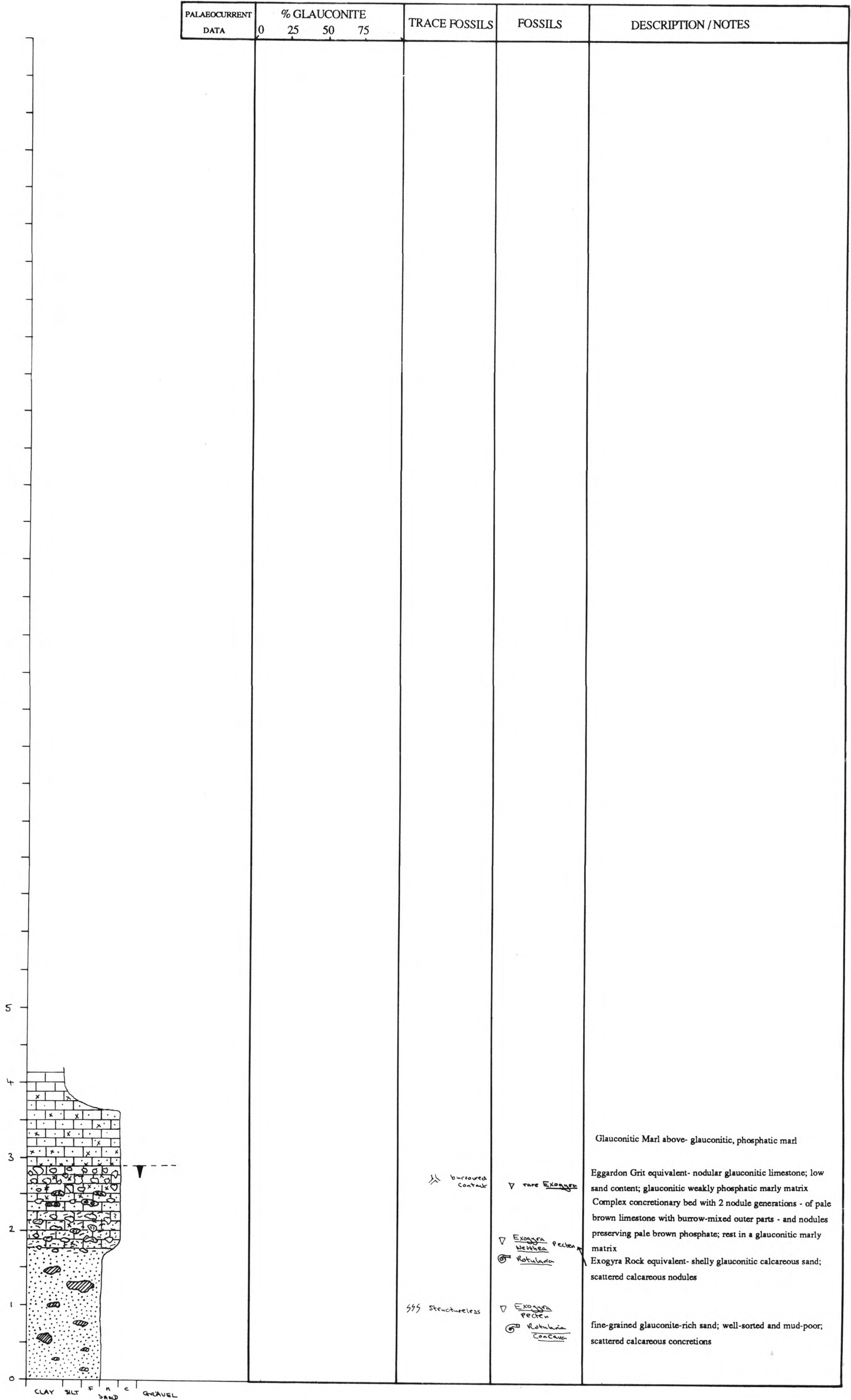
CLAY SILT F M C GRAVEL SAND

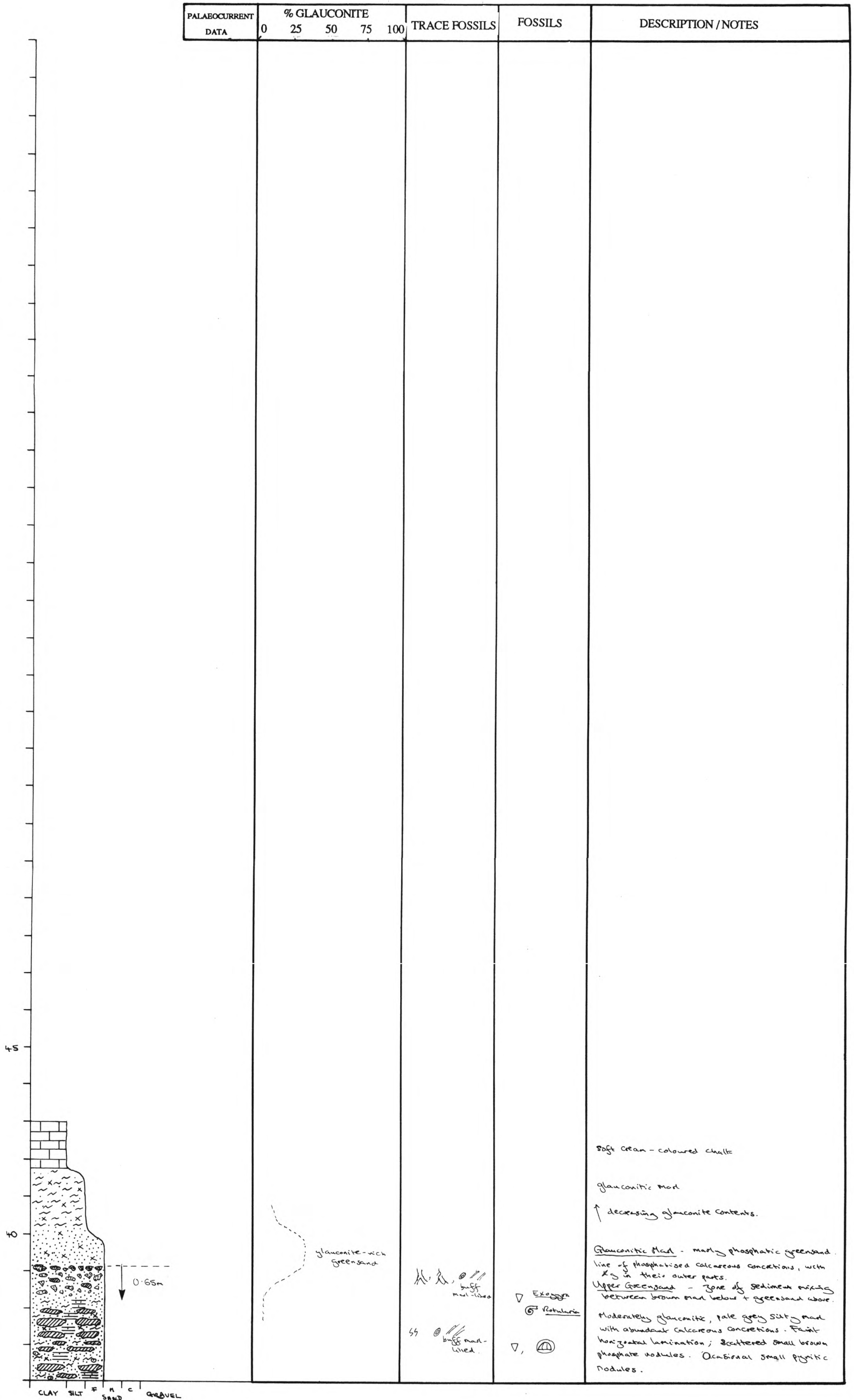


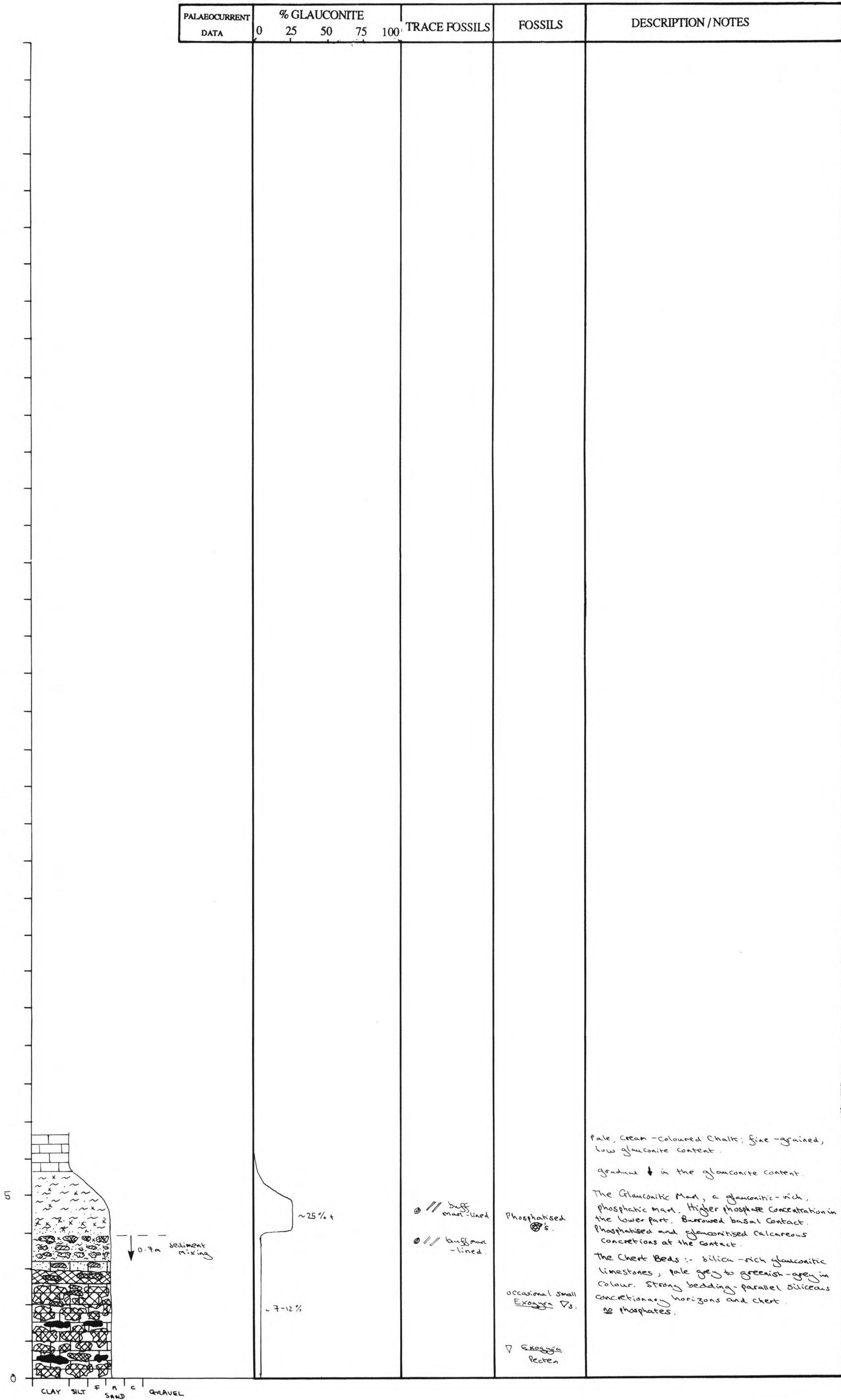
CLAY SILT F M C GRAVEL SAND



CLAY SILT F N C GRAVEL SAND







PALAEOCURRENT DATA	% GLAUCONITE					TRACE FOSSILS	FOSSILS	DESCRIPTION / NOTES
	0	25	50	75	100			
						some bilobed		Fine-grained, indurated marly, silty sand well-developed line of silico-calcareous concretions.
						buff mud-lined & common	occasional small <i>Exogyra</i>	Grey-brown, fine marly silty sand, scattered small phosphate nodules.
						buff mud-lined	<i>Exogyra</i> <i>Entolium</i> <i>Rotularia</i>	Fine-grained, silty, marly sand, only slightly glauconitic; rare small phosphate nodules, 1-2mm in diameter. Sediment a pale grey-brown in colour.
	very low, few %.					occasional small clusters of Ph. nods		Faces change from more muddy sediment matrix below, to a more marly matrix above.
						mostly buff mud-lined, a few black mud-lined	<i>Rotularia</i> <i>Concava</i>	Strongly bioturbated, structureless, fine-grained, muddy silty sand. Scattered small dark brown phosphate nodules
						occasional buff mud-lined	Small <i>Exogyra</i> <i>Rotularia</i>	Compact muddy siltstone, with well-developed lines of calcareous concretions.
	~ 2-3% maximum concentration					black mud-lined	scattered <i>Rotularia</i>	
						but few discrete	<i>Rotularia</i> <i>Concava</i> reptile tooth	Fine-grained calcareous siltstone, only weakly muddy/marly. Slightly micaceous (muscovite); very weakly glauconitic (2-3%).
	not glauconitic							
								<u>The Passage Beds</u> Rhythmically bedded, variably muddy siltstones, with calcareous concretions. Rhythmic fluctuations in the mud contents of successive beds. All strongly bioturbated and mottled. Pale grey to darker grey in colour. Scattered small pyrite nodules. Some beds of silty clay at finest end of the spectrum; range up to weakly muddy siltstones.
					black mud-lined	rare <i>Rotularia</i> rare <i>Entolium</i>		
					throughout	rare/occasional <i>Entolium</i>		
						rare		
							compact, very muddy silt to silty clay. Dark grey; scattered incipient pyritic nodules.	
					black mud-lined			
						common ind. <i>Entolium</i>	very muddy silt. Muddy fine silt	
					bul.			

CLAY SILT F M C GRAVEL SAND

PALAEOCURRENT DATA	% GLAUCONITE				TRACE FOSSILS	FOSSILS	DESCRIPTION / NOTES
	0	25	50	75			
	<p>estimated ~ 8% glauconite</p>				<p> rare @ buff-marl-lined</p> <p>@ </p>	<p>▽ scattered <u>Exogyra</u></p> <p>▽ <u>Exogyra</u> α @ <u>Kobulekia</u> <u>Concava</u></p> <p>scattered small ▽ <u>Exogyra</u></p>	<p><u>Chest Beds</u> Pale greenish-grey siliceous marly limestones/marls. Scattered small pale brown + dark brown phosphate nodules. Slightly silty. Strong bedding parallel siliceous to chert concretionary horizons. Weakly glauconitic sediment.</p>
							<p>Indurated, fine grained, marly fine silt around 7% glauconite. Pale greenish, brownish grey in colour. Scattered small phosphate nodules and phosphatised AS.</p>
							<p>strongly-silicified concretionary horizon. Fine-grained, slightly glauconitic, marly fine sand. Scattered small phosphate nodules. included phd. ▽ infills.</p>
CLAY SILT F SAND C GRAVEL							

